OL. 21 NO. 1 APRIL 1969
UBLISHED MONTHLY

of 89

OURNAL OF ELECTROANALYTICAL CHEMISTRY

AND INTERFACIAL ELECTROCHEMISTRY

ternational Journal devoted to all Aspects
f Electroanalytical Chemistry, Double Layer
tudies, Electrokinetics, Colloid Stability, and
lectrode Kinetics.

HIS ISSUE IS
EDICATED TO THE
IEMORY OF
RUNO BREYER

L S E V I E R

GENERAL INFORMATION

Types of contributions

(a) Original research work not previously published in other periodicals.
(b) Reviews on recent developments in various fields.
(c) Short communications.
(d) Preliminary notes.

Languages

Papers will be published in English, French or German.

Submission of papers

Papers should be sent to one of the following Editors:
Professor J. O'M. Bockris, John Harrison Laboratory of Chemistry, University of Pennsylvania, Philadelphia 4, Pa. 19104, U.S.A.
Dr. R. H. Ottewill, Department of Chemistry, The University, Bristol 8, England.
Dr. R. Parsons, Department of Chemistry, The University, Bristol 8, England.
Professor C. N. Reilley, Department of Chemistry, University of North Carolina, Chapel Hill, N.C. 27515, U.S.A.

Authors should preferably submit two copies in double-spaced typing on pages of uniform size. Legends for figures should be typed on a separate page. The figures should be in a form suitable for reproduction, drawn in Indian ink on drawing paper or tracing paper, with lettering etc. in thin pencil. The sheets of drawing or tracing paper should preferably be of the same dimensions as those on which the article is typed. Photographs should be submitted as clear black and white prints on glossy paper. Standard symbols should be used in line drawings, the following are available to the printers:

▼ ▽ ■ □ ● ◎ ▪ ◘ ◈ ▣ ▪ + ×

All references should be given at the end of the paper. They should be numbered and the numbers should appear in the text at the appropriate places.
A summary of 50 to 200 words should be included.

Reprints

Fifty reprints will be supplied free of charge. Additional reprints (minimum 100) can be ordered at quoted prices. They must be ordered on order forms which are sent together with the proofs.

Publication

The *Journal of Electroanalytical Chemistry and Interfacial Electrochemistry* appears monthly. For 1969, each volume has 3 issues and 4 volumes will appear.
Subscription price: Sfr. 316.— (U.S. $ 74.60) per year incl. postage. Additional cost for copies by air mail available on request. For subscribers in the U.S.A. and Canada, 2nd class postage paid at Jamaica, N.Y. For advertising rates apply to the publishers.

Subscriptions

Subscriptions should be sent to:

ELSEVIER SEQUOIA S.A., P.O. Box 851, 1001 Lausanne 1, Switzerland

JOURNAL OF ELECTROANALYTICAL CHEMISTRY AND INTERFACIAL ELECTROCHEMISTRY

VOL. 21 (1969)

JOURNAL
of
ELECTROANALYTICAL CHEMISTRY
and
INTERFACIAL ELECTROCHEMISTRY

AN INTERNATIONAL JOURNAL DEVOTED TO ALL
ASPECTS OF ELECTROANALYTICAL CHEMISTRY,
DOUBLE LAYER STUDIES, ELECTROKINETICS,
COLLOID STABILITY AND ELECTRODE KINETICS

VOL. 21 1969

ELSEVIER SEQUOIA S.A.

LAUSANNE

BRUNO BREYER 1900–1967
to whose memory the papers in this issue are dedicated

Bruno Breyer was a man of remarkable personality and deep culture, whose gusto for life expressed itself in a wide range of activities.

Readers of this journal will know Breyer as the father of alternating current polarography. Over the course of some twenty years, he laid the foundation for studies now represented in the literature by hundreds of articles from many countries. Breyer began with oscilloscopic studies along the lines of the work of Boeke and van Suchtelen, adding a microammeter "to see what would happen". He immediately grasped the analytical possibilities of a technique that is now routinely used in industrial and in academic laboratories, and published a series of articles on the behaviour of inorganic cations and anions. (In later years, he enjoyed showing letters from two of the leading journals in the English-speaking world, rejecting his first papers on the analytical applications of a.c. polarography—a fate that still awaits contributions that are too novel and portentous.) Subsequently, Breyer studied systematically the behaviour of organic compounds, anticipating the more recent recognition by other workers of the roles of adsorption and changes in double-layer capacity. He explored applications to the study of the double-layer itself, of non-electroactive surfactants, of anodic processes with film formation, and many other aspects of the field. All this is available in the literature, and its significance is attested by the later work that has built on and/or rediscovered his ideas. What is probably not so well known is that all the basic studies in a.c. polarography and tensammetry were made in the space of a decade, with the assistance of a total of three co-workers in this area, using self-constructed apparatus made largely from war-surplus material.

But Breyer's interests and accomplishments ranged far beyond his work in a.c. polarography. While some 50 papers dealt with this work, there are close to a dozen each in general analytical and physical chemistry, on the relation of molecular structure to biological activity, and on fundamental studies in clinical chemistry.

As a youth, Breyer had been active on stage, screen, and radio in Zagreb, had become a polished cabaret compère, tapdancer, and pianist, and had been elected *honoris causa* member of the German Guild of Magicians. In later years, he could sometimes be persuaded to display these talents, particularly in the presence of children, whom he loved.

Breyer's formal studies were carried out at the Universities of Vienna, Leipzig, Berlin, and Bonn. His Ph.D., from the latter institution, was awarded in 1928, *summa cum laude*, for work on "Stereoisomeric Betaines" with Paul Pfeiffer. After teaching briefly at Bonn, Breyer joined I.G. Farbenindustrie and was responsible for a number of patents in the areas of drugs, pesticides, dyestuffs, and water-based emulsion paints. In 1931, Breyer began the study of medicine, at Bonn, Zagreb, and finally Padua, where he graduated M.D. with honours with a thesis on "Application to the field of biology of some recent theories of physical chemistry." Work in the Department of Pharmacology ensued, chiefly on the relation of molecular structure to biological activity. Political tyranny forced Breyer to move once again, this time to Fribourg in Switzerland, where he carried out work on local anaesthetics with prolonged action. In 1939, he joined Rideal's group in Cambridge and there introduced the then-novel technique of polarography; he also assisted the Cambridge Instrument Co. in the design of a polarograph. Upon the outbreak of war, Breyer turned to work on sulphanilamides, chemotherapy of gas gangrene, and developed materials impregnable to mustard gas. He was commended for this work by the War Office, but nevertheless,

like many refugees, was interned as an enemy alien. Given the choice of which country he wished to be moved to, Breyer opted for the U.S.A. and subsequently, in a group of others with the same preference, found himself instead in Australia.

From 1942, Breyer worked at the University of Sydney. As a member of the war-time Drug Research Team, he contributed to the discovery of acridine-type antiseptics and helped found the production of sulpha drugs. He frequently lectured on polarography and did much to spur the development of polarographic work in Australia; many Australians now active in this area were first introduced to it by Breyer. He was attached at first to the Department of Organic Chemistry, then from 1946 worked in Agricultural Chemistry of which he later became Head. Apart from teaching and research there, he was active in clinical studies: from 1951 as Director of the Section for Clinical Biophysics at Prince Henry Hospital, and from 1956 in the Unit of Clinical Investigation at Lidcombe State Hospital. After early retirement from the University of Sydney, he was at the University of Kyoto as visiting professor, and then Head of the Section of Biophysical Chemistry at the Institute for Pharmacology of the University of Milan.

Breyer was passionately devoted to scientific work, and received many honours. But he was first and foremost a warm human being, and more than these honours enjoyed the friendships across the globe that stemmed from his scientific contacts. In 1956, Breyer visited Japan for the first time and was immediately captivated by the charm of the country; he returned whenever he could, and made many firm friendships there. Breyer was an accomplished linguist—when one was with him when the phone rang, it was a matter of conjecture in which of four or five languages he would talk; yet Japanese was the only language he learnt because he wanted to, the others had come of necessity.

People of my generation have studied in a sheltered world, and emerged into an environment of numerous grants and fellowships with virtually ensured employment. It is worth pondering the contrast with a man who was three times exiled, beginning new careers in his mid-thirties and yet again in his forties—the latter making him famous—and withal achieving more in several areas than most of us will in one.

I will remember Breyer as a friend who set the example of a man striving intellectually and in his relations with others to accomplish the best that he was capable of; without stuffiness or snobbery, enjoying the good things of life to the full yet totally undependent on them. A man who gave his students absolute loyalty and encouraged them to become independent workers, smoothing the passage from student and disciple to colleague and friend. A man of great honesty, aware of his shortcomings, who tried always to do what was right irrespective of his own possible preferment or material security. An intensely warm and passionate man, who loved children and gave his affection readily to people whom he met—too readily at times. A man that it is impossible not to miss. Mourning the dead, he told me once, is but self-pity; yet Breyer can also be mourned because he had still so much of lasting value to do when he died.

Breyer's friends can feel what this loss has meant to his beloved companion of many years; she brought much happiness to his life, for which we remain grateful.

HENRY BAUER

ELECTROANALYTICAL CHEMISTRY AND INTERFACIAL ELECTROCHEMISTRY
Elsevier Sequoia S.A., Lausanne – Printed in The Netherlands

ALTERNATING CURRENT POLAROGRAPHY: THEORETICAL PREDICTIONS FOR SYSTEMS WITH FIRST-ORDER CHEMICAL REACTIONS FOLLOWING THE CHARGE TRANSFER STEP*

THOMAS G. McCORD**, HOYING L. HUNG AND DONALD E. SMITH***
Department of Chemistry, Northwestern University, Evanston, Illinois 60201 (U.S.A.)
(Received September 12th, 1968)

INTRODUCTION

The electrode reaction mechanism involving a first-order homogeneous chemical reaction following the heterogeneous charge transfer step,

$$O + ne \rightleftharpoons R \underset{k_1}{\overset{k_2}{\rightleftharpoons}} Y \qquad (R1)$$

has stimulated considerable interest among electrochemists as evidenced by the extensive literature involving both experimental[1-14] and theoretical[5-31] studies. The reasons for this interest are quite evident. To the chemical kineticist, this mechanism when operative affords an ideal and often unique possibility for the evaluation of homogeneous chemical rate parameters of rapid decomposition processes[1-14]. A thorough understanding of the perturbations on electrochemical observables introduced by the following chemical reaction is also essential to the kineticist who is primarily interested in the heterogeneous charge transfer step, simply because Mechanism R1 is likely to be encountered frequently.

The theory of the a.c. polarographic wave of systems involving following chemical reactions has been given due consideration. The earliest efforts[15-18] contributed much to the quantitative understanding of effects of first-order following chemical reactions on the a.c. polarographic response. However, only the phase angle expression was developed with sufficient rigor and scope for general application[16]. The current amplitude expressions were either limited to rather specific conditions[15,18] or were based on a stationary plane mass transfer model[17,18] which is somewhat imprecise. To alleviate some of these restrictions, a theory of greater rigor and generality was developed recently for systems with first-order chemical reactions coupled to a single charge transfer step[32] which incorporates as a special case the theory for the mechanism under consideration. The predictions of these recently derived theoretical relationships for Mechanism R1 have been accorded detailed study to obtain more extensive quantitative insights into the manifestations on the a.c. polarographic

* Work supported by National Science Foundation Grants GP5778 and GP7985.
** NIH Graduate Fellow: present address, General Electric Corp., Materials and Processes Laboratory, Schenectady, New York, 12305.
*** To whom correspondence should be addressed.

response of first-order homogeneous chemical reactions following the charge transfer step. Such theoretical insights are essential in assessing the capabilities of the a.c. polarographic method for investigating systems involving Mechanism R1. The results of this study are presented here.

THEORETICAL

The theoretical relationships considered below are based on the expanding plane model of the dropping mercury electrode (DME)[33]. This model, which accounts for mercury drop growth, is expected to yield current amplitude expressions which are slightly inexact under some conditions[17,34,35], owing to neglect of drop curvature. However, the error is not likely to be serious, particularly with judicious choice of data analysis procedures. Indeed, this model of the DME is the most popular for careful d.c. polarographic work[33] because it represents an excellent compromise between the somewhat incompatible goals of complete theoretical rigor and simplicity of mathematical relationships. Other assumptions or approximations incorporated in the theory have been enumerated elsewhere[16].

General relationships

The general a.c. polarographic theory for systems with first-order homogeneous chemical reactions coupled to a single charge transfer step[32] has shown, within the framework of the expanding plane electrode model, that the theoretical formulation of the a.c. polarographic wave for an electrode reaction following Mechanism R1 may be written (notation definitions are given below):

$$I(\omega t) = I_{\text{rev.}} F(t)\, G(\omega) \sin(\omega t + \Phi) \tag{1}$$

where

$$I_{\text{rev.}} = \frac{n^2 F^2 A C_O^* (\omega D_O)^{\frac{1}{2}} \Delta E}{4RT \cosh^2\left(\frac{j}{2}\right)} \tag{2}$$

$$F(t) = \frac{1+M_f}{M_f}\left\{\frac{K}{1+K} + \left[(\gamma_f - \beta)e^{-j} - \frac{K\beta}{1+K}\right]\frac{\psi(\xi)}{\gamma_f}\right\} \tag{3}$$

$$G(\omega) = \left[\frac{2}{V^2+U^2}\right]^{\frac{1}{2}} \tag{4}$$

$$\cot \Phi = \frac{V}{U} \tag{5}$$

$$\psi(\xi) = 1 + \sum_{p=1}^{\infty} (-1)^p \prod_{n=1}^{p} \frac{\Gamma\{(3n+7)/14\}}{\Gamma\{(3n+14)/14\}} (\sqrt{\tfrac{3}{7}}\,\xi)^p \tag{6}$$

$$\xi = \frac{\lambda_f t^{\frac{1}{2}}}{\gamma_f} \tag{7}$$

$$M_f = K + e^{-j}(1+K) \tag{8}$$

$$\gamma_f = 1 + \frac{\lambda}{k^{\frac{1}{2}}(1+K)(1+e^{-j})} \tag{9}$$

$$\lambda_f = \frac{k_s f}{D^{\frac{1}{2}}}\left(e^{-\alpha j} + \frac{K e^{\beta j}}{1+K}\right) \tag{10}$$

$$\lambda = \frac{k_s f}{D^{\frac{1}{2}}}(e^{-\alpha j} + e^{\beta j}) \tag{11}$$

$$V = \frac{\sqrt{2\omega}}{\lambda} + \frac{1}{1+e^{j}}\left\{\frac{e^{j}}{1+K}\left[\frac{(1+g^2)^{\frac{1}{2}}+g}{1+g^2}\right]^{\frac{1}{2}} + \frac{Ke^{j}}{1+K} + 1\right\} \tag{12}$$

$$U = \frac{1}{1+e^{j}}\left\{\frac{e^{j}}{1+K}\left[\frac{(1+g^2)^{\frac{1}{2}}-g}{1+g^2}\right]^{\frac{1}{2}} + \frac{Ke^{j}}{1+K} + 1\right\} \tag{13}$$

$$j = \frac{nF}{RT}(E_{d.c.} - E^{r}_{\frac{1}{2}}) \tag{14}$$

$$E^{r}_{\frac{1}{2}} = E^{0} - \frac{RT}{nF}\ln\left(\frac{f_R}{f_O}\right)\left(\frac{D_O}{D_R}\right)^{\frac{1}{2}} \tag{15}$$

$$D = D_O^{\beta} D_R^{\alpha} \tag{16}$$

$$f = f_O^{\beta} f_R^{\alpha} \tag{17}$$

$$\beta = 1-\alpha \tag{18}$$

$$g = k/\omega \tag{19}$$

$$k = k_1 + k_2 \tag{20}$$

$$K = k_1/k_2 \tag{21}$$

This set of relationships accounts for the influence on the a.c. polarographic response of three rate processes: diffusion, heterogeneous charge transfer and the coupled chemical reaction. The only restrictions imposed on the relevant kinetic parameters are that $kt \geqq 10$ and $D_R = D_Y$[32]. Both restrictions are of negligible significance for most situations.

The physical significance of various terms in eqn. (1) is readily recognized, as discussed previously[16,17]. Briefly, the $I_{rev.}$-term represents the amplitude of the purely diffusion-controlled a.c. polarographic current (chemical reaction non-existent). The $F(t)$-term is responsive to effects of heterogeneous charge transfer kinetics and/or the kinetic–thermodynamic effects of the homogeneous chemical reaction on the *d.c. process*. The $G(\omega)$-term is responsive to the same effects on the *a.c. process*.

The potential-dependent parameter in the foregoing formulation, j, refers the applied d.c. potential, $E_{d.c.}$, to the quantity $E^{r}_{\frac{1}{2}}$ which is the reversible (diffusion-controlled) d.c. polarographic half-wave potential in *absence* of the following chemical reaction. However, $E^{r}_{\frac{1}{2}}$ usually is not the best reference potential choice for systems with following chemical reactions, particularly when the equilibrium constant, K, is small and the chemical reaction is reasonably close to equilibrium in the d.c. sense.

For the latter situation, the a.c. polarographic wave is usually located at potentials far-removed from $E^{r}_{\frac{1}{2}}$. For systems with reversible following chemical reactions a more rational choice of potential-dependent parameter would refer the applied d.c. potential to the reversible d.c. polarographic half-wave potential in the presence of the chemical equilibrium. The relevant half-wave potential is[36]

$$E^{rc}_{\frac{1}{2}} = E^{r}_{\frac{1}{2}} + \frac{RT}{nF} \ln\left(\frac{1+K}{K}\right) \tag{22}$$

so that the desired potential-dependent quantity is

$$J = \frac{nF}{RT}\left[E_{d.c.} - E^{r}_{\frac{1}{2}} - \frac{RT}{nF} \ln\left(\frac{1+K}{K}\right)\right]. \tag{23}$$

One can readily reformulate the above theoretical expressions for the a.c. polarographic wave in terms of the parameter, J. One obtains

$$I(\omega t) = I_{J,rev.} F_J(t) G_J(\omega) \sin(\omega t + \Phi_J) \tag{24}$$

where

$$I_{J,rev.} = \frac{n^2F^2AC^*_O(\omega D_O)^{\frac{1}{2}}\Delta E}{4RT \cosh^2\left(\frac{J}{2}\right)} \tag{25}$$

$$F_J(t) = 1 + [(\gamma_f - \beta)e^{-J} - \beta]\frac{\psi(\xi)}{\gamma_f} \tag{26}$$

$$G_J(\omega) = \left[\frac{2}{V_J^2 + U_J^2}\right]^{\frac{1}{2}} \tag{27}$$

$$V_J = \frac{\sqrt{2\omega}}{\lambda_f} + \frac{K^{-1}}{(1+e^{-J})}\left[\frac{(1+g^2)^{\frac{1}{2}}+g}{1+g^2}\right]^{\frac{1}{2}} + 1 \tag{28}$$

$$U_J = \frac{K^{-1}}{(1+e^{-J})}\left[\frac{(1+g^2)^{\frac{1}{2}}-g}{1+g^2}\right]^{\frac{1}{2}} + 1 \tag{29}$$

$$\cot \Phi_J = \frac{V_J}{U_J}. \tag{30}$$

The quantities λ_f and γ_f (eqns. (9) and (10)) in terms of the parameter, J, are

$$\gamma_f = 1 + \frac{\lambda_f}{(1+e^{-J})Kk^{\frac{1}{2}}} \tag{31}$$

$$\lambda_f = \frac{k_s f\left(\frac{K}{1+K}\right)^{\alpha}}{D^{\frac{1}{2}}}(e^{-\alpha J} + e^{\beta J}) \tag{32}$$

and all other quantities are the same as above.

Both formulations of the a.c. polarographic wave are valid for $kt > 10$ and

either may be preferred, depending on the system under study. The theoretical expression in terms of j is preferred whenever the equilibrium constant is moderately large ($K > 0.5$, approx.) and/or when the chemical kinetics are relatively slow ($kt < 50$, approx.)—*i.e.*, whenever the d.c. and a.c. waves are located in the vicinity of $E^{r}_{\frac{1}{2}}$. The equations given in terms of J are most useful with fast kinetics and small equilibrium constants—*i.e.*, when the waves are far removed from $E^{r}_{\frac{1}{2}}$, but close to $E^{rc}_{\frac{1}{2}}$.

It should be recognized that under special circumstances other choices of potential-dependent parameter may be preferred as, for example, the parameter δ given by

$$\delta = \frac{nF}{RT}\left\{E_{d.c.} - E^{r}_{\frac{1}{2}} - \frac{RT}{nF}\ln\left[1.349(kt)^{\frac{1}{2}}\right]\right\} \tag{33}$$

which has been previously shown to be the most rational choice with totally irreversible chemical reactions[37].

Special cases and simplifications

By accounting for kinetic contributions of three rate processes, diffusion, heterogeneous charge transfer and the coupled homogeneous chemical reaction, the foregoing general solution assumes a somewhat cumbersome form. A number of special cases can be envisioned where the general solution is notably simplified because one or two of these rate processes are kinetically unimportant. The number of possibilities is rather large, particularly if one recognizes that the a.c. polarographic response manifests kinetic effects on two time scales: that attending the d.c. perturbation (drop life) and that of the a.c. perturbation (period of applied alternating potential). Thus, one can distinguish between the cases where a particular rate process is kinetically unimportant only in the d.c. time scale, only in the a.c. time scale, or in both time scales.

The cases where the homogeneous chemical reaction is thermodynamically inoperative ($K \gg 1$) and kinetically inoperative ($k \rightarrow 0$) have already been discussed[32] where it was shown that the theoretical expressions will reduce to those for the simple quasi-reversible case (rate control by diffusion and heterogeneous charge transfer only).

Table 1 lists other important mathematical conditions which allow simplification of the general theory, together with the physical significance of these conditions. With the aid of these relationships and algebraic manipulation, the general theory given above can be easily reduced to the simplified formulations appropriate to each special situation. Of course, combinations of these simplifying conditions may be invoked when appropriate. For example, systems characterized by an irreversible chemical reaction (Condition 5 of Table 1) in combination with Nernstian behavior (Conditions 3 and 4) may be encountered frequently. When one considers the possible combinations of the simplifying assumptions of Table 1 which can be envisioned as definite possibilities in experimental work, it becomes apparent that the number of special cases represented greatly exceeds the number of individual simplifying conditions listed. It also should be recognized that the validity of certain conditions listed in Table 1 automatically validates a second condition. For example, if Nernstian conditions prevail in the a.c. sense (Condition 4), this demands the existence of Nernstian conditions in the d.c. sense (Condition 3). The converse is not true, however.

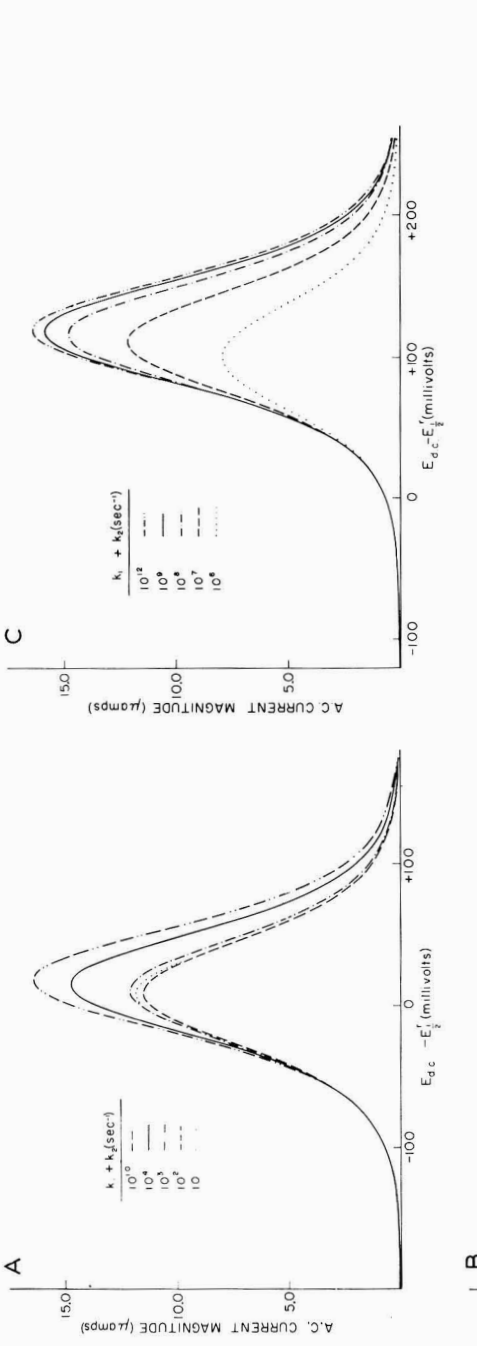

Fig. 1. Fundamental harmonic a.c. polarograms with Nernstian behavior. Parameter values: $n=1$, $T=298°K$, $A=0.035$ cm^2, $\Delta E=5.00$ mV, $C_O^*=1.00\cdot10^{-3}$ M, $D_O=D_R=1.00\cdot10^{-5}$ cm^2 sec^{-1}, $k_s=\infty$, $\omega=1.00\cdot10^3$ sec^{-1}, $f=1$. k-Values (k_1+k_2 in sec^{-1}) shown in the curves: (A), $K=1.00$, $t=12.0$ sec; (B), $K=0.100$, $t=6.00$ sec; (C)–(D), $K=1.00\cdot10^{-2}$, $t=6.00$ sec.

TABLE 1

Mathematical condition	*Physical significance*
(1) $\dfrac{\lambda_f}{(1+e^{-J})Kk^{\frac{1}{2}}} \ll 1$	Chemical equilibrium exists in the d.c. sense.
(2) $\dfrac{K^{-1}}{(1+e^{-J})}\left[\dfrac{(1+g^2)^{\frac{1}{2}}\pm g}{1+g^2}\right]^{\frac{1}{2}} \ll 1$	Chemical equilibrium exists in the a.c. sense.
(3) $\dfrac{\lambda_f}{(1+e^{-J})Kk^{\frac{1}{2}}} \gg 1$	Nernstian conditions (equilibrium with respect to heterogeneous charge transfer step) prevail in the d.c. sense.
(4) $\dfrac{(2\omega)^{\frac{1}{2}}}{\lambda_f} \ll 1 + \dfrac{K^{-1}}{(1+e^{-J})}\left[\dfrac{(1+g^2)^{\frac{1}{2}}+g}{1+g^2}\right]^{\frac{1}{2}}$	Nernstian conditions prevail in the a.c. sense.
(5) $1.349\,K(kt)^{\frac{1}{2}}e^{\delta} \ll 1$ (δ is given by eqn. (33))	Following chemical reaction is effectively irreversible —*i.e.*, one may assume $K=0$.
(6) $\left[\dfrac{(1+g^2)^{\frac{1}{2}}-g}{1+g^2}\right]^{\frac{1}{2}} \cong 0$ and $\left[\dfrac{(1+g^2)^{\frac{1}{2}}+g}{1+g^2}\right]^{\frac{1}{2}} \cong \left(\dfrac{2}{g}\right)^{\frac{1}{2}}$	Chemical reaction rate constant greatly exceeds applied angular frequency—*i.e.*, $k \gg \omega$
(7) $\left[\dfrac{(1+g^2)^{\frac{1}{2}}\pm g}{1+g^2}\right]^{\frac{1}{2}} \cong 1$	Chemical reaction rate is much smaller than applied angular frequency so that the chemical reaction is kinetically inoperative in the a.c. sense—*i.e.*, $k \ll \omega$

RESULTS AND DISCUSSION

An extensive investigation of the predictions of the foregoing theory has been carried out. All calculations utilized the general relationships of eqns. (1)–(21). A Control Data Corporation Model 3400 digital computer was the main computational aid. Computer readout was provided in an analog form with the aid of a Calcomp Model 565 digital incremental plotter, as well as in the usual digital form. The Fortran program used for this purpose is available on request.

A sampling of the calculational results is illustrated in Fig. 1–13. Because the phase angle response has been illustrated and discussed in moderate detail previously[16,17], emphasis is placed on the current amplitude response. Nevertheless, some phase angle predictions are given for reference, as the relation between the amplitude and phase response is of interest. The k_s-values were widely varied so that the calculations encompassed both equilibrium (Nernstian) and non-equilibrium (non-Nernstian) conditions with regard to the heterogeneous charge transfer step.

(*a*) *Nernstian conditions*

The case where k_s is sufficiently large that Nernstian conditions prevail in both the a.c. and d.c. sense warrants special consideration for several reasons. First, such circumstances are expected to occur frequently in experimental investigations, particularly at lower frequencies. Second, this situation represents an ideal case to

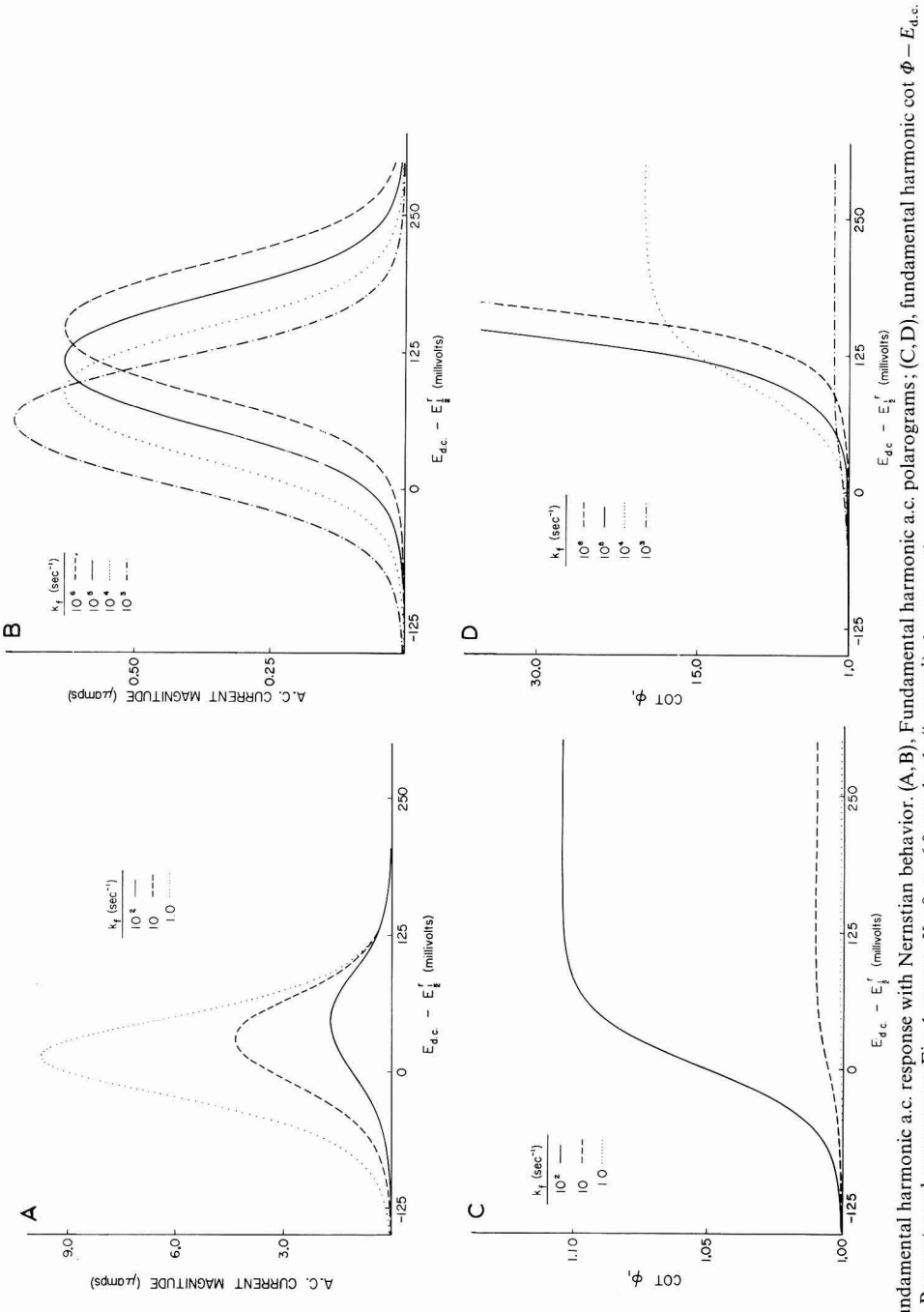

Fig. 2. Fundamental harmonic a.c. response with Nernstian behavior. (A,B), Fundamental harmonic a.c. polarograms; (C,D), fundamental harmonic cot $\Phi - E_{d.c.}$ response. Parameter values: same as Fig. 1 except, $K = 0$, $t = 6.0$ sec, $k \equiv k_f$ (in sec^{-1}) shown on the curves.

the kineticist interested primarily in the homogeneous chemical reaction rate. Only the chemical reaction and diffusion are rate-determining and a notable simplification of the mathematical formulation results which facilitates data analysis. Finally, the predicted effects of the homogeneous chemical reaction on the a.c. wave are more readily recognized when the wave is uncomplicated by charge transfer kinetic effects.

Figure 1 illustrates some typical predictions for systems characterized by reversible following chemical reactions and Nernstian conditions. The curves show the variation in the a.c. polarographic wave characteristics as the rate parameter, k, is varied for three values of the equilibrium constant, K. All other relevant parameters are held constant and are of typical magnitude. One sees that as the rate of the chemical reaction increases, the a.c. wave height first decreases from its diffusion-controlled limit for $k=0$ (curve not shown), passes through a minimum and increases again, eventually achieving the diffusion-controlled limit corresponding to the state where the chemical reaction is at equilibrium in the a.c. and d.c. sense (see Conditions 1 and 2 of Table 1). The waves for the largest k-values in each of the three sets of curves ($K=1$, 0.1, 0.01) represent this diffusion-controlled limit. The diffusion-controlled wave for $k=0$ is not shown, but is identical with the waves for the largest k's in magnitude and shape, and is centered about the potential, $E_{\text{d.c.}}=E^{\text{r}}_{\frac{1}{2}}$. The initial decrease in wave magnitude as k increases manifests the onset of rate control by the following chemical reaction. The effect first appears only in the d.c. responsive term, $F_J(t)$ (*i.e.*, $F_J(t)$ deviates from unity), but as k increases the chemical effect eventually appears in the a.c. term, $G_J(\omega)$. With increasing k the wave magnitude continues to decrease owing to increased rate of chemical removal of electroactive reduced material. However, increasing k also permits a closer approach to chemical equilibrium, an effect which tends to oppose the wave attenuation. Thus, as k becomes sufficiently large the latter becomes predominant and the wave magnitude begins to increase with k. As one would expect, the minimum a.c. polarographic wave magnitude and the k-value corresponding to this minimum depend on the magnitude of the equilibrium constant. Decreasing K decreases the minimum current magnitude and increases the k-value associated with the minimum. This simply illustrates the obvious principle that with smaller K-values, the reduced form concentration resulting from the electrode reaction is farther removed from the chemical equilibrium state so that kinetic effects of the chemical reaction are accentuated. For example, in Fig. 1A where $K=1$, the minimum a.c. polarographic peak magnitude is about 70% of the diffusion-controlled limit and is found for a k-value of about $10^2\ \text{sec}^{-1}$. Reducing K to 0.01 (Fig. 1C, and D) changes these values to about 8% and $10^3\ \text{sec}^{-1}$, respectively. In the limit of a totally irreversible chemical reaction ($K=0$) with Nernstian behavior, where an approach to chemical equilibrium is precluded, a minimum in the wave magnitude *versus* k profile is not observed. With increasing k, the wave magnitude decreases monotonically until a k-independent lower limit is realized[37] as shown in Fig. 2, A and B.

It is of interest to inquire as to the magnitude of K required to validate the assumption that the following chemical reaction is *unconditionally* irreversible—*i.e.*, the equations for $K=0$ are accurate for all conceivable values of the rate parameter, k. For the Nernstian situation under consideration, the appropriate K-value is readily estimated on the basis of Condition 5 of Table 1. Based on sample calculations, it is found that, for reasonable accuracy over the entire potential range encompassed by the a.c. wave, Condition 5 is equivalent to the statement

$$K(kt)^{\frac{1}{2}} \leq 10^{-3} \tag{34}$$

We estimate the upper conceivable limit of k as of the order of $10^{12}\,\mathrm{sec}^{-1}$. This value is obtained by assuming that k is a pseudo first-order rate constant whose value is the product of a second-order rate constant which has a collision-controlled upper limit of about 10^{10}–$10^{11}\,\mathrm{l\,mole}^{-1}\,\mathrm{sec}^{-1}$ [38] and a concentration of the species reacting with the electrode product which has a generously estimated upper limit of 10–10^2 (the larger value is approachable when the reacting species is the solvent). Inserting $k=10^{12}\,\mathrm{sec}^{-1}$ and a typical t-value of 4 sec, one concludes

$$K \leqq 5\cdot 10^{-10} \tag{35}$$

Although this demands a rather small equilibrium constant, one must keep in mind that K-values fulfilling eqn. (35) allow one to assume irreversible behavior, unconditionally. If K exceeds the $5\cdot 10^{-10}$ limit, a response characteristic of an irreversible chemical reaction can still be realized provided the magnitude of k remains below the limit established by eqn. (34). Thus, for example, if $K=10^{-4}$ it is required that $k\leqq 25\ \mathrm{sec}^{-1}$ (for $t=4$ sec) for essentially irreversible behavior.

In addition to wave magnitudes, other features of Figs. 1 and 2 worth noting are the peak potentials, wave shapes and phase angles. The effect of the following chemical reaction on the peak potential causes an anodic shift, analogous to the corresponding effect on the d.c. polarographic half-wave potential. For a reversible chemical reaction, the peak potential must be found between the extremes of $E_{\mathrm{d.c.}}=E^{\mathrm{r}}_{\frac{1}{2}}$, and $E_{\mathrm{d.c.}}=E^{\mathrm{r}}_{\frac{1}{2}}+(RT/nF)\ln\{(1+K)/K\}$ where the latter value corresponds to $k\rightarrow\infty$. Thus, for such systems the magnitude of the peak potential shift relative to $E^{\mathrm{r}}_{\frac{1}{2}}$ is limited by the equilibrium constant. For an irreversible chemical reaction, the peak potential will lie between the extremes of $E_{\mathrm{d.c.}}=E^{\mathrm{r}}_{\frac{1}{2}}$ $(k\rightarrow 0)$ and

$$E_{\mathrm{d.c.}} = E^{\mathrm{r}}_{\frac{1}{2}} + \frac{RT}{nF}\ln\left[1.349\,(kt)^{\frac{1}{2}}\right] - \frac{RT}{2nF}\ln\left[1.907\,(\omega t)^{\frac{1}{2}}\right] \tag{36}$$

(for $k\rightarrow\infty$)[37]. Figures 1 and 2 show that wave symmetry is not degraded significantly by the following chemical reaction, although the width of the wave may be noticeably altered. With reversible chemical reactions the predicted width at half-height (half-width) passes through a maximum as k is varied, approaching the $90/n$ mV value characteristic of diffusion-control at the extreme limits of $k\rightarrow 0$ and $k\rightarrow\infty$. With irreversible chemical reactions the half-width increases with increasing k from the $90/n$ mV value until $k\gg\omega$ where it assumes a k-independent limit noticeably exceeding $90/n$ mV[37]. The sigmoidal character of the cot $\Phi - E_{\mathrm{d.c.}}$ profile shown in Fig. 2, C and D, represents typical phase angle behavior for Nernstian systems with following chemical reactions, regardless of whether the chemical reaction is irreversible or reversible. The most significant difference between the cases of reversible and irreversible chemical reaction lies in the variation of cot Φ with k. In general, the cot Φ magnitude at the plateau (largest cot Φ) increases monotonically with increasing k when irreversible chemical reactions are operative (Fig. 2, C and D), whereas systems with reversible chemical reactions exhibit a maximum cot Φ-value as k is varied, with a unity value (diffusion-control) characterizing the limits of $k\rightarrow 0$ and $k\rightarrow\infty$. The magnitude of this maximum cot Φ-value and the associated k-value depend on the equilibrium constant, K, in a manner very similar to systems with coupled preceding chemical reactions[39]. This similarity to the latter type of system is quite general for

the phase angle under Nernstian conditions. The major difference is that with preceding chemical reactions the cot Φ increases as $E_{d.c.}$ becomes more negative, rather than the converse as with following reactions. More quantitatively, the cot $\Phi - E_{d.c.}$ plots with following reactions and Nernstian behavior have a mirror-image correspondence about the point $E_{d.c.} = E^r_{\frac{1}{2}}$ to the corresponding plots with preceding reactions. Thus, the influence of the equilibrium constant of reversible following reactions on phase angle behavior is readily ascertained from appropriate plots for systems with preceding reactions[39].

Some aspects of the predicted frequency-dependence of a.c. wave parameters are illustrated in Figs. 3 and 4. Figure 3A shows that kinetic effects of following chemical reactions can lead to substantial deviations from the well-known linear peak current–$\omega^{\frac{1}{2}}$ response characteristic of diffusion-controlled systems. The curve for $k = 10^9$ in Fig. 3A corresponds to the latter state. Figure 3B shows how the same effects manifest themselves when the peak current (i_p) relative to the diffusion-controlled

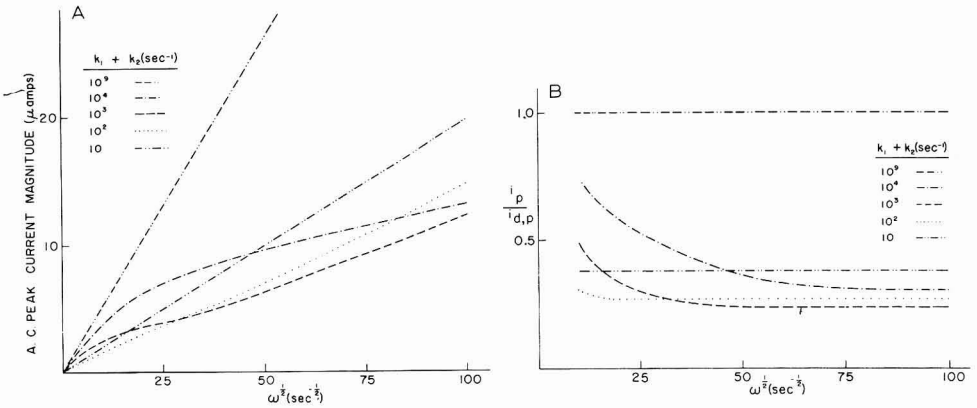

Fig. 3. Frequency-dependence of fundamental harmonic peak current with Nernstian behavior. Parameter values: same as Fig. 1 except $K = 0.100$, $t = 6.00$ sec, ω given by abscissa. k-Values ($k_1 + k_2$ in sec^{-1}) shown on curves.

peak current ($i_{d,p}$) is plotted *versus* $\omega^{\frac{1}{2}}$. The effects of K on the observables considered in Fig. 3 are not illustrated here as they are quite similar to the predictions obtained for preceding chemical reactions[39]. The general characteristics of the phase angle–frequency response also are illustrated elsewhere[16,17]. Figure 4 shows the variation of the experimental observables, $i_p/i_{d,p}$, half-width, and peak potential with the dimensionless kinetic parameter $\log(k/\omega)$ for $K = 0.1$. The curves were constructed by selecting a particular k-value and varying ω. For each k-value only those values of k/ω corresponding to experimentally realistic ω-values were considered. Thus, also established is the general range where experimental data is likely to fall in such plots with particular k-values. In addition to the obvious trends which were already qualitatively apparent in Figs. 1 and 2, one should note that predicted variations of the observables do not lie on a single continuous curve, but depend on the particular k-value in question unless k exceeds about 10^3 sec^{-1} (for $K = 0.1$). This effect arises from the above-mentioned duality in the time scale operative in the a.c. polarographic experiment.

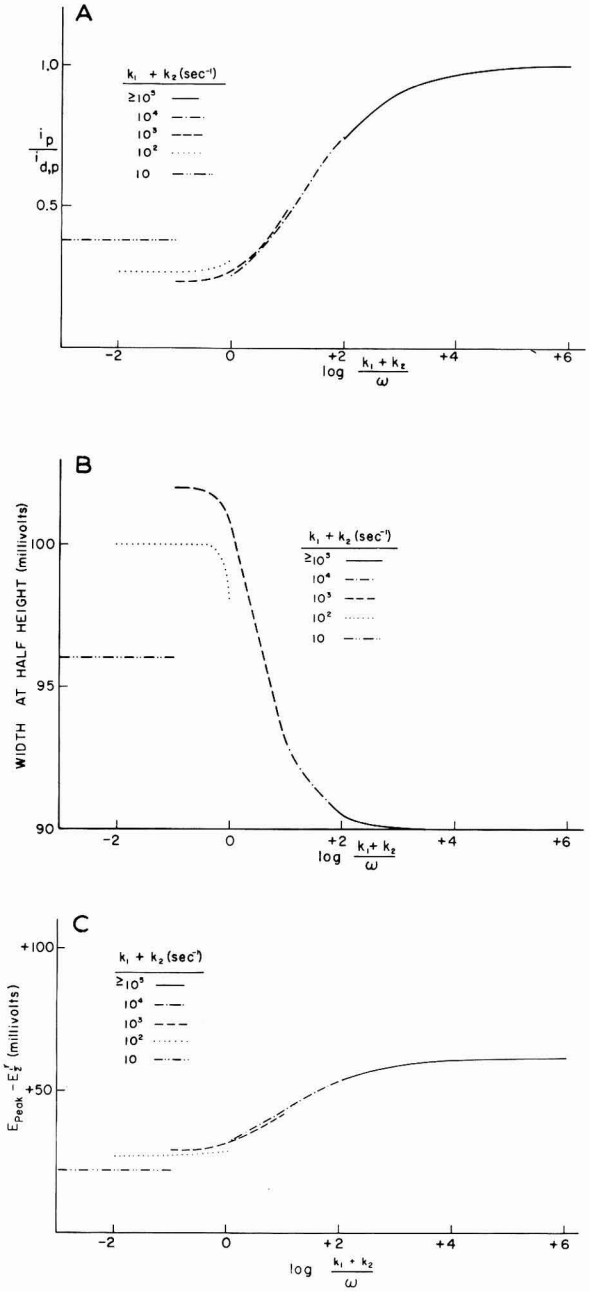

Fig. 4. Dependence of several a.c. polarographic characteristics *vs.* $\log(k/\omega)$ with Nernstian behavior. Parameter values: same as Fig. 3. $k_1 + k_2$ ($\sec^{-1}$) shown on curves.

Unless the d.c. process is diffusion-controlled, k/ω is not a unique kinetic parameter in determining the contribution of the coupled chemical reaction. Rather, k/ω shares a role with the parameter which is a measure of the d.c. chemical kinetic contributions, ξ [$\xi = (1+e^{-J})K(kt)^{\frac{1}{2}}$ with Nernstian conditions]. This has obvious implications regarding data analysis as it precludes the possibility that working curves of experimental observables *versus* a single dimensionless kinetic parameter will, in general, uniquely describe the kinetic situation for a particular K-value. It should be noted that the curves illustrated in Fig. 4 are notably more sensitive to the k-value than the corresponding curves with preceding chemical reactions[39]. On the other hand, the effect of K on such plots is similar to that obtained with preceding reactions[39].

Figures 1–4 establish the existence of rather substantial effects of following chemical reactions on various aspects of the a.c. polarographic response. It would be useful to have quantitative analytical relationships for the variation in observables such as peak height, peak potential, half-width, etc. as a function of the various kinetic parameters. Unfortunately, even with the mathematical simplifications attending Nernstian conditions, the complexity of the theoretical formulation appears to preclude the deduction of generally applicable expressions for such observables so that normally one must rely on theoretical working curves for data analysis[17,40–42]. Only in rather restricted situations are expressions of some utility obtainable for such experimental quantities. These are discussed elsewhere[37,43] and may be deduced easily by utilizing appropriate combinations of the simplifying assumptions listed in Table 1.

Another important aspect of the a.c. polarographic wave is its time-dependence (mercury drop-life dependence) which can arise whenever the d.c. surface concentration components are either in a non-equilibrium state with respect to the heterogeneous charge transfer process, coupled chemical reactions, adsorption steps[15,17,18,44,45] and/or when spherical diffusion effects are important[17,35,46]. Figure 5 illustrates some typical predictions for the drop-life dependence under Nernstian conditions where the time-dependence originates solely in the coupled chemical reaction. The most noteworthy features are the reduction in peak current magnitude and anodic shift of peak potential with increasing drop life, the negligible effect of drop life on wave symmetry and the relatively large drop-life dependence associated with small K-values. This drop-life dependence is noticeably larger in magnitude and opposite in direction to that predicted for preceding reactions[39]. Time-dependence predicted for irreversible chemical reactions is closely approximated by Fig. 5D (smallest K considered) and has been discussed previously for special circumstances[15,18,37].

(*b*) *Non-Nernstian conditions*

As one would expect, the existence of slow charge transfer kinetics can substantially alter the predicted characteristics of the a.c. polarographic response from that shown in the foregoing section. Included is a notable influence on the magnitude and nature of the contribution of the following chemical reaction. With two slow rate processes in addition to diffusion, the combination of kinetic conditions which might be considered are too numerous to allow complete presentation in the present work. However, calculational results sufficient to establish the most significant trends in the effects of slow charge transfer kinetics will be presented.

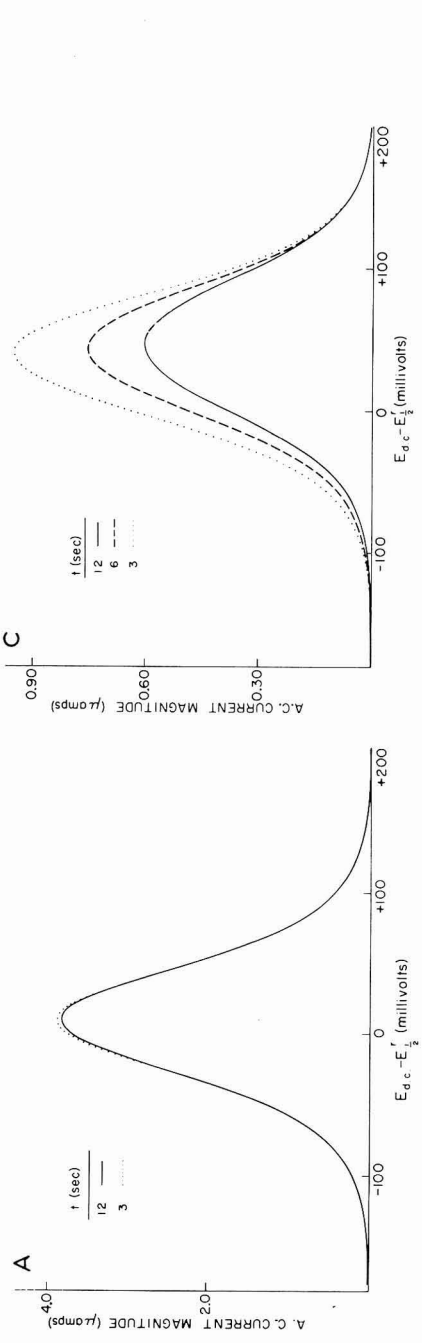

Fig. 5. Fundamental harmonic a.c. polarograms with Nernstian behavior-drop life dependence. Parameter values: same as Fig. 1 except $k = 1.00 \cdot 10^{2}$ sec^{-1}, $\omega = 1.00 \cdot 10^{2}$ sec^{-1}. t-Values shown on the curves: (A), $K = 1.00$; (B), $K = 1.00 \cdot 10^{-1}$; (C), $K = 1.00 \cdot 10^{-2}$; (D), $K = 1.00 \cdot 10^{-3}$.

Figures 6–8 illustrate some of the effects of slow charge transfer kinetics on the a.c. polarographic wave and on the attendant phase angle–d.c. potential profile. Some of the more obvious and anticipated effects are the reduction in the magnitude of the wave (current amplitude), the cathodic shift in its peak potential and the substantial increase in its width. Although not always obvious from qualitative inspection, wave symmetry usually is significantly degraded, particularly when $k_s < 10^{-2}$ cm sec^{-1}. The most readily apparent manifestation of charge transfer kinetic effects on the phase angle response is the tendency toward an asymmetric peak-shaped profile in the cot Φ–$E_{d.c.}$ plot as k_s is decreased, rather than the sigmoidal behavior characterizing Nernstian conditions.

Some of the interactions between the heterogeneous charge transfer and following chemical reaction rate processes are readily discernible. In general, one expects that the slower the following chemical reaction, the less important the contribution of heterogeneous charge transfer kinetics, and *vice versa*. That the calculational results manifest this expectation is clearly illustrated in Figs. 6–8 (*e.g.*, compare Figs. 7A and 7B). Conversely, slow charge transfer kinetics tend to suppress the importance of the following chemical reaction. Thus, the polarograms of Figs 6–8 corresponding to the smallest k_s-values are closely approximated by those predicted from the theory for a simple quasi-reversible process[15,17]. A judicious comparison of Figs. 6 and 8 suggests that decreasing the equilibrium constant, K, of the chemical reaction tends to enhance the effects of slow charge transfer .This principle can be vividly illustrated for the extreme of very rapid chemical kinetics (chemical equilibrium), where only the diffusion and charge transfer steps are rate-controlling, by inspection of the appropriate mathematical relationships. The a.c. polarographic wave equation obtained upon assuming chemical equilibrium (apply Conditions 1 and 2 of Table 1) is formally identical with the expression for the simple quasi-reversible case[17], except for differences in the definitions of the d.c. potential-dependent parameter (J in place of j) and the parameter dependent on charge transfer and diffusion kinetics (λ_f in place of λ). Thus, whereas the parameter, k_s, determines the magnitude of the charge transfer kinetic contribution for the simple quasi-reversible case where the following chemical reaction is non-existent, the corresponding parameter with a following chemical reaction at equilibrium is $k_s[K/(1+K)]^{\alpha}$. In the latter case, reduction of the equilibrium constant K (all other parameters invariant) will reduce the magnitude of the relevant charge transfer kinetic parameter, enlarging the contributions of slow charge transfer to the a.c. polarographic response. For example, with a simple quasi-reversible system the requirement for Nernstian behavior in the a.c. sense may be written[17]

$$\frac{(2\omega)^{\frac{1}{2}}}{\lambda} \ll 1 \tag{37}$$

which implies, approximately,

$$k_s \gg (\omega D)^{\frac{1}{2}} \tag{38}$$

whereas, with a following chemical reaction at equilibrium these requirements become

$$\frac{(2\omega)^{\frac{1}{2}}}{\lambda_f} \ll 1 \tag{39}$$

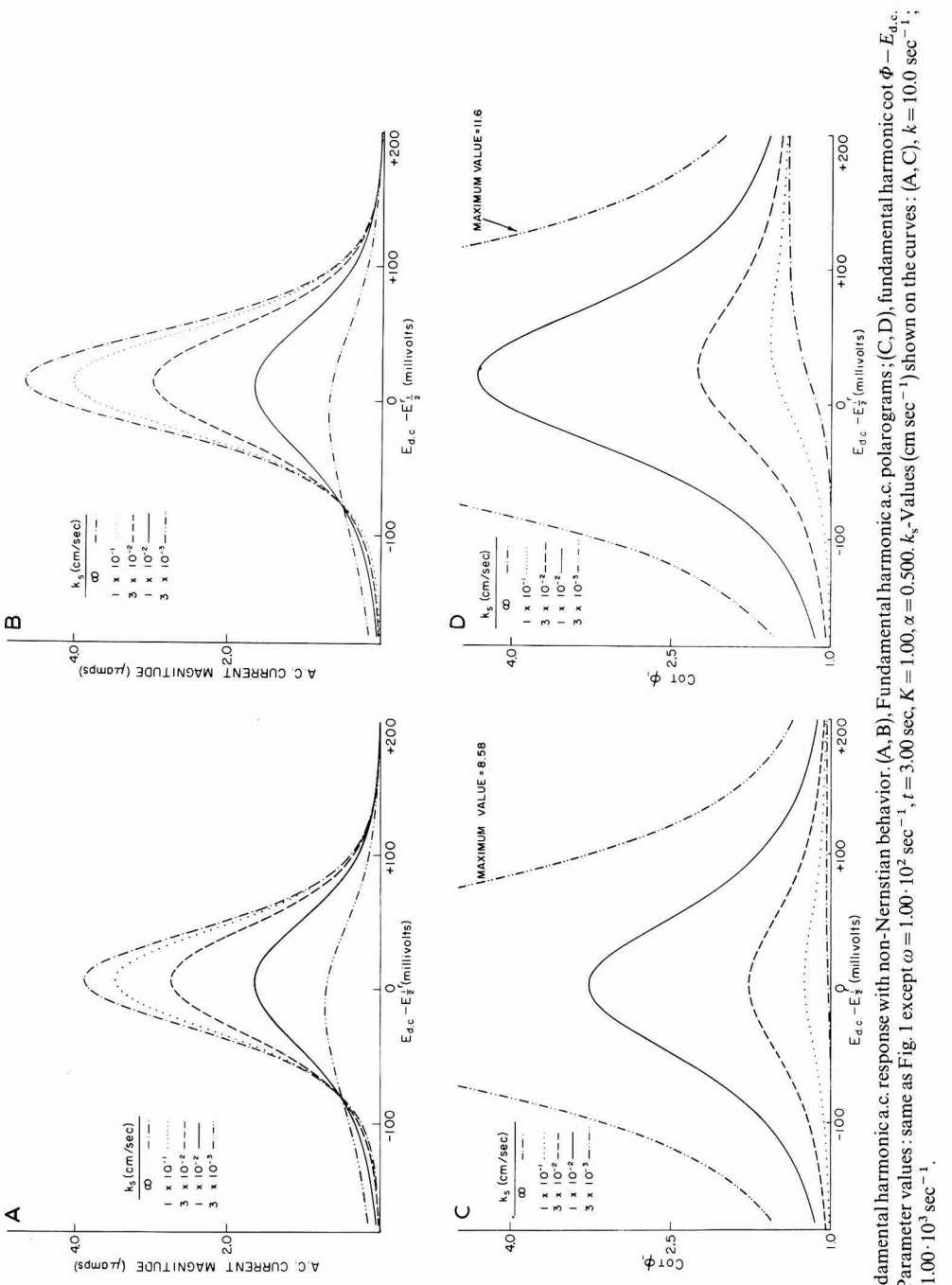

Fig. 6. Fundamental harmonic a.c. response with non-Nernstian behavior. (A, B), Fundamental harmonic a.c. polarograms; (C, D), fundamental harmonic cot $\Phi - E_{d.c.}$ response. Parameter values: same as Fig. 1 except $\omega = 1.00 \cdot 10^2$ sec^{-1}, $t = 3.00$ sec, $K = 1.00$, $\alpha = 0.500$. k_s-Values (cm sec^{-1}) shown on the curves: (A, C), $k = 10.0$ sec^{-1}; (B, D), $k = 1.00 \cdot 10^3$ sec^{-1}.

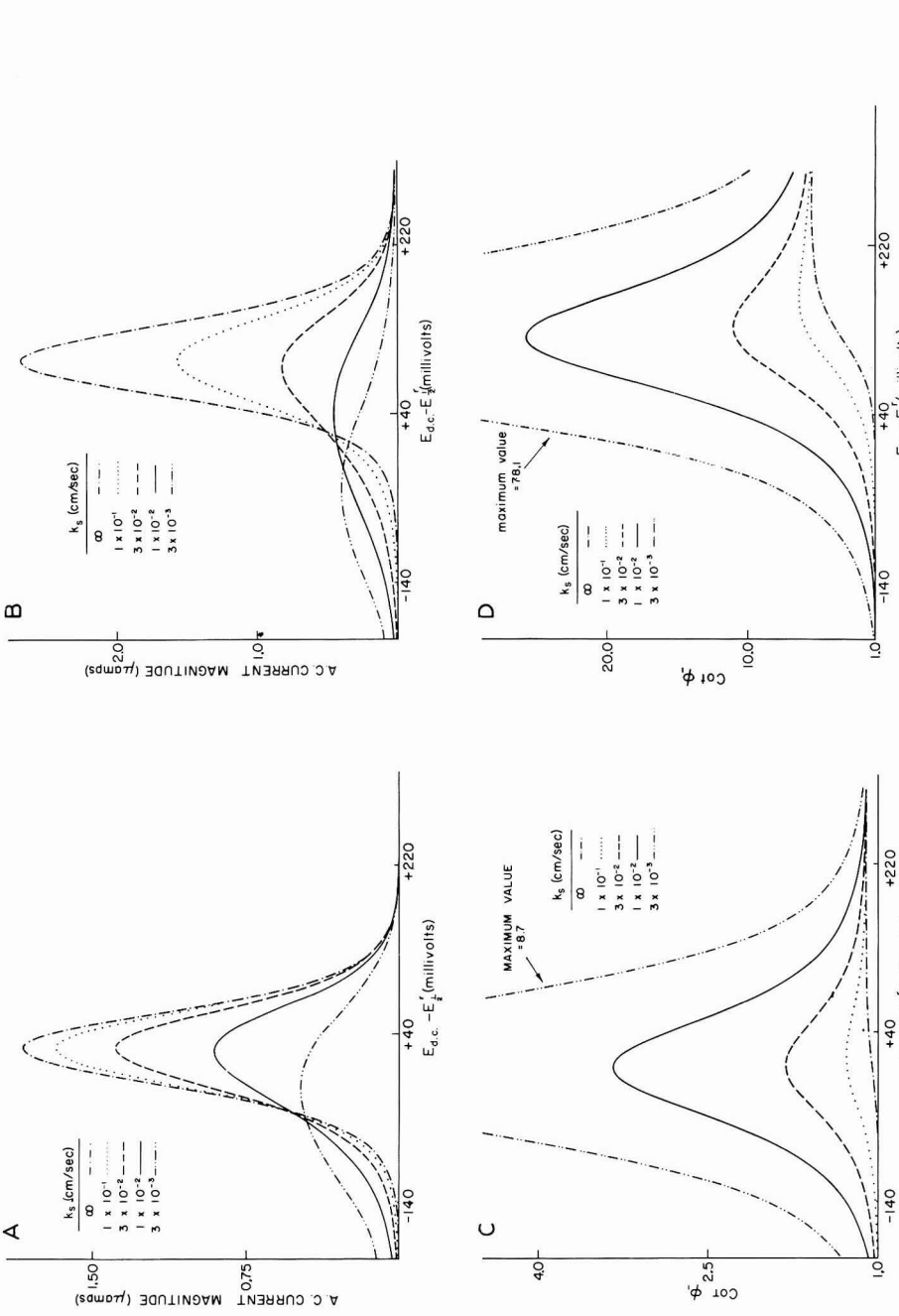

Fig. 7. Fundamental harmonic a.c. response with non-Nernstian behavior. (A, B), Fundamental harmonic a.c. polarograms; (C, D), fundamental harmonic cot $\Phi - E_{d.c.}$ response. Parameter values: same as Fig. 1 except $\omega = 1.00 \cdot 10^2\ \mathrm{sec}^{-1}$, $t = 3.00$ sec, $K = 1.00 \cdot 10^{-2}$, $\alpha = 0.500$. k_s-Values (cm sec^{-1}) shown on the curves: (A, C), $k = 10.0\ \mathrm{sec}^{-1}$; (B, D), $k = 1.00 \cdot 10^5\ \mathrm{sec}^{-1}$.

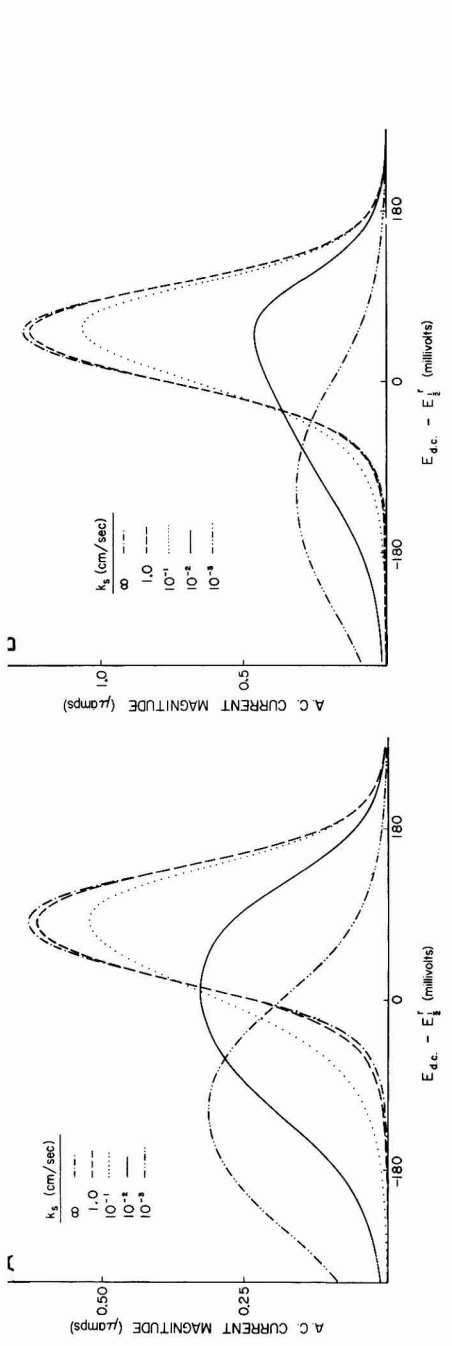

Fig. 8. Fundamental harmonic a.c. response with non-Nernstian behavior. (A, B). Fundamental harmonic a.c. polarograms; (C, D), fundamental harmonic cot $\phi - E_{d.c.}$ response. Parameter values: same as Fig. 1 except $t = 6.00$ sec, $K = 0$, $\alpha = 0.500$. k_s-Values (cm sec^{-1}) shown on the curves: (A, C), $k = 5.00 \cdot 10^3$ sec^{-1}; (B, D), $k = 2.00 \cdot 10^2$ sec^{-1}.

or

$$k_s\left(\frac{K}{1+K}\right)^{\alpha} \gg (\omega D)^{\frac{1}{2}} . \tag{40}$$

Clearly, the latter condition demands a larger value of k_s than that of eqn. (38). For example, with $\alpha=0.5$ and $K \ll 1$, a factor of 100 decrease in K increases by an order of magnitude the k_s-value required for Nernstian behavior. As the rate of the chemical reaction is decreased, the demands on the k_s-value for Nernstian behavior are reduced, approaching the value required by eqn. (38) as $k \rightarrow 0$. This effect of the following chemical reaction equilibrium state arises partly from its influence on the surface concentration term for the reduced form in the rate expression for heterogeneous charge transfer. In addition, because the chemical reaction shifts the position of the a.c. wave, it also influences the magnitudes of the potential-dependent terms in the heterogeneous rate law. These results establish that requirements for Nernstian behavior depend intimately on the status of the following chemical reaction.

Figure 9 illustrates effects of slow charge transfer on the frequency response of the peak current magnitude. It is seen that the importance of charge transfer kinetics is enhanced considerably by increasing frequency and that this effect leads to a frequency-independent limiting value at high frequency. With strictly Nernstian behavior the high frequency case corresponds to a linear peak current–$\omega^{\frac{1}{2}}$ plot (Fig. 3). Again, the magnitude and nature of the charge transfer kinetic contribution to the frequency response depends on the following chemical reaction rate parameters and *vice versa*. Earlier work[16-18] may be consulted for the effect of k_s on cot Φ–$\omega^{\frac{1}{2}}$ behavior.

When charge transfer kinetics are slow enough that non-Nernstian conditions prevail in the d.c. sense, then this rate process can substantially influence the predicted drop-life dependence of the a.c. polarographic wave. Some results are shown in Figs. 10 and 11. Although usually difficultly discernible, a cross-over point[44] (change in direction of drop-life dependence) is predicted for the drop-life dependence of the current magnitude *versus* $E_{d.c.}$ under appropriate conditions (Fig. 10D). This contrasts to the negative drop-life dependence (decreasing drop life increases current) at all potentials characterizing Nernstian systems (Fig. 5). The potential of the cross-over point is difficult to express in a simple analytical form, except in special circumstances. For example, for $\alpha=0.5$, one can easily show that the cross-over point occurs at the d.c. potential, $E^*_{d.c.}$ given by

$$E^*_{d.c.} = E^{rc}_{\frac{1}{2}} + \frac{2RT}{nF} \sinh^{-1}(H) \tag{41}$$

where

$$H = \frac{k_s f\left(\frac{K}{1+K}\right)^{\frac{1}{2}}}{K(kD)^{\frac{1}{2}}} \tag{42}$$

Equation (41) predicts that the cross-over point shifts anodically as the kinetic effects of the following chemical reaction become more important, relative to charge transfer kinetics (increasing H), a fact evident in Fig. 10 and in calculational results for α-values other than 0.5. Slow charge transfer may also introduce a marked dependence of wave symmetry on drop life, in contrast to the Nernstian case. This is most readily seen in

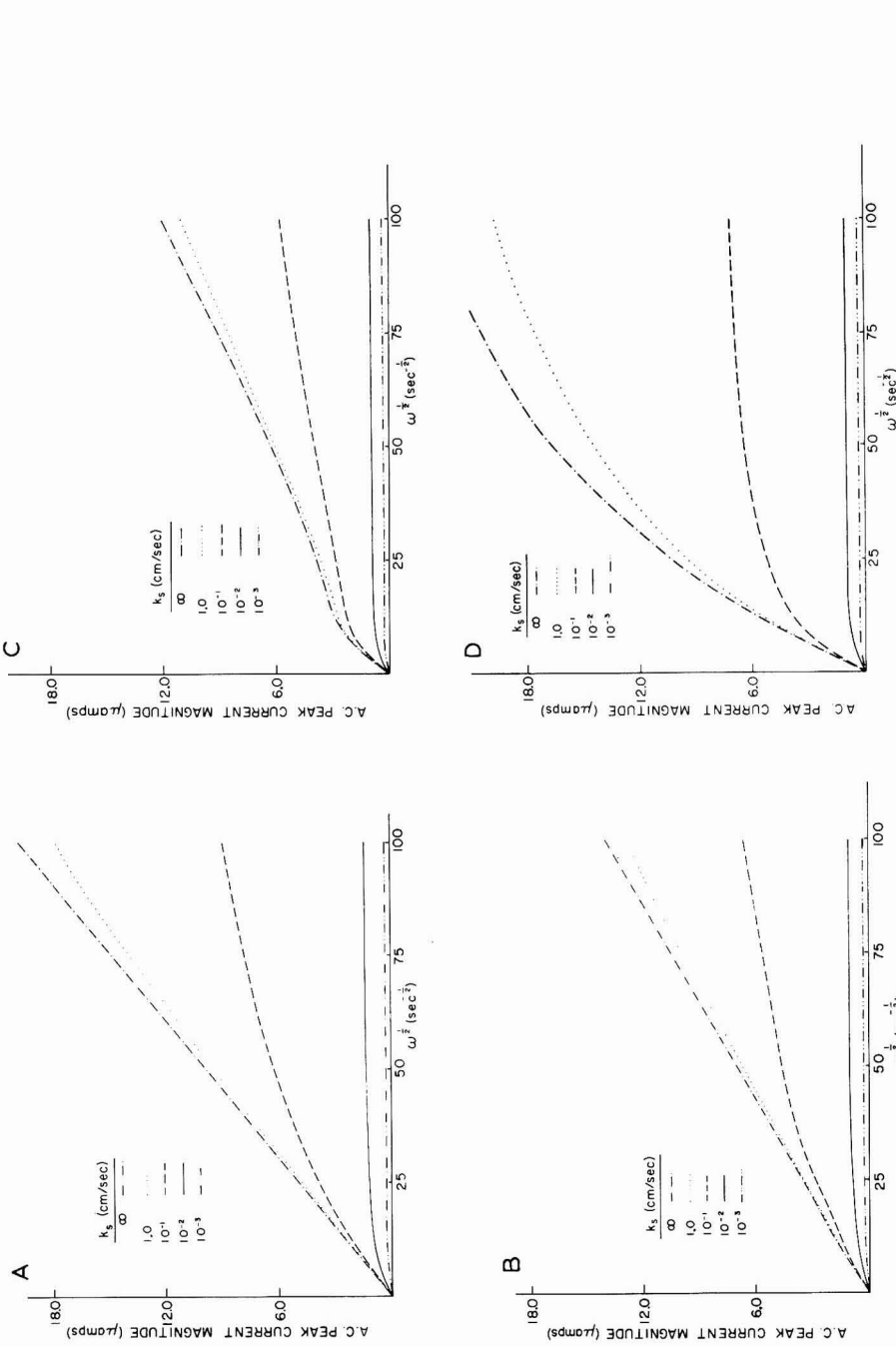

Fig. 9. Frequency dependence of fundamental harmonic peak current with non-Nernstian behavior. Parameter values: same as Fig. 1 except $K = 0.100$, $t = 6.00$ sec, ω given by abscissa, $\alpha = 0.500$. k_s-Values (cm sec^{-1}) shown on the curves: (A), $k = 10.0$ sec^{-1}; (B), $k = 100$ sec^{-1}; (C), $k = 1.00 \cdot 10^{-3}$ sec^{-1}; (D), $k = 1.00 \cdot 10^{5}$ sec^{-1}.

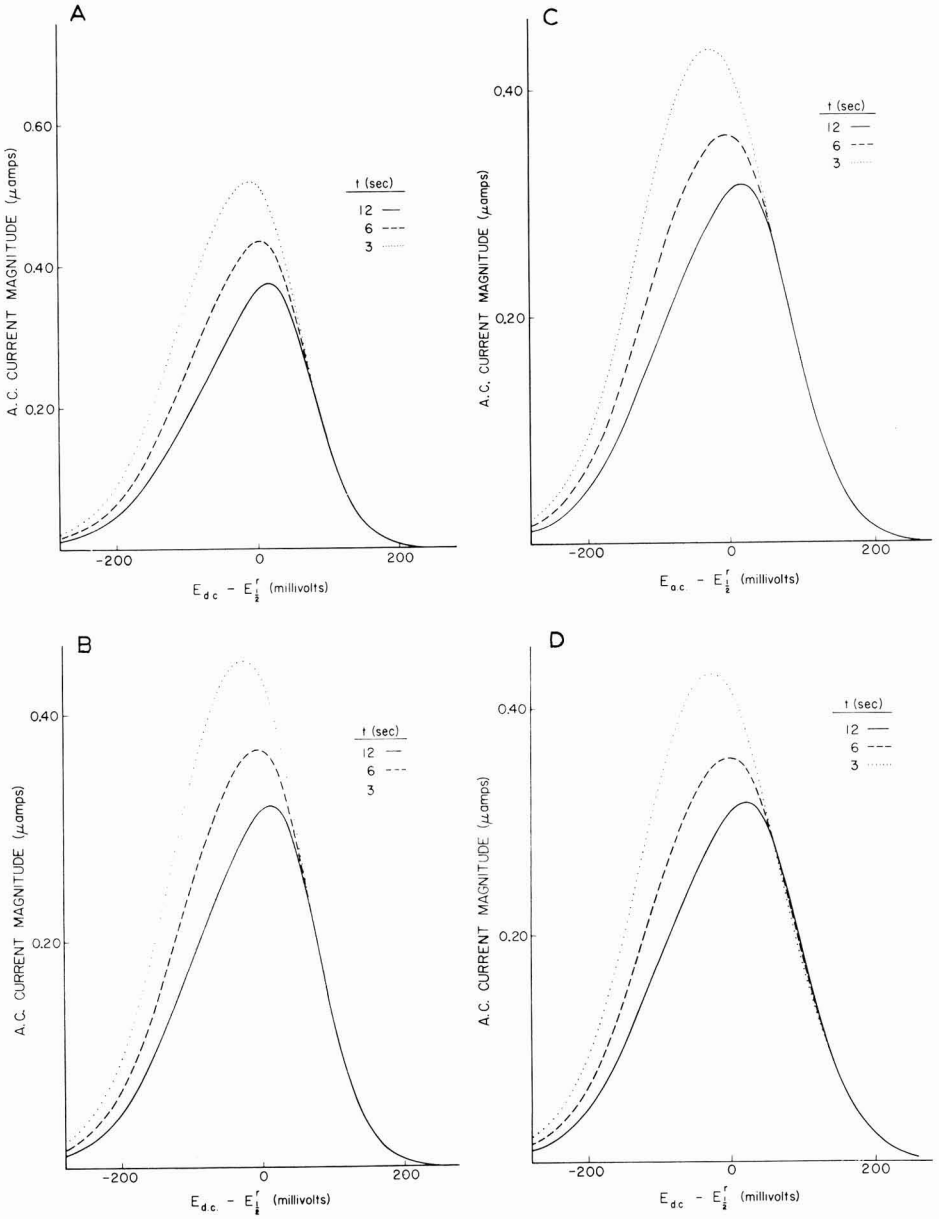

Fig. 10. Fundamental harmonic a.c. polarograms with non-Nernstian behavior-drop life dependence. Parameter values: same as Fig. 1 except $K = 0.100$, $k_s = 3.00 \cdot 10^{-3}$ cm sec^{-1}, $\omega = 1.00 \cdot 10^{2}$ sec^{-1}, $\alpha = 0.500$. t-Values (sec) shown on the curves: (A), $k = 10.0$ sec^{-1}; (B), $k = 100$ sec^{-1}; (C), $k = 1.00 \cdot 10^{3}$ sec^{-1}; (D), $k = 1.00 \cdot 10^{8}$ sec^{-1}.

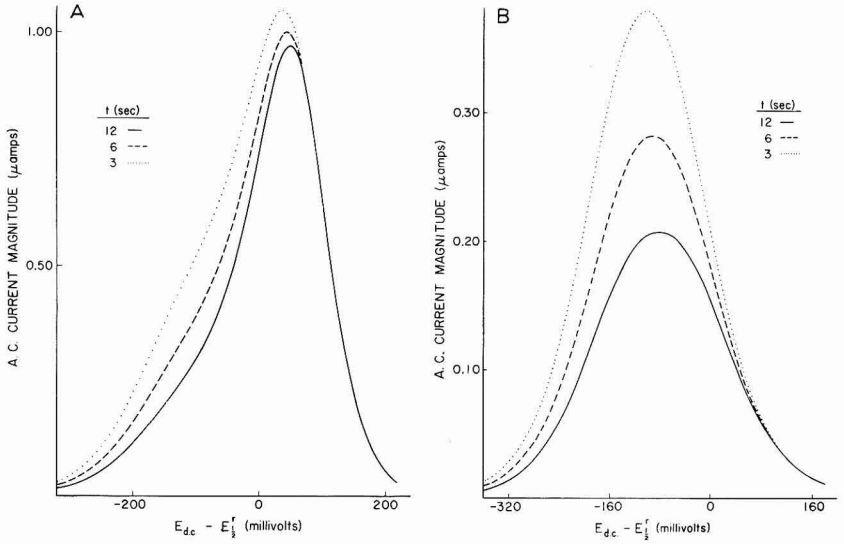

Fig. 11. Fundamental harmonic a.c. polarograms with non-Nernstian behavior-drop life dependence. Parameter values: same as Fig. 1 except (A), $K=0.100$, $\omega=1.00\cdot10^{4}$ sec^{-1}, $k_s=1.00\cdot10^{-2}$ cm sec^{-1}, $k=1.00\cdot10^{3}$ sec^{-1}, $\alpha=0.500$; (B), $K=1.00\cdot10^{-2}$, $\omega=1.00\cdot10^{2}$ sec^{-1}, $k_s=1.00\cdot10^{-3}$ cm sec^{-1}, $k=1.00\cdot10^{10}$ sec^{-1}, $\alpha=0.500$. t-Values (sec) shown on the curves.

Fig. 11A. A comparison of Figs. 11A and 11B shows that the general characteristics of the predicted drop life effect can vary considerably, depending on the kinetic situation. Note the relatively small drop-life dependence of the peak current in Fig. 11A in contrast to the rather large effect in Fig. 11B.

(*c*) *Data analysis*

Quantitative evaluation of data obtained from systems characterized by following chemical reactions using the foregoing theoretical formulation varies in complexity depending on the kinetic situation. Although not always the simplest, judicious use of theoretical working curves appears to be the most generally applicable approach. Accordingly, this method will be given emphasis.

Probably the simplest situation arises when an irreversible chemical reaction exists in combination with Nernstian conditions. In such cases, the forward chemical reaction rate constant is the only unknown rate parameter, other than the diffusion coefficient which is readily evaluated from the limiting d.c. polarographic current. As Aylward *et al.*[13-15] have already shown, if these circumstances are combined with $k \ll \omega$, the a.c. polarographic peak current is expressible in terms of a single dimensionless chemical rate parameter, kt. Thus, a single working curve of $i_p/i_{d,p}$ *vs.* kt suffices, provided the foregoing conditions apply. Experimental measurements of $i_p/i_{d,p}$ are then easily related to the chemical rate constant through the working curve. Figure 12 illustrates three such theoretical working curves, each calculated with the aid of a different theoretical model for the d.c. process. The importance of accurately accounting for effects of drop growth is evident. If the value of $E_{\frac{1}{2}}^{r}$ is known, another very convenient data analysis approach, which does not demand that $k \ll \omega$, may be

formulated from phase angle measurements. For irreversible chemical reactions and Nernstian conditions, cot Φ at any particular d.c. potential is determined uniquely by the parameter, g. Knowledge of $E^{r}_{\frac{1}{2}}$ allows one to calculate a working curve of cot Φ *vs.* g for a convenient $E_{d.c.}$-value, from which the chemical rate constant is obtainable using experimental cot Φ measurements at a known frequency. Lacking the simpli-

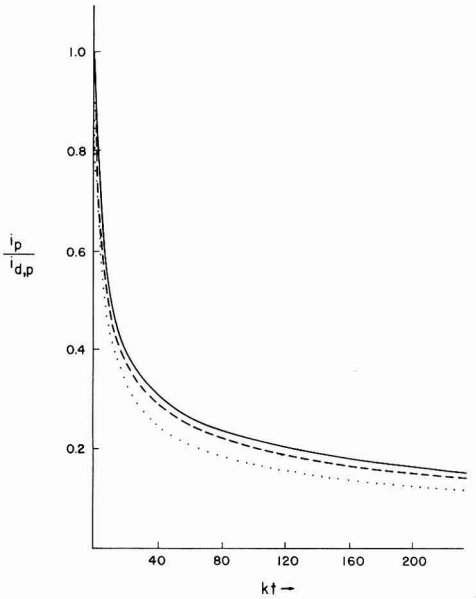

Fig. 12. Working curve of $i_p/i_{d,p}$ *vs.* kt for irreversible following reaction, Nernstian behavior and $k \ll \omega$. (———), Present theory; (– – –), Aylward, Hayes, Tamamushi theory[15]; (· · · · · ·), stationary plane theory.

fications attending $k \ll \omega$ or knowledge of $E^{r}_{\frac{1}{2}}$ is not serious for the case under consideration as some rather effective approaches of greater generality are evident. Among the most appealing is one based on the relationship

$$I(\omega t) = \frac{nF\Delta E\, i_{d.c.}(t) g^{-\frac{1}{2}}}{RT(1+e^{-j})}\, G(\omega) \sin(\omega t + \varphi) \tag{43}$$

which is obtained from the general theory by invoking the assumptions of Nernstian behavior and irreversibility for the chemical step, inserting the expression relating $\psi(\xi)$ to the direct current $i_{d.c.}(t)$ for Mechanism R1 with $K=0$[47], and rearranging. This relationship shows that the experimental observable consisting of the ratio of fundamental harmonic a.c. polarographic current over the d.c. polarographic current times $(nF\Delta E/RT)$ is simply a function of g and the d.c. potential-dependent parameter, j. From eqn. (43) one can construct a series of working curves of

$$\frac{I(\omega t)}{(nF\Delta E/RT) i_{d.c.}(t)}$$

vs. $E_{d.c.} - E^{r}_{\frac{1}{2}}$, each corresponding to a different g-value. Figure 13 illustrates such a

set of working curves. The theoretical working curve best matching the shape of the corresponding experimental plot with an abscissa of $E_{d.c.}$ provides the k-value. The position of the experimental data on the working curve abscissa which yields the best agreement between theory and experiment provides the $E^r_{\frac{1}{2}}$-value. Because cot Φ also depends only on g and j, an identical procedure may be adopted for obtaining k and $E^r_{\frac{1}{2}}$ from cot Φ measurements—*e.g.*, construct and employ a set of working curves of cot Φ *vs.* $E_{d.c.} - E^r_{\frac{1}{2}}$ for different g-values (see Fig. 2, C and D). Although the foregoing methods should suffice for systems with irreversible chemical reactions and Nernstian charge transfer, some alternative procedures are worth mentioning as they might prove useful for confirming rate constants obtained from the above approaches and they are important for the analysis of more complex systems. At a particular frequency and drop life, the peak alternating current dependence on k is described by a single working curve of $i_p/i_{d.p}$ *vs.* k. Similarly, the cot Φ-value at the potential of

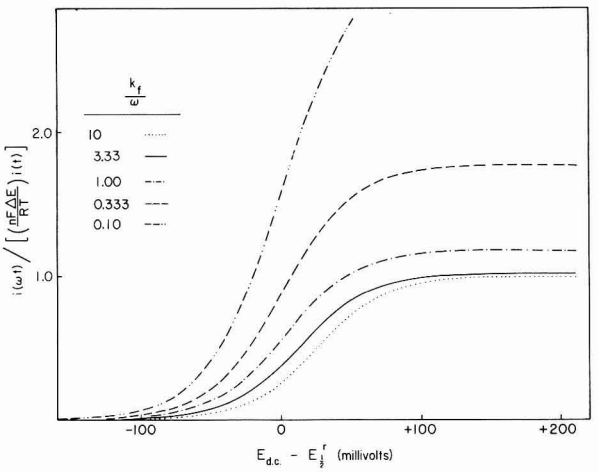

Fig. 13. Working curve of $I(\omega t)/[nF\Delta E/RT)i_{d.c.}(t)]$ for irreversible following reaction and Nernstian behavior. k_f/ω-Values shown on the curves.

the peak alternating current is defined by a single working curve of cot Φ *vs.* k for any particular combination of ω and t. Thus, the peak current and associated phase angle of an a.c. polarogram may be used to obtain the chemical rate constant by constructing such working curves for the appropriate ω- and t-values. Obviously such experiments should be repeated at various ω- and t-values to assess the self-consistency of the calculated k-values. From k-values thus obtained, one can calculate $E^r_{\frac{1}{2}}$ from the theoretical value of $E_{d.c.} - E^r_{\frac{1}{2}}$ at the wave peak, or from the d.c. polarographic half-wave potential using the Koutecky equation[48]

$$E^{rI}_{\frac{1}{2}} = E^r_{\frac{1}{2}} + \frac{RT}{nF} \ln \left[1.349(kt)^{\frac{1}{2}}\right] \tag{44}$$

The added unknown parameter, K, attending the existence of a reversible chemical reaction does not complicate data analysis significantly if Nernstian conditions prevail. In such circumstances a number of procedures are potentially appli-

cable. Frequently, the equilibrium constant is known or obtainable from independent, non-electrochemical means. Sometimes it is readily calculated from electrochemical measurements such as cell potential data, d.c. polarographic half-wave potentials or a.c. polarographic peak potentials at low frequencies where fast chemical reactions yield reversible behavior. In any such situation where K is obtainable by simple means, its value then may be inserted in the theoretical current amplitude and phase angle relationships, and data analysis procedures analogous to those just described for irreversible chemical reactions may be invoked. If K is unknown, one may employ an extension of the procedure described above involving the use of working curves of peak current ($i_p/i_{d,p}$) and the associated cot Φ-value *vs.* k at a particular $\omega - t$ combination. With reversible chemical reactions a set of working curves corresponding to different K-values must be constructed for each observable. The intersection of the experimental value of peak current with each working curve of peak current *versus* k in the set defines a curve of K *vs.* k. A second K *vs.* k curve is generated by the same operation with the cot Φ-value. The intersection of these two K *vs.* k curves corresponds to the correct values of K and k from which one can then calculate $E^r_{\frac{1}{2}}$ using the peak potential measurement. Repetition of this procedure with different combinations of ω and t should establish experimental uncertainty levels. In the special case where the d.c. process is diffusion-controlled, plots such as those of Fig. 4 may be used effectively as working curves because a single unique curve is obtained for each K-value under these conditions. Thus, sets of working curves of either experimental observable considered in Fig. 4 may be compared to experimental plots of the observable *vs.* log ω^{-1}. The working curve whose shape best fits the experimental plot yields the K-value, while the difference in abscissa values of the theoretical and experimental plots which corresponds to best agreement defines the k-value.

When non-Nernstian conditions are encountered, the data analysis problem becomes substantially more complex, but the situation is by no means intractable. The key to conveniently handling non-Nernstian systems lies in first finding conditions of frequency or d.c. potential where chemical kinetic effects are unimportant, and evaluating the charge transfer rate parameters. This knowledge of k_s and α then allows evaluation of the chemical kinetic parameters using data obtained under conditions where the chemical reaction is kinetically important. Data analysis routines of the type outlined above will suffice. Such ideas often can be applied when measurements are made over a reasonably wide frequency range. This may allow realization of the state where $\omega \gg k$ which validates the well-known phase angle relation

$$\cot \Phi = 1 + \frac{(2\omega)^{\frac{1}{2}}}{\lambda} \tag{45}$$

Equation (45) is the relationship followed by simple quasi-reversible systems so that established procedures may be utilized for the evaluation of k_s and α[16,17], provided $E^r_{\frac{1}{2}}$ is known (neglecting the activity correction, as usual). Once obtained, the k_s- and α-values may be substituted in the theoretical expressions leaving only k and K as unknowns. At this point, procedures such as those outlined above for Nernstian systems can be applied to evaluate k and K using data at lower frequencies where the chemical kinetic effect is important. When $E^r_{\frac{1}{2}}$ is unknown, the high frequency phase angle data still provide the important parameter λ as a function of $E_{d.c.}$. Substituting

the λ-value into the theoretical equations (the relationships in terms of j are most appropriate—*i.e.* eqns. (1)–(21)) yields a relationship which contains the unknowns, k, K, $E_{\frac{1}{2}}^{r}$ and α. The unknown α appears in the $F(t)$-term (eqn. (3)), but only when the d.c. process is non-Nernstian. If the d.c. process is Nernstian, the resulting expressions do not depend on α and the unknowns, k, K and $E_{\frac{1}{2}}^{r}$ are, again, obtainable as suggested for Nernstian systems, with the aid of lower frequency data. Obtaining $E_{\frac{1}{2}}^{r}$ then allows one to calculate experimental values of k_s and α from the high frequency phase angle data. If the d.c. process is non-Nernstian, the four unknowns, α, k, K and $E_{\frac{1}{2}}^{r}$, are probably most simply obtained by inserting trial values of α into the $F(t)$ expression, using one of the described data analysis procedures for obtaining k, K and $E_{\frac{1}{2}}^{r}$ with Nernstian systems, and repeating the process until an α-value yielding a set of k, K and $E_{\frac{1}{2}}^{r}$ which is self-consistent over a range of ω- and t-values is obtained. In situations where the chemical reaction is so rapid that the $\omega \gg k$ state cannot be reached with experimental conditions, chances are good that at the lower end of the frequency scale one will have $k \gg \omega$, chemical equilibrium will exist, and eqn. (46) is validated.

$$\cot \Phi = 1 + \frac{(2\omega)^{\frac{1}{2}}}{\lambda_f}. \tag{46}$$

Thus, phase angle values at lower frequencies may provide the λ_f-value unless charge transfer kinetics are overly rapid. Inserting λ_f in the theoretical relationships (the relationships in terms of J are most appropriate—eqns. (24)–(32)) yields relationships dependent on the unknowns, k, K, $E_{\frac{1}{2}}^{r}$ and α, which may be handled as just outlined for the case where λ is known. In cases where neither the upper nor lower ends of the available frequency scale provide an a.c. response in which chemical kinetic contributions are truly absent, another principle may be applied to minimize such contributions and facilitate evaluation of heterogeneous charge transfer kinetic parameters. The principle in question is that contributions of the following chemical reaction decrease as the d.c. potential becomes more cathodic and, in appropriate circumstances, may even be negligible over much of the cathodic side of the a.c. wave (*e.g.*, see Fig. 1, A and C). Thus, combining extreme frequencies and measurements on the cathodic side of the a.c. wave may improve the situation in borderline cases. Even when such extreme efforts fail to yield conditions under which only the charge transfer process and diffusion are rate-controlling, the possibility of unambiguous calculation of the relevant heterogeneous charge transfer and following chemical reaction rate parameters through even more sophisticated working curve procedures and/or trial-and-error methods, should not be overlooked. One must keep in mind that a.c. polarographic current amplitude and phase angle data over a reasonable frequency and d.c. potential range represents a pool of empirical knowledge in which much quantitative kinetic information is hidden.

One might note that some of the data analysis procedures outlined demand calculation of numerous working curves which may apply to one particular system only so that the calculations must be repeated for each system. Despite the complexity of the theoretical formulation, this is a minor problem with modern computational aids such as the computer utilized in the present work.

CONCLUSIONS

Earlier theoretical and experimental studies have suggested, at least in a preliminary manner, that a.c. polarography might be profitably applied to studying systems with following homogeneous chemical reactions[15-18]. That the results presented here both confirm and provide additional support for this concept is clearly indicated, representing the most significant conclusion one can draw from this study. Careful perusal of the calculational results seems to support this view regardless of whether one's interest lies in the heterogeneous charge transfer step or the following homogeneous chemical reaction (or both).

Measurement of the heterogeneous charge transfer kinetic parameters, k_s and α, has been one of the most successful areas of application of the a.c. polarographic method. However, such data has been forthcoming from simple quasi-reversible systems only. The present study shows that, although a complicating factor, the existence of kinetic effects of a following chemical reaction need not preclude the evaluation of k_s and α. The above theory provides guide-lines to various approaches for eliminating and/or correcting for the perturbations introduced by the chemical reaction.

Although evaluation of kinetic parameters of following chemical reactions represents a rare application of a.c. polarography, this is not likely to be a continuing situation. The marked sensitivity of the a.c. polarographic response to both the kinetic and thermodynamic status of the following chemical reaction indicated by the present calculations provides a sound basis for attempting such measurements. A.c. polarography offers both advantages and disadvantages relative to the many other electrochemical techniques that have been suggested for characterizing following chemical reactions[1-14], so that its use may be recommended for many systems, but certainly not all. Important advantages of a.c. polarography for such measurements are its high inherent accuracy, the extensive data provided on the effects of d.c. potential and the fact that both k and K may be evaluated simultaneously with many systems involving reversible following chemical reactions (which is not usually the case with other methods). Although not yet part of the established methodology, modern computer-oriented approaches to a.c. polarographic measurements[49-50] may enable acquisition of a.c. polarographic data for the entire frequency range of interest in the time required for a single sweep of the d.c. potential range (10–20 min). Such an advance would add rapidity of experimental investigation to the advantages of a.c. polarography. The main disadvantage of a.c. polarography for the characterization of following chemical reactions lies in the possibility that non-Nernstian behavior will complicate and, in some cases, preclude such measurements. Such difficulties can be avoided through the use of certain large amplitude relaxation techniques[10,11,41]. However, it should be recognized that many of the currently most studied classes of electrode processes in which following chemical reactions are prevalent—*e.g.*, electrode reactions of organic or organometallic species in aprotic solvents[51]— involve rapid heterogeneous charge transfer processes. For such systems one expects at worst small deviations from Nernstian behavior and minor difficulty in evaluating the chemical kinetic parameters by a.c. polarography.

SUMMARY

Results are presented of a detailed study of theoretical predictions for the fundamental harmonic a.c. polarographic response with systems involving rate control by diffusion, first-order following chemical reactions and/or heterogeneous charge transfer kinetics. A general theoretical formulation based on a rigorous solution of the expanding plane boundary value problem by the Matsuda method is the subject of study. The calculated a.c. polarographic behavior is examined for a wide range of kinetic conditions. Approaches to data analysis are recommended.

APPENDIX

Notation definitions

C_O^* initial concentration of species O.
D_i diffusion coefficient of species i.
f_i activity coefficient of species i.
$E_{d.c.}$ d.c. component of applied potential.
ΔE amplitude of applied alternating potential.
$E_{\frac{1}{2}}^r$ reversible d.c. polarographic half-wave potential (planar diffusion theory).
$E_{\frac{1}{2}}^{rc}$ d.c. polarographic half-wave potential with chemical equilibrium following Nernstian charge transfer.
$E_{\frac{1}{2}}^{rI}$ polarographic half-wave potential with irreversible chemical reaction following Nernstian charge transfer.
$E_{d.c.}^*$ potential of cross-over point in a.c. polarographic drop-life dependence.
$i_{d.c.}(t)$ instantaneous d.c. faradaic current component.
$I(\omega t)$ instantaneous fundamental harmonic faradaic alternating current.
i_p peak fundamental harmonic faradaic alternating current amplitude.
$i_{d,p}$ peak fundamental harmonic faradaic alternating current amplitude for diffusion-controlled process.
Φ phase angle of fundamental harmonic faradaic alternating current.
F Faraday's constant.
R ideal gas constant.
T absolute temperature.
A electrode area.
n number of electrons transferred in heterogeneous charge transfer step.
t time.
ω angular frequency of applied alternating potential.
k_s heterogeneous charge transfer rate constant at E^0.
α charge transfer coefficient.
k_1 backward rate constant for chemical reaction following charge transfer.
k_2 forward rate constant for chemical reaction following charge transfer.
K equilibrium constant for chemical reaction following charge transfer ($=k_1/k_2$).
Γ Euler gamma function.

REFERENCES

1 D. HAWLEY AND R. N. ADAMS, *J. Electroanal. Chem.*, 10 (1965) 376.
2 P. A. MALACHESKY, K. B. PRATER, G. PETRIE AND R. N. ADAMS, *J. Electroanal. Chem.*, 16 (1968) 41.
3 S. P. PERONE AND W. J. KRETLOW, *Anal. Chem.*, 38 (1966) 1760.
4 L. K. J. TONG, K. LIANG AND W. R. RUBY, *J. Electroanal. Chem.*, 13 (1967) 245.
5 W. JAENICKE AND H. HOFFMAN, *Z. Elektrochem.*, 66 (1962) 808.
6 W. JAENICKE AND H. HOFFMAN, *Z. Elektrochem.*, 66 (1962) 814.
7 A. A. VLCEK, *Collection Czech. Chem. Commun.*, 25 (1960) 668.
8 W. M. SCHWARZ AND I. SHAIN, *J. Phys. Chem.*, 70 (1966) 845.
9 L. B. ANDERSON AND C. N. REILLEY, *J. Electroanal. Chem.*, 10 (1965) 538.
10 A. C. TESTA AND W. H. REINMUTH, *Anal. Chem.*, 32 (1960) 1512.
11 H. B. HERMAN AND A. J. BARD, *Anal. Chem.*, 36 (1964) 511.
12 W. K. SNEAD AND A. E. REMICK, *J. Am. Chem. Soc.*, 79 (1957) 6121.
13 G. H. AYLWARD AND J. W. HAYES, *Anal. Chem.*, 37 (1965) 195.
14 G. H. AYLWARD AND J. W. HAYES, *Anal. Chem.*, 37 (1965) 197.
15 G. H. AYLWARD, J. W. HAYES AND R. TAMAMUSHI, *Proceedings of the First Australian Conference on Electrochemistry, 1963*, edited by J. A. FRIEND AND F. GUTMANN, Pergamon Press, Oxford, 1964, pp. 323–331.
16 D. E. SMITH, *Anal. Chem.*, 35 (1963) 602.
17 D. E. SMITH, *Electroanalytical Chemistry*, Vol. 1, edited by A. J. BARD, Marcel Dekker, Inc., New York, 1966, chap. 1.
18 H. L. HUNG, Doctoral Thesis, Northwestern University, Evanston, Illinois, 1967.
19 C. FURLANI AND G. MORPURGO, *J. Electroanal. Chem.*, 1 (1960) 351.
20 O. DRACKA, *Collection Czech. Chem. Commun.*, 25 (1960) 338.
21 O. DRACKA, *Collection Czech. Chem. Commun.*, 32 (1967) 3987.
22 R. S. NICHOLSON AND I. SHAIN, *Anal. Chem.*, 36 (1964) 706.
23 R. S. NICHOLSON, *Anal. Chem.*, 38 (1966) 1406.
24 M. L. OLMSTEAD AND R. S. NICHOLSON, *J. Electroanal. Chem.*, 14 (1967) 133.
25 J. H. CHRISTIE, *J. Electroanal. Chem.*, 13 (1967) 79.
26 R. KOOPMAN, *Ber. Bunsengesellsch. Physik. Chem.*, 70 (1966) 121.
27 C. M. GRODEN, G. H. AYLWARD AND J. H. HAYES, *Australian J. Chem.*, 17 (1964) 16.
28 C. M. GRODEN AND R. F. MATLAK, *Australian J. Chem.*, 19 (1966) 923.
29 J. M. SAVEANT AND E. VIANELLO, *Compt. Rend.*, 256 (1963) 2597.
30 J. KOUTECKÝ, *Collection Czech. Chem. Commun.*, 20 (1955) 116.
31 D. M. H. KERN, *J. Am. Chem. Soc.*, 75 (1953) 2473.
32 T. G. MCCORD AND D. E. SMITH, *Anal. Chem.*, 40 (1968) 1959.
33 J. HEYROVSKÝ AND J. KŮTA, *Principles of Polarography*, Academic Press, New York, 1966, pp. 77–83.
34 J. R. DELMASTRO AND D. E. SMITH, *J. Electroanal. Chem.*, 9 (1965) 192.
35 J. R. DELMASTRO AND D. E. SMITH, *Anal. Chem.*, 38 (1966) 169.
36 J. HEYROVSKÝ AND J. KŮTA, *Principles of Polarography*, Academic Press, New York, 1966, pp. 156–158.
37 D. E. SMITH AND T. G. MCCORD, *Anal. Chem.*, 40 (1968) 474.
38 L. ONSAGER, *J. Chem. Phys.*, 2 (1934) 599.
39 T. G. MCCORD AND D. E. SMITH, *Anal. Chem.*, 41 (1969) 116.
40 T. G. MCCORD AND D. E. SMITH, *Anal. Chem.*, 40 (1968) 289.
41 W. M. SCHWARZ AND I. SHAIN, *J. Phys. Chem.*, 69 (1965) 30.
42 A. C. TESTA AND W. H. REINMUTH, *J. Am. Chem. Soc.*, 83 (1961) 784.
43 T. G. MCCORD, Doctoral Thesis, Northwestern University, Evanston, Illinois, 1969.
44 H. L. HUNG AND D. E. SMITH, *Anal. Chem.*, 36 (1964) 922.
45 G. H. AYLWARD, J. W. HAYES, H. L. HUNG AND D. E. SMITH, *Anal. Chem.*, 36 (1964) 2218.
46 J. R. DELMASTRO AND D. E. SMITH, *Anal. Chem.*, 39 (1967) 1050.
47 D. E. SMITH, T. G. MCCORD AND H. L. HUNG, *Anal. Chem.*, 39 (1967) 1149.
48 J. KOUTECKÝ, *Collection Czech. Chem. Commun.*, 18 (1953) 597.
49 E. R. BROWN, D. E. SMITH AND D. D. DEFORD, *Anal. Chem.*, 38 (1966) 1130.
50 B. J. HUEBERT AND D. E. SMITH, unpublished work, Northwestern University, Evanston, Illinois, 1968.
51 M. E. PEOVER, *Electroanalytical Chemistry* Vol. 2, edited by A. J. BARD, Marcel Dekker, Inc., New York, 1967, chap. 1.

ELECTROANALYTICAL CHEMISTRY AND INTERFACIAL ELECTROCHEMISTRY
Elsevier Sequoia S.A., Lausanne – Printed in The Netherlands

THE EFFECT OF SPECIFIC ADSORPTION ON THE RATE OF AN ELECTRODE PROCESS

ROGER PARSONS
Department of Physical Chemistry, The University, Bristol (England)
(Received September 19th, 1968)

1. INTRODUCTION

The importance of the structure of the double layer for the quantitative interpretation of electrode processes was first pointed out by Frumkin[1]. It is to him and his school that we owe the broad picture of the effect of double layer changes on the rate of electrode reactions which has been built up in the last twenty years[2]. It was originally assumed that the electrochemical reaction can occur when the reacting species from the solution is adsorbed at the inner boundary of the diffuse layer. This has two consequences: first the rate of the reaction is affected, not by the whole of the metal–solution potential difference (ϕ^M), but by this less the potential difference across the diffuse layer (ϕ_2), *i.e.*, the rate equation for a reduction is of the form:

$$i = k[A]_2 \exp[-\alpha(\phi^M - \phi_2)f] \tag{1.1}$$

where $[A]_2$ is the concentration of the reducible species at the inner boundary of the diffuse layer and $f = F/RT$. Second, the concentration $[A]_2$ differs from the concentration in the bulk of the solution and is given by:

$$[A]_2 = [A] \exp(-z\phi_2 f) \tag{1.2}$$

where z is the valency of A (positive for cation, negative for anion), if we assume equilibrium across the diffuse layer and that there is no concentration polarization. Hence

$$i = k[A] \exp -(\alpha\phi^M f) \cdot \exp(\alpha - z)\phi_2 f \tag{1.3}$$

This equation was first used by Frumkin[1] and Levina and Zarinskii[3] to account for the independence of hydrogen overpotential on acid concentration in dilute acid solutions. A more recent successful application[4] is to the reduction of polyvalent anions in dilute solution. Here z is negative and near the point of zero charge, $\phi_2 \gg \phi^M - \phi_2$, so that the effect of electrode potential on the reaction rate is expressed primarily through the double layer term. Consequently, we have the striking effect of a reduction rate reduced by a shift of electrode potential in the negative direction.

2. DEVIATIONS FROM THE SIMPLE THEORY

In general, it seems that the simple theory is capable of quantitative results so long as no specific adsorption occurs on the electrode surface. In the presence of specific adsorption there are two obvious possibilities:

(a) the reacting particle is still located at the outer Helmholtz plane, but the potential, ϕ_2, of this layer is altered by the presence of specifically adsorbed particles;

(b) the reacting particle moves closer to the electrode before reaction occurs and ϕ_2 must be replaced by the potential at this point.

Many effects may be accounted for qualitatively in terms of (a), but frequently, additional hypotheses are required. For example, in the reduction of $S_2O_8^{2-}$ in the presence of 0.01 *N* chloride solutions[5] the marked effect of the nature of the cation seems inconsistent with the insensitivity of the double layer capacity to the nature of the cation[6]. Alternative but possibly equivalent explanations have been proposed for this: that the detailed structure of the double layer must be taken into account[7] and that there is some ion-pair formation between $S_2O_8^{2-}$ and the cations[8].

Another type of deviation is exhibited in the effect of tetraalkylammonium ions on electrode process. In qualitative agreement with (1.3), hydrogen evolution is retarded when these specifically adsorbed cations are present in solution[9]. However, the reduction of H_2O_2, for which $z=0$, should be accelerated; but it is also found to be retarded[10]. Here, it seems likely that the large size of the adsorbed ions causes a blocking effect which outweighs the electrostatic effect. This blocking may be due to the increase in dimension of the inner part of the double layer causing an increase in the energy of activation of the reaction. Similar effects are observed with adsorbed neutral particles.

In view of these, more obvious, reasons for deviation from the simple theory, it is particularly interesting to examine the effect of adsorbed halide ions on the rate of hydrogen evolution on mercury. The properties of the double layer in the presence of these ions are now quite well known. It is improbable that these ions would cause any appreciable blocking effect and the dissociation constants of the acids are so large that complex formation may be assumed to be completely absent. Consequently, it seems reasonable to expect that a simple electrostatic interpretation should be possible.

3. APPLICATION OF THE SIMPLE THEORY TO HYDROGEN EVOLUTION IN THE PRESENCE OF HALIDES

The effect of chloride, bromide and iodide ion on hydrogen evolution was observed about 20 years ago by Iofa *et al.*[11]. Their striking results are shown in Fig. 1.

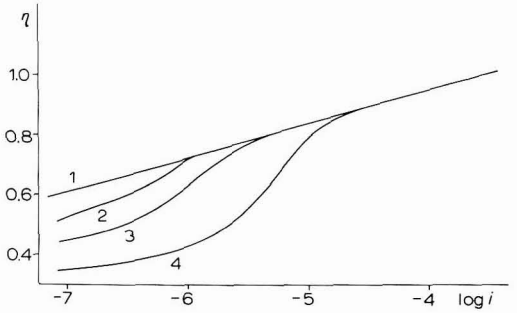

Fig. 1. Hydrogen overpotential at 25° on a mercury electrode *vs.* log current density in acidified 1*N* solns. of the following salts: (1), Na_2SO_4; (2), KCl; (3), KBr; (4), KI (data from Iofa *et al.*[11]).

They have been interpreted in terms of eqn. (1.3), but it seems unlikely that this is correct. From Grahame's excellent measurements[12], accurate values of ϕ_2 can now be calculated. These are shown in Fig. 2, for 1N KI solution and for 1N KF solution in which the anion is not specifically adsorbed (this will differ to a negligible extent from the results for the Na_2SO_4 solution used in the overvoltage work).

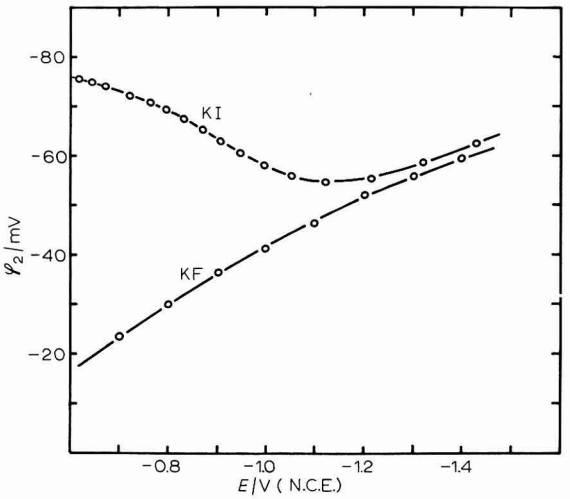

Fig. 2. Outer Helmholtz potential (ϕ_2) *vs.* potential (E) of a mercury electrode (*vs.* NCE) at 25° in solns. of 1N KF and 1N KI (data of Grahame[12]).

If the current density and concentration of hydrogen ions remain constant it follows from (1.3) that

$$\phi^M = \left(\frac{\alpha-1}{\alpha}\right)\phi_2 + \text{const.} \tag{3.3}$$

since $z=+1$.

At a current density of 10^{-6} A/cm^2 the electrode potential becomes 0.30 V more positive as the sulphate solution is changed to iodide. At the same time, ϕ_2 becomes 0.024 V more negative. Thus, although (3.3) accounts correctly for the direction of the effect, if α is taken as 0.5, the magnitude is wrong by a factor of more than 10. Similar large discrepancies have been observed in the effect of halides on the reduction of O_2 at mercury[10]. Further, it may be noted from Figs. (1) and (2) that the variation in ϕ_2 in the course of the Tafel line in the iodide solution amounts to only 18 mV which is almost the same as the variation in the sulphate solution, although in the opposite direction.

From these results it must be concluded that the change of the potential at the outer Helmholtz plane due to specific adsorption is quite inadequate to account for the observed results.

The second alternative proposed above has been investigated by Frumkin[13] and by Breiter *et al.*[14]. Frumkin replaced ϕ_2 by a potential calculated from a very simple model of the double layer in the presence of specific adsorption and obtained reasonable agreement with the observed effect at very low concentrations of the

specifically adsorbed ions though divergences occurred at higher concentrations. Breiter *et al.* used inner Helmholtz potentials, ϕ_1, calculated by Grahame[12]. The use of these potentials has been criticized[15] and more recently the significance of the potentials calculated by Grahame has been questioned[16]. There is, however, a more general difficulty with this approach. In order to account for the fact that specific adsorption of halide ions accelerates the evolution of hydrogen, it is clearly necessary that the potential which replaces ϕ_2 in eqn. (1.3) must become considerably more negative as the halide ion is specifically adsorbed. If the simple derivation of (1.3) is accepted, then according to (1.2) hydrogen ions should be much more strongly adsorbed in the presence of specifically adsorbed halides than in their absence. In particular, if ϕ_2 is replaced by ϕ_1, this implies that hydrogen ions are specifically adsorbed in the presence of specifically adsorbed halide ions. There is no evidence for this.

On the other hand eqn. (1.3) can be obtained in another way in which the effect of the electric field on the activated complex is considered directly rather than indirectly as in (1.1) and (1.2). The formal nature of eqn. (1.3) has been discussed[2,13] but no very clear model on which quantitative calculations can be based has emerged.

4. THE EFFECT OF SPECIFICALLY ADSORBED IONS ON THE RATE OF AN ELECTRODE REACTION

An alternative way of accounting for the effect of specifically adsorbed ions seems to be possible by retaining the ideas behind eqns. (1.1) and (1.2) but introducing the interaction between the activated complex of the electrode reaction and the adsorbed ions in the form of an activity coefficient.

According to the theory of absolute reaction rates[17], the rate constant of a reaction is of the form:

$$k = (\mathrm{k}T/h) \exp(-\Delta G^{\ddagger}/kT)/\gamma^{\ddagger} \tag{4.1}$$

where $\mathrm{k}T/h$ is the universal frequency factor, $\Delta G^{\ddagger}$ the standard free energy of activation (for an electrode reaction, corresponding to some standard potential) and $\gamma^{\ddagger}$ the activity coefficient of the activated complex. So far, in the use of eqns. (1.1) and (1.3) it has been assumed implicitly that $\gamma^{\ddagger}$ is independent of potential and of solution composition. This is probably a good approximation in the absence of specific adsorption if the active complex is located in the inner layer. The effect of the electrical field on the energy of the activated complex in this case is sufficiently accurately expressed by the exponential term in the potential, $\phi^{\mathrm{M}} - \phi_2$, in eqn. (1.1). In the presence of specific adsorption, however, this assumption is less plausible. The effect of the double layer on the energy of the activated complex may then be expressed in two parts: first, the direct effect of the charge on the electrode which is expressed in the same way as in the absence of specified adsorption; and second, the interaction between the activated complex and the specifically adsorbed ions, which is expressed through the activity coefficient of the activated complex.

It has already been shown[18] that specifically adsorbed anions behave as if they constituted a two-dimensional imperfect gas and that the deviations from ideality are sufficiently accurately expressed by a term in the second virial coefficient. It seems reasonable, therefore, to regard the present system as a two-dimensional imperfect

gas mixture. Temkin[19] has shown that for such a system the adsorption isotherms may be expressed in the form:

$$\sum_{k=1}^{k=c} 2B_{i,k}\Gamma_k = \ln \beta_i a_i - \ln (\Gamma_i/\Gamma_s) \tag{4.2}$$

where Γ_i is the surface concentration of the species in question whose activity in the bulk is a_i and whose standard free energy of adsorption on a bare surface is $-RT \ln \beta_i$. Γ_s is the saturation value of Γ_i. The second virial coefficients, $B_{i,k}$, are defined as

$$B_{i,k} = \pi \int_0^\infty \{1 - \exp(-\varepsilon_{i,k}/kT)\}\, r\,dr \tag{4.3}$$

where $\varepsilon_{i,k}$ is the energy of interaction between a particle of species i and one of species k when they are a distance r apart. The summation in eqn. (4.2) is carried out over all the c species of particles k including k = i.

In the absence of any appreciable amount of adsorbed species, (4.2) reduces to

$$\Gamma_i/\Gamma_s = \beta_i a_i \tag{4.4}$$

which is Henry's law. If we take the ideal dilute film as the reference state then it is clear from comparison of (4.4) with (4.2) rearranged in the form

$$\Gamma_i/\Gamma_s \exp\left\{\sum_k 2B_{i,k}\Gamma_k\right\} = \beta_i a_i \tag{4.5}$$

that $\exp\{\Sigma\, 2B_{i,k}\Gamma_k\}$ may be regarded as the two-dimensional activity coefficient of the species i. Thus, the required activity coefficient of the activated complex may be written

$$\gamma_\ddagger = \exp\left\{\sum_k 2B_{\ddagger k}\Gamma_k\right\}$$

where the subscript $\ddagger$ refers to the activated complex. Since the concentration of the activated complex ($\Gamma_\ddagger$) is always very small, the term, $B_\ddagger\Gamma_\ddagger$, which arises from interactions of activated complexes alone, may be omitted from the sum.

In the presence of a single species of specifically adsorbed ion, as in acidified alkali halide solution, the expression for the activity coefficient reduces to

$$\gamma_\ddagger = \exp 2B_{\ddagger,1}\Gamma_1 \,. \tag{4.7}$$

From (4.1) and (4.7) the ratio of the rate in the presence to that in the absence of specific adsorption is readily obtained

$$\ln [k/k(\Gamma_1 = 0)] = \ln [i/i(\Gamma_1 = 0)] = -2B_{\ddagger,1}\Gamma_1 \,, \tag{4.8}$$

the comparison being made at constant potential and concentration of reactants, as well as with neglect of the much smaller effect described in eqn. (1.3). Thus, the logarithm of the rate constant depends approximately linearly on the amount of substance specifically absorbed.

The value of the second virial coefficient, $B_{\ddagger,1}$, will depend on the detailed structure of the double layer, but it may reasonably be expected to be related to the virial coefficient $B_{1,1}$ expressing the first-order interaction between the specifically adsorbed ions themselves. The activated complex, being a transient species, will not

seriously perturb the configuration of the specifically adsorbed ions during its passage to the final state. Hence, to a first approximation it may be suggested that

$$B_{\ddagger,1} = (z_\ddagger/z_1)B_{1,1} \tag{4.9}$$

where $z_\ddagger e$ is the effective charge on the activated complex and $z_1 e$ the charge on the specifically adsorbed ions. This assumes that the interactions are entirely electrostatic, which is probably a good approximation at the densities for which (4.2) is valid. It also assumes that the activated complex occurs in the inner Helmholtz plane and deviations from (4.9) will obviously arise if it does not. It is also possible that these deviations will depend on the nature of the specifically adsorbed ions and perhaps also on their concentration.

5. COMPARISON WITH EXPERIMENT

The data of Fig. 1 was analysed by measuring the increase in log i between the results in sulphate solution and those in the halide solutions at a series of constant potentials. These values of Δ log i are plotted in Fig. 3 against the amounts of speci-

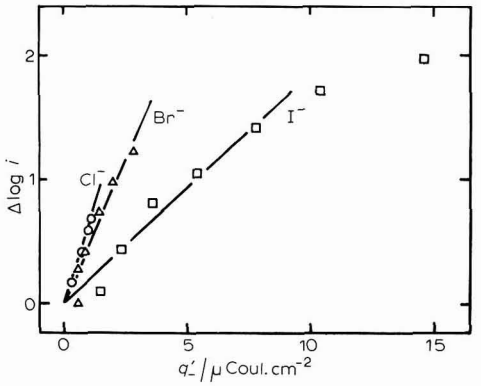

Fig. 3. Increase in rate of hydrogen evolution at constant potential when the anion is changed from SO_4^{2-} to a halide *vs.* amount of specifically adsorbed halide ion (data from Fig. 1 and from Grahame[12], Lawrence *et al.*[21] and Grahame and Parsons[20]).

fically adsorbed halide ion at each potential obtained from data in 1 M potassium halide solutions[12,20,21]. Approximately straight lines are found, although the results for iodide show significant curvature at the highest concentration. Values of $B_{\ddagger,1}$ calculated according to (4.8) from the slopes of the linear sections are -340, -630 and -1215 A^2 ion^{-1} for iodide, bromide and chloride, respectively. This is in the same sequence as the values of $-B_{1,1}$ for these ions, although the values of $B_{1,1}$ obtained[20,21] for bromide and chloride vary considerably with adsorbed density. The value of $B_{1,1}$ calculated from Grahame's[12] iodide data[18] is about $+350$ A^2 ion^{-1} which suggests that $z_\ddagger \simeq +1$, which is perhaps surprising as an effective charge of about $+\frac{1}{2}$ might be expected (*cf.* ref. 22).

More recently, Sluyters *et al.*[23,24] have studied the effect of specifically adsorbed ions on the kinetics of the deposition of Zn^{2+} on mercury. In their first paper[23]

they obtained a linear relation like that predicted by eqn. (4.8) when they varied the concentration of the adsorbed ion at constant potential. The slope of this line corresponds to a value of $B_{\ddagger,1}$ in iodide solutions of -280 A^2 ion^{-1}. In the second paper[24], experiments at varying potentials in solutions of constant composition were carried out and these are more closely analogous to those of Fig. 1 for hydrogen. The initial parts of the plots of log k against Γ_1 are linear and have slopes corresponding to $B_{\ddagger,1} = -440$A^2 ion^{-1} for iodide, and -2060A^2 ion^{-1} for chloride and bromide. The value for bromide is much higher than can be explained on the basis of eqn. (4.9), but those for the other two ions are consistent with this equation if the charge on the activated complex is between $+1$ and $+2$. A simple view based on the theory of electron transfer reactions would lead to the expectation of an effective charge of $+2(1-\alpha)$, where α is the transfer coefficient. Sluyters *et al.*[24] suggest that the true value of α is about 0.2. It must be noted that, for this reaction, like the hydrogen reaction, there is no evidence for specific adsorption of the initial state so that a model of the general type described here must be invoked. However, for the zinc reaction there is the possibility of participation of halide complexes. This has been thoroughly discussed by Sluyters *et al.*[23].

The occurrence of a decrease in the slope of the plot of log rate against specifically adsorbed charge at the higher adsorbed densities may be a result of the environment of the activated complex becoming constant at the higher densities or of the effect of the size of the adsorbed species as discussed in the next section. Nevertheless, it is very difficult to explain the sharp change in direction observed by Sluyters *et al.*[24] in their work in bromide solutions.

6. EXTENSION TO OTHER TYPES OF SYSTEM

The use of eqn. (4.9) implies that the interaction between the activated complex and the specifically adsorbed ions is predominantly electrostatic. It has already been mentioned above that blocking effects may occur which do not seem to be connected with electrostatic interaction. A possible modification of eqn. (4.2) which would allow for this type of effect is the Frumkin isotherm[25] in the more general semi-empirical form proposed recently[26]

$$\sum_{k=1}^{k=c} 2B_{i,k}\Gamma_k - r_i \ln\left[r_i\left(1-\sum_{k=1}^{k=c}\Gamma_k/\Gamma_s\right)\right] = \ln \beta_i a_i - \ln(\Gamma_i/\Gamma_s) \qquad (6.1)$$

where r_i is the number of solvent molecules replaced by the adsorption of one molecule of species i. The additional term in (6.1) compared with (4.2) allows for the finite number of adsorbed molecules which can be accommodated on the surface. It is not a rigorous equation because the first term on the left-hand side has been derived only for low coverage of the surface; however, it is probably of the right form.

In the presence of a single adsorbed species (other than the solvent), each of the sums in (6.1) may be reduced to a single term, as discussed above, because of the infinitesimal surface concentration of the activated complex. For this simple situation the activity coefficient of the latter reduces to

$$\ln \gamma_\ddagger = 2B_{\ddagger,1}\Gamma_1 - r_1 \ln[r_1(1-\Gamma_1/\Gamma_s)] \qquad (6.2)$$

and the effect on the rate of the electrode reaction becomes

$$\ln [k/k(\Gamma_1=0)] = -2B_{\ddagger,1}\Gamma_1 + r_1 \ln [r_1(1-\Gamma_1/\Gamma_s)] \quad (6.3)$$

If $B_{\ddagger,1}=0$ and $r_1=1$, this reduces further to the simple equation which has been used frequently[8,27-29] to express the idea that the electrode reaction occurs rapidly on "uncovered" regions of the surface and very slowly, if at all, on "covered" regions. In a recent paper, Sathyanarayana[30] found that the effect of butanol on the deposition of Cu^{2+}, Cd^{2+} and Zn^{2+} on mercury required the use of an expression of the form:

$$\ln k = \text{const.} + b \ln (1-\Gamma_1/\Gamma_s) \quad (6.4)$$

He described b as expressing the lateral repulsive interaction on the surface. Presumably, b includes the effect of both terms on the right-hand side of (6.3) because it varies with the nature of the reacting ion, being 1.74 for Zn^{2+}, 1.93 for Cd^{2+} and 3.97 for Cu^{2+}; the latter two values were obtained from data at high coverages only. According to the present model, r_1 should be characteristic of the nature of the inhibitor only, while $B_{\ddagger,1}$, of course, depends on the nature of both reactant and inhibitor. At present, not much is known from equilibrium measurements about the interaction between neutral molecules and specifically adsorbed ions, except that it seems to be repulsive[31,32] in the case of anions.

The ideas used in eqn. (6.1) can clearly be extended to include the effect of reorientation of the adsorbed inhibitor following the model already presented for the *p*-toluene sulphonate ion[26].

7. DISCUSSION

The simple model proposed above goes some way towards a semi-quantitative interpretation of the limited amount of experimental data available. The general framework should be suitable for an improved approach based on a more detailed model of the inner layer and on a better estimate of the charge and position of the activated complex.

There is one difficulty concerning the general framework which should be discussed here. The adsorption isotherm for an ionic species alone, which has the form of eqn. (4.2) with $c=1$, has been obtained experimentally for concentration variations at constant charge; that is, the adsorption coefficient derived by extrapolation to low adsorbed densities is found to be a function (linear for simple ions[18]) of the charge on the electrode. If it is assumed that the adsorption coefficient of the activated complex has similar properties, then the standard electrochemical potential of the activated complex should be dependent on the charge of the electrode rather than directly on the potential as is usually assumed. This means that, in the condition of constant potential imposed on eqn. (4.8), the standard chemical free energy of activation will not be held constant because the charge of the electrode changes as a result of the adsorption of halide ions, for example. In the comparison with experiment carried out in section 5, this effect is included in the apparent second virial coefficient. Correction for it will tend to increase the value of the second virial coefficient calculated. In the present rudimentary state of the model a more detailed analysis of this problem seems scarcely worthwhile.

Finally, it should be noted that Krishtalik[33] has recently discussed the properties of the activity coefficient of the activated complex in terms of the Brønsted rule.

The situation discussed in the present paper is one in which the Brønsted rule does not apply, since, for example, the Tafel lines are non-linear. The basic reason for this departure from the Brønsted rule is that the environment of the activated complex is quite different from that of the reactants or products and cannot be derived from the latter in a simple linear way.

SUMMARY

A simple model is proposed to account for the effect of adsorbed species on the rate of an electrode reaction. It is assumed that this effect can be expressed by the activity coefficient of the activated complex which can be calculated from the adsorption isotherm. This approach gives a reasonable account of experimental data already published and provides a framework for future experimental and theoretical work.

REFERENCES

1 A. N. FRUMKIN, *Z. Physik. Chem.*, 164 (1933) 121.
2 R. PARSONS, *Advances Electrochem. Electrochem. Eng.* 1 (1961) 1.
3 S. D. LEVINA AND W. ZARINSKII, *Acta Physicochim. U.R.S.S.*, 6 (1937) 491; 7 (1937) 485.
4 A. N. FRUMKIN AND G. M. FLORIANOVICH, *Zh. Fiz. Khim.*, 29 (1955) 1827.
5 A. N. FRUMKIN AND N. V. NIKOLAEVA-FEDOROVICH, *Vestn. Mosk. Univ., Ser. Mat. Mekh. Astron. Fiz. Khim.* 2 (1957) 169.
6 D. C. GRAHAME, *J. Electrochem. Soc.*, 98 (1951) 343.
7 A. N. FRUMKIN, *Z. Elektrochem.* 59 (1955) 807.
8 L. GIERST, Thèse d'agrégation, Université Libre de Bruxelles, 1958.
9 E. P. ANDREEVA, *Zh. Fiz. Khim.*, 29 (1955) 699.
10 J. M. PARRY AND R. PARSONS, unpublished work.
11 Z. A. IOFA, B. KABANOV, E. KUCHINSKII AND F. CHISTYAKOV, *Acta Physicochim., U.R.S.S.*, 10 (1939) 317.
12 D. C. GRAHAME, *J. Am. Chem. Soc.*, 80 (1958) 4201.
13 A. N. FRUMKIN, *Advan. Electrochem. Electrochem. Eng.* 1 (1961) 65.
14 M. BREITER, M. KLEINERMAN AND P. DELAHAY, *J. Am. Chem. Soc.*, 80 (1958) 5111.
15 R. PARSONS, *Trans. Symp. Electrode Processes*, edited by E. YEAGER, Wiley, New York, 1961, p. 265.
16 J. M. PARRY AND R. PARSONS, *Trans. Faraday Soc.*, 59 (1963) 241.
17 S. GLASSTONE, K. J. LAIDLER AND H. EYRING, *Theory of Rate Processes*, McGraw-Hill, New York, 1941.
18 R. PARSONS, *Trans. Faraday Soc.*, 55 (1959) 999.
19 M. I. TEMKIN, *Zh. Fiz. Khim.*, 15 (1941) 296.
20 D. C. GRAHAME AND R. PARSONS, *J. Am. Chem. Soc.*, 83 (1961) 1291.
21 J. LAWRENCE, R. PARSONS AND R. PAYNE, *J. Electroanal. Chem.*, 16 (1968) 193.
22 M. I. TEMKIN, *Tr. Soveshch. po Elektrokhim. Akad. Nauk SSSR, Otdel. Khim. Nauk*, 1950 (1953) 181.
23 P. TEPPEMA, M. SLUYTERS-REHBACH AND J. H. SLUYTERS, *J. Electroanal. Chem.*, 16 (1968) 165.
24 M. SLUYTERS-REHBACH, J. S. M. C. BREUKEL AND J. H. SLUYTERS, *J. Electroanal. Chem.*, 19 (1968) 85.
25 A. N. FRUMKIN, *Z. Physik. Chem.*, 116 (1925) 466.
26 J. M. PARRY AND R. PARSONS, *J. Electrochem. Soc.*, 113 (1966) 992.
27 W. LORENZ AND W. MÜLLER, *Z. Physik. Chem. N. F.*, 18 (1958) 142.
28 R. W. SCHMID AND C. N. REILLEY, *J. Amer. Chem. Soc.*, 80 (1958) 2087.
29 J. WEBER, J. KOUTECKÝ AND J. KORYTA, *Z. Elektrochem.*, 63 (1959) 583.
30 S. SATHYANARAYANA, *J. Electroanal. Chem.*, 10 (1965) 119.
31 R. PARSONS AND F. G. R. ZOBEL, *Trans. Faraday Soc.*, 62 (1966) 3511.
32 R. PARSONS AND P. C. SYMONS, *Trans. Faraday Soc.*, 64 (1968) 1077.
33 L. I. KRISHTALIK, *Electrochim. Acta*, 13 (1968) 715.

ELECTROANALYTICAL CHEMISTRY AND INTERFACIAL ELECTROCHEMISTRY
Elsevier Sequoia S.A., Lausanne – Printed in The Netherlands

SUPPORTING-ELECTROLYTE EFFECTS IN TENSAMMETRY

HENRY H. BAUER, H. R. CAMPBELL AND A. K. SHALLAL
Department of Chemistry, University of Kentucky, Lexington, Kentucky 40506 (U.S.A.)
(Received October 23rd, 1968)

In virtually all studies of the adsorption of surfactants at electrodes, attention has been focussed on the properties of the surfactant itself. The process involved, however, is actually the displacement of water and of the ions of the background electrolyte, so that properties of the latter should be taken into account. The role of water has recently been emphasised by Bockris and his co-workers[1]. The influence of the supporting electrolyte has been briefly mentioned in a number of studies, but the only attempts at systematic investigation appear to be those of Breyer and Hacobian[2] and of Damaskin *et al.*[3].

We have been making studies of supporting-electrolyte effects in tensammetry partly with a view to the use of tensammetric processes to characterise the structure of the double layer—*e.g.*, at solid electrodes. It soon became apparent that, before the competitive adsorption of surfactants and ions could be quantitatively investigated, it would be necessary to take into account the salting effect on the surfactant of the various electrolytes. Results illustrating this point are reported here.

EXPERIMENTAL

Tensammetric curves were obtained with apparatus described elsewhere[4]. Double-layer capacity values were obtained in some experiments by use of phase-selective observation using an Ad-Yu Phase-Vector voltmeter Type 248 A.

Salting effects were measured by determining the solubility of the alcohol (*n*-amyl) in the various salt solutions used. The concentration of alcohol in saturated solutions was determined spectrophotometrically using the color developed by *p*-dimethylaminobenzaldehyde; this is similar to the method, described by Boruff[5], for estimation of fusel oils; details will be published elsewhere.

RESULTS AND DISCUSSION

Region of surfactant adsorption

Usually, the difference in potentials of the tensammetric waves—the *wave-spread*—increases with increasing concentration of surfactant[6]. The wavespread might therefore be used as a measure of adsorbability in comparing different surfactants and supporting electrolytes. This procedure is more advantageous than measuring changes in the peak potential of either wave, since the individual potentials are affected by the liquid-junction potentials. The utility of the wavespread as a criterion was investi-

gated by examining the effects of various electrolytes, at different concentrations, on the behavior of *n*-amyl alcohol (Table 1).

The wavespread was found to be unaffected by the frequency of the alternating current (40 Hz–4 kHz). The magnitude decreased as the electrolyte concentration (KF or KCl) increased, in accordance with the idea that electrolyte and surfactant are competitively adsorbed. However, in sodium sulfate solutions the opposite effect was observed in solutions not saturated with the alcohol. Clearly, two effects are

TABLE 1

TENSAMMETRIC WAVESPREAD AND CONCENTRATION OF AMYL ALCOHOL

Concn. of	*Salt soln.*					
alcohol	*KF*		Na_2SO_4		*KCl*	
(*M*)	0.1 *M* (*mV*)	1 *M*	0.1 *M* (*mV*)	1 *M*	0.1 *M* (*mV*)	1 *M*
0.01	810	770	740	920	620	550
0.02	1033	954	903	1078	788	745
0.03	1100	1070	990	1170	900	860
0.04	1218	1154	1071	1211	950	902
0.05	1270	1210	1120	1220	1020	960
satd.	1577	1420	1436	1315	1463	1345

present: salting out of the alcohol by the salt, and competitive adsorption of electrolyte and surfactant. The former effect outweighs the latter with sodium sulfate, but not with potassium chloride or fluoride.

Results in Table 1 can be converted to results at constant activity of *n*-amyl alcohol by using the ratio of alcohol concentration to the saturation concentration

TABLE 2

TENSAMMETRIC WAVESPREAD AND ACTIVITY OF AMYL ALCOHOL

Activity	*Salt soln.*					
of	*KF*		Na_2SO_4		*KCl*	
alcohol	0.1 *M* (*mV*)	1 *M*	0.1 *M* (*mV*)	1 *M*	0.1 *M* (*mV*)	1 *M*
0.079	986	757	858	748	768	606
0.143	1132	914	988	876	908	748
0.224	1254	1038	1098	979	1020	862
0.316	1342	1132	1178	1056	1105	948
1.0	1577	1420	1436	1315	1463	1345

for each salt solution. Table 2 shows that the "anomaly" in sulfate solutions then disappears—the wavespread at constant activity of alcohol always decreases as the concentration of sulfate increases (changes in the activity coefficient of the alcohol with changing concentration of alcohol are neglected here; such changes are much less than the salting effects[7]).

Isotherm parameters

Measurements of the decrease in double-layer capacity near the point of zero charge showed that, in the systems studied, adsorption closely followed the Frumkin isotherm[8]

$$Bc = \frac{\theta}{1-\theta} \exp(-2a\theta) \tag{1}$$

where B is an adsorption coefficient, c the concentration of surfactant in the solution, a an interaction parameter, and θ the fraction of surface covered. The latter was obtained by the approximation that

$$C_{dl} = (1-\theta)C_0 + \theta C_s \tag{2}$$

where C_{dl} is the observed capacity and C_0, C_s are the capacities for $\theta=0$ and $\theta=1$, respectively.

Values of B are shown in Table 3. Once again, there are anomalies in that B

TABLE 3

ADSORPTION COEFFICIENTS OF AMYL ALCOHOL

Salt soln.	B (*see eqn.* (1))[a] ($l/mole^{-1}$)	B_a (*see eqn.* (3)) ($l/mole^{-1}$)
0.1 *M* KF	37.0	34.3
1 *M* KF	60.9	30.1
0.1 *M* Na_2SO_4	64.1	55.4
1 *M* Na_2SO_4	147	35.5
0.1 *M* KCl	34.8	32.5
1 *M* KCl	18.9	11.5

[a] All values of B were obtained from measurements at -0.5 V *vs.* SCE. The qualitative trend was the same as at -0.45 V and at -0.55 V.

apparently increases as the electrolyte concentration increases. To allow for activity changes, one can use a different adsorption coefficient, B_a, defined by

$$B_a = \frac{S}{S_0} B \tag{3}$$

where S is the solubility of the alcohol in the given salt solution and S_0 its solubility in water. Results in Table 3 show that B_a-values decrease as the salt concentration increases, as would be expected.

Thus, apparently anomalous results are obtained when one seeks to compare the adsorptive effects of amyl alcohol and of various electrolytes, if allowance is not made for salting effects. The corrected data do not, however, provide a straightforward measure of adsorbability; for instance, the largest wavespread (0.1 *M* KF, Table 2) is not found in the same system as the largest value of the adsorption coefficient (in 0.1 *M* Na_2SO_4, Table 3). Indeed, one would not expect otherwise in view of the change of specific adsorbability of anions with changes in the electrode potential.

Work is continuing on the relative adsorbabilities of surfactants and of electrolytes.

ACKNOWLEDGEMENTS

This work was supported in part by funds from the Office of Water Resources Research, U.S. Department of the Interior, under P.L. 88-379; by the Water Resources Institute of the University of Kentucky; and by the Petroleum Research Fund.

SUMMARY

The adsorption of *n*-amyl alcohol has been studied by tensammetry in the presence of various electrolytes. The apparent adsorbability of the alcohol increased with increasing concentration of sodium sulfate under certain circumstances. This apparent anomaly disappears when corrections are made for changes of the activity coefficient of the alcohol, resulting from salting out.

REFERENCES

1 J. O'M. Bockris, E. Gileadi and K. Müller, *Electrochim. Acta*, 12 (1967) 1301.
2 B. Breyer and S. Hacobian, *Australian J. Chem.*, 9 (1956) 7.
3 B. B. Damaskin, A. A. Survila and L. E. Rybalka, *Soviet Electrochemistry*, 3 (1967) 818.
4 H. H. Bauer, D. Britz and D. C. S. Foo, *J. Electroanal. Chem.*, 9 (1965) 481.
5 C. S. Boruff, *J. Assoc. Offic. Agri. Chemists*, 42 (1959) 331; 44 (1961) 383.
6 B. Breyer and S. Hacobian, *Australian J. Sci. Res.*, A5 (1952) 500.
7 F. A. Long and W. F. McDevit, *Chem. Rev.*, 51 (1952) 119.
8 A. N. Frumkin and B. B. Damaskin, *Mod. Aspects Electro-chem.*, 3 (1964) 149.

ELECTROANALYTICAL CHEMISTRY AND INTERFACIAL ELECTROCHEMISTRY
Elsevier Sequoia S.A., Lausanne – Printed in The Netherlands

EFFECT OF THE EXTERNAL RESISTANCE ON THE HIGH-FREQUENCY POLAROGRAPHIC WAVE HEIGHT

TOMIHITO KAMBARA, SHIGEYUKI TANAKA AND KIYOSHI HASEBE
Department of Chemistry, Faculty of Science, Hokkaido University, Sapporo 060 (Japan)
(Received October 4th, 1968)

INTRODUCTION

The high-frequency (HF) polarographic method developed by Barker[1] using Faradaic rectification is now accepted as one of the most elegant polarographic methods of analysis of high sensitivity and resolving power. The methodology has been treated theoretically and reviewed by several authors[1-4]. This method has also been applied to the practical analysis of micro-constituents, such as zinc, cobalt and nickel[5], magnesium and calcium[6], arsenic[7] in food, and carbon disulfide[8] in carbon tetrachloride, and some trace components[9] in high purity metals and alloys. The temperature-dependence of the HF polarographic wave height is also clarified[10].

It has been emphasized that in the analytical applications of the HF polarographic method the electrical resistance of the electrolysis cells should be as low as possible[5-7]. The present study reports on the decrease in the HF wave height caused by the external resistance.

THEORETICAL

According to Barker[1], the HF polarographic signal, i_{HF}, is proportional to the square of the amplitude of the superimposed HF alternating current. If the external resistance, R_{ext}, is not small enough compared with the electrode–solution interface impedance, Z, the effective potential difference at the interface, ΔE_{eff}, will be decreased compared with the total applied potential difference, ΔE_{HF}. Therefore,

$$i_{HF} = k\Delta E_{HF}^2 C \left(\frac{1}{Z+R_{ext}}\right)^2 \quad (1)$$

where k denotes the proportionality factor and C the concentration of depolarizer.

Another interpretation of the HF polarographic signal is proposed by Yasumori *et al.*[11] on the basis of the Senda–Tachi theory[12] for the Fournier polarogram. The theory regards the HF method as a sort of Breyer a.c. polarography, in which the mean potential during the half-period with the HF modulation differs from the unmodulated constant potential. According to this theory, the HF polarographic signal is proportional to the difference between the usual d.c. polarographic step and the Fournier current. Thus, the HF wave for a reversible redox system is expressed by:

$$i_{HF} = \frac{i_d}{4}\left(\frac{nF}{2RT}\right)^2 \frac{d^2 j}{dx^2} \cdot \Delta E_{HF}^2 \quad (2)$$

where

$$j = \tfrac{1}{2}(1 - \tanh x)$$

$$x = \frac{nF(E - E_{\frac{1}{2}})}{2RT}$$

and the other symbols have their usual significance. Consequently, one may expect that the resulting HF signal would be decreased by the factor, $Z/(Z + R_{ext})$, analogously to the Breyer a.c. wave height, *i.e.*,

$$i_{HF} = k\Delta E_{HF}^2 C \frac{1}{Z + R_{ext}} \tag{3}$$

An experimental investigation as to the validity of eqn. (1), eqn. (3) or neither, now follows.

EXPERIMENTAL

Apparatus and reagents

The HF polarograph used was a Yanagimoto product, type PF-500, in which a 200-Hz square-wave voltage is modulated by a HF potential of 455 kHz.

The mercury pool at the bottom of the electrolysis cell was used as the anode. The electrical connection to the mercury pool was made by means of a sealed platinum wire of 1-mm diam. If ordinary cells made of *ca.* 0.2-mm diam. platinum wire are used, the recorded HF wave height fluctuates from cell to cell.

The characteristics of the dropping mercury electrode were: $m = 1.04$ mg sec^{-1} in pure water, $t = 4.88$ sec in 1 M KCl at open circuit at $h = 85$ cm. Other operating conditions are: synchro. = 1.5–3.0 sec after drop fall, gate = 2–7, and span voltage, 2.0 V.

The reagents employed were all of analytical grade. The deionized water was distilled and used immediately.

Control chart

Three electrolysis cells each equipped with a 1-mm diam. platinum wire were labelled as No. 1, 2, and 3, respectively. With a standard polarographic solution, (10^{-6} M in cadmium and 0.5 M in potassium chloride), the mean of four data of the HF wave height was obtained ten times with the three cells. The method of one-factor analysis of variance was then applied to the data sets. It was confirmed that there was no significant difference in three means of wave heights obtained with the three cells, as shown in Table 1.

The daily mean, $\bar{x}$, and the range, R, were measured for ten days and the grand mean, $\bar{\bar{x}}$, and the mean of daily range, $\bar{R}$, were evaluated. Then, the $\bar{x}$ control chart corresponding to the three-sigma deviation from the central line was constructed.

After the establishment of the above control chart, the HF wave height (with the same standard solution) was each day confirmed at first to lie between two critical lines, *i.e.*, the working function of the HF polarograph was maintained under controlled conditions, and then the appropriate measurements made under varying conditions. An example of such a control chart for several days is shown in Fig. 1.

TABLE 1

ANALYSIS OF VARIANCE FOR HF WAVE HEIGHTS OBSERVED WITH THREE ELECTROLYSIS CELLS

Source of variation	*Sum of squares*	*Degree of freedom*	*Mean square*	F_o	$F(2, 27, 0.05)$
Between cells	18.5	2	9.3	1.86	3.35
Error	134.1	27	5.0		
Total	152.6	29			

Conclusion: The three cells are equivalent.

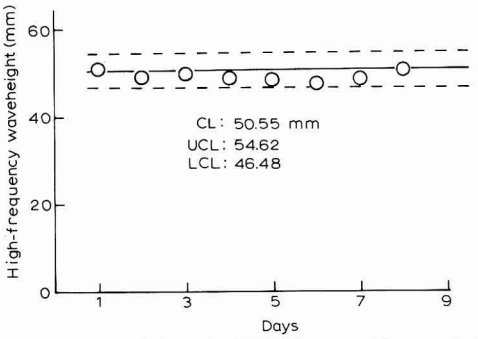

Fig. 1. $\bar{x}$ control chart for HF polarographic wave height. Standard electrolysis solution, $1 \cdot 10^{-6}$ *M* Cd^{2+} in 0.5 *M* KCl (25°); recorder sensitivity, 0.020 μA mm^{-1}; amplifier sensitivity, $\frac{1}{2}$; damping, 1 μF; HF amplitude ΔE_{HF}, 5 V; electrode distance, 1 cm.

Effect of the electrode distance

The HF polarographic wave height tends to decrease with increasing distance between the DME and mercury pool anode, as shown in Fig. 2. It is evident from Fig. 2 that if the electrodes are more than 1.5 cm apart the wave height is definitely lowered. Sets of data obtained with electrode distances of 0.5 and 1.0 cm, confirm, by means of the familiar *t*-test, that there is no significant difference between the means

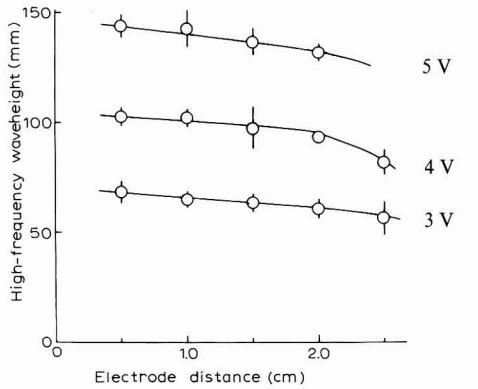

Fig. 2. Effect of electrode distance on HF wave height. Electrolysis soln., $1 \cdot 10^{-5}$ *M* Pb^{2+} in 0.5 *M* KNO_3 (25°). Figures indicate ΔE_{HF} in volts. The vertical line shows the 95% confidence limits. Recorder sensitivity, 0.020 μA mm^{-1}; amplifier sensitivity, $\frac{1}{5}$; damping, 1 μF.

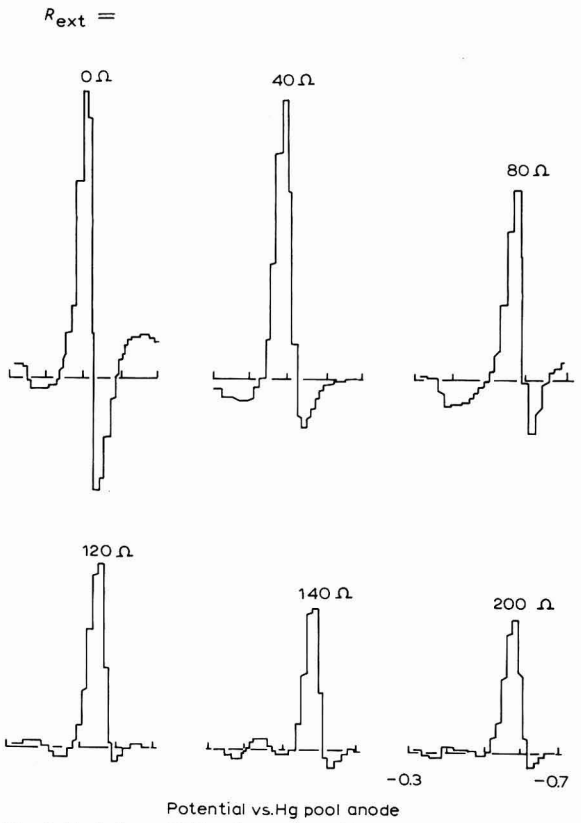

Fig. 3. Variation of HF polarogram with external resistance. The amplitude, ΔE_{HF}, of the HF modulation voltage was kept to 4 V. Other experimental conditions as in Fig. 2.

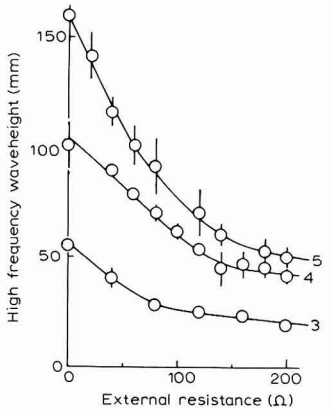

Fig. 4. Effect of external resistance on HF wave height. Experimental conditions as in Fig. 2. Figures indicate ΔE_{HF} in volts.

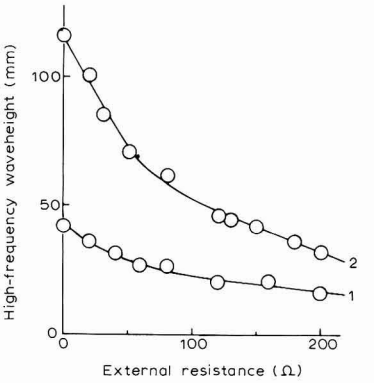

Fig. 5. Effect of external resistance on HF wave height. Experimental conditions as in Fig. 2, except that amplifier sensitivity = 1/1.

of wave heights. Thus, the electrode distance was kept at 1.0 cm throughout the experiments.

Effect of the external resistance

Furutani *et al.*[5-7] report that at a constant depolarizer concentration the HF wave height decreases with decreasing concentration of supporting electrolyte. This may be caused by the increase in the cell resistance.

In the present study, the change of HF wave height produced by connecting a standard resistor of variable resistances in series to the electrolysis cell, was measured. Some examples of the HF polarograms recorded are shown in Fig. 3. The results are given in Figs. 4 and 5.

The question as to whether the relationship that the HF wave height is proportional to the square of the HF amplitude (as expected from eqns. (1) and (3)), holds even under the condition of the external resistance connection, was first examined experimentally. Zinc ions in potassium halides and lead ions in potassium nitrate were used as depolarizers. These have various degrees of reversibility.

The results are given in Fig. 6. The double-logarithmic plot shown in Fig. 7 is treated statistically and the results are summarized in Table 2.

It was found that the mean values of the slope, m, for each solution in Table 2 do not differ significantly. The correlation coefficient, r, approaches very closely to unity, so that it may be safe to say that the relationship:

$$i_{HF} = k\Delta E_{HF}^2$$

holds even under the condition of resistance connection.

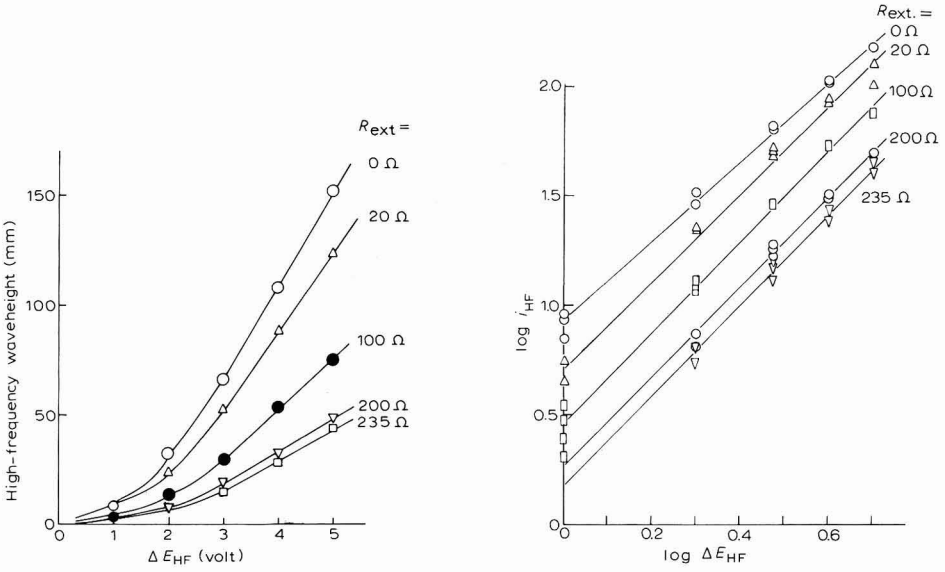

Fig. 6. Variation of HF wave height with amplitude, ΔE_{HF}, of HF pulse. Figures indicate the resistance connected in series to the cell (in ohm).
Electrolysis soln., $1 \cdot 10^{-4}$ M Pb^{2+} in 0.5 M KNO_3 (25°); recorder sensitivity, 0.060 μA mm^{-1}; amplifier sensitivity, $\frac{1}{20}$; damping, 1 μF.

Fig. 7. Double-logarithmic plot of the data shown in Fig. 6.

TABLE 2

RESULTS OF THE CORRELATIONAL ANALYSIS OF $\log i_{HF}$ *vs.* $\log \Delta E_{HF}$
r = correlation coefficient and m = slope

Depolarizer	$1 \cdot 10^{-4}$ *M* Zn^{2+}						$1 \cdot 10^{-4}$ *M* Pb^{2+}	
Supporting electrolyte	1 *M KCl*		1 *M KBr*		1 *M KI*		0.5 *M* KNO_3	
R_{ext} (Ω)	r	m	r	m	r	m	r	m
0	0.992	2.047	1.000	1.753	1.000	2.021	0.991	1.805
20							1.000	2.043
50	1.000	1.882	0.991	1.858	1.000	2.033		
100	0.999	1.782	0.992	1.923	1.000	1.953	0.832	2.091
150	0.974	1.898	1.000	1.943	0.945	2.305		
200	0.962	2.176	1.000	1.908			0.958	2.063
235							0.979	2.084

It is expected from eqn. (1) that the plot of $(C\Delta E_{HF}^2/i_{HF})^{\frac{1}{2}}$ *vs.* R_{ext} would give a straight line; on the other hand, it is seen from eqn. (3) that the plot of $(C\Delta E_{HF}^2/i_{HF})$ *vs.* R_{ext} should give a straight line. With zinc ion in various concentrations and with a fixed amplitude ($\Delta E_{HF} = 5$ V), the HF wave heights were measured and the results treated by the method of least squares. Analogous measurements and statistical treatment of data were carried out using lead ion as depolarizer and with varying HF amplitudes. The sequence of measurements was completely randomized.

The results are given in Table 3 and Figs. 8 and 9. Application of the *t*-test to the correlation coefficients listed in Table 3 has shown that there is a linear relationship for each plot in Table 3.

Two sets of correlation coefficients shown in Table 3 are now analysed according to the method described by Doerffel[13]. The *k*-value in Table 3 is calculated by

$$k = 1.1513 \sqrt{\frac{(N_1-3)(N_2-3)}{N_1+N_2-6}} \log \frac{(1+r_1)(1-r_2)}{(1-r_1)(1+r_2)}$$

TABLE 3

RESULTS OF REGRESSION ANALYSIS

Electrolysis soln.	*Mathematical expression obtained*[a]	*Correlation coefficient*	*Degree of freedom*	*k-Value*
Zn^{2+} in 1 *M* KCl	$C/i_{HF} = (0.65 \pm 0.03) \cdot 10^{-4} + (10.8 \pm 0.4) \cdot 10^{-7} R_{ext}$	0.948	92	7.50
	$(C/i_{HF})^{\frac{1}{2}} = (8.4 \pm 0.4) \cdot 10^{-3} + (4.8 \pm 0.7) \cdot 10^{-5} R_{ext}$	0.586	92	
Pb^{2+} in 0.5 *M* KNO_3	$C\Delta E_{HF}^2/i_{HF} = (8.42 \pm 0.88) \cdot 10^{-4} + (95 \pm 14) \cdot 10^{-7} R_{ext}$	0.796	28	1.26
	$(C\Delta E_{HF}^2/i_{HF})^{\frac{1}{2}} = (2.8 \pm 0.6) \cdot 10^{-2} + (13 \pm 10) \cdot 10^{-5} R_{ext}$	0.643	28	

[a] C in mM, i_{HF} in mm, ΔE_{HF} in volts, and R_{ext} in ohms.

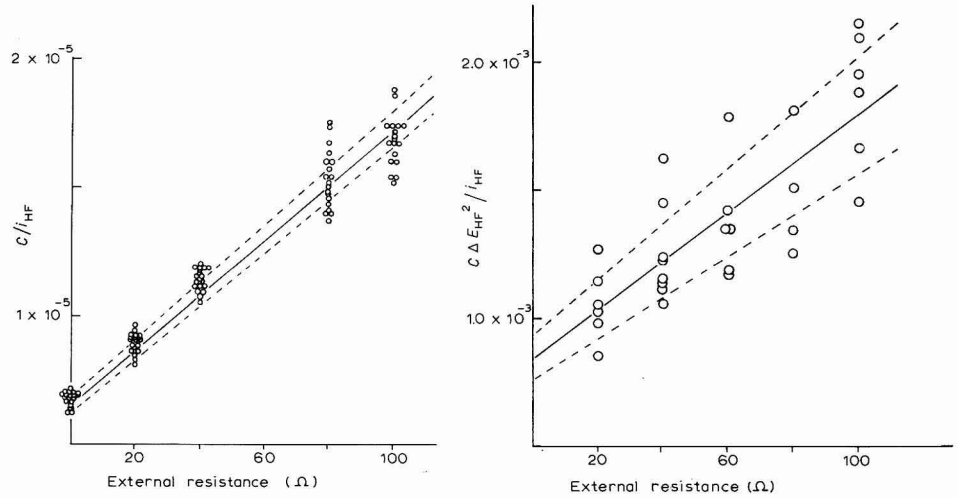

Fig. 8. C/i_{HF} *vs.* R_{ext}. Electrolysis soln., $=2\cdot10^{-5}$–$1\cdot10^{-4}$ *M* Zn^{2+} in 1 *M* KCl (25°); recorder sensitivity, 0.020 μA mm^{-1}; amplifier sensitivity, $\frac{1}{20}$; ΔE_{HF}, 5 V; damping, 1 μF.

Fig. 9. $C\,\Delta E_{HF}^2/i_{HF}$ *vs.* R_{ext}. Electrolysis soln., $2\cdot10^{-5}$–$1\cdot10^{-4}$ *M* Pb^{2+} in 0.5 *M* KNO_3 (25°); ΔE_{HF}, 3, 4 and 5 V; recorder sensitivity, 0.020, 0.040 and 0.060 μA mm^{-1}; amplifier sensitivity, $\frac{1}{10}$; damping, 1 μF.

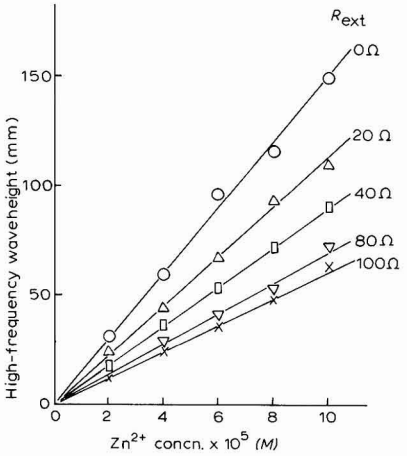

Fig. 10. Calibration curves for Zn(II) in 1 *M* KCl (25°). ΔE_{HF}, 5 V; recorder sensitivity, 0.020 μA mm^{-1}; amplifier sensitivity, $\frac{1}{20}$; damping, 1 μF.

where r_1 and r_2 are the correlation coefficients and N_1 and N_2 are the corresponding number of measurements. There is a significant difference in the coefficients 0.948 and 0.586 observed with zinc ion, since the calculated *k*-value of 7.50 is much larger than 4.00 (99.99% certainty) listed in the Table. The data obtained with lead ion show that eqn. (3) fits better experimentally than eqn. (1), but the theoretical *k*-value for 95% certainty being 1.96, it is impossible to judge whether there is a significant difference between two coefficients of 0.796 and 0.643.

Calibration curve

While the HF polarographic wave height is influenced by the external resistance, the wave height is proportional to the depolarizer concentration provided that the circuit resistance is kept constant. Calibration curves obtained with zinc ion are shown in Fig. 10. It is desirable, however, to maintain the resistances of cell, capillary and lead wire as low as possible for high sensitivity analysis.

SUMMARY

Two expressions as shown by eqns. (1) and (3) are postulated and verified experimentally for the dependencies of the HF polarographic wave height, i_{HF}, on the depolarizer concentration C, the amplitude ΔE_{HF} of the HF pulse, and the external resistance R_{ext}. The statistical analysis of data has shown that eqn. (3) holds more accurately than eqn. (1) (see Table 3). The importance of lowering the circuit resistance in HF polarography is emphasized.

REFERENCES

1 G. C. BARKER, *Trans. Symp. Electrode Processes*, Philadelphia, 1959, edited by E. YEAGER, New York, J. Wiley, 1961, chap. 19.
2 P. DELAHAY, *Advan. Electrochem. Electrochem. Eng.*, 1 (1961) p. 233.
3 B. BREYER AND H. H. BAUER, *Alternating Current Polarography and Tensammetry*, Interscience Publishers, New York, 1963.
4 H. SCHMIDT AND M. VON STACKELBERG, *Die neuartigen polarographischen Methoden*, Verlag Chemie, Weinheim, 1962.
5 S. FURUTANI, *Japan Analyst*, 16 (1967) 103.
6 Y. OSAJIMA, M. NAKASHIMA AND S. FURUTANI, *Japan Analyst*, 16 (1967) 1297.
7 S. FURUTANI AND Y. OSAJIMA, *Nippon Nogei Kagaku Kaishi*, 41 (1967) 145.
8 T. KAMBARA, S. TANAKA AND K. HASEBE, *J. Chem. Soc. Japan, Pure Chem. Sect.*, 88 (1967) 644.
9 G. WOLFF AND H. W. NÜRNBERG, *Z. Anal. Chem.*, 224 (1967) 332.
10 T. KAMBARA AND S. WATARAI, *Bull. Chem. Soc. Japan*, 39 (1966) 521.
11 Y. YASUMORI, M. KUROSAKI AND T. NISHIMURA, *Yakushin-suru Kiki (Yanagimoto Tech. Review)*, 6 (No. 3) (1961) 14.
12 M. SENDA AND I. TACHI, *Bull. Chem. Soc. Japan*, 28 (1955) 632.
13 K. DOERFFEL, *Z. Anal. Chem.*, 185 (1962) 1.

ELECTROANALYTICAL CHEMISTRY AND INTERFACIAL ELECTROCHEMISTRY
Elsevier Sequoia S.A., Lausanne – Printed in The Netherlands

FURTHER STUDIES ON PERIODIC PHENOMENA IN PASSIVATING SYSTEMS

K. S. INDIRA AND S. K. RANGARAJAN
Central Electrochemical Research Institute, Karaikudi (India)
K. S. G. DOSS
India Cements Limited, Madras (India)
(Received October 15th, 1968)

INTRODUCTION

The anodic behaviour of metals makes a fascinating field of study. Amongst the various phenomena that may take place we have: metallographic etching, polishing, roughening, pitting, passivity, porous film formation and formation of flocs, indefinite growth of film proportional to the potential applied, oxygen evolution, formation of higher oxidation products and anode effect. The potentiostatic current–potential curve taken under near steady conditions can be very complicated and considerably differs in form with the electrolyte used; the curve for nickel in sulphuric acid and perchloric acid is given in Fig. 1. Similarly, the galvanostatic potential-time

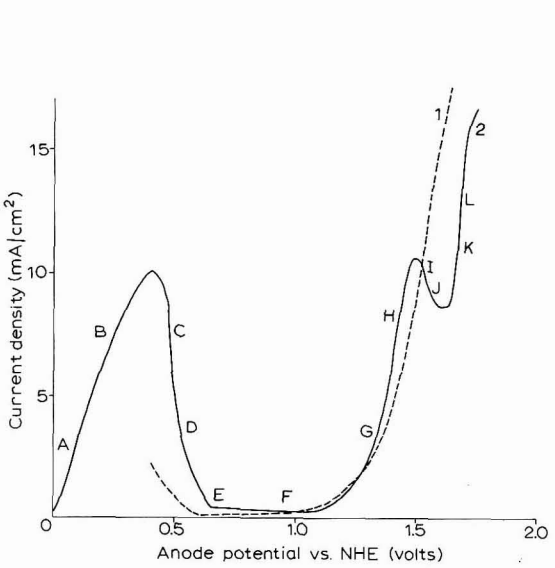

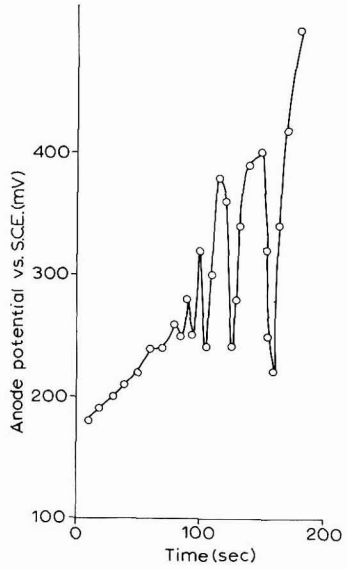

Fig. 1. Potentiostatic current–potential curve for nickel. (1), Anode, nickel wire embedded in araldite with the cross-section exposed; apparent area, 0.0079 cm^2; electrolyte, 0.5 *M* perchloric acid; time given for obtaining stationary conditions, *ca.* 5 min. (2), As (1) with 0.5 *M* sulphuric acid as electrolyte.

Fig. 2. Galvanostatic potential–time curve for silver in hydrochloric acid. Anode, silver wire embedded in araldite with its cross-section exposed; electrolyte; 2 *M* HCl; current density, 10 mA/cm^2.

curve can be exceedingly complicated. The curve obtained for silver in hydrochloric acid[1] is given in Fig. 2; a galvanostatic curve for nickel in sulphuric acid is given in Fig. 3. One striking aspect of the latter curves is the potential oscillations over a period of time. Under controlled galvanostatic conditions, steady oscillations can be obtained for a number of hours[2]. A typical oscillogram for potential oscillations in the nickel–sulphuric acid system is given in Fig. 4. The present paper presents a new

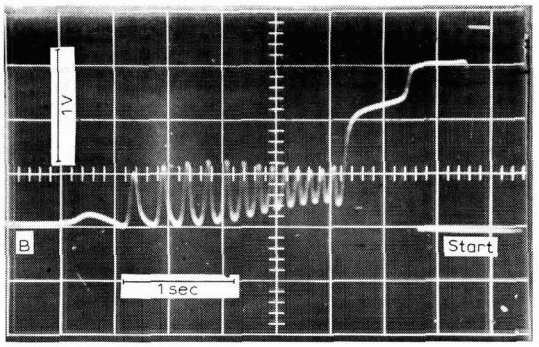

Fig. 3. Galvanostatic potential–time curve for nickel in sulphuric acid. Anode, as in Fig. 1; electrolyte, 50% H_2SO_4; current density, 200 mA/cm^2. The main oscillogram sweep (CDEF) starts 1.5 sec after switching on the current. There is no recognisable change of potential for the first 1.5 sec (*vide* AB).

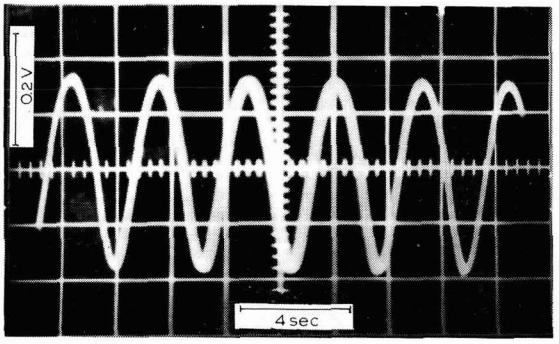

Fig. 4. Potential oscillations in nickel–sulphuric system under galvanostatic conditions. Anode, as in Fig. 1; electrolyte, 0.5 *M* H_2SO_4 + 0.2 *M* $NiSO_4$; pH adjusted to 2.0 ($NiSO_4$ is added to make the system less dependent on fluctuations in nickel ion concn. in solution near the electrode); current density, 10 mA/cm^2.

approach to explain the occurrence of oscillations and comments on the significance of the potentiostatic curve referred to above.

PREVIOUS WORK

Oscillations have been observed in a wide variety of systems and a few that have been discussed in the literature are given in Table 1. Most of the explanations are based on: (a) film formation and dissolution; (b) the exhaustion, followed by

TABLE 1

No.	*Metal system*	*Details*	*Explanation*
1	Silver	KCN	Film formation and dissolution[13] SR mechanism (slow oscillations at lower current density) PNJ mechanism (fast oscillations at high current densities)[1]
2	Silver	HCl	
3	Silver	KCl	Rearrangement in solid film; recrystallisation[14]
4	Silver	KOH	A change in the semi-conducting property of surface oxide layers Development of a genuine electroactive surface and change in the mechanism of electrode reactions[15]
5	Aluminium	lead laurate + 5 p.p.m. Cl^- 0.5 A/cm^2, 25°, 20 osc./min	Creation of "*n*"-type defects[16]
6	Cobalt	40% H_2SO_4	pH changes at the film–solution[17]
7	Cobalt	0.4 *M* CrO_3 + 1 *N* HCl, +0.3 V to −0.2 V, 0.5 osc./sec	Reducibility of CrO_3 depends on the concentration near the electrode[18]
8	Copper	HCl	Film formation and dissolution[19]
9	Copper	HCl	Depletion of H^+ and Cl' followed by replenishment[20]
10	Copper	HCl	Rise of potential due to dearth of H^+ and the fall to dissolution of film[21]
11	Copper	HCl	Convection controlled. Concentration changes in the pores are important [22]
12	Copper	H_3PO_4, 0.65–0.85 V	Formation and dissolution or destruction of oxide film[23]
13	Copper	NaOH	Change in semi-conducting property of surface oxide layers[15]
14	Gold	4 *N* HCl, 1 A/cm^2, 1.8 V, 0.2 osc./sec	pH changes[18]
15	Iron	Na_2SO_4 + NaCl	Connected with differences in c.d. distribution[24]
16	Iron	Sodium borate + NaCl	Oscillations stop on stirring. Reaction product-control[25]
17	Stainless steel	0.1 *N* NaCl, 2 A/cm^2, 30°, 0.1 kc/sec	Diffusion-controlled. Pitting type; c.d. around a pit being different at different times[26]
18	Iron	H_2SO_4, 10^4 osc/sec, 600 c/sec (20°), 4000 c/sec (47°)	Dissolution and formation of film[27]
19	Iron	H_2SO_4, 0.2 A/cm^2, 0.1 osc/sec	pH Changes[18]
20	Nickel	50% H_2SO_4, 35°, 60 mA/cm^2, 12 c/sec	Film formation and O_2 evolution[28]
21	Nickel	1 *N* H_2SO_4	Instability phenomena are described by second-order linear differential equation[29]
22	Nickel	H_2SO_4	Progressive decrease of H^+ concentration in the electrolyte next to the anode; the pH becomes high enough for oxide precipitation and passivity sets in[30]
23	Nickel	H_2SO_4	SR and PNJ mechanisms[2]
24	Tin	NaOH	pH changes[31]
25	Titanium	Formic acid	Film puncturing and simultaneous O_2 evolution[32]
26	Zinc	4 *N* NaOH, 0.2 A/cm^2, $E = -1.1$ V, 0.3 osc/sec	pH changes[18]
27	Zinc	NaOH + silicate	Dielectric breakdown and fresh film formation[33]

replenishment, of acceptor ions; (c) pH changes in the anode film caused by gas evolution leading to alternate dissolution and deposition of film; (d) gas evolution disturbing the stationary diffusion film; (e) periodic dielectric breakdown; and (f) recrystallisation. Explanations (a), (b), (e) and (f) do not indicate the factors that cause the periodicity. Explanations (c) and (d) completely fail where gas evolution is not observed, as for instance the oscillations observed by us (Fig. 2 and 3).

It will be shown later that even the observed association of the dissolution or bubble formation, or the dielectric breakdown, with the oscillations in some of the systems can be interpreted as a result of the SR or PNJ present near the film–solution interface breaking down by the internal field emission, or an avalanche breakdown.

STOICHIOMETRIC REGION FOR SLOW OSCILLATIONS

On the basis of literature reports and our own observations with silver–hydrochloric acid and nickel–sulphuric acid systems, we[1,2] have formulated the following mechanism for passivation and potential oscillations.

Let us first consider a system in which the electrode reaction is mainly, or entirely, the dissolution of the metal. Since we are dealing with high overvoltages (>0.1 V), nucleation would take place all over the metal surface and complications due to differential effects of nucleation and growth[3] do not arise. Also we need not go into the controversy[4] as to whether the film is formed by direct anodic conversion (Thirsk) or by a dissolution–deposition mechanism (Bockris) as it is not relevant to our mechanism.

Let us consider the oscillations in the nickel–sulphuric acid system.

Metals like nickel have a film of oxide (hydrated or otherwise) even when there is no anodic current passing. The oxide film appears[5] before passivity sets in. The anodic process in such a system would consist of a number of successive steps. Ammar and Darwish[6] established that the conduction in such systems is not through any active pores in the film but by a solid state conduction through the film. Three important stages mark the passage of nickel ions into solution are: (i) the entry of the nickel ion from the metal into the solid oxide film; (ii) migration through the oxide film and (iii) transfer to the solution forming the *aquo* or other complex. All these three steps are more or less field–dependent. In the absence of electronic conduction a positive potential on the metal would cause nickel ions to leave the metal and enter the film, forming a non-stoichiometric nickel excess region at the metal–film interface. Simultaneously, some nickel ions in the oxide film would get into solution causing a nickel deficient non-stoichiometric region in the oxide film, near the film–solution interface. These defects would tend to get concentrated in grain boundaries as well as at the dislocation tubes inside the grains. Stoichiometric nickel oxide (even if polycrystalline) is a bad ionic (and a bad electronic) conductor at ordinary temperatures. The (field-produced) non-stoichiometric defect regions however would exhibit high ionic conductivity (this is a well-known phenomenon in silver halide[1]). The positively-charged excess nickel ions would migrate from the metal–film interface towards the solution. Similarly, the negatively-charged cation vacancies (corresponding to nickel deficit) move from the film–solution interface towards the metal. The excess nickel ions and the vacancies would interact on meeting each other and a *stoichiometric region* (SR) may be expected to be formed (Fig. 5). The position of the SR would be

determined by various factors of which the rate of production of nickel ion excess and the vacancies and their rates of migration are significant (we have not taken into account the possibility of conduction by interstitial anions and anion vacancies; it would require further investigation to determine the relative contributions of anions and cations towards the ionic conductivity of the film). The SR would be a badly conducting domain causing a large field in the region. This would lead to tunnelling of electrons from the valence band of nickel oxide on the solution side of the SR to the conduction band of the nickel oxide on the metal side of the SR. The charge on excess nickel ions thus gets partially neutralised by the electrons. Similarly, the holes produced (in the process of tunnelling) on the solution side of the SR partly neutralise the negative charge of cation vacancies. The electrons and holes are perhaps mostly in traps. The SR then builds up further in thickness. A stage is reached when tunnelling of the electron becomes difficult and a further passage of current causes more nickel excess and/or vacancies to be formed on the two sides of the SR. This leads to a strong

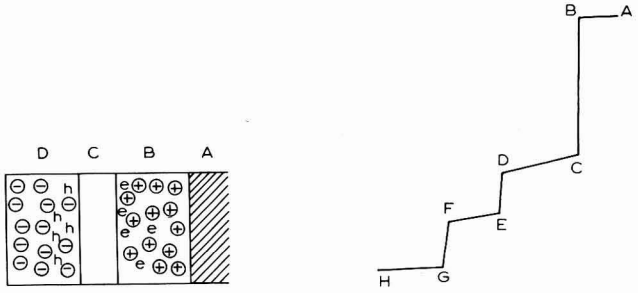

Fig. 5. Picture of the SR in the oxide film. (e), electron; (h), hole; (⊕), excess nickel ion; (⊖), nickel ion vacancy; (A), metal; (B), "nickel ion excess" region; (C), stoichiometric region; (D), "nickel ion deficit" region.

Fig. 6. Schematic diagram for potential drop in the nickel–sulphuric acid system. (AB), potential in metal; (BC), potential drop at the metal–oxide film interface; (CD), potential drop in "nickel ion excess" region; (DE), potential drop in SR; (EF), potential drop in the "nickel ion deficit" region; (FG), potential drop in electric double layer at the film–solution interface; (GH), potential in solution.

field in the SR. The potential drop in the badly conducting domain of the SR is the main cause of rise of potential during the oscillation. A schematic representation of potential drop distribution is given in Fig. 6. When the field reaches a sufficiently high value, internal field emission occurs from the valence band of the nickel oxide on the solution side of the SR to the conduction band of nickel oxide on the metal side of the SR across the SR. This causes a breakdown of the SR, forming highly conducting (because of high defect concentration) filaments. This brings down the potential drop across the SR and the overall potential drop. The SR then again begins to form. The repeated formation and breakdown of the SR is thus the main cause of oscillations.

The dissolution of the film in the electrolyte may take place not only by creation of cation vacancies in the film but also by the direct dissolution of holes (present in the film) giving rise to higher valency *aquo*–nickel ions.

The SR mechanism was further supported by our experiments[2] on the effect

of an additional anode pulse during the oscillation. At the crest where the SR is about to break down, an additional pulse causes a more severe breakdown and the next peak is, therefore, smaller. An additional anodic pulse given at the trough, however, has little effect since the SR is already in the broken-down state.

If the SR is close to the solution–film interface, its formation and breakdown may cause large changes in the structure of the film at the film–solution interface, thereby causing corresponding large changes in the rates of dissolution. The picture given by us is not, however, limited to homogeneous corrosion. The formation and breakdown of the SR may cause preferential attack of metal in grain boundaries on other appropriate types of localised defects in metal. In such cases, the oscillations could as well be associated with the pitting type of corrosion[7].

The observation of Tomashov[8] that a change from an active to passive state can be brought about by passing an extremely small current (insufficient even to cover the apparent surface by a unimolecular layer of oxygen) can be interpreted as follows. The active state is presumably caused by a few conducting filaments across

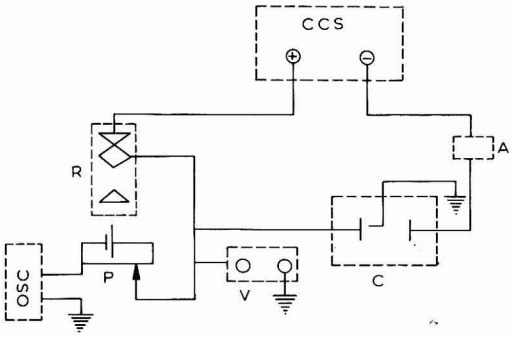

Fig. 7. Experimental set-up for decay studies. (CCS), constant current source: 90-V battery with a high resistance in series; (A), milliammeter; (C), experimental cell having a nickel anode, a platinum cathode and the Luggin capillary of the reference electrode (Hg, Hg_2SO_4, 0.5 *M* H_2SO_4); (V), vacuum tube voltmeter: Philips GM 6020, input impedance 1 MΩ; (R), mercury-wetted relay: OSC Tektronix oscilloscope 531 A, input impedance 1 MΩ.

the SR. As the cross-sectional area of the filaments is only a small fraction of the total surface, the build-up of the SR in the filament would require the passage of a very small amount of electricity. Further experiments are necessary to establish the minimum thickness of oxide film necessary for causing passivation, and the number and cross-section of the conducting filaments, and for substantiating the interpretation given above.

DECAY STUDIES

These experiments on potential decay were carried out on the nickel–sulphuric acid system. The experimental arrangement is given in Fig. 7. Figures 8 and 9 give the decay curves at the crest and trough of the oscillations. The fast decay is 125–130 mV at the crest and 165 mV at trough (the *iR* drop in the electrolyte between the Luggin capillary and the anode is small and does not exceed a few millivolts). There-

fore, the initial drop is *lower* at the crest than at the trough in spite of the potential at the crest being higher by about 300 mV. This phenomenon can be interpreted as follows.

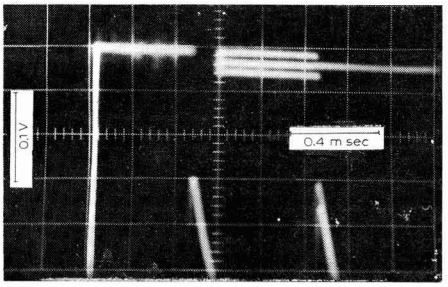

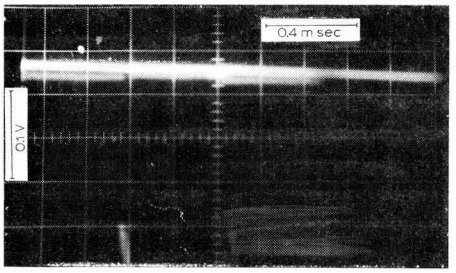

Figs. 8–9. Decay of potential in nickel–sulphuric acid system on cutting off anodising current at the *crest* of the oscillation (Fig. 8) and at the *trough* of the oscillation (Fig. 9), respectively. Anode, electrolyte and current density as in Fig. 4.

The charge separation is mainly across the SR. When the polarising current is cut off, the charges tend to neutralise. This can happen either across the external circuit or through the SR. The resistance of the external circuit (*i.e.*, input impedance of the oscillograph and of the VTVM, each of which is 1 MΩ) is very high. The neutralisation is therefore almost solely across the SR. As the SR is in the broken-down state in the trough of the oscillation, there is a quick neutralisation of charge through the conducting filaments across the SR. A large drop in potential therefore takes place in a short time. At the crest, however, the well-formed badly conducting domain of SR allows a slower neutralisation of charge and therefore much of the drop has a long time of relaxation. *It is also clear from this that the voltage build-up from trough to crest is not due to an increase in iR drop, but to a polarisation having a large time of relaxation.*

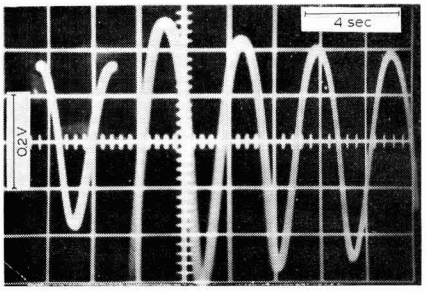

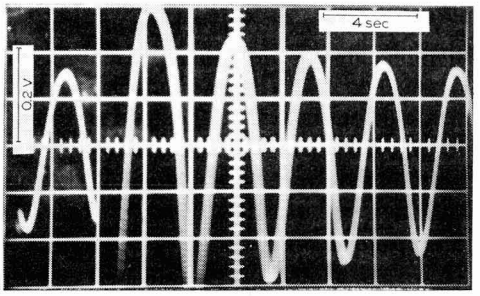

Figs. 10–11. Effect of momentary breaking of the circuit on oscillations. Electrode, electrolyte, current density, as in Fig. 4. Momentary break of circuit at the second trough (Fig. 10) and at the second crest (Fig. 11), respectively.

It is further of interest to examine the effect of momentarily breaking the circuit during the oscillations. Whether this is done at the trough or the crest, the next oscillation is found to have a higher amplitude, as can be seen in Figs. 10 and 11.

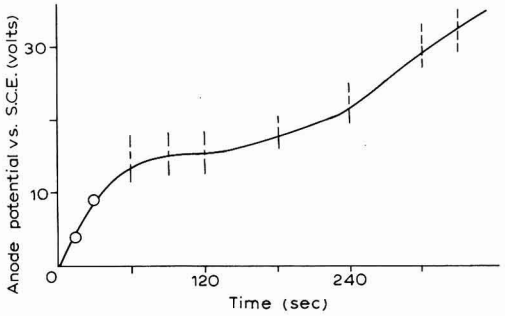

Fig. 12. Fast potential oscillations in silver–hydrochloric acid system under galvanostatic conditions. Anode, as in Fig. 2; electrolyte, 10 *M* HCl; current density, 10 mA/cm^2. Observations of oscillations are recorded at intervals. The dotted lines indicate the amplitude of the potential oscillation as observed at the different times of anodisation.

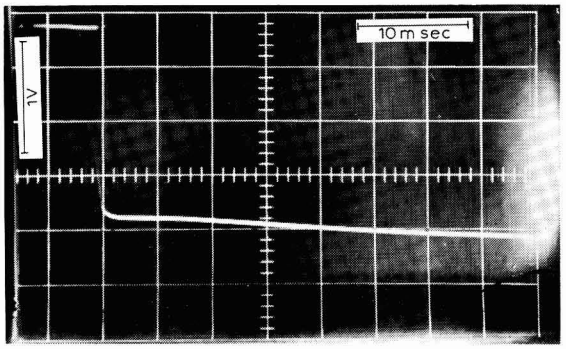

Fig. 13. Decay in a polishing system. Conditions as in Fig. 3; experimental arrangement as in Fig. 7; circuit broken at oxygen evolution potential.

This is due presumably to a better formation of the SR, which offers a higher resistance than that existing under stationary oscillation conditions.

The decay can be very fast if the SR does not exist, as in electropolishing conditions (nickel in 50% H_2SO_4; 200 mA/cm^2). As can be seen in Fig. 13, the whole of the potential drop takes place in less than 0.1 msec. Several seconds would be needed for the decay to occur under passivating conditions where the SR is present (see Fig. 14).

PN JUNCTION (PNJ) MECHANISM FOR HIGH FREQUENCY OSCILLATIONS

We now come to the anodic processes involving electronic conduction in the film. One example (Fig. 12) is the behaviour of Ag–10 *M* HCl[1]. The potential shoots up to as high as 50 V and shows rapid though irregular oscillations (higher than 100 kHz as observed in the oscillograph) of amplitude of 5 V or higher. This continues for several minutes, while the mean potential goes on rising. There is chlorine evolution, showing that electronic conduction is occurring. These can be inter-

preted as follows. The anodic film of silver chloride consists of three regions. Near the metal–film interface we have the silver ion excess region and near the film–solution interface, we have the silver ion deficit region. The SR is formed somewhere between. Under the conditions of the experiment, a good proportion of the associated electrons in the silver ion excess region is in the conduction band, making it an N-type conductor. Similarly, the associated holes in the silver ion deficit region make it the P-type. In between, a badly conducting PN junction (PNJ) can be expected to be formed. There is a considerable potential drop across the PNJ domain. When the field goes beyond a certain limit, the PNJ gets broken down by an avalanche type of breakdown and causes highly conducting filaments to form. This brings down the potential. The PNJ again builds up. The repeated formation and breakdown of the PNJ causes the rapid oscillations.

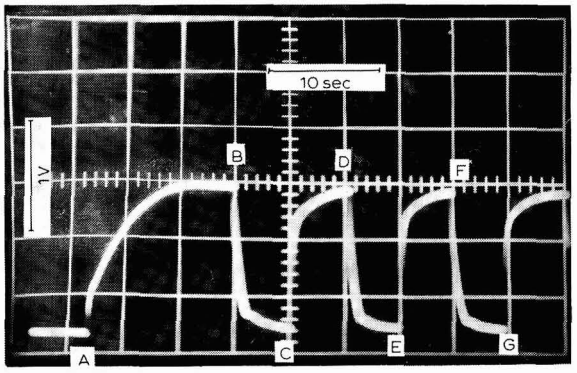

Fig. 14. Build-up and decay curves in a passivating system. Nickel anode as in Fig. 1; electrolyte, 0.5 *M* $NiSO_4$; pH = 3. "On" at A, C, E, G; "Off" at B, D, F.

The PNJ mechanism explains the abnormal transfer coefficients for the Fe^{2+}, Fe^{3+} system at passivated nickel electrodes, observed by Makrides[9], which are connected with the significant changes in PNJ in the film by even small amounts of current passing in the cathodic and anodic directions.

Similarly, if the PNJ is near the film–solution interface, there can be sudden gas evolution during the breakdown of the PNJ. Furthermore, a large breakdown of the PNJ may cause dielectric breakdown in solution causing the anode effect.

INTERPRETATION OF THE POTENTIOSTATIC CURVE

A working hypothesis for interpreting the potentiostatic curve (Fig. 1, curve 2) for nickel in sulphuric acid is now presented.

The first rising portion, AB, shows the nickel ion entry from the metal into the film is the rate-determining step. The curve should rise exponentially, but, in fact, starts falling along CD because a compact film starts building up as the current tends to reach the value necessary for the build-up[5] of the necessary concentration of dissolved Ni (*i.e.*, $NiOH^+$?) near the electrode. The film is mostly a Ni^{2+} excess film. The part covered by the compact film dissolves much more slowly than the bare metal or

the non-compact film and by the mechanism of excess Ni^{2+} in the film entering the solution to meet the acceptor molecules or ions in solution. The horizontal portion, EF, corresponds to the rate of removal of excess Ni^{2+} from a surface completely covered by the excess Ni^{2+} film, and the current is controlled by this step. GH represents the formation of vacancies, and conduction by movement of vacancies which is better than by interstitials. IJ represents formation of a thick SR, and KL the progressive breakdown of the SR. Beyond 1.7 V, electronic conduction causes oxygen evolution.

INTERPRETATION OF THE FORMS OF ANODIC DISSOLUTION

(a) At low overvoltages in suitable etching electrolytes, the dissolution is controlled by the *rate of entry of Ni^{2+} from the metal into the film which is different for grain boundaries and for the different faces of the grains.* This gives metallographic etching.

(b) Under conditions when a *compact solid structureless film* or a *viscous liquid film of electrolyte* forms, the rate of dissolution becomes identical at the hills and valleys and leads to polishing by the Edwards mechanism[10,11].

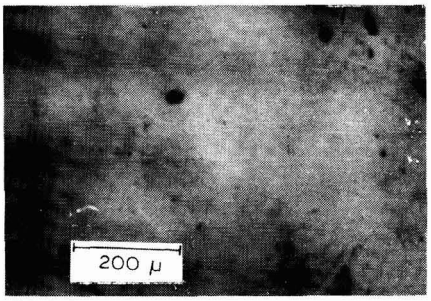

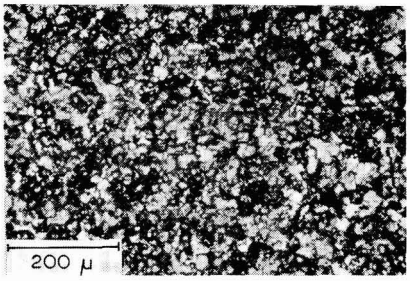

Figs. 15–16. Microphotographs of nickel anodically treated under potentiostatic conditions. Anode, as in Fig. 1; electrolyte, 0.5 *M* H_2SO_4; steady current density, 5 mA/cm^2; time of treatment, 15 min. Potential 1.35 V (Fig. 15) and 0.15 V (Fig. 16).

(Figure 15 is a microphotograph of nickel after it was anodically dissolved at a potential of 1.35 V (NHE) under conditions corresponding to (a) and Fig. 16 gives that dissolved at 0.15 V under conditions corresponding to (b). Both were subjected to the *same current density*. Conditions corresponding to (a) have resulted in etching whereas those in (b) have resulted in polishing. The true current densities no doubt would have been somewhat different, but the results would not be different even at equivalent true current densities.)

(c) Polishing can also be obtained *by a reversible unimolecular adsorption film* of an addition agent, the dissolution taking place through the adsorption-free sites which go on changing with time and statistically produce a uniform dissolution at hills and valleys. Since in polishing, the hills and valleys to be levelled out are numerous and are of very small magnitude, *field-controlled preferential dissolution of hills does not occur to any large extent.*

(d) If the film present is a thick solid film having a *coarse structure* of its own, the dissolution is patterned on the structure of the solid film and this leads to roughening.

(e) Passivity is caused by a film which has an extremely low ionic conductance which may, nevertheless, be sufficiently electronically conducting.

(f) Porous films and flocks are formed by *fast creation of vacancies by acceptor ions or molecules.* The porous film may bring down convection and help the formation of the compact film.

(g) Ions such as Cl^- *may replace* O^{2-} in the oxide film and would induce more of the cation vacancies (to bring about electroneutrality) and cause higher ionic conduction and enhance the corrosion. They may also act as good acceptor ions to remove cations from the oxide film or the metal.

(h) The oscillations may be associated with pitting if the metal shows gross heterogeneity in the initial solution processes. Once the dissolution is localised for a short time, the chloride ions may accumulate in the solid film near the spot and make it easier for anion transport and hence accentuate the dissolution at this point, causing the pitting.

(i) Indefinite growth of film is ensured in a *film full of electron and hole traps* so that electronic conduction becomes impossible.

(j) Electronically conducting films would cause oxygen evolution.

(k) A sudden breakdown of a PNJ near the film–solution interface could cause the anode effect.

CONCLUSION

We have shown in an earlier paper that the remarkable reversibility of the calomel electrode and the systematic variation of the thermodynamic properties of the solid halides of mercury and silver in contact with aqueous solutions having varying concentrations of halide ions, are caused by solid-state effects[12]. Future progress in the study of passivity and even some cathodic processes is intimately bound up with a clearer understanding of solid-state effects in the films formed on the electrodes.

SUMMARY

The SR and PNJ mechanisms of Indira and Doss for explaining potential oscillations in galvanostatic systems have been described. Additional evidence, based on decay studies, in favour of the mechanism has been presented. The SR is shown to give a good picture of passivity and is also useful for explaining the abnormal behaviour of passivated nickel electrodes, and how an apparent coverage of even a fraction of the metal surface by oxygen atoms can cause passivity. A working picture has been given to the potentiostatic curve for nickel in sulphuric acid, on the basis of the SR. The mechanism of various forms of anodic dissolution and related phenomena is discussed in relation to SR and PNJ.

REFERENCES

1 K. S. INDIRA AND K. S. G. DOSS, *Proceedings of Symposium on Electrode Processes*, Jodhpur University, Jodhpur, India, 1966, pp. 7–16.
2 K. S. INDIRA AND K. S. G. DOSS, *Proc. Indian Acad. Sci.*, A, 66 (1967) 69–76.
3 H. GERISCHER, *Anal. Chem.*, 31 (1959) 39; B. E. CONWAY AND J. O'M. BOCKRIS, *Electrochim. Acta*, 3 (1961) 340.
4 J. O'M. BOCKRIS, A. K. N. REDDY AND B. RAO, *J. Electrochem. Soc.*, 113 (1966) 1142.
5 J. O'M. BOCKRIS, A. K. N. REDDY AND B. RAO, *J. Electrochem. Soc.*, 113 (1966) 1139.
6 I. A. AMMAR AND S. DARWISH, *Electrochim. Acta*, 11 (1966) 1541.
7 K. S. RAJAGOPALAN, K. VENU AND M. VISWANATHAN, unpublished data.
8 N. D. TOMASHOV, *Corrosion Sci.*, 4 (1964) 315.
9 A. C. MAKRIDES, *J. Electrochem. Soc.*, 113 (1966) 1158, 1162.
10 K. S. G. DOSS, K. S. INDIRA, K. VIJAYALAKSHMI AND B. A. SHENOI, *Bull. Acad. Polon. Sci. Ser. Sci. Chim.*, 8 (1960) 629–633.
11 J. EDWARDS, *J. Electrochem. Soc.*, 100 (1953) 223 C.
12 K. S. INDIRA AND K. S. G. DOSS, *Current Sci. India*, 36 (1967) 145–147.
13 L. I. GILBERTSON AND O. M. FORTNER, *J. Electrochem. Soc.*, 81 (1942) 199.
14 H. LAL, H. R. THIRSK AND W. F. K. WYNNE-JONES, *Trans. Faraday Soc.*, 47 (1951) 70, 999.
15 V. N. FLEROV, *Zh. Fiz. Khim.*, 37 (1963) 1243–50.
16 M. J. PRYOR, *Z. Elektrochem.*, 62 (1958) 782.
17 E. S. HEDGES, *J. Chem. Soc.*, (1926) 2878.
18 U. F. FRANCK, *Z. Elektrochem.*, 62 (1958) 649–55.
19 J. H. BARTLETT, *J. Electrochem. Soc.*, 87 (1945) 521.
20 E. S. HEDGES, *J. Chem. Soc.*, (1926) 1533; (1929) 1029.
21 K. F. BONHOEFFER AND H. GERISCHER, *Z. Elektrochem.*, 52 (1948) 24.
22 R. S. COOPER AND J. H. BARTLETT, *J. Electrochem. Soc.*, 105 (1958) 109.
23 V. A. DMITRIYER AND E. V. RZHEVSKAYA, *Zh. Fiz. Khim.*, 35 (1961) 871.
24 A. RINS AND R. LIZARBE, *Electrochim. Acta*, 7 (1962) 513.
25 K. VENU AND K. S. RAJAGOPALAN, unpublished data.
26 I. L. ROSENFELD AND I. S. DANILOV, *Corrosion Sci.*, 7 (1967) 129.
27 Y. TORIGOE, *Denki Kagaku*, 35 (1967) 206.
28 T. P. HOAR AND J. A. S. MOWAT, *Nature*, 165 (1950) 64.
29 J. OSTERWALD AND H. G. FELLER, *J. Electrochem. Soc.*, 107 (1960) 473; *Electrochim. Acta*, 7 (1962) 523.
30 T. P. HOAR, *J. Electrochem. Soc.*, 99 (1952) 275.
31 A. M. SHAMS EL DIN AND F. M. ABD EL WAHAB, *Electrochim. Acta*, 9 (1964) 883.
32 A. R. PIGGOTT, H. LECKIE AND L. L. SHREIR, *Corrosion Sci.*, 5 (1965) 165.
33 L. L. GRUSS AND W. MCNEILL, *Electrochem. Tech.*, 1 (1963) 283.

ELECTROANALYTICAL CHEMISTRY AND INTERFACIAL ELECTROCHEMISTRY
Elsevier Sequoia S.A., Lausanne – Printed in The Netherlands

EIN VERFAHREN ZUR SYNCHRONISATION POLAROGRAPHISCHER MESSVORGÄNGE MIT DER TROPFZEIT

GÜNTER WILLEMS UND ROLF NEEB
Institut für Anorganische Chemie und Kernchemie, Johannes Gutenberg-Universität, Mainz (Deutschland)
(Eingegangen am 4. November, 1968)

EINFÜHRUNG

Vielfach ist bei polarographischen Untersuchungen eine Synchronisation von Schaltvorgängen mit der Tropfzeit notwendig. Die Synchronisationsverfahren lassen sich in zwei Gruppen einteilen. Einmal wird der Tropfenabfall durch mechanisches Abklopfen[1-4], einen elektrischen Stromstoss[4,5] oder einen Druckimpuls[6] erzwungen. Der Tropfenabfall wird hier von einem periodischen Programm selbst bestimmt. Bei einer anderen Gruppe von Verfahren liefert der freie Tropfenabfall das Startsignal zum Ablauf des Programms. Das Startsignal wird auf elektroakustischem[7], auf photoelektronischem[8-10] Wege oder aus dem sprunghaften Stromabfall[11,12] oder Impedanzwandel[13-22] beim Tropfenabfall erhalten.

Das von uns vorgeschlagene Verfahren benutzt ein natürliches Synchronisationssignal der polarographischen Zelle, das beim Tropfenabfall zwischen Tropf- und Vergleichselektrode auftritt (siehe Abb. 1). Diese negativen Spannungssprünge sind in der Literatur bereits mehrfach beschrieben[23-25], ohne aber bisher zu Synchronisationszwecken ausgenutzt zu werden. Die Spannungssprünge können mit Hilfe der Deutung der Potentiale von Metallen in eigenionenfreien Lösungen erklärt werden[26,29].

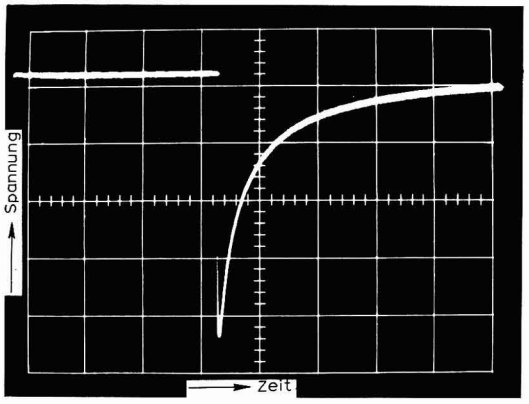

Abb. 1. Spannung einer polarographischen Zelle bei Tropfenabfall in Abhängigkeit von der Zeit. Keine äusseren Spannungen oder Ströme angelegt. Grundelektrolyt: 1.2 *N* HCl; X-Ablenkung: 200 msec/cm (Raster = 1 cm); Y-Ablenkung: 50 mV/cm; Eingangswiderstand des Oszillographen (= Zellaussenwiderstand): 10 MΩ; Niveauhöhe: 650 mm; Kapillare: 0.05 mm ∅; Tropfzeit in 1 *N* KCl bei offener Zelle: 3.1 sec.

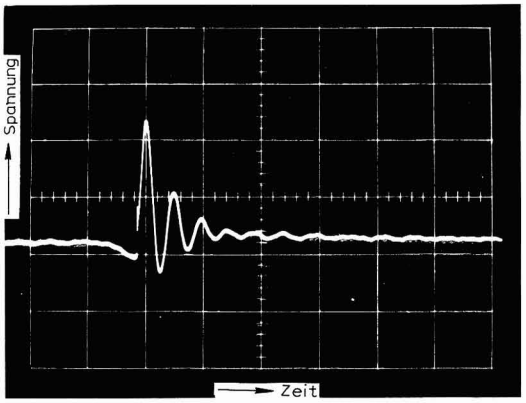

Abb. 2. Spannungsverlauf an einer Stationärelektrode (stehende Extrusionselektrode nach Lit.[30]) bei Abstreifen mit mechanischem Abstreifer. Keine äusseren Spannungen oder Ströme angelegt. Grundelektrolyt: 1.2 *N* HCl; Oszillograph: X-Ablenkung 100 msec/cm, Y-Ablenkung 10 mV/cm; Eingangswiderstand (= Zellaussenwiderstand) 10 MΩ; Kapillare: 0.5 mm ∅; Tropfengrösse: 0.9 mm ∅.

Streift man den Tropfen einer stationären Quecksilberelektrode (stehende Extrusionselektrode nach Lit.[30]) mit Hilfe eines mechanischen Abstreifers[31] ab, so erhält man einen schwingungsförmigen Spannungsverlauf (siehe Abb. 2) ohne die deutliche Spannungsspitze* der Abb. 1. Einen Spannungsimpuls, ähnlich der Abb. 1, erhält man jedoch bei der Neubildung des Tropfens an der Stationärelektrode, wobei die Höhe des Spannungsimpulses mit der Bildungsgeschwindigkeit des Tropfens ansteigt (vergl. im folgenden die Abhängigkeit des Spannungsimpulses von der Niveauhöhe). Die Entstehung der Impulse ist also ursächlich mit der Neubildung der Elektrodenoberfläche verknüpft. Die Schwingungsfrequenz bei Abstreifen an der Stationärelektrode (vergl. Abb. 2) stimmt nicht überein mit den bei Tropfkapillaren gleichen Durchmessers beim Tropfenabfall auftretenden Frequenzen[23,24,32,33]. Wahrscheinlich handelt es sich bei der beobachteten Schwingung an der Stationärelektrode um eine Säulenschwingung des Quecksilbers in der Kapillare. Eine in Abb. 2 erkennbare höhere Schwingungsfrequenz ist vermutlich Oberflächenschwingungen zuzuordnen, die an Quecksilbertropfelektroden beobachtet werden und die bei höherer Auflösung auch in Abb. 1 zu erkennen sind.

Die Höhe des Spannungssprunges (vergl. Abb. 1) hängt von der Art des Anions und des Kations der Grundlösung ab[28]. Die meist nicht zu vermeidende Anwesenheit geringster Spuren von Depolarisatoren (z.B. Sauerstoff, Quecksilberionen) führt zu einer Dämpfung und einem Abklingen des ursprünglich bei Tropfenabfall auftretenden Spannungssprunges, aus dem dadurch der in Abb. 1 gezeigte Spannungsimpuls entsteht. Ein Aussenwiderstand an der polarographischen Zelle vermindert ebenfalls die Impulshöhe (siehe Abb. 3). Ebenso wirkt sich die Zunahme der Tropfzeit (Verringerung der Quecksilberniveauhöhe) aus (siehe Abb. 4).

* Der kleine negative Anstieg unmittelbar nach Abstreifen, in Abb. 2 links zu erkennen, stellt möglicherweise einen geringfügigen Potentialanstieg gleicher Art wie in Abb. 1 dar. Es ist denkbar, dass beim Abstreifvorgang kurzzeitig ähnliche Verhältnisse herrschen wie beim frisch heranwachsenden Tropfen an der Tropfkapillare.

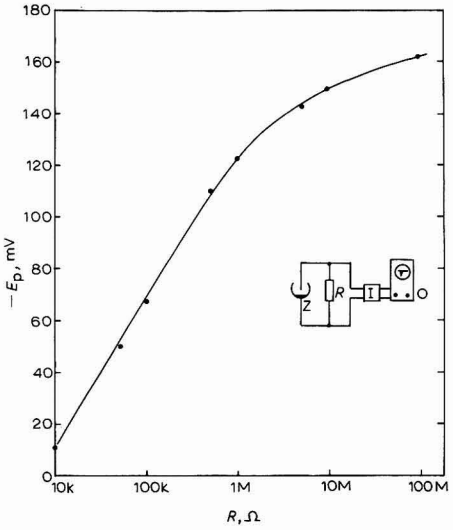

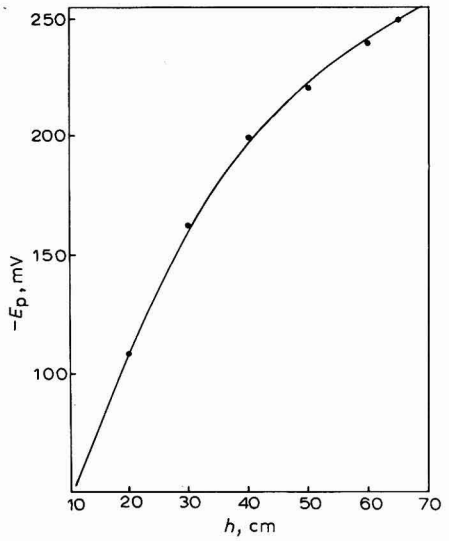

Abb. 3. Abhängigkeit der Höhe der Spannungsspitze vom Aussenwiderstand R. Grundelektrolyt: 1.2 *N* HCl; Kapillare: wie Abb. 1, jedoch Niveauhöhe 40 cm. (E_p), Spitzenhöhe; (Z), Zelle; (I), Impedanzwandler (Eingangswiderstand $10^{10}\Omega$); (O), Oszillograph.

Abb. 4. Abhängigkeit der Höhe E_p, der Spannungsspitze von der Quecksilberniveauhöhe *h*. Grundelektrolyt 1.2 *N* HCl; Zellaussenwiderstand 10 MΩ; Kapillare wie Abb. 1.

BESCHREIBUNG DER ANORDNUNG

Die von uns vorgeschlagene Synchronisationsmethode ist für polarographische und voltammetrische Verfahren geeignet, die die Polarisationsspannung(en) während des Tropfenabfalles abschalten (siehe z.B. Lit.[34]). Dabei entlädt sich die Doppelschichtkapazität der Elektrode infolge stets vorhandener Depolarisatorspuren (Quecksilberionen)* oder äusserer Widerstände, was zu einem zeitlichen Abfall der an der Elektrode vorhandenen Spannung führt. Die am Tropfen bei Tropfenabfall noch auftretende "Restspannung" beeinflusst auch die in Abb. 1 gezeigten Spannungsimpulse. Im allgemeinen wird bei steigender Restspannung die Höhe des in Abb. 1 gezeigten Spannungsimpulses geringer. Soll der Abschaltzeitpunkt der Pola-

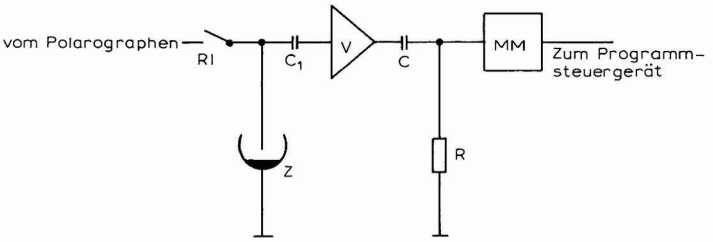

Abb. 5. Prinzipanordnung der Pulsformerstufe. (RI), Relais; (Z), Polarographische Zelle; (V), Verstärker; (MM), Monovibrator.

* Vergleiche Coulostatische Analyse[35].

risationsspannung dicht (z.B. 50 msec) an den Tropfenabfall gelegt werden, so kann die dann noch hohe Restspannung stören. Es zeigte sich, dass die Verkleinerung der Restspannung durch einen Zellaussenwiderstand günstig ist, obwohl dieser auch den Spannungsimpuls dämpft (vergl. Abb. 3).

Das Prinzipschaltbild einer Anordnung, die aus dem Zellsignal einen Synchronisationsimpuls bildet, zeigt Abb. 5. Relais Rl schaltet, vom Programmgerät* gesteuert, die Polarisationsspannungen. Das Zellsignal (Abb. 1) gelangt über C_1 auf den Verstärker V. Die verstärkte Anstiegsflanke des Signals erzeugt am Differenzierglied CR eine scharfe Spitze, deren Vorderflanke am Monovibrator einen Rechteckimpuls auslöst, der das Programmsteuergerät startet.

Bei polarographischen Verfahren mit angelegter Wechselspannung können Störungen auftreten, da Wechselspannungen (ausreichender Amplitude) kurz vor dem Abschalten noch Synchronisationssignale verursachen, die das Programmsteuergerät sofort wieder starten. Auch wäre der Verstärker bei grossen Wechselspannungsamplituden übersteuert. Weiterhin ist es günstiger, die Anordnung während der Messvorgänge von der Zelle zu trennen. Legt man den Verstärker V an einen Ruhekontakt des Relais Rl, so lassen sich die genannten Störungen umgehen. Die Anordnung wird jedoch etwas komplizierter, da das Verbinden des Verstärkers V mit der jeweiligen Restspannung der Zelle einen steilen negativen Impuls darstellt, der ein

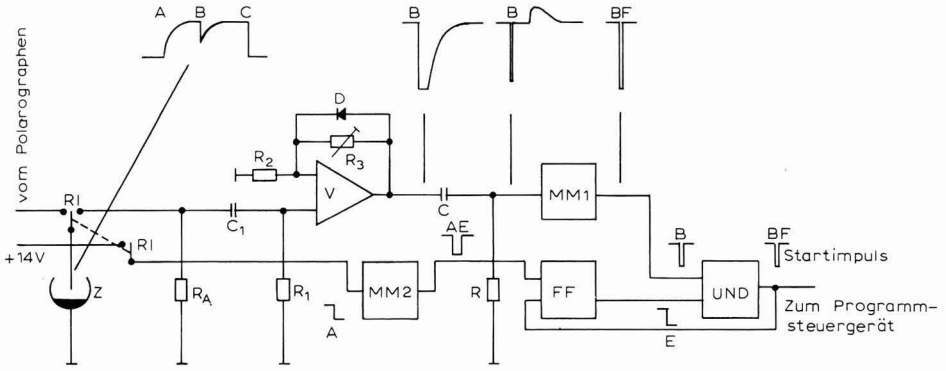

Abb. 6. Blockschaltbild der Pulsformerstufe mit Verzögerungskreis. (A), Abschalten der Gleichspannung; (B), Vorderflanke des Synchronimpulses; (C), Einschalten der Gleichspannung; (E), Ende Verzögerungsimpuls; (F), Ende Synchronimpuls (richtet sich nach Programmsteuergerät). Inverterstufen sind im Blockschaltbild weggelassen. (V), Verstärker Philbrick P85 AU, (Rl), Relais Clare International N.V. Typ HG 2A–1003; (R_a), 470 k; (R_1), 470 k; (R_2), 68 Ω; (R_3), Trimmpotentiometer 20 k; (R), 1.5 k; (C_1), 30 nF; (C), 220 nF; (D), OA 95.

Synchronisationssignal erzeugt. Die in Abb. 6 gezeigte Anordnung vermeidet dies durch einen Verzögerungskreis: über einen zweiten Kontakt des Relais Rl wird bei Abschalten der Gleichspannung eine monostabile Kippstufe MM2 angesteuert, die einen Rechteckimpuls liefern muss, der länger ist als die Schaltzeit des Relais und die Pulsdauer von MM1 zusammen. Die Rückflanke dieses von MM2 gelieferten

* Das verwendete Programmsteuergerät arbeitet digital mit Quarz-Zeitbasis und vier beliebig kombinierbaren Zeitvorwahlen.

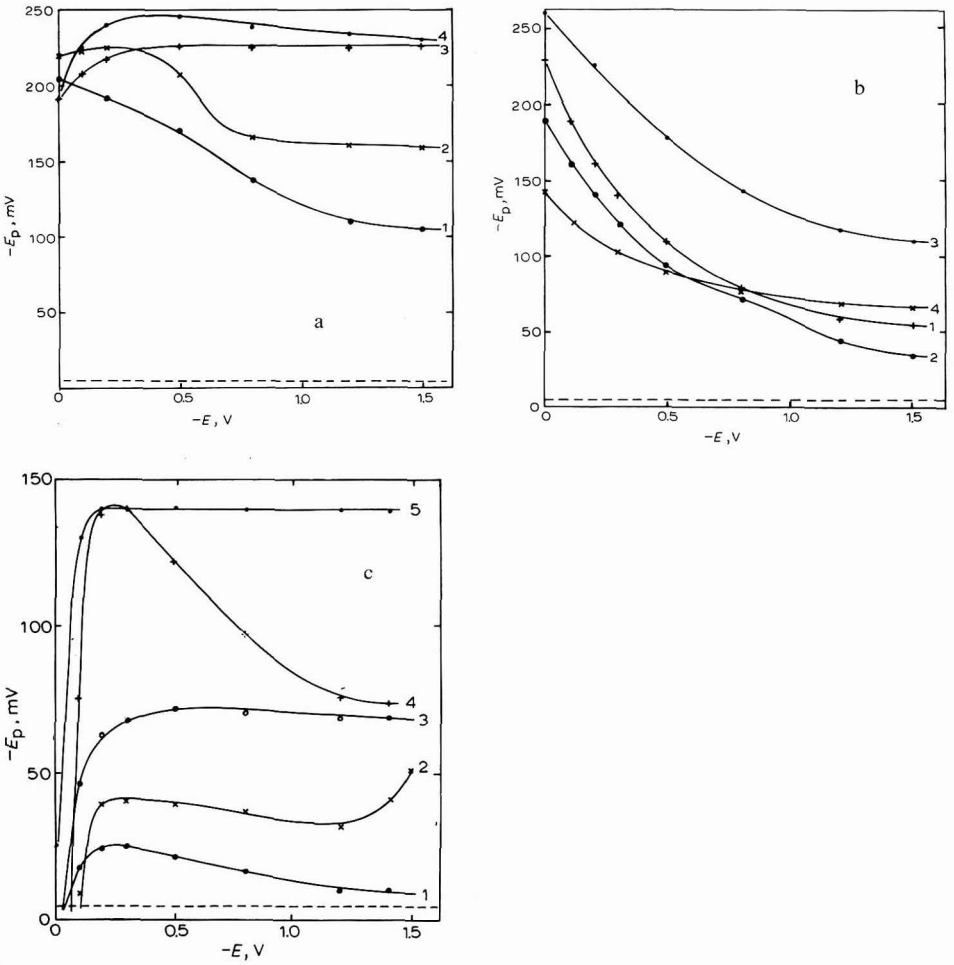

Abb. 7. Abhängigkeit der Höhe E_p, der Spannungsimpulse von der Vorpolarisationsspannung E. Schaltintervall der Gleichspannung: 0.5–3 sec nach Tropfenbeginn eingeschaltet. Kapillare: 0.05 mm ∅, Tropfzeit: 3.5 sec in 1 *M* KCl bei unbelasteter Zelle, Niveauhöhe 52 cm Zellaussenwiderstand R_a (vergl. Abb. 6.) $= \infty$. Messung mit Oszillograph (vergl. Abb. 1). (– – –), Empfindlichkeitsgrenze der Anordnung.
(a) Einfluss des Entlüftens auf die Spannungsimpulse. Entlüftung 5 min bei -0.1 V mit nachgereinigtem Stickstoff. (1), 2 *M* $HClO_4$, entlüftet; (2), 1.2 *M* HCl, entlüftet; (3), 1.2 *M* HCl, nicht entl.; (4), 2 *M* $HClO_4$, nicht entl. (b) Spannungsimpulse in entlüfteten Salzlösungen. (1), gilt angenähert für: $AlCl_3$(2.4 *M*), $MgCl_2$(2 *M*), $CaCl_2$(bei 20° gesättigt), $Ca(NO_3)_2$(4 *M*), $MgSO_4$(2.6 *M*), $NaCH_3COO$(1 *M*). (2), $NaNO_3$(7.1 *M*); (3), $(NH_4)_2SO_4$(3.6 *M*); (4), K_2CO_3(0.1 *M*). (c) Einfluss von Komplexbildnern auf den Spannungsimpuls. (1), 1 *M* Na-Tartrat/2 *M* NaOH; (2), 0.1 *M* Titriplex III/2 *M* NaOH; (3), 0.2 *M* K-Oxalat/2 *M* NH_4OH; (4), 1 *M* KBr; (5), 1 *M* NH_4Cl/1 *M* NH_4OH. Gegenelektrode bei allen Versuchen: Ag/AgCl.

Impulses öffnet über ein Flipflop FF ein Tor des UND-Gates. Erst dann kann ein auf den Verstärker V gelangendes Signal am Ausgang des UND-Gates ein Synchronisationssignal erzeugen, dessen hintere Flanke das Flipflop zurückstellt. Diode D über dem Verstärker verhütet, dass positive Impulse die Anordnung ansteuern.

EIGENSCHAFTEN DES SYNCHRONISATIONSVERFAHRENS

Das Synchronisationsverfahren bewährte sich in vielen Grundlösungen. Der Verstärker V (vergl. Abb. 5) wurde so ausgelegt, dass ein Spannungssprung (vergl. Abb. 1) von 5 mV noch zur Ansteuerung ausreichte. Im allgemeinen sind die Spannungssprünge bei Tropfenabfall sehr viel grösser (siehe Abb. 7).

Für viele mineralsalzhaltige, entlüftete Lösungen ist die Abhängigkeit des Spannungsimpulses E_p von der Vorpolarisationsspannung E ähnlich (siehe Kurve 1 in Abb. 7b). In nichtentlüfteten Lösungen zeigen die Kurven einen etwas anderen Verlauf (siehe Abb. 7a). Die Abnahme der Spannungsimpulse zu negativerer Vorpolarisation E hin ist wegen der Zunahme der Restspannung verständlich, jedoch sind auch die Änderung der Tropfzeit, nachdem das Polarisationsintervall konstant gehalten wurde, und der Gang der Doppelschichtkapazität mit E von Einfluss auf die Restspannung. Dies mag erklären, warum nicht alle Kurven der Abb. 7 nach negativeren Potentialen hin abfallen.

Depolarisatoren vermögen oberhalb ihres Abscheidungspotentials die Spannungsspitze zu dämpfen. In Kupfer-, Cadmium-, Wismut- und Bleilösungen arbeitete das Verfahren jedoch bis zu Konzentrationen von 10^{-3} M einwandfrei. Zur Bestimmung so hoher Depolarisationskonzentrationen sind synchronisierte Messvorgänge meist nicht erforderlich. Die Dämpfung durch Depolarisatoren zeigt sich auch im Gebiet der Quecksilberauflösung (vergl. Abb. 7). In nichtentlüfteten Lösungen (vergl. Abb. 7a) tritt deshalb bei kleinen negativen Vorspannungen E ein Abfall der Spannungsspitze auf. Gleichzeitig erhält man in solchen Lösungen im negativeren Gebiet eine Stabilisierung der Spannungsspitze, da die Restspannung durch den Depolarisatorgehalt verkleinert wird.

Lösungen von Komplexbildnern, die die Quecksilberauflösung in negativere Bereiche verschieben, zeigen eine starke Dämpfung der Spannungsimpulse, so dass das Verfahren gelegentlich bei positiveren Potentialen versagt. Dies tritt ein, sobald eine Kurve die Empfindlichkeitsgrenze (5 mV – gestrichelte Linie in Abb. 7) der Anordnung unterschreitet. In Gebieten so starker Quecksilberauflösung ist auch die Bestimmung anderer Elemente gestört, sodass dies keine Einschränkung des Verfahrens bedeutet.

Tenside, wie Eulan NK, Sulfetal K90, Triton X 100, können in höheren Konzentrationen (0.1% und mehr) die Spannungsspitze in manchen Potentialbereichen ungünstig beeinflussen. Bei den analytisch angewandten, kleineren Konzentrationen (vergl. z.B. Lit.[36]) reichte jedoch die Spannungsspitze zur Synchronisation aus.

Das von uns vorgeschlagene Synchronisationsverfahren benötigt keinerlei (eventuell störende) Hilfsspannungen oder Hilfsströme zur Feststellung des Tropfenabfalles.

Über das Tropfzeitverhalten der frei tropfenden Elektrode bei synchronisierten Schaltprogrammen wird in einer späteren Arbeit berichtet.

Die vorliegende Arbeit wurde in dankenswerter Weise durch Mittel der Deutschen Forschungsgemeinschaft und des Verbandes der Chemischen Industrie ermöglicht.

ZUSAMMENFASSUNG

Eine Anordnung zur Synchronisation von Schaltprogrammen mit der Tropfzeit der Quecksilbertropfelektrode mit Hilfe eines natürlichen Signals der polarographischen Zelle wird beschrieben. Das Signal wird bei offener Zelle, ohne Anschluss äusserer Spannungen oder Ströme erhalten. Einflüsse von Grundlösungen, Depolarisatoren, Tensiden und Komplexbildnern auf das Zellsignal werden untersucht.

SUMMARY

An arrangement for the synchronisation of a switching programme with the drop-time of a dropping mercury electrode using the natural signals of the polarographic cell is described. The signal is from the open cell circuit without recourse to any external potential or current. The effect of base electrolyte, depolarisers, surfactants and complex formation on the cell signal has been investigated.

LITERATUR

1 P. O. KANE, *J. Electroanal. Chem.*, 11 (1966) 276.
2 H. W. NÜRNBERG UND G. WOLF, *Chem.-Ing.-Tech.*, 37 (1965) 977.
3 S. WOLF, *Angew. Chem.*, 72 (1960) 449.
4 L. AIREY UND A. A. SMALES, *Analyst*, (1950) 287.
5 A. SEVCIK, *Collection Czech. Chem. Commun.*, 13 (1948) 349.
6 O. NESVADBA, *Proc. Intern. Congr. Polarography 1st, Prague*, III (1951) 758.
7 G. HAUCK, *Dissertation*, Universität Bonn, 1955.
8 J. RIHA, *Advances in Polarography*, Vol. I, edited by I. S. LONGMUIR, Pergamon Press, London, 1960, 210.
9 P. CORBUSIER UND L. GIERST, *Anal. Chim. Acta*, 15 (1956) 254.
10 H. P. RAAEN UND H. C. JONES, *Anal. Chem.*, 34 (1962) 1994.
11 E. C. SNOWDEN UND H. T. PAGE, *Anal. Chem.*, 22 (1950) 969.
12 L. MEITES UND J. STURTEVANT, *Anal. Chem.*, 24 (1952) 1183.
13 S. SATHYANARAYANA, *Indian J. Chem.*, 2 (1964) 474.
14 G. C. BARKER UND L. L. JENKINS, *Analyst*, 77 (1952) 685.
15 W. A. BROCKE UND H. W. NÜRNBERG, *Z. Instr.*, 75/9 (1967) 291.
16 G. C. BARKER UND A. W. GARDNER, *AERE-Report C/R 2297*, 1958.
17 H. KRONENBERGER, H. STREHLOW UND A. W. ELBEL, *Polarograph. Ber.*, 5 (1957) 62.
18 B. KASTENING, *Ber. Bunsenges. Physik. Chem.*, 68/10 (1964) 979.
19 M. BECKER UND G. KÖHLER, *Ber. Bunsenges. Physik. Chem.*, 67/7 (1963) 690.
20 B. NYGARD, E. JOHANSSON UND J. OLOFSSON, *J. Electroanal. Chem.*, 12 (1966) 564.
21 R. C. PROBST UND M. H. GOOSEY, *Anal. Chem.*, 36 (1964) 2383.
22 J. W. HAYES, D. E. LEYDEN UND C. N. REILLEY, *Anal. Chem.*, 37 (1965) 1445.
23 R. I. NEWCOMBE UND D. A. JENKINS, *Proc. Australian Conf. Electrochemistry 1st, 1963*, Herausgegeben von J. A. FRIEND UND F. GUTMANN, Pergamon Press, London, 1965, S. 743.
24 R. I. NEWCOMBE UND R. WOODS, *Advances in Polarography*, Vol. II, Herausgegeben von I. S. LONGMUIR, Pergamon Press, London, 1960, S. 482.
25 R. I. NEWCOMBE UND R. WOODS, *Trans. Faraday Soc.*, 457 (1961) 130.
26 K. VETTER, *Elektrochemische Kinetik*, Springer-Verlag, Berlin, Göttingen, Heidelberg, 1961, S. 79ff.
27 H. I. OEHL UND H. STREHLOW, *Z. Physik. Chem. N.F.*, 4 (1955) 89.
28 T. ERDEY-GRUZ UND P. SZARVAS, *Z. Physik. Chem.*, 177 (1936) 277.
29 H. I. OEHL UND H. STREHLOW, *Naturwiss.*, 39 (1952) 478.
30 R. NEEB, *Z. Anal. Chem.*, 171 (1959) 321.
31 R. NEEB UND D. SAUR, *Z. Anal. Chem.*, 222 (1966) 200.
32 R. DOPPELFELD UND M. VON STACKELBERG, *Collection Czech. Chem. Commun.*, 25 (1960) 2958.

33 R. C. KAYE, *Trans. Faraday Soc.*, 60 (1964) 584.
34 G. WOLFF UND H. W. NÜRNBERG, *Z. Anal. Chem.*, 224 (1967) 332.
35 P. DELAHAY, *Anal. Chem.*, 34 (1962) 1267.
36 R. NEEB, *Z. Anal. Chem.*, 222 (1966) 291.

ELECTROANALYTICAL CHEMISTRY AND INTERFACIAL ELECTROCHEMISTRY
Elsevier Sequoia S.A., Lausanne – Printed in The Netherlands

DOPPELSCHICHTKAPAZITÄTSMESSUNG MIT DER BREYER-WECHSELSTROMPOLAROGRAPHIE (TENSAMMETRIE)

H. JEHRING

Forschungsbereich Physikalische Methoden der Analytischen Chemie, Zentralinstitut für Physikalische Chemie, Deutsche Akademie der Wissenschaften zu Berlin, Berlin-Adlershof (DDR)

(Eingegangen am 7. November, 1968)

1. DEFINITION

Nach der bereits im Titel verwendeten Definition verstehen wir unter Tensammetrie den Einsatz einer speziellen Messtechnik (Wechselstrompolarographie oder -voltammetrie nach Breyer[1,2]) für die Untersuchung bestimmter Elektrodenerscheinungen (Kapazität der Phasengrenze Elektrode/Elektrolyt und deren Beeinflussung durch Adsorption).

Wegen der Abhängigkeit der Kapazität und der Adsorption vom Elektrodenpotential werden Kapazitäts–Potential-Kurven aufgenommen. Methodisch erfolgt dies durch Einspeisung einer kleinen konstanten Wechselspannung und Registrierung des resultierenden Wechselstromes als Funktion der angelegten veränderlichen Gleichspannung.

Das zweite und ursprüngliche Anwendungsgebiet der Methode mit überlagerter Wechselspannung ist die Untersuchung der Durchtrittsprozesse (von Breyer als eigentliche Wechselstrompolarographie bezeichnet zur Unterscheidung von der Tensammetrie, die Vorgänge ohne Ladungsdurchtritt erfasst)[3]. Die Bezeichnung Wechselstrompolarographie ist folglich sowohl als Überbegriff der Tensammetrie als auch als gleichgestellter Begriff im Gebrauch.

Für die Untersuchung des hier gewählten Messobjektes, der Doppelschichtkapazität, stehen noch andere, einfachere und kompliziertere elektrochemische Methoden bereit, z.B. Impedanzmessbrücken oder auch die einfache Gleichstrompolarographie und oszillographische Polarographie[4–7]. Diese Untersuchungen fallen nach unserer Definition nicht unter den Begriff der Tensammetrie, obgleich für das Untersuchungsobjekt dieselben elektrochemischen Grundlagen bestehen.

Das ihr entgegengebrachte Interesse verdankt die Doppelschichtkapazität in erster Linie ihrer ausgeprägten Sensibilität gegenüber Adsorption an der Elektrode, die in allen elektrochemischen Problemkreisen eine wesentliche Rolle spielt und ferner die analytische Erfassung nicht reduzierbarer grenzflächenaktiver Stoffe möglich macht. In der Untersuchung der Adsorption liegt damit auch das eigentliche Einsatzfeld der Breyerschen Tensammetrie.

2. HISTORISCHE ENTWICKLUNG

Auf die Adsorption an Elektroden spricht nicht nur die Kapazität C, sondern z.B. auch die Grenzflächenspannung γ der elektrisch geladenen Phasengrenze Elek-

trode/Elektrolyt an, die nach Lippman über eine einfache Beziehung mit der Kapazität verknüpft ist:

$$\gamma = \gamma_{E_0} - \int_{E_0}^{E} q\,\mathrm{d}E = \gamma_{E_0} - \iint_{E_0}^{E} C\,\mathrm{d}E^2 \tag{1}$$

Die Beeinflussung der Ladungsdurchtrittsprozesse durch Adsorption (z.B. die Inhibition) gehört nicht mehr unmittelbar zu den Kapazitätseffekten und bleibt deshalb hier ausser Betracht.

An der Änderung der Grenzflächenspannung (Elektrokapillarkurve) wurde nun auch erstmalig das Adsorptionsphänomen von Gouy[8] gefunden und näher untersucht. Die Entdeckung des Adsorptionseinflusses auf die Doppelschichtkapazität (mit einem Substitutionsverfahren) geht auf Proskurnin und Frumkin[9] zurück. Durch den Einsatz geeigneter Präzisionsbrückenmesstechniken konnte das Gebiet dann später näher exakt bearbeitet und theoretisch interpretiert werden[10,11]. Die Breyerschen Untersuchungen mit der Wechselstrompolarographie ergaben dieselben Erscheinungen und wurden daraufhin auf verschiedene grenzflächenaktive Stoffe ausgedehnt[12,13].

Der Einsatz der Breyer-Tensammetrie erbrachte zwar durch die einfache Messtechnik viele interessante Phänomene, hatte jedoch an der quantitativen Erforschung der Kapazitäts- und Adsorptionsgesetzmässigkeiten zunächst nur einen geringeren Anteil. Auch der Vorteil der gegenüber den Brückenmethoden sehr viel einfacheren Aufnahmetechnik wurde nicht ausgenützt. Erst die in den letzten Jahren erfolgte stärkere Beachtung der Wechselstrompolarographie im Gerätebau ermöglicht eine volle Leistungserprobung der Tensammetrie.

Voraussetzung ist jedoch eine exakte (bisher häufig etwas zu grosszügig und mehr qualitativ geübte) Mess- und Auswertetechnik unter Anwendung der mit den (zeitlich und apparativ sehr viel aufwendigeren) Präzisionsbrückenmethoden erhaltenen theoretischen Grundlagen.

3. MESSTECHNIK

Die Polarisation der Elektrode mit der Gleichspannung E erfolgt nach der in der klassischen Polarographie üblichen Weise und in den auch dort üblichen Potentialbereichen. Die Einspeisung der Wechselspannung U und die Messung des Wechselstromes I kann parallel oder in Reihe zur Gleichspannung erfolgen. Besonders in hochohmigen Lösungen ist eine potentiostatische Arbeitsweise hinsichtlich E und U zweckmässig[14,15].

Die Empfindlichkeit nimmt nach

$$I = 2\pi\nu UC \qquad (\omega = 2\pi\nu) \tag{2}$$

mit der Amplitude U und Frequenz ν der Wechselspannung zu, das Auflösungsvermögen nimmt dagegen mit U ab. Die gebräuchlichen U-Werte liegen zwischen 1 und 20 mV.

Die Frequenzen können zwischen 10 Hz und 10 kHz betragen. Mit steigender Frequenz gehen jedoch die nicht interessierenden Reihenwiderstände R_M der Messanordnung (Zelle, Elektronik) zunehmend verfälschend nach

$$I = U\{(\omega C)^{-2} + R_{M^2}\}^{-\frac{1}{2}} = U\omega C(R_M^2\omega^2C^2 + 1)^{-\frac{1}{2}} \tag{3}$$

mit in das Messergebnis ein[16,17]. Diese müssen durch Sondermassnahmen (Überbrückung mit hohen Kapazitäten, hohe Leitsalzkonzentration) weitestgehend eliminiert oder bei der Auswertung rechnerisch berücksichtigt werden[18-20]. Die Anwendung der einfachen Gl. (2) setzt voraus, dass in Gl. (3) $R_M^2\omega^2C^2 \ll 1$ gilt[21]. Das übliche Frequenzgebiet liegt daher zwischen 10 und 300 Hz (bezüglich der tensammetrischen Wellen, die nicht rein kapazitiven Charakter besitzen und zusätzlich frequenzabhängig sind, siehe Abschnitt 5.3).

Als Wechselspannungsquelle kann das Netz über Transformator oder besser ein RC-Generator (Ausschaltung von Störungen durch Netzfrequenz und variable Frequenz) dienen. Die Strommessung erfolgt an einem in Reihe geschalteten Arbeitswiderstand als Spannungsabfall. Die Messempfindlichkeit, aber auch der parasitäre Einfluss nach Gl. (3) nimmt mit dem Arbeitswiderstand zu. Der Wert sollte daher bei 0.1–10 Ω liegen, wenn die Empfindlichkeit des nachfolgenden Verstärkers ausreicht. In Sonderfällen (hohe analytische Empfindlichkeit und Eichkurvenauswertung) kann der Wert bis zu 200 Ω gesteigert werden.

Die Verstärkung des Wechselspannungssignals über dem Arbeitswiderstand wird zur Ausschaltung von Fremdsignalen (höhere Empfindlichkeit und Genauigkeit) möglichst frequenzselektiv durchgeführt. Nach der Gleichrichtung (und evtl. Dämpfung der Tropfenoszillationen) erfolgt die Registrierung auf einem gesonderten Schreiber oder dem Schreiber des Gleichstrom-Stammgerätes (das auch die Gleichspannung liefert) als Funktion des Elektrodenpotentials.

Zur Auswertung kann direkt die Wechselstromstärke I_E als Mass für die Elektrodenkapazität C_E benutzt werden, was für die meisten analytischen Aufgaben ausreicht. Besser ist die Eichung des Ausschlages bei jeder Messreihe mit Präzisionskapazitätsdekaden (anstelle der Zelle geschaltet), gegebenenfalls unter Zuschaltung von Reihenwiderständen zur Berücksichtigung unerwünschter Serienwiderstände. Dies gilt besonders bei Einsatz höherer Frequenzen.

Günstigere Bedingungen hinsichtlich des R_M-Einflusses mit gleichzeitiger Möglichkeit der Phasenwinkelmessung verspricht die von Bauer[22] vorgeschlagene Wechselspannungspolarographie (Überlagerung eines konstanten Wechselstromes und Messung der Wechselspannung über der Elektrode)[19,23].

An stationären Elektroden ist die Umrechnung der Elektrodenkapazität C_E (μF) über die Oberfläche A (cm^2) in die spezifische Kapazität pro Flächeneinheit C (μF cm^{-2}) leicht möglich nach

$$C_E = CA \tag{4}$$

Dies gilt auch für ungedämpfte Kurven bei der tropfenden Elektrode mit dem Maximalwert C_m bei der Tropfzeit t_m aus A_m. Bei starker Dämpfung der Tropfenoszillationen kann C aus dem Mittelwert der Tropfenzacken $\bar{C}$ mit der mittleren Oberfläche $\bar{A} \simeq 0.6\, A_m$ annähernd berechnet werden. (Der theoretische Wert 0.6 wird nicht exakt erreicht, da die Messanordnung keine einfache Integration liefert)[18].

Abweichungen von der einfachen A–t-Funktion, z.B. durch Rückdruckeinfluss[24,25], müssen gegebenenfalls rechnerisch mit berücksichtigt werden. Beim Arbeiten mit einer selbsttätig tropfenden Elektrode (ohne Tropfkontroller oder Tasteinrichtung) ist ferner die Abhängigkeit der Grenzflächenspannung γ vom Elektrodenpotential E und von der Adsorption und damit die Auswirkung auf die Tropfzeit t_m bzw. A_m und $\bar{A}$ (bei konstanter Ausflussgeschwindigkeit) zu beachten[18,26] (Abb. 1c).

Die umständliche manuelle Aufnahmetechnik (Auftragen des Voltmeterausschlages gegen das schrittweise von Hand veränderte Elektrodenpotential) sollte eigentlich, von Sonderfällen wie Phasenwinkelmessung udgl. abgesehen, nur noch historische Bedeutung besitzen, weil hiermit der markante Vorteil der Breyer-Technik (Schnelligkeit, Automation) auch nicht annähernd genutzt wird. Seit Erscheinen der Monographie von Breyer und Bauer[3] ist die Wechselstrompolarographie messtechnisch soweit verbessert worden, dass heute tensammetrische Untersuchungen mit dergleichen Routine durchgeführt werden können wie gleichstrompolarographische. In den vergangenen Jahren sind nicht nur mehrere Publikationen über Laboraufbauten mit Schreiberregistrierung und über Laborzusatzeinrichtungen für Gleichstrompolarographen erschienen[5,6,14,15,19,22,23,26-49], es sind auch bereits für die Kapazitätsmessung geeignete Geräte kommerziell erhältlich[26,50-54].

Auch der Barkersche Square-Wave-Polarograph eignet sich bei Einbau eines gesonderten Integrationsgliedes zur Kapazitätsmessung[6,55,56]. In der ursprünglichen Form (mit Kapazitätsstromunterdrückung) können damit nur die tensammetrischen Wellen aufgenommen werden[57]; dies gilt ebenfalls für die in Japan eingeführte oszillographische Square-Wave-Polarographie[58,59]. Auch noch andere angebotene Wechselstrompolarographen bzw. Zusatzgeräte sind speziell für Durchtrittsprozesse (Depolarisatoren) ausgelegt. Die zur Empfindlichkeitssteigerung fest eingebaute Einrichtung zur Kapazitätsstromkompensation (z.B. phasenempfindliche Anzeige mit fixiertem Phasenwinkel) macht diese Geräte für Kapazitätsmessungen ungeeignet[32,60]. Vorteilhaft, aber mit Vorsicht einzusetzen, sind Geräte zur Aufnahme der Frequenzabhängigkeit.

Die der Breyer-Methode zugrundeliegende einfache Strom–Spannungs-Messung ermöglicht nicht nur eine schnelle Registrierung, sondern weiterhin eine wenig aufwendige Automation in der Prozess-Kontrolle und -Steuerung[26,61-63] sowie auch die rasche Computer-Auswertung der Ergebnisse[14,64-66].

4. KURVENVERLAUF UND AUSWERTUNG

In der Regel werden Wechselstrom–Potential- (I_E–E-) bzw. Kapazitäts–Potential- (C_E–E-)Kurven aufgenommen, an der tropfenden Elektrode zweckmässig mit entsprechender Dämpfung[26] (Abb. 1a). Daneben haben noch Wechselstrom–Zeit- (I_E–t-) bzw. Kapazitäts–Zeit- (C_E–t-)Kurven bei konstantem Elektrodenpotential E Bedeutung[18,41,57,67-77], z.B. für die Untersuchung der Zeitabhängigkeit der Adsorption oder für die Verfolgung in der Lösung ablaufender Reaktionen bzw. Konzentrationsänderungen. An stationären Elektroden ist der Zeitraum nahezu unbegrenzt. An der tropfenden Elektrode haben wir einmal die Möglichkeit, innerhalb eines Tropfenlebens ($t < t_m$) z.B. Änderungen an der Elektrode (Adsorptionsgeschwindigkeit) zu untersuchen (C_E–t-Kurven ungedämpft). Zweitens können Änderungen in der Lösung über den Zeitraum mehrerer Tropfen ($t > t_m$) über längere Zeit hin verfolgt werden ($\bar{C}$–t-Kurven, gedämpft) (Abb. 1b). Die Darstellung der C_E–t-Kurven kann sowohl vor der Gleichrichtung auf einem Kathodenstrahloszillographen (Abb. 1d) als auch nach der Gleichrichtung mit Galvanometer oder Schreiber (kurze Ansprechzeit) (Abb. 1c) erfolgen. Schliesslich ist es möglich, noch kürzere zeitliche Veränderungen, nämlich innerhalb der einzelnen Wechselspannungsperioden, oszillographisch zu erfassen. Letzteres ist besonders als zusätzliche Überprüfung der Ap-

paratur bei der Aufnahme aller Arten von Kurven und als Möglichkeit der Phasenwinkelmessung empfehlenswert.

Die am häufigsten verwendeten $\bar{C}$–E-Kurven, d.h. die eigentlichen tensammetrischen Wechselstrompolarogramme (oder Kapazitogramme), liefern folgende,

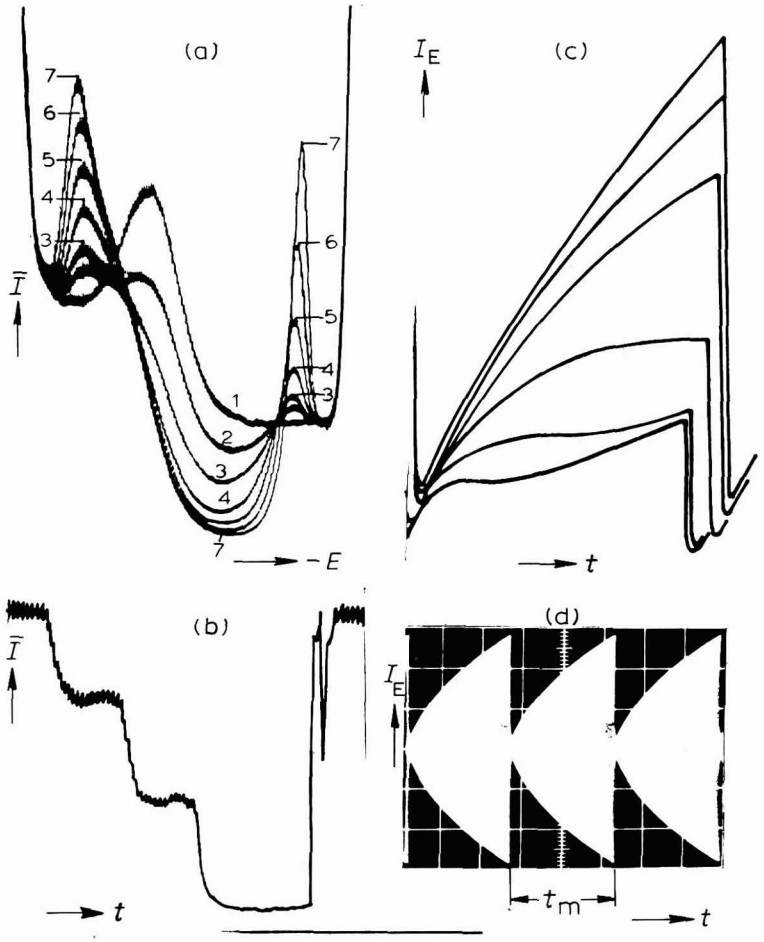

Abb. 1. Registrier- und Auswertemöglichkeiten. (a), Wechselstrom–($\bar{I}$–) Potential-(E-) Kurven (verschiedene Konzentrationen); (b), Wechselstrom–($\bar{I}$–) Zeit-(t-) Kurven bei konstantem Potential E (zeitliche Änderung der Konzentration c in der Lösung; (c), Wechselstrom–(I_E–) Zeit-(t-) Kurven bei konstantem Potential E nach der Gleichrichtung mit Schreiber registriert (verschiedene Konzentrationen); (d), Wechselstrom–(I_E–) Zeit-(t-) Kurven bei konstantem Potential E vor der Gleichrichtung oszillographisch registriert.

für die Untersuchung der Adsorption auswertbare Grössen (Abb. 1a):

1. Die durch die Adsorption hervorgerufene Kapazitätserniedrigung $\Delta\bar{C}$ in der Umgebung des Ladungsnullpunktes E_0 als Funktion der Konzentration in der Lösung c und als Funktion der Tropfzeit t_m;

2. die Sättigungskapazität $\bar{C}_S$ bzw. die Sättigungskapazitätserniedrigung $\Delta\bar{C}_S$ bei völliger Bedeckung der Elektrode;

3. das positive bzw. negative Desorptionspotential E_+ bzw. E_-, d.h. die Scheitelpotentiale der tensammetrischen Wellen beiderseits des Adsorptionsgebietes als Funktion der Konzentration c:

4. die Höhe der tensammetrischen Wellen $\bar{h}_+$ bzw. $\bar{h}_-$ als Funktion der Konzentration c (u. evtl. auch der Tropfzeit t_m); im Gegensatz zur Kapazitätserniedrigung $\Delta\bar{C}$ ist die Wellenhöhe $\bar{h}$, bedingt durch die Geschwindigkeit des Ad-Desorptionsprozesses, zusätzlich noch abhängig von der Frequenz ν;

5. die Gestalt der Wellen bzw. die Wellenbreite.

Bei einigen Systemen treten zusätzlich potentialabhängige Umorientierungen in der Adsorptionsschicht auf, begleitet von Umorientierungswellen. Bei Vorliegen mehrerer grenzflächenaktiver Stoffe gleichzeitig ergibt sich eine starke gegenseitige Beeinflussung des Kurvenverlaufs (s. 5.4).

Da der Schreiber nicht die spezifische Kapazität pro Flächeneinheit C (μF cm^{-2}), sondern die von der Elektrodenoberfläche A abhängige Gesamtelektrodenkapazität C_E bzw. die Mittelwerte $\bar{C}$ registriert, andererseits die A–t-Charakteristik bei gleichen Versuchsbedingungen (Elektrode, Behälterhöhe) praktisch unverändert bleibt, ist es für die quantitative Auswertung zweckmässig, anstelle der C_E-, ΔC_E- und h_E-Werte die entsprechenden relativen (dimensionslosen) Grössen (auf den Grundstrom beim gleichen Potential bezogen) auszuwerten, d.h. C_E/C_{0E}, $\Delta C_E/C_{0E}$ und h_E/h_{0E}. Man umgeht damit die Berechnung der Tropfenoberfläche und kompensiert gleichzeitig systematische Fehler bzw. Abweichungen der Messeinrichtung. Dies gilt auch für Mittelwerte $\bar{C}$ usw.[18,26,71] (s. dazu 5.2 und 5.3).

5. THEORIE DER ADSORPTIONSUNTERSUCHUNG MIT DER TENSAMMETRIE

5.1. *Adsorptionsgleichgewicht und Doppelschichtskapazität*

Der Adsorption an der Elektrode unterliegen sowohl die Moleküle und Ionen des umgebenden Elektrolyten als auch besonders der Lösung zugesetzte (meist organische) Moleküle (bzw. Ionen). Die Adsorption z.B. organischer Teilchen an der Elektrodenoberfläche ist als Austauschadsorption anzusehen, d.h. sie ist verbunden mit einer gleichzeitigen Verdrängung von Molekülen und Ionen der Grundlösung aus der Phasengrenzschicht. Bei der Adsorptionsenergie spielen eine Rolle sowohl die Wechselwirkungsenergien Elektrode-Partikel als auch die Partikel–Partikel-Wechselwirkung gleicher und verschiedener Natur (z.B. Lösungsmittel, Gelöstes). Im Gegensatz zur allgemeinen Adsorption liegt jedoch an der elektrisch geladenen Phasengrenze Elektrode/Elektrolyt eine elektrochemische Adsorption vor. Die freie elektrochemische Adsorptionsenthalpie ist damit nicht nur bestimmt durch die Konzentration c (genauer Aktivität) in der Lösungsphase, sondern auch eine Funktion der Oberflächenkonzentration Γ bzw. des Bedeckungsgrades θ (Γ-Abhängigkeit der Wechselwirkungsanteile) sowie des Elektrodenpotentials E[78–86].

Wechselwirkungskräfte der adsorbierten organischen Moleküle untereinander werden z.B. in der durch Frumkin[84,87] erweiterten Langmuir-Gleichung berücksichtigt:

$$bc = \theta(1-\theta)^{-1} \exp(-2a\theta) \tag{5}$$

Die Potentialabhängigkeit des Adsorptionskoeffizienten b und des Wechselwirkungskoeffizienten a (z.B. bei Neutralmoleküladsorption)[81,84] kann ausgedrückt werden

durch

$$\ln b = \ln b_0 - \beta(E - E_0)^2 \quad \text{bzw.} \quad a = a_0 + \alpha E \qquad (6)\ (7)$$

Unter annähernd idealen Bedingungen ($\theta \ll 1$, Anfangsteil der Adsorptionsisotherme) geht Gl. (5) in die lineare Form über:

$$bc = \theta \qquad (8)$$

Durch die thermodynamische Verknüpfung der freien Standardenthalpie der Löslichkeit mit derjenigen der Adsorption (entgegengesetztes Vorzeichen)[88] ergibt sich auch der entgegengesetzte Temperaturkoeffizient beider, der sich u.a. im unterschiedlichen Vorzeichen zwischen einfacheren Stoffen und Makromolekülen äussert[3].

Ausgehend von der (zunächst vereinfachten) Annahme, dass die Kapazitätsänderung pro Flächeneinheit ΔC (μF cm^{-2}) direkt proportional der Oberflächenkonzentration Γ (Mol cm^{-2}) ist,

$$\Delta C = \Delta C_n \Gamma \qquad (9)$$

bietet sich für die Auswertung das bewährte Modell parallelgeschalteter Kapazitäten[84] an:

$$C = C_0(1 - \theta) + C_S\theta + (q_S - q_0)(\mathrm{d}\theta/\mathrm{d}E) \qquad (10)$$

Die ersten beiden Glieder auf der rechten Seite der Gleichung genügen für die Auswertung der Kapazitätserniedrigung im Potentialgebiet maximaler Adsorption ($\mathrm{d}\theta/\mathrm{d}E = 0$). Das dritte Glied, die Zusatzkapazität, besitzt Bedeutung für die Wellenhöhe beim Desorptionspotential. ($\mathrm{d}\theta/\mathrm{d}E$-Maximum).

5.2. *Kapazitätserniedrigung*

Nach Gl. (10) ergibt sich mit $\mathrm{d}\theta/\mathrm{d}E = 0$

$$\theta = (C - C_0)(C_S - C_0)^{-1} = \Delta C/\Delta C_S \qquad (11)$$

Aus den Adsorptionsisothermen $\Delta C/C_0 = f(c)$ bzw. $\theta = f(c)$ ist damit nicht nur die quantitative Tensidanalyse möglich, sondern auch die Ermittlung von a und b. Voraussetzung für letzteres ist, dass sich das Adsorptionsgleichgewicht zwischen c und Γ eingestellt hat, d.h. Γ zeitunabhängig ist[68,82].

Als Kriterien hierfür sind anzusehen: an stationären Elektroden zeitlich konstante Elektrodenkapazität C_E; an der tropfenden Elektrode ist C_E proportional der Tropfenoberfläche, d.h. proportional $t^{\frac{2}{3}}$ bzw. C_E, $\Delta C_E/C_{0E}$ oder C_E/C_{0E} sind zeitunabhängig; die Mittelwerte $\bar{C}$ sind unabhängig von der Behälterhöhe H bzw. der Tropfzeit t_m. Das Verhältnis Mittelwert $\bar{C}$ zu Maximalmomentanwert (bei t_m) C_m, liegt bei 0.6[18,26]. Sofortige Gleichgewichtseinstellung findet man bei relativ schwach grenzflächenaktiven Stoffen (keine Diffusionshemmung wegen der relativ hohen eingesetzten Konzentrationen c in der Lösung). Die Konzentration c_0 in der Lösungsschicht unmittelbar vor der Oberfläche ist gleich der in der Lösung ($c_0 = c$).

Bei mittelstark grenzflächenaktiven Stoffen liegen die Lösungskonzentrationen c für Gleichgewichtsbedeckung im θ-Bereich < 1 schon so niedrig, dass die Gleichgewichtseinstellung wegen messbarer Diffusionshemmung bis zu einigen Sekunden Zeit erfordert. Γ steht zwar im Gleichgewicht mit c_0, aber nicht mit c ($c_0 < c$; während der Gleichgewichtseinstellung: $c_0 \rightarrow c$). Bis zur Gleichgewichtseinstellung

ist daher Γ eine komplizierte Funktion der Zeit[68]. Erst nach Erreichen des Gleichgewichtes gelten die Kriterien des ersten Falles, und die Gleichgewichtswerte sind bestimmbar ($c_0 = c$)[73]. Auf Grund der komplizierteren Γ–t-Funktion kann keine zeitlich konstante Beziehung für das Verhältnis Mittelwert zu Maximalwert gegeben werden.

Bei sehr stark grenzflächenaktiven Substanzen wird in den untersuchbaren (niedrigen) Konzentrationen jedes andiffundierende Teilchen sofort so fest aus der Oberflächenlösungsschicht heraus adsorbiert, dass c_0 zunächst immer null bleibt und die Adsorption schliesslich zu $\theta = 1$ führt. Das Diffusionsproblem liegt hier einfacher, so dass wieder einfachere Beziehungen für die Zeiten bis zur völligen Bedeckung gegeben werden können[46,68] (z.B. für die tropfende Elektrode):

$$\theta = 7.36 \cdot 10^{-4} D^{\frac{1}{2}} S c t^{\frac{1}{2}} \tag{12}$$

(S = Oberflächenbedarf (cm^2 Mol^{-1}) = Γ_s^{-1}).

Kriterien sehr starker Adsorption mit Diffusionshemmung sind: ΔC_E wächst linear mit $t^{7/6}$, und $\Delta C_E / C_{0E}$ steigt linear mit $t^{\frac{1}{2}}$ während des Tropfenwachstums; für die Mittelwerte gilt analog $\Delta \bar{C} / \bar{C}_0 \sim t_m^{\frac{1}{2}}$ (Tropfzeit) bzw. $\sim H^{-\frac{1}{2}}$ (Behälterhöhe)[26,71,89]. Für das Verhältnis Mittelwert zu Maximalmomentanwert ergibt sich $\Delta \bar{C} / \bar{C}_0 = 0.77\, \Delta C_m / C_{0m}$[18]. Nach Erreichen der Adsorptionssättigung $\theta = 1$ gelten die Beziehungen für den Gleichgewichtsfall. Gl. (12) kann z.B. zur Ermittlung des Oberflächenbedarfes benutzt werden[72].

Im Potentialgebiet maximaler Adsorption kann die Elektrodenkapazität als verlustfreier Kondensator und als unabhängig von Amplitude und Frequenz (in den üblichen Grenzen) der Messpannung angesehen werden. Die gemessene Wechselstromstärke ist (unter den eingangs erwähnten messtechnischen Gesichtspunkten) als eindeutiges Kapazitätsmass anzuerkennen.

5.3. *Kapazitätsmaxima (tensammetrische Wellen)*

Beim Scheitelpotential der tensammetrischen Welle liegt das Maximum der Potentialabhängigkeit der Kapazität. Während im Potentialgebiet maximaler Adsorption praktisch nur durch das Abreissen des Tropfens und die Bildung eines neuen das Adsorptionsgleichgewicht immer wieder neu eingestellt werden muss, wird beim Ad-Desorptionspotential zusätzlich durch die überlagerte Wechselspannung das Gleichgewicht periodisch im Rythmus der Frequenz laufend um kleine Beträge gestört und ein zeitlich verzögerter Pendelvorgang zwischen Adsorption und Desorption aufgezwungen. Im Gegensatz zur Kapazitätserniedrigung ist die Gesamtkapazität im Potentialbereich der tensammetrischen Wellen damit durch das 3. Glied in Gl. (10) verlustbehaftet (ohmsche Anteile) und stark frequenzabhängig (Adsorptionskinetik). Durch die starke Nichtlinearität der Elektrodenkennlinie $C = f(E)$ treten ausserdem Oberwellen und Gleichrichtereffekte auf.

Da in der Tensammetrie (mit der üblichen einfachen Schalttechnik) nur die komplexe Gesamtadmittanz (Z^{-1}) registriert wird, ist bei der quantitativen Interpretation der Wellenhöhe (wegen der kapazitiven und ohmschen Anteile der Zusatzkapazität) zunächst Vorsicht geboten. Eine einfache Korrektur wie beim Elektrolytwiderstand ist nicht möglich, eine gesonderte Bestimmung des Phasenwinkels φ daher erforderlich.

Es besteht damit eine gewisse Parallelität mit den wechselstrompolarographi-

schen Durchtrittswellen[90] von Depolarisatoren, mit dem Unterschied jedoch, dass im Gegensatz zu Durchtrittswellen bei tensammetrischen Wellen kein Ladungsdurchtritt durch die Phasengrenze, sondern lediglich eine Umstrukturierung und Ladungsänderung des Phasengrenzkondensators (Wechsel des Dielektrikums und des Ladungsabstandes) erfolgt. Während bei Durchtrittswellen die Kinetik des elektrochemischen Redox-Vorganges in Verbindung mit der Diffusion (und evtl. chemischen Reaktionen) bestimmend wirkt, ist bei tensammetrischen Wellen die Ad–Desorptionskinetik (ohne elektrochemische Umwandlung) in Verbindung mit der Diffusion massgebend (Bei adsorbierten Depolarisatoren können beide Vorgänge in einer Welle vereinigt auftreten[3]).

Auf Grund der Parallelität zwischen Durchtritts- und Ad–Desorptionswellen (ohmsche Anteile, Nichtlinearität) kann eine weitere Verstärkung der tensammetrischen Wellen und damit eine Empfindlichkeitssteigerung mit den auch bei Durchtrittsprozessen üblichen Methoden[5,6,14,91,92] zur Unterdrückung des hohen kapazitiven Grundstromes (phasenempfindliche Anzeige, Rechteckwellenpolarographie, Oberwellentechnik) erreicht werden[56,57,93-96].

Hinweise für die Unterscheidung beider Wellentypen[97] ergeben sich zunächst aus der Kapazitätserniedrigung. Aufschlussreich ist die Aufnahme von Gleichstrompolarogrammen (z.B. mit einem kombinierten Gleich–Wechselstrom-Polarographen). Tensammetrische Prozesse rufen (auch bei höheren Konzentrationen) nur eine kleine Kapazitätsstufe hervor. Unterschiede zeigen auch die Phasenwinkel, besonders hinsichtlich der Frequenzabhängigkeit.

Die im Inneren des Adsorptionspotentialbereiches mitunter zusätzlich auftretenden tensammetrischen Wellen werden durch eine Umstrukturierung der adsorbierten Teilchen (z.B. etwa beim Übergang von positiver zu negativer Elektrodenaufladung) verursacht. Da der Umstrukturierungsvorgang schneller verläuft als der mit Stofftransport verbundene Ad–Desorptionsvorgang, findet man bei den Wellen des ersteren eine geringere Frequenzabhängigkeit als bei den Wellen des letzteren[21].

Die theoretischen Grundlagen für die Frequenzabhängigkeit entwickelten* Frumkin und Melik-Gaykasjan[98], Berzins und Delahay[99] sowie Lorenz und Möckel[100,101]. Aus dem Ersatzschaltbild und dem Zeigerdiagramm (Abb. 2) ergeben sich folgende wichtige Grössen:

(a) für die Zusatzadmittanz der Welle:

$$Z_T^{-1} = (\omega^2 C_T^2 + R_T^{-2})^{\frac{1}{2}} \quad \text{und} \quad \tan\delta = (\omega C_T R_T)^{-1} \tag{13}$$

(b) für die Gesamtadmittanz beim Scheitelpotential (ohne R_M):

$$Z^{-1} = \{\omega^2 (C_\infty + C_T)^2 + R_T^{-2}\}^{\frac{1}{2}} \quad \text{und} \quad \tan\varphi = \omega(C_\infty + C_T)R_T \tag{14}$$

Für die ohmschen (R_T) und kapazitiven (C_T) Anteile der kinetischen Admittanz (Z_T^{-1}) bzw. für den kinetischen Verlustfaktor tan δ wurden von den genannten Autoren quantitative Beziehungen für die Frequenzabhängigkeit unter Berücksichtigung beider Teilschritte (Adsorption, Diffusion) aufgestellt und teilweise auch mit Brückenmessungen überprüft[82,98,100-102]. Lorenz berücksichtigte noch als dritten Teilschritt die zweidimensionale Assoziation in der Adsorptionsschicht[103] und schliesslich später noch den partiellen Ladungsübergang Partikel-Elektrode[104].

Mit zunehmender Frequenz nimmt die kinetische Zusatzadmittanz Z_T^{-1} ab**

* Vgl. auch Breyer und Hacobian[12]. ** Über C_T und $1/R_T$.

und der kinetische Verlustwinkel δ (d.h. die Abweichung von $\varphi = 90°$) zu. Bei sehr hohen Frequenzen verschwinden schliesslich die tensammetrischen Wellen (Abb. 2c) und es verbleibt der I_E–E-Verlauf der "wahren" oder "HF-Kapazität" C_∞, bestimmt durch die ersten beiden Glieder in Gl. (10). Der relativ langsame Ad–Desorptionsprozess (einschliesslich Diffusion) vermag dem sehr schnellen Wechselspannungsfeld nicht mehr zu folgen, das 3. Glied in Gl. (10), die kinetische Zusatzadmittanz, fällt weg.

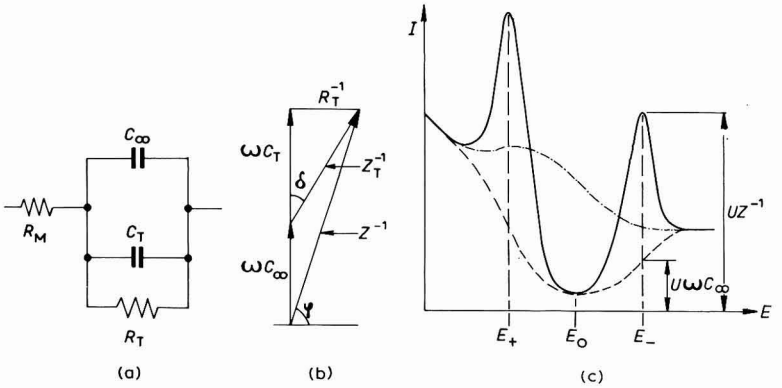

Abb. 2. Elektrische Eigenschaften tensammetrischer Wellen. (a), Ersatzschaltbild; (b), Zeigerdiagramm (ohne R_M); (c), I–E-Kurven. (–·–·–·–), leere Lösung (praktisch frequenzunabhängig); (– – – –), Strom der wahren oder Hochfrequenzkapazität ($\omega = \infty$); (———), Strom der vektoriellen Summe aus wahrer und Zusatzkapazität (mit Verlustanteil) bei der Messfrequenz ($0 < \omega < \infty$). (Erklärung im Text, Symbole s. unten). UZ^{-1} und $U_\infty C_\infty$ sind in der I-Achse mit verschiedenen Masstäben dargestellt. Der Strom der bei hohen Frequenzen allein messbaren wahren Kapazität liegt praktisch nach Gl. (2) wesentlich höher, als jener der bei niedrigen Frequenzen aufgenommenen Gesamtadmittanz.

Da ausserdem der Einfluss der parasitären Reihenwiderstände nach Gl. (3) mit Z^{-1} wächst, ist es gerade bei Wellen nötig, mit möglichst niedrigen Frequenzen zu messen, und möglichst für quantitative Interpretationen den Phasenwinkel φ gesondert zu bestimmen. Mit einem mehr oder weniger grossen elektronischen Aufwand ist letzteres ohne weiteres möglich[3,14,20,23,29,44,105]. Damit könnte der Tensammetrie auch das Gebiet komplizierterer theoretischer Untersuchungen erschlossen werden, methodisch in einem Grenzgebiet zwischen der einfachen Messtechnik und den aufwendigen Methoden. Es sollte jedoch vor dem Einsatz der Tensammetrie geprüft werden, welcher Aufwand der Problemstellung entsprechend tatsächlich unbedingt erforderlich ist.

Die auf $\omega = 0$ extrapolierte, verlustfreie ($\delta = 0$) Gesamtkapazität C beim Scheitelpotential der Welle ergibt sich nach Hansen[106] sowie Frumkin und Damaskin[84] als eine lineare Funktion von log c:

$$C = K_1 + K_2 \log c \tag{15}$$

Die Gestalt der tensammetrischen Welle wird im wesentlichen durch das Verhältnis Höhe zu Breite bestimmt. Einen grossen Einfluss übt die Wechselwirkungskonstante a aus. Da die Höhe mit a zu-, die Breite mit a dagegen abnimmt, werden die Wellen nach Frumkin und Damaskin[84] mit zunehmendem a immer schmaler und spitzer bis zu einer vertikalen Linie bei $a = 2$. Bei $a > 2$ treten in Übereinstimmung mit Ergebnissen von Lorenz[103] Hysteresiserscheinungen in der Potentialachse und folglich auch keine Wellen mehr auf.

Die Scheitelpotentiale der positiven (E_+) und negativen (E_-) tensammetrischen Welle und damit das Potentialgebiet der Adsorption hängen von der Natur des adsorbierten Stoffes (und besonders von der Ladung) sowie von der Zusammensetzung der Grundlösung ab[3,84]. Durch den starken Einfluss der Konzentration sind sie (im Gegensatz zu Depolarisatoren) nur in wenigen Fällen geeignet für die Identifizierung der Stoffe[26]. Bei einigen Makromolekülen jedoch nehmen die (negativen) Scheitelpotentiale mit dem Molgewicht zu. Da sie hier gleichzeitig praktisch unabhängig von der Konzentration sind, ergibt sich die Möglichkeit der Molgewichtsbestimmung und der getrennten analytischen Erfassung in Mischungen (vgl. z.B. Abb. 3)[26,35,72]. Für die Konzentrationsabhängigkeit der Scheitelpotentiale einfacherer organischer Stoffe wurden von verschiedenen Autoren unterschiedliche Beziehungen gefunden und interpretiert. Eine Diskussion hierüber erfolgte in der Arbeit von Frumkin und Damaskin[84], wo u.a. eine kritische Auseinandersetzung mit den Vorstellungen von Doss[13] und Breyer[12] ($\Delta E_T \sim \log c$) sowie von Lorenz und Möckel[100] ($(\Delta E_T)^2 \sim \log c$) erfolgt. Eine wesentliche Rolle hierbei spielt wieder der Wechselwirkungskoeffizient a.

Für die Zeitabhängigkeit der tensammetrischen Wellenhöhe, genauer des registrierten Wechselstromes (z.B. während des Tropfenwachstums), gelten wieder etwa analoge Beziehungen zur Kapazitätserniedrigung. Im Gleichgewichtsfalle ist die Gesamtelektrodenkapazität C_E wieder proportional der Tropfenoberfläche A, d.h. an der Tropfelektrode (in erster Näherung) proportional $t^{\frac{2}{3}}$ und unabhängig von der Behälterhöhe[26,56,69,107]. Das Verhältnis Mittelwert zu Maximalmomentanwert $\bar{C}/C_m \simeq 0.6$. Eine Auswertung aus der Mitte der Tropfenzacken ist damit möglich. Bei diffusionsgehemmter Adsorption, d.h. vor beendeter Gleichgewichtseinstellung (niedrige Konzentrationen starker Tenside) sind die bei der Kapazitätserniedrigung gefundenen Gesetzmässigkeiten durch die Potentialabhängigkeit nach Gl. (6) nicht ohne weiteres übertragbar. Für das Verhältnis Mittelwert $\bar{C}$ zu Maximalmomentanwert C_m ergeben sich unterschiedliche Werte zwischen beiden Grenzfällen, wodurch die Auswertung der Mittelwerte erschwert wird[56].

5.4. *Mischadsorption und Adsorptionsverdrängung*

Die Mischadsorption an Elektroden wurde bisher, wenn man alle elektrochemischen Methoden einbezieht, etwa in fünfzig Arbeiten mehr oder weniger ausführlich behandelt[12,26,35,51,57,59,62,69,79,89,94,101,108-132]. Diese relativ geringe Zahl zeigt im Vergleich zu den mehreren hundert Veröffentlichungen auf dem Gebiet der Einzeladsorption die Vernachlässigung, aber auch die besonderen Schwierigkeiten dieses Problems.

Die für die Einzelstoffadsorption gültigen Beziehungen können auf die Mischadsorption (im folgenden für zwei Substanzen A und B in der Grundlösung) erweitert werden. Bei niedrigen Bedeckungsgraden $\theta_{A'}, \theta_{B'} \ll 1$ und $\theta_{A'} + \theta_{B'} \ll 1$ ergeben sich zunächst wieder, wie bei der Einzeladsorption (Gl. (8)), lineare Beziehungen

$$\theta_{A'} = bc_A \quad \text{bzw.} \quad \theta_{B'} = bc_B \tag{16}$$

θ_A, θ_B = Bedeckungsgrad bei Einzeladsorption
$\theta_{A'}, \theta_{B'}$ = Bedeckungsgrad bei Mischadsorption.
Beide Partner werden folglich unabhängig voneinander gleichzeitig adsorbiert. Es gilt

$$\theta_A = \theta_{A'};\ \theta_B = \theta_{B'};\ \theta_{A'B'} = \theta_A + \theta_B = \theta_{A'} + \theta_{B'} \tag{17}$$

Bei höheren Bedeckungsgraden macht sich im Adsorptionsgleichgewicht die gegenseitige Konkurrenz im Platzbedarf an der begrenzt aufnahmefähigen Elektrodenoberfläche und damit eine gegenseitige Adsorptionsverdrängung bemerkbar. Es gilt hier z.B. die auf Mischadsorption erweiterte[111] Langmuir-Gleichung

$$b_A c_A = \theta_{A'}(1 - \theta_{A'} - \theta_{B'})^{-1} \tag{18}$$

Wechselwirkungskräfte A–A, B–B und A–B in der Adsorptionsschicht werden schliesslich in der durch Tedoradze u. M.[131] erweiterten Frumkin-Gleichung berücksichtigt: Zusätzlich zur Adsorptionskonkurrenz können folglich noch starke Wechselwirkungskräfte den Gesamtverlauf der Adsorption beim Übergang von der Einzel- zur Mischadsorption beeinflussen. So gilt analog zu Gl. (5) für die Mischung mit $a_{A'}$(= Wechselwirkungskoeffizient der gleichartigen Partner A in der Mischung) zunächst

$$b_A c_A = \theta_{A'}(1 - \theta_{A'} - \theta_{B'})^{-1} \exp(-2a_{A'}\theta_{A'}) \tag{19}$$

Bei Erweiterung um den Wechselwirkungskoeffizienten der verschiedenartigen Partner A und B untereinander ergibt sich

$$b_A c_A = \theta_{A'}(1 - \theta_{A'} - \theta_{B'})^{-1} \exp(-2a_{A'}\theta_{A'} - 2a_{A'B'}\theta_{B'}) \tag{20}$$

Untersuchungen bei eingestelltem Adsorptionsgleichgewicht ergeben wie bei Einzeladsorption (mit je einer positiven und negativen tensammetrischen Welle) einen Potentialbereich der Kapazitätserniedrigung durch Mischadsorption oder auch durch Einzeladsorption des sehr viel stärker grenzflächenaktiven Partners bei völliger Verdrängung des schwächeren Partners. Das Potentialgebiet der Adsorption wird wieder durch je eine Desorptionswelle eingeschlossen, verursacht durch die Desorption beider Partner oder (bei starken Unterschieden in der elektrochemischen Adsorptionsenergie) des nur noch allein adsorbierten stärkeren Partners. Eine Erfassung der Einzelpartner über getrennte tensammetrische Wellen ist damit nicht möglich. Bei genauer Kenntnis der qualitativen Zusammensetzung der Untersuchungslösung kann über Eichkurven die Bestimmung des einen Partners erfolgen, wobei der Gehalt des anderen Partners bekannt oder konstant sein sollte. Anderenfalls ist vor der analytischen Bestimmung eine stoffliche Trennung (z.B. chromatographisch)[133,134] erforderlich.

Für die Trennung günstigere Voraussetzungen liegen nach Untersuchungen von Jehring[26,35,51,57,69,94,117–119] vor bei Systemen, in denen bei einem oder bei mehreren beteiligten Partnern bis zur Messzeit das Adsorptionsgleichgewicht noch nicht eingestellt ist (z.B. durch Diffusionshemmung). Der langsame Diffusionsvorgang führt zu einer gewissen Stofftrennung. Sehr stark grenzflächenaktive Stoffe (niedrige Konzentration→langsame Diffusion) sind in der Lösungsschicht unmittelbar an der Elektrode nur in stark begrenzter Menge vorhanden und können damit schwächer adsorbierte nur zum Teil verdrängen. Es kommt damit auch zur Ausbildung der Einzeladsorptionswellen beider Partner. Dadurch ist es möglich, schwach grenzflächenaktive Stoffe neben stark aktiven und mehrere starke Tenside nebeneinander (Abb. 3) zu bestimmen, wenn möglichst kurze Messzeiten (Tropfzeiten) gewählt werden. Das gesamte System bzw. das Mischadsorptionsverhältnis ist damit stark,

aber reproduzierbar zeitabhängig. Die Zeitabhängigkeit kann an C_E–t-Kurven verfolgt werden. Für die zunehmende Verdrängung eines sofort adsorbierten schwach grenzflächenaktiven Stoffes durch langsamer andiffundierende starke Tensidmoleküle gilt die für Einzeladsorption bei Diffusionshemmung abgeleitete Gl. (12). Aber auch mit den Schreibermittelwerten kann die Mischadsorption in Abhängigkeit von

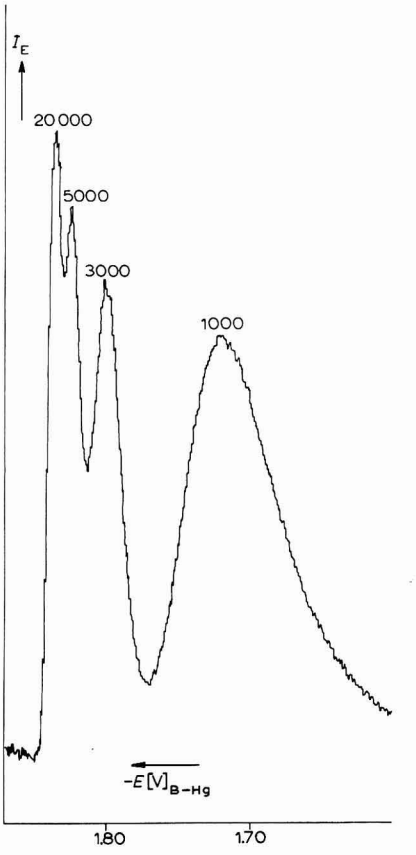

Abb. 3. Tensammetrisches Spektrum einer Mischung: Polyäthylenglykolen verschiedenen mittleren Molekulargewichtes $\overline{M}$ in 1 M LiCl. $\overline{M}$ (c): 1000 (20.0), 3000 (7.5), 5000 (3.0), 20000 (15.0) {c in (mg l^{-1})}. Gerät: Mervyn Modular Square-Wave-Polarograph in der ursprünglichen Schaltung zur Grundstromkompensation (Tastung innerhalb des Tropfenlebens und innerhalb der Rechteckperiode); Amplitude 2 mV.

der Tropfzeit t_m (bzw. Behälterhöhe H) und der Konzentration untersucht werden. Mit zunehmender Tropfzeit wächst die Welle des stärker adsorbierten Stoffes (höheres Desorptionspotential) auf Kosten der Welle der schwächer adsorbierten Substanz (Abb. 4)[118]. Hier zeigt sich der grosse Vorteil der einfachen Breyer-Methode, die eine sehr wenig aufwendige Verfolgung des zeitlichen Verlaufes der Doppelschichtkapazität und damit der Adsorption ermöglicht.

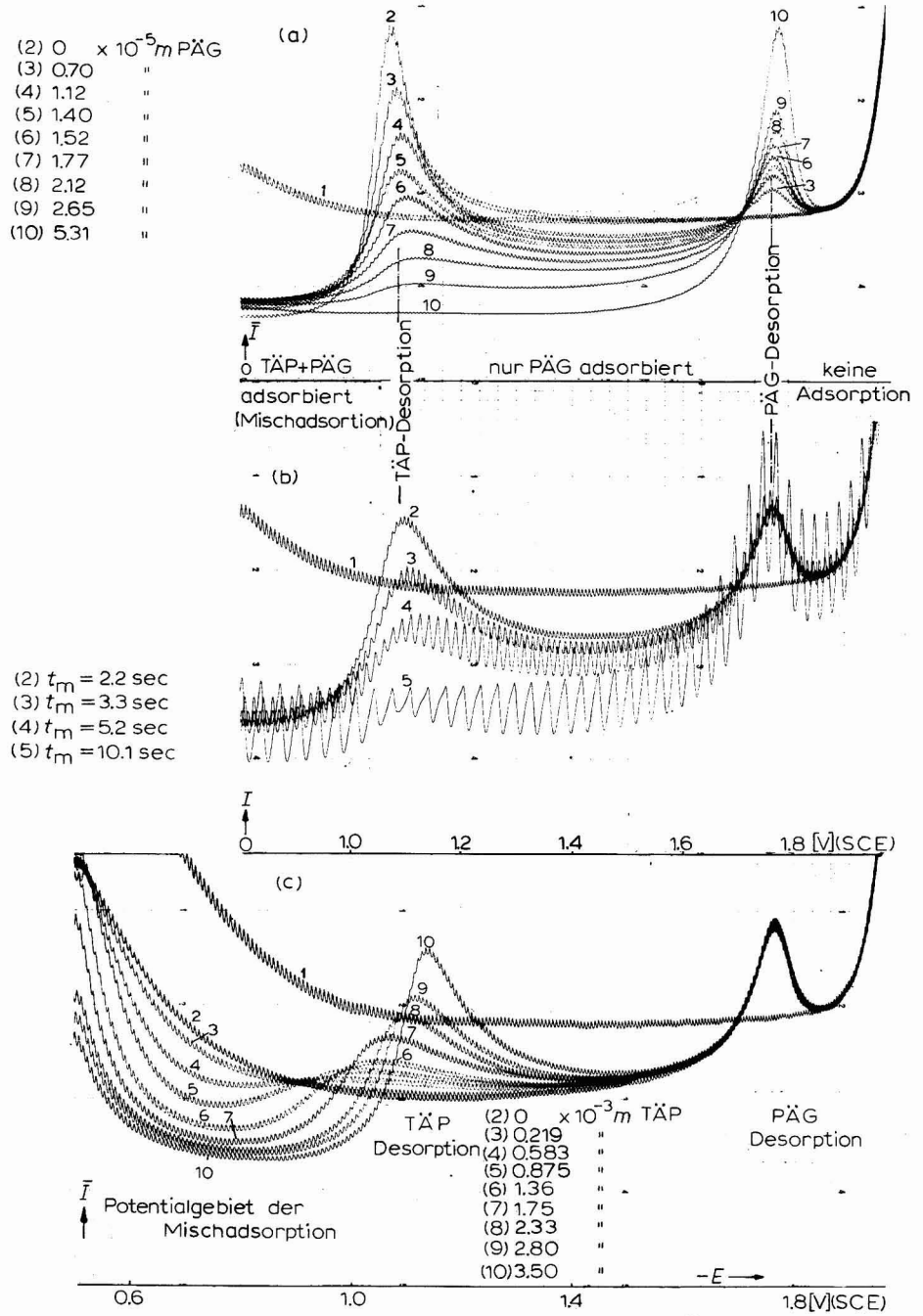

Abb. 4. c- und t_m-Abhängigkeit der Mischadsorption von Triäthylphosphat (TÄP) und Polyäthylenglykol (PÄG) $\bar{M} = 1000$ in 1 M KCl. Gerät: GWP 563 (Deutsche Akademie der Wissenschaften zu Berlin); Amplitude: 6 mV; Frequenz: 78 Hz. (a), Kurve 1, KCl; Wellen 2–10, $c_{TÄP}$ $2.50 \cdot 10^{-3}$ m, $c_{PÄG}$ verändert; t_m 2.1 sec. (b), Kurve 1, KCl, t_m 2.2 sec. Wellen 2–5, $c_{TÄP}$ $2.5 \cdot 10^{-3}$ $m + c_{PÄG}$ $1.33 \cdot 10^{-5}$ m; t_m verändert; (c), Kurve 1, KCl; Wellen 2–10, $c_{PÄG}$ $1.7 \cdot 10^{-5}$ m, $c_{TÄP}$ verändert; t_m 2.1 sec.

6. ERGEBNISSE UND ANWENDUNGEN

Die Ergebnisse über die Adsorption an Elektroden resultieren aus Messungen mit verschiedenen Methoden neben der Tensammetrie. Die Überprüfung der wichtigsten quantitativen theoretischen Grundlagen erfolgte jedoch hauptsächlich mit komplizierten Impedanzmessbrücken. Über die Theorie der Struktur und der Eigenschaften der Doppelschicht einschliesslich der Adsorption liegen moderne Übersichtsartikel und Monographien vor[80-85]. Im letzten Abschnitt dieser Arbeit soll nur über die speziell mit der Tensammetrie gewonnenen Resultate berichtet werden, ausgehend etwa vom Stand in der Monographie von Breyer und Bauer[3]. Inhibitionseffekte an Depolarisatoren und grenzflächenaktive Depolarisatoren, d.h. der Einfluss auf Durchtrittsprozesse[4,24,123,135], werden nur am Rande behandelt.

In zahlreichen der im folgenden kurz zitierten Arbeiten wurde die eingangs dargelegte Mess- und Auswertetechnik nur unzureichend berücksichtigt, einige besitzen daher in wissenschaftlicher Sicht nur qualitativen oder halbquantitativen bzw. empirischen Wert. Während beim Einsatz der selbstentwickelten komplizierten Brückenmethoden theoretisch fundiert gearbeitet wurde, ging man an den Einsatz der einfacheren, aber mit zahlreichen zusätzlichen Faktoren belasteten Tensammetrie häufig ohne gründliche vorherige Auseinandersetzung mit den messtechnischen Realitäten.

Die Tensammetrie hat insgesamt gesehen bei der Erforschung des Adsorptionsverhaltens wertvolle Dienste geleistet und lässt in der Zukunft noch zahlreiche vielseitige Einsatzgebiete, nicht nur auf dem Gebiet der Analytik, erwarten. Gerade die einfache—gegenüber der Gleichstrompolarographie apparativ nicht aufwendigere—Aufnahmetechnik ermöglicht eine breite Anwendung der Tensammetrie. Die Reproduzierbarkeit liegt mit zuverlässigen Apparaturen bei $\pm 1\%$. In derselben Grössenordnung können die Abweichungen von den theoretisch geforderten Kapazitätswerten, z.B. in der Kapazitätserniedrigung, gehalten werden. Die hohe Empfindlichkeit erlaubt bei sehr starken Tensiden eine Bestimmung bis zu 1 mg l^{-1} mit kurzen Tropfzeiten[26,61]. Mit längeren Zeiten (langsamtropfende oder stationäre Elektroden) kann die Nachweisgrenze noch um ein bis zwei Grössenordnungen herabgedrückt werden. Eine weitere Empfindlichkeitssteigerung ist durch Einsatz besonderer Messtechniken (z.B. Oberwellen) für die Wellenuntersuchung möglich[57,95]. Das Auflösungsvermögen benachbarter tensammetrischer Wellen (unter den in Abschn. 5.4 gegebenen Voraussetzungen) hängt naturgemäss von der Wellenbreite ab und ist bei schmalen Wellen sehr hoch, teilweise bis zu 10 mV (vgl. Abb. 3).

Die aus der Literatur zu entnehmenden tensammetrischen Untersuchungen erstrecken sich über eine breite Substanz-Palette; vielseitig sind auch die Anwendungsgebiete (z.B. polarographisch inaktive Stoffe, Tenside, Makromoleküle, Inhibitoren, Fungizide sowie Biochemie und Flotation). Über die Adsorption anorganischer Stoffe liegen, wenn man von einfachen Ionen, z.B. des Leitelektrolyten, absieht, naturgemäss nur wenig Arbeiten vor. Bei organischen Verbindungen erstreckt sich dagegen das Stoffspektrum von den einfachsten Verbindungen bis zu ausgesprochenen Tensiden und Makromolekülen. In der abschliessenden Übersicht werden nach der Breyer–Bauer-Monographie erschienene Arbeiten, nach Substanz-Gruppen gegliedert, stichwortartig kurz zitiert. Tatsächlich ist der Bereich der Ergebnisse und Anwendungen wesentlich grösser als diese Übersicht vermittelt, da hier nur speziell

mit der Breyer-Methode durchgeführte Untersuchungen einbezogen wurden. Letztere lassen sich grösstenteils auf die mit anderen Methoden bearbeiteten Gebiete ausweiten.

Alkohole
Kettenlänge, Isomerie, Mehrfachbindung[26,89,116,136–138]
Mischadsorption und Lösungsmittel[26,59,94,115,116,120,130,139,140]
Zeitabhängigkeit und C–t-Kurven[18,26,71]
Inhibition[26,51,70,140,141], Wechselwirkungskoeffizient[26]
Oszillographische Square-Wave-Polarographie[58,59]
Oberwellen- und Doppeltonpolarographie[96]

Kationaktive Tenside
Alkylamin- und Alkylammoniumverbindungen[39,46,62,116,130,142,143]
Einfluss der Kettenlänge und t-Abhängigkeit[73]
Oszillographische Square-Wave-Polarographie[59]
Alkylpyridiniumverbindungen[26,35,89,117,138]
Fluortenside[26,51]
Zeitabhängigkeit[26,41,46,73], Mischadsorption[94]

Anionaktive Tenside
Sulfate[26,61,142,144,145], Osz.Squ.-W.-Pol.[59]
Sulfonate[26,35,69,89,117,142,146], Best. in PVC-Pulver:[147]
Fluortenside[26], Mischadsorption[26,89,94]

Nichtionogene Tenside
Polyglykoläther[26,35,69,89,117]
Einfluss des Äthoxylierungsgrades[56,148]
Mischadsorption[26,51,69,89,117], Prozesskontrolle[61]
Einfluss auf Durchtrittsprozesse[26,57,89,107,149–151]
Oszillographische Square-Wave-Polarographie[59]

Makromoleküle
Methylcellulose[56,116]; Mischadsorption und Inhibition[26]
Na-Carboxymethylcellulose: $\overline{M}$-Abhängigkeit[56], Mischadsorption[94]
Polyvinylalkohol[26,51,116,130]
Polyäthylenglykole: $\overline{M}$-, t-Abhängigkeit[18,26,35,72]; $\overline{M}$-Abhängigkeit, Oberflächenbedarf[72]; c-, t-Abh. d. Mischadsorption[26,35,57,94,118]; versch. tensammetrische Meth. (z.B. Oberwellen)[57,95]
Difo-P(Polydiglykolformal)[56]
Polyvinylpyrrolidon: $\overline{M}$-, t-Abh., Oberflächenbedarf[72]
Biopolymere: Umwandlungen und Grundkörper[152,153]

Verschiedenes
Struktureinfluss[26,137,138]
Kohlenwasserstoffe[26,138,145,154]
Dioxan[39], Cyclohexan[155], Resorcin, Phloroglucin[156]
Komplexe[157–159], Farbstoffe[139,160]

Organoschwefelverbindungen[145,161]; Inhibitoren[26,70,116,130]; Flotationsmittel[62,127,128,162]; Fungizide[163]
Organophosphorverbindungen[26,35,69,117,118,133,159,164]
Organozinnverbindungen[120,140,165]
Mischungen[26,35,51,57,59,69,89,94,115,116–119,127,130,140,142]
Vergleich mit Oszillopolarographie[37,117,121,166,167]
Oberwellen- und Doppeltonpolarographie[96]
Chromato-Tensammetrie[134]
Anorganische Stoffe: Polyphosphate (hydrolytischer Abbau)[168]

ZUSAMMENFASSUNG

Es wird eine Übersicht gegeben über den gegenwärtigen Stand der Mess- und Auswertetechnik, der Theorie sowie der Leistungsfähigkeit und Anwendung der Tensammetrie nach Breyer. Bei Einhaltung exakter Versuchsbedingungen und Berücksichtigung der Einflussgrössen besitzt die Tensammetrie nicht nur analytischen Wert, sondern auch Bedeutung für theoretische Untersuchungen des Gleichgewichtes und der Kinetik der Adsorption. Die wichtigsten Parameter vor allem für letzteres sind die Frequenz, die ohmschen Anteile (bzw. der Phasenwinkel) und die Zeit. Die theoretische Interpretation erfolgt nach den mit aufwendigeren Präzisionsmethoden erarbeiteten und überprüften Grundlagen. Durch Variation der wechselstrompolarographischen Messtechnik kann die Aussage in wissenschaftlicher und analytischer Hinsicht erweitert und vertieft werden. Durch den relativ geringen apparativen und zeitlichen Aufwand wurden tensammetrische Untersuchungen bereits in zahlreichen Anwendungsgebieten eingesetzt.

SUMMARY

A short review is given of the present development of the measurement and evaluation technique, of the theory as well as the performance and use of Breyer's Tensammetry. Provided that exact experimental conditions are observed and the parameters are taken into account, tensammetry has not only value in analysis, but also significance for the theoretical investigation of equilibria and kinetics of adsorption. The most important parameters are the frequency, the ohmic component (or the phase angle) and the time. The theoretical interpretation follows on the basis of fundamentals which have been developed and tested with the more tedious precision methods. By variation of a.c. polarographic techniques the scientific and analytical information value can be expanded and deepened. With relatively small expenditure of apparatus and time tensammetric investigations have been applied in numerous fields.

VERZEICHNIS DER VERWENDETEN SYMBOLE

a	= Wechselwirkungskoeffizient
A	= Elektrodenoberfläche (s. unten)
b	= Adsorptionskoeffizient
c_i	= Konzentration in der Lösung

c_0 = Konzentration in unmittelbarer Elektrodennähe
C = Differentialkapazität pro Flächeneinheit (s. unten)
ΔC_n = molare Kapazitätserniedrigung
C_T = kapazitiver Anteil der Zusatzimpedanz Z_T
C_∞ = "wahre" oder HF-Kapazität ($\omega = \infty$)
D = Diffusionskoeffizient
E = Elektrodenpotential
E_0 = Null-Ladungs-Potential
E_T, E_+, E_- = Scheitelpotentiale tensammetrischer Wellen
h = Höhe tensammetrischer Wellen (s. unten)
H = Behälterhöhe
I = Wechselstromdichte (s. unten)
$\overline{M}$ = mittleres Molekulargewicht von Makromolekülen
q = Ladungsdichte (s. unten)
R = Widerstand
R_L = Elektrolytwiderstand
R_M = Reihenwiderstände im Messkreis
R_T = ohmscher Anteil der Zusatzimpedanz Z_T
S = Oberflächenbedarf
t = Zeit
t_m = Tropfzeit
U = Wechselspannungsamplitude
Z = Gesamtimpedanz
Z_T = Zusatzimpedanz der tensammetrischen Welle
Z^{-1} = Admittanz pro Flächeneinheit (s. unten)
α = Konstante
β = Konstante
γ = Grenzflächenspannung
Γ = Oberflächenkonzentration
Γ_S = Oberflächenkonzentration bei $\theta = 1$
δ = Verlustwinkel
θ = Bedeckungsgrad
ν = Frequenz
φ = Phasenwinkel zwischen Strom und Spannung
ω = $2\pi\nu$

NÄHERE BEZEICHNUNG EINIGER GRÖSSEN

	Oberfläche	*Kapazität*		
		allgemein	$\theta = 0$	$\theta = 1$
pro Flächeneinheit		C	C_0	C_S
beliebige Oberfläche	A	C_E	C_{0E}	C_{SE}
maximale Oberfläche	A_m	C_m	C_{0m}	C_{Sm}
mittlere Oberfläche	$\bar{A}$	$\bar{C}$	$\bar{C}_0$	$\bar{C}_S$

gilt entsprechend für q, h, I und Z^{-1}.

LITERATUR

1 B. BREYER UND F. GUTMANN, *Trans. Faraday. Soc.*, 42 (1946) 645.
2 P. DELAHAY, *New Instrumental Methods in Electrochemistry*, Interscience, New York, 1954, S. 146, 375.
3 B. BREYER UND H. H. BAUER, *Alternating Current Polarography and Tensammetry*, Interscience, New York, 1963.
4 H. W. NÜRNBERG UND M. VON STACKELBERG, *J. Electroanal. Chem.*, 4 (1962) 1.
5 H. W. NÜRNBERG UND G. WOLFF, *Chem. Ing.-Tech.*, 37 (1965) 977.
6 H. W. NÜRNBERG UND G. WOLFF, *Chem. Ing.-Tech.*, 38 (1966) 160.
7 H. SCHMIDT UND M. VON STACKELBERG, *Die neuartigen polarographischen Methoden, ihr Prinzip und ihre Möglichkeiten*, Verlag Chemie, Weinheim/Bergstr., 1962.
8 G. GOUY, *Ann. Chim. Phys.*, 8 (1906) 291.
9 M. PROSKURNIN UND A. N. FRUMKIN, *Trans. Faraday Soc.*, 31 (1935) 110.
10 P. J. DOLIN UND B. V. ERSHLER, *J. Phys. Chim. USSR*, 14 (1940) 886.
11 D. C. GRAHAME, *J. Am. Chem. Soc.*, 63 (1941) 1207; 71 (1949) 2975; *Chem. Rev.*, 41 (1947) 441.
12 B. BREYER UND S. HACOBIAN, *Australian J. Sci. Res. Ser. A*, 5 (1952) 500.
13 K. S. G. DOSS UND A. KALYANASUNDARAM, *Proc. Indian Acad. Sci.*, 35A (1952) 27.
14 D. E. SMITH, *Advances in Electroanalytical Chemistry*, Vol. 1, herausgegeben von A. J. BARD, Marcel Dekker, New York, 1966, S. 1.
15 D. E. WALKER, R. N. ADAMS UND J. R. ALDEN, *Anal. Chem.*, 33 (1961) 308.
16 J. H. SLUYTERS, *Rec. Trav. Chim.*, 79 (1960) 1092.
17 H. SCHMIDT UND M. VON STACKELBERG, *J. Electroanal. Chem.*, 1 (1959) 133.
18 H. JEHRING, *J. Electroanal. Chem.*, 20 (1969) 33.
19 J. H. M. REK, M. D. WIJNEN UND J. H. SLUYTERS, *Rec. Trav. Chim.*, 84 (1965) 1035.
20 M. SLUYTERS-REHBACH, D. J. KOOIJMAN UND J. H. SLUYTERS, *Proc. IIIrd Intern. Congr. Polarography*, herausgegeben von G. J. HILLS, Macmillan, London, 1966, S. 135.
21 A. N. FRUMKIN UND B. B. DAMASKIN, *J. Electroanal. Chem.*, 3 (1962) 36.
22 H. H. BAUER, *Rev. Polarog. (Kyoto)*, 11 (1963) 58; *Proc. Ist Australian Conf. on Electrochemistry*, herausgegeben von J. A. FRIEND UND F. GUTMANN, Pergamon Press, New York, 1965, S.282; *Mod. Aspects Polarog.*, (1966) 58; H. H. BAUER, D. BRITZ UND D. C. S. FOO, *J. Electroanal. Chem.*, 9 (1965) 481.
23 J. H. SLUYTERS UND J. J. C. OOMEN, *Rec. Trav. Chim.*, 79 (1960) 1101.
24 J. HEYROVSKÝ UND J. KŮTA, *Grundlagen der Polarographie*, Akademie-Verlag, Berlin, 1965.
25 G. H. NANCOLLAS UND C. A. VINCENT, *Electrochim. Acta*, 10 (1965) 97.
26 H. JEHRING, *Habilitationsschrift*, T. U. Dresden, 1965.
27 H. BECKMAN UND W. O. GAUER, *Anal. Chem.*, 38 (1966) 1434.
28 B. BREYER, *Proc. IIIrd Intern. Congr. Polarography*, Vol. I, herausgegeben von G. J. HILLS, Macmillan, London, 1966, S. 49.
29 D. BRITZ UND H. H. BAUER, *J. Sci. Instr.*, 44 (1967) 843.
30 I. EPELBOIN UND L. VIET, *J. Chim. Phys.*, 60 (1963) 857; *Proc. Ist Australian Conf. on Electrochemistry*, herausgegeben von J. A. FRIEND UND F. GUTMANN, Pergamon, New York, 1965, S.261.
31 R. F. EVILIA UND A. J. DIEFENDERFER, *Anal. Chem.*, 39 (1967) 1885.
32 J. W. HAYES UND H. H. BAUER, *J. Electroanal. Chem.*, 3 (1962) 336.
33 J. W. HAYES UND C. N. REILLEY, *Anal. Chem.*, 37 (1965) 1322.
34 Heathkit-Geräte, Sprendlingen: Heath Malmstadt-Enke EUW-401 Polarography System.
35 H. JEHRING, *Proc. Anal. Chem. Conf., Budapest, 1966.*
36 H. JEHRING UND J. SCHMIDT, in Vorbereitung.
37 R. KALVODA, *J. Electroanal. Chem.*, 1 (1959–60) 314.
38 D. J. KOOIJMAN UND J. H. SLUYTERS, *Rec. Trav. Chim.*, 83 (1964) 587.
39 Z. KOWALSKI UND J. SRZEDNICKI, *J. Electroanal. Chem.*, 8 (1964) 399.
40 N. G. LORDI, *Anal. Chem.*, 34 (1962) 1832.
41 L. NĚMEC, *Collection Czech. Chem. Commun.*, 31 (1966) 1162.
42 E. NIKI, H. SIRAI UND T. KYOYA, *Japan Analyst*, 15 (1966) 257.
43 T. F. RETAJCZYK UND D. K. ROE, *J. Electroanal. Chem.*, 16 (1968) 21.
44 D. E. SMITH, *Anal. Chem.*, 35 (1963) 1811.
45 E. M. L. VALERIOTE UND R. G. BARRADAS, *J. Electroanal. Chem.*, 12 (1966) 67.
46 S. VAVRIČKA, L. NĚMEC UND J. KORYTA, *Collection Czech. Chem. Commun.*, 31 (1966) 947; J. KORYTA, *Collection Czech. Chem. Commun.*, 18 (1953) 206.

47 A. WATANABA, F. TSUJI UND S. UEDA, *J. Electrochem. Soc. Japan.*, 22 (1954) 521.
48 H. YAMAOKA, *Acta Chem. Scand.*, 21 (1967) 2559.
49 S. B. ZFASSMAN, *Zavodsk. Lab.*, 26 (1960) 888; 30 (1964) 8; S. B. ZFASSMAN UND R. M. SALICHSHDANOWA, *Zavodsk. Lab.*, 30 (1964) 133.
50 Deutsche Akademie der Wissenschaften zu Berlin: Gleich-Wechselstrompolarograph GWP 563.
51 H. JEHRING, *Proc. IIIrd Intern. Congr. Polarogr.*, Vol. 1, herausgegeben von G. J. HILLS, Macmillan, London, 1966, S.349.
52 Polnische Akademie der Wissenschaften, Warschau: AC-Polarograph Type PZP-67.
53 W. SKALWEIT UND H. JEHRING, *Chem. Tech. Berlin*, 16 (1964) 290.
54 T. TAKAHASHI UND E. NIKI, *Talanta*, 1 (1958) 245.
55 G. C. BARKER UND R. L. FAIRCLOTH, *Advances in Polarography*, Vol. I, herausgegeben von I. S. LONGMUIR, Pergamon, New York, 1960, S. 313; G. C. BARKER UND A. W. GARDNER, *At. En. Res. Eestab. Gr. Br. Rept. C/R 1606*, 1955.
56 H. JEHRING, unveröffentlicht.
57 H. JEHRING, E. HORN, A. REKLAT UND W. STOLLE, *Collection Czech. Chem. Commun.*, 33 (1968) 1038.
58 K. OKAMOTO, *Mod. Aspects Polarog.*, (1966) 225.
59 K. OKAMOTO, *Bul. Chem. Soc. Japan*, 37 (1964) 293.
60 Metrohm AG Herisau (Schweiz): AC-Modulator E393 zum Polarecord E 261 R.
61 H. JEHRING, *Abhandl. Deut. Akad. Wiss. Kl. Chem., Geol. Biol.*, (1966) 197.
62 W. PÖTSCH, *Freiberger Forschungsh.*, A302 (1963) 53.
63 G. W. TUJEW UND L. S. SARETZKI, *Zavodsk. Lab.*, 29 (1963) 1291.
64 R. G. BARRADAS, F. M. KIMMERLE UND E. M. L. VALERIOTE, *J. Polarog. Soc.*, 13 (1967) 30.
65 M. W. BREITER, *J. Electrochem. Soc.*, 112 (1965) 845.
66 E. R. BROWN, D. E. SMITH UND D. D. DE FORD, *Anal. Chem.*, 38 (1966) 1130.
67 T. BIEGLER, *Australian J. Chem.*, 15 (1962) 34; B. BREYER, H. H. BAUER, J. R. BEEVERS UND T. BIEGLER, *Proc. Ist Australian Conf. on Electrochemistry*, herausgegeben von J. A. FRIEND UND F. GUTMANN, Pergamon, New York, 1965, S.292.
68 P. DELAHAY UND C. FIKE, *J. Am. Chem. Soc.*, 80 (1958) 2628; P. DELAHAY UND J. TRACHTENBERG, *J. Am. Chem. Soc.*, 79 (1957) 2355; 80 (1958) 2094.
69 H. JEHRING, *Z. Physik. Chem. Leipzig*, 225 (1964) 116.
70 H. JEHRING, *Z. Physik. Chem. Leipzig*, 226 (1964) 59.
71 H. JEHRING, *Z. Physik. Chem. Leipzig*, 229 (1965) 39.
72 H. JEHRING UND E. HORN, *Monatsber. Deut. Akad. Wiss. Berlin*, 10 (1968) 295.
73 H. KRAUS, H. JEHRING UND E. HORN, *Tenside*, in Vorbereitung.
74 H. A. LAITINEN UND B. MOSIER, *J. Am. Chem. Soc.*, 80 (1958) 2363.
75 C. N. REILLEY UND W. STUMM, *Progress in Polarography*, Vol. 1, herausgegeben von P. ZUMAN UND I. M. KOLTHOFF, Interscience, New York, 1962, S.81.
76 W. H. REINMUTH, *Advan. Anal. Chem. Instr.*, 1 (1960) 241.
77 J. H. M. REK, M. D. WIJNEN UND J. H. SLUYTERS, *Rec. Trav. Chim.*, 84 (1965) 1071.
78 J. O'M. BOCKRIS, M. A. V. DEVANATHAN UND K. MÜLLER, *Proc. Roy. Soc. (London) Ser. A*, 274 (1963) 55.
79 J. O'M BOCKRIS, E. GILEADI UND K. MÜLLER, *Electrochim. Acta*, 12 (1967) 1301.
80 B. E. CONWAY, *Theory and Principles of Electrode Processes*, The Ronald Press, New York, 1965.
81 P. DELAHAY, *Double Layer and Electrode Kinetics*, Interscience, New York, 1965.
82 R. PARSONS, *Advan. Electrochem. Electrochem. Eng.*, 1 (1961) 1.
83 M. A. V. DEVANATHAN UND B. V. K. S. R. A. TILAK, *Chem. Rev.*, 65 (1965) 635.
84 A. N. FRUMKIN UND B. B. DAMASKIN, *Modern Aspects of Electrochemistry*, Vol. III, herausgegeben von J. O'M. BOCKRIS UND B. E. CONWAY, Butterworths, London, 1964.
85 D. M. MOHILNER, *Advances in Electroanalytical Chemistry*, Vol. I, herausgegeben von A. J. BARD, Marcel Dekker, New York, 1966, S.241.
86 R. PARSONS, *J. Electroanal. Chem.*, 7 (1964) 136.
87 A. N. FRUMKIN, *Z. Physik. Chem.*, 116 (1925) 466.
88 E. BLOMGREN, J. O'M. BOCKRIS UND C. JESCH, *J. Phys. Chem.*, 65 (1961) 2000; J. O'M. BOCKRIS UND G. A. RAZUMNEY, *Fundamental Aspects of Electrocrystallization*, Plenum Press, New York, 1967.
89 H. JEHRING, *Abhandl. Deut. Akad. Wiss. Berlin, Kl. Chem., Geol. Biol.*, (1964) 472.
90 K. J. VETTER, *Elektrochemische Kinetik*, Springer, Berlin, 1961.
91 P. DELAHAY, *Advan. Electrochem. Electrochem. Eng.*, 1 (1961) 233.

92 R. NEEB, *Fortschr. Chem. Forsch.*, 4 (1963) 333.
93 H. H. BAUER UND D. C. S. FOO, *Australian J. Chem.*, 19 (1966) 1103.
94 H. JEHRING, in Vorbereitung.
95 H. JEHRING UND W. STOLLE, *Collection Czech. Chem. Commun.*, 33 (1968) 1670.
96 R. NEEB, *Z. Anal. Chem.*, 208 (1965) 168.
97 B. BREYER, T. BIEGLER UND H. H. BAUER, *Rev. Polarog. (Kyoto)*, 11 (1963) 50.
98 A. N. FRUMKIN UND W. I. MELIK-GAYKASJAN, *Dokl. Akad. Nauk SSSR*, 77 (1951) 855; W. I. MELIK-GAYKASJAN, *Zh. Fiz. Khim.*, 26 (1952) 500.
99 T. BERZINS UND P. DELAHAY, *J. Phys. Chem.*, 59 (1955) 906.
100 W. LORENZ UND F. MÖCKEL, *Z. Elektrochem.*, 60 (1956) 507.
101 W. LORENZ UND F. MÖCKEL, *Z. Elektrochem.*, 60 (1956) 939.
102 R. PARSONS UND P. C. SYMONS, *Trans. Faraday Soc.*, 64 (1968) 1077.
103 W. LORENZ, *Z. Elektrochem.*, 62 (1958) 192.
104 W. LORENZ UND G. KRÜGER, *Z. Physik. Chem. Leipzig*, 221 (1962) 231; 236 (1967) 253; *Z. Physik. Chem. N. F.*, 56 (1967) 268.
105 H. H. BAUER UND P. J. ELVING, *Australian J. Chem.*, 12 (1959) 343; *J. Am. Chem. Soc.*, 82 (1960) 2091.
106 R. S. HANSEN, R. E. MINTURN UND D. A. HICKSON, *J. Phys. Chem.*, 60 (1956) 1185; 61 (1957) 953.
107 G. H. AYLWARD UND J. W. HAYES, *J. Electroanal. Chem.*, 8 (1964) 442.
108 R. A. ARAKEIJAN UND G. A. TEDORADZE, *Elektrokhimiya*, 4 (1968) 144.
109 E. D. BELOKOLOS, *Elektrokhimiya*, 1 (1965) 498.
110 D. BRITZ UND H. H. BAUER, *Electrochim. Acta*, 13 (1968) 347.
111 J. A. V. BUTLER UND CH. OCKRENT, *J. Phys. Chem.*, 34 (1930) 2286, 2841; CH. OCKRENT UND J. A. V. BUTLER, *J. Phys. Chem.*, 34 (1930) 2297.
112 C.-S. TZA, Y.-H. CHOU, G.-Y. CHOU UND C.-T. LO, *Sci. Sinica Peking*, 14 (1965) 63.
113 G. A. DOBRENKOW UND R. K. BANKOWSKI, *Izv. Vysshikh. Uchebn. Zavednii, Khim. i Khim. Tekhnol.*, 5 (1962) 75.
114 K. EDA UND K. TAKAHASHI, *Nippon Kagaku Zasshi*, 85 (1964) 828.
115 S. L. GUPTA UND S. K. SHARMA, *Electrochim. Acta*, 10 (1965) 151.
116 H. JEHRING, *Dissertation*, Dresden, 1958.
117 H. JEHRING, *Chem. Zvesti*, 18 (1964) 313.
118 H. JEHRING, *Abhandl. Deut. Akad. Wiss. Berlin, Kl. Chem., Geol. Biol.*, (1966) 652.
119 H. JEHRING, Chemie-Dozententagung, Dresden, 1967.
120 H. JEHRING UND H. MEHNER, *Z. Chem.*, 3 (1963) 34; *Z. Anal. Chem.*, 224 (1967) 136.
121 R. KALVODA, *Acta Chim. Acad. Sci. Hung.*, 32 (1962) 293.
122 B. KASTENING, *Ber. Bunsenges. Physik. Chem.*, 68 (1964) 979; *J. Electroanal. Chem.*, 9 (1965) 41; B. KASTENING UND L. HOLLECK, *Z. Elektrochem.*, 64 (1960) 823.
123 B. KASTENING UND L. HOLLECK, *Talanta*, 12 (1965) 1259.
124 P. A. KIRKOW, *Dokl. Akad. Nauk SSSR*, 135 (1960) 651.
125 S. G. MAIRANOVSKI, *Talanta*, 12 (1965) 1299.
126 Z. OSTROWSKI UND H. FISCHER, *Electrochim. Acta*, 8 (1963) 1, 37.
127 A. POMIANOWSKI UND J. PAWLIKOWSKA-CZUBAK, *Przemysl Chem.*, 46 (1967) 481.
128 W. PÖTSCH UND K. SCHWABE, *J. Prakt. Chem.*, 18 (1962) 1.
129 F. W. SCHAPINK, M. OUDEMAN, K. W. LEU UND J. N. HELLE, *Trans. Faraday Soc.*, 56 (1960) 415.
130 K. SCHWABE UND H. JEHRING, *Z. Anal. Chem.*, 173 (1960) 36.
131 G. A. TEDORADZE, R. A. ARAKELJAN UND E. D. BELOKOLOS, *Elektrokhimiya*, 2 (1966) 563.
132 S. I. ZDANOW UND B. A. KISELEV, *Zh. Fiz. Khim.*, 40 (1966) 484.
133 H. JEHRING UND A. REKLAT, in Vorbereitung.
134 Polnische Akademie der Wissenschaften, Warschau: Chromatopolarograph CHP-67; W. KEMULA, B. BEHR, K. CHELBICKA UND D. SYBILSKA, *Roczniki Chem.*, 39 (1965) 1315.
135 L. GIERST, D. BERMANE UND P. CORBUSIER, *Ric. Sci., Suppl.*, 29 (1959) 75.
136 S. L. GUPTA UND S. K. SHARMA, *Kolloid-Z.*, 190 (1963) 40.
137 S. L. GUPTA UND S. K. SHARMA, *J. Indian Chem. Soc.*, 41 (1964) 384, 663, 668; 42 (1965) 855; 43 (1966) 53.
138 S. L. GUPTA UND S. K. SHARMA, *Abhandl. Deut. Akad. Wiss. Berlin., Kl. Med.*, (1966) 611.
139 S. L. GUPTA, M. K. CHATTERJI UND S. K. SHARMA, *J. Electroanal. Chem.*, 7 (1964) 81.
140 H. MEHNER, *Dissertation*, Berlin, 1967.
141 S. L. GUPTA UND S. K. SHARMA, *Talanta*, 11 (1964) 105.

142 P. DIETRICH, *Abhandl. Deut. Akad. Wiss. Berlin, Kl. Chem., Geol. Biol.*, (1966) 208.
143 A. POMIANOWSKI, *Abhandl. Deut. Akad. Wiss. Berlin, Kl. Chem., Geol. Biol.*, (1966) 642.
144 G. KRETZSCHMAR UND D. VOLLHARDT, *Ber. Bunsenges. Physik. Chem.*, 71 (1967) 410.
145 R. NARAYAN, *Proc. Nat. Inst. Sci. India*, A32 (1966) 63.
146 H. JEHRING UND GY. PALYI, *Magyar Kem. Folyoir.*, 71 (1965) 427; 72 (1966) 29; GY. PALYI, A. MERENY, H. JEHRING UND L. MOLNAR, *Magyar Kem. Folyoir.*, 73 (1967) 98.
147 E. SCHRÖDER, M. HELMSTEDT UND H. JEHRING, *Plaste und Kautschuk*, 12 (1965) 666.
148 H. JEHRING UND A. WEISS, Vortragstagung des Fachverbandes Anal. Chem. zur Haupttagung der Chem. Ges. der DDR, Berlin, 1967.
149 M. ISHIBASHI, T. FUJINAGA UND M. SATO, *J. Electrochem. Soc. Japan (Overseas Ed.)*, 27 (1959) 28.
150 H. JEHRING UND W. STOLLE, *Z. Chem.*, 4 (1964) 309.
151 N. TANAKA, R. TAMAMUSHI UND A. TAKAHASHI, *Collection Czech. Chem. Commun.*, 25 (1960) 3016.
152 H. BERG, *Abhandl. Deut. Akad. Wiss. Berlin, Kl. Med.*, (1966) 479; H. BERG UND H. BÄR, *Monatsber. Deut. Akad. Wiss. Berlin*, 7 (1965) 210; *Studia Biophys. (Berlin)*, 3 (1967) 133; H. BERG, H. BÄR UND F. A. GOLLMICK, *Biopolymers*, 5 (1967) 61; H. BERG UND F. A. GOLLMICK, *Abhandl. Deut. Akad. Wiss. Berlin, Kl. Med.*, (1966) 533; J. FLEMMING UND H. BERG, *Abhandl. Deut. Akad. Wiss. Berlin, Kl. Med.*, (1966) 559; L. KITTLER UND H. BERG, *Abhandl. Deut. Akad. Wiss. Berlin, Kl. Med.*, (1966) 547.
153 E. PALEČEK, *J. Mol. Biol.*, 20 (1966) 263; E. PALEČEK UND V. VETTERL, *Biopolymers*, 6 (1968) 917; V. VETTERL, *Abhandl. Deut. Akad. Wiss. Berlin, Kl. Med.*, (1966) 493.
154 B. A. SHENOI UND K. S. NARASIMHAN, *J. Sci. Ind. Res. (India)*, B21 (1962) 262.
155 K. TSUJI, *Rev. Polarog. (Kyoto)*, 11 (1964) 233; *Mod. Aspects Polarog.*, (1966) 233.
156 R. NARAYAN, *Electrochim. Acta*, 7 (1962) 111.
157 T. M. FLORENCE UND G. H. AYLWARD, *Australian J. Chem.*, 15 (1962) 65.
158 S. L. GUPTA, J. N. JAITLY UND R. N. SONI, *J. Indian Chem. Soc.*, 42 (1965) 384; S. L. GUPTA, S. K. SHARMA UND R. N. SONI, *Electrochim. Acta*, 10 (1965) 549.
159 H. SOHR UND K'H. LOHS, *Monatsber. Deut. Akad. Wiss. Berlin.*, 9 (1967) 327.
160 S. L. GUPTA, L. SARASWATHI UND S. K. SHARMA, *Indian J. Chem.*, 1 (1963) 283.
161 K. OKAMOTO, *Bull. Chem. Soc. Japan*, 34 (1961) 920, 1063.
162 A. POMIANOWSKI, *Roczniki Chem.*, 41 (1967) 775.
163 H. SAÜBERLICH, H. WOGGON UND H. JEHRING, im Druck.
164 H. SOHR, *Dissertation*, Leuna-Merseburg, 1963.
165 H. JEHRING UND H. MEHNER, *Z. Chem.*, 4 (1964) 273.
166 G. DUSINSKI, *Abhandl. Deut. Akad. Wiss. Berlin, Kl. Chem., Geol. Biol.*, (1964) 176.
167 GY. PALYI UND H. JEHRING, *Collection Czech. Chem. Commun.*, 30 (1965) 4339.
168 V. VETTERL UND J. BOHÁČEK, *J. Electroanal. Chem.*, 16 (1968) 313.

ELECTROANALYTICAL CHEMISTRY AND INTERFACIAL ELECTROCHEMISTRY
Elsevier Sequoia S.A., Lausanne – Printed in The Netherlands

INFLUENCES ON HOMOGENEOUS CHEMICAL REACTIONS IN THE DIFFUSE DOUBLE LAYER

H. W. NÜRNBERG AND G. WOLFF
Zentrallabor für Chemische Analyse, Kernforschungsanlage Jülich, GmbH (Germany)
(Received November 28th, 1968)

INTRODUCTION

Much of the credit for the remarkable general development of voltammetry during the last 20 years goes to the late Professor Breyer, "the father of a.c. polarography"[1].

Meanwhile, a.c. polarography has developed in many ways[2,3]. One significant trend of fundamental interest has been the increase in potentialities offered by high frequency methods with very short measuring times, t_1. The shorter the accessible t_1-values, the more sensitive becomes a given voltammetric technique for the kinetics of charge transfer reactions and of very fast chemical steps involved in the overall electrode process. The application of these advanced techniques, among them Breyer's a.c. polarography, to the study of the current–voltage curve, has led to many fundamental conclusions, one of the most important being that very fast chemical steps are involved in most electrode processes. Thus, these advances have forced electrochemists to depart from simple, conventional views and models, but, on the other hand, have rewarded them by the more detailed and accurate knowledge obtainable about the complicated phenomenon called the electrode process.

Besides these general aspects, certain voltammetric techniques provide an attractive and advantageous alternative[4,5] to other non-electrochemical relaxation methods[6–9] for the study of the kinetics of several types of fast homogeneous chemical reactions in solution. The basic condition for the voltammetric approach is to find a suitable electrode reaction to couple to the chemical system. The charge transfer step then achieves by rapid consumption of one of the chemical reactants a very rapid shift of the chemical equilibrium in the neighbourhood of the test electrode. At the same time, the current, or one of its components, being partly dependent on the rate of the chemical reaction initiated by the equilibrium shift, provides experimental access to the kinetics of the forward and backward reaction of the chemical system, if suitable conditions have been selected.

An example of this application of voltammetry to fast homogeneous chemical kinetics in solution is the study of the dissociation and recombination of carboxylic acids and other weak acids containing no further electrochemically reactive substituents. For several years we have studied intensively this type of reaction[4,5,10–13] using an advanced technique of polarographic character called high level faradaic rectification (HLFR)[14–16]. This technique allows the application of measuring times, t_1, down to 1 μsec, thus giving a kinetic determination limit for first-order rate constants up to $3 \cdot 10^8$ sec^{-1}.

In the study of these proton transfer processes, the reduction of the H^+-ions at a mercury electrode serves as the coupled electrode reaction, and as overall electrode process one has:

$$HA \underset{k_r}{\overset{k_d}{\rightleftarrows}} H^+ + A^- \qquad \text{(I)}$$

$$H^+ + e^- \xrightarrow{k_{ct}} \tfrac{1}{2} H_2 \qquad \text{(II)}$$

The reactants are naturally hydrated in aqueous solution.

FUNDAMENTAL ASPECTS OF THE APPLICATION OF VOLTAMMETRIC METHODS

As the electrode reaction is restricted to the electrode/solution phase boundary, the resulting gradual shift of the chemical equilibrium in the direction of dissociation is limited in the pseudo-stationary state established after the relaxation time to a

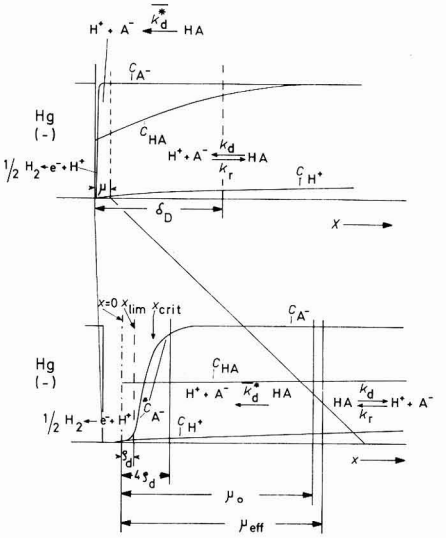

Fig. 1. Schematic model of the surroundings of the test electrode and the concn. profiles of reactants in this range. Upper part: diffusion layer (δ_D) with reaction layer (μ); lower part: formal (μ_0) and effective (μ_{eff}) reaction layer thickness with effective diffuse double layer of diameter, 4 ρ_d. The outer Helmholtz-plane is at $x=0$ and the region between electrode surface and $x=0$ corresponds to the inner or compact part of the double layer. The position of the planes, x_{lim} and x_{crit}, is indicated by arrows.

reaction layer with a thickness defined generally by eqn. (1). This reaction layer surrounds the test electrode (see Fig. 1).

$$\mu = (D_{H^+}/k_r c_{A^-})^{\frac{1}{2}} \qquad (1)$$

D_{H^+} is the diffusion coeffficient of the H^+-ions, k_r the recombination rate constant and c_{A^-} the concentration of the carboxylate anions. For the proton transfer reactions considered, μ equals 20–60 Å according to the adjusted value of c_{A^-}.

This situation, typical of the voltammetric approach, creates two major problems[4,5].

(i) The participation of mass transfer of the reactants towards and from the test electrode region is unavoidable. Restriction of the mass transfer to diffusion or convective diffusion by using suitable techniques allows easy elimination of the mass transfer contribution to the overall rate of the electrode process in the evaluation of the electrical signal measured. However, as the rate of diffusion decays with the time elapsed from the start of the overall process, (I + II), by polarization of the test electrode, the time, t_1, has to be restricted to sufficiently small values so that the overall rate and the corresponding electrical signal are at least less than 90% (preferably less than 75%) controlled by diffusion. In this respect, the HLFR-method with its t_1-values down to 1 μsec has allowed access to the kinetics of a large number of very fast reactions not accessible hitherto by any other voltammetric technique.

(ii) There remains as a second problem, increasing in importance with the amount by which the electrode potential differs from the electrocapillary zero potential, the fact that the inner part of the reaction layer coincides with the diffuse part of the double layer (see Fig. 1). Consequently, the homogeneous chemical reaction —for instance the dissociation and recombination of acid (I)—proceeds partly in an electric field increasing progressively over the diffuse double layer in direction towards the outer Helmholtz plane (O.H.P.). Thus, the chemical steps will be influenced diversely and to a different extent by several double-layer effects. The present paper deals with the resulting problems. The dissociation and recombination of weak acids will be taken as example for the treatment. However, it must be stressed that the conclusions are generally valid for all chemical reactions in which a charged or uncharged particle dissociates into two differently charged products according to:

$$U^z \underset{k_r}{\overset{k_d}{\rightleftarrows}} X^{z+} + Y^{z-} \qquad \text{(III)}$$

Important further examples would be metal complexes and ion-pairs. The various double-layer effects to be considered are:

(i) A static ψ-effect on the stationary concentration of charged reactants.

(ii) A dynamic ψ-effect on the reactant of the charge transfer step, *i.e.*, the H^+-ions in our example. As the evaluation is restricted to the limiting current region, this effect will not affect the rate of the overall process in this range[4].

(iii) The progressive decrease of the dielectric constant, ε, of the medium in the solution layers of the diffuse part of the double layer adjacent to the outer Helmholtz plane caused by the growing electric field strength and by the total of all solute particles present. This decrease of ε is related to the polarization of the solvent.

(iv) A dissociation field effect increasing the dissociation rate in the solution layers adjacent to the outer Helmholtz plane. This effect is substantial for larger differences between the electrode potential and the potential of the electrocapillary zero (and, consequently, high charge densities of the electrode) and may even become the dominating double-layer effect on chemical reactions prior to the charge transfer.

Thus, an electrode is not an ideal probe for determining the kinetics of fast homogeneous chemical reactions in solution and it is evident that the evaluation of relevant and sufficiently exact values for the rate constants requires corrections for double-layer effects.

Although several authors[17-20] have already deduced corrections for ψ-effects and effect (iii) has also been treated[21-24], a quantitative treatment of the dissociation

field effect (iv) was missing until recently although the need for it had often been indicated[17,20,25,42]. Barker[26] has proposed an empirical global correction for the sum of *all* these double-layer effects on the rate of homogeneous chemical reactions prior to the charge transfer step. We have demonstrated the potentialities and range of this correction[4,5,10,12,13]. It applies if the condition: $\mu \geqslant 4\ \rho_d$ is met, where ρ_d is the formal thickness of the diffuse double layer which for a 1,1-electrolyte medium of ionic strength, I, is given by:

$$\rho_d = 1.988 \cdot 10^{-10}\ (\varepsilon T/I)^{\frac{1}{2}} \qquad (2)$$

The advantage of this empirical correction, dicussed in detail elsewhere[4,5,27], is that it relies on experimental data for a given system and remains independent of special theoretical models for the structure of the double layer and their mode of action as well as of possible errors in the relative distribution of the global effect on the four effects mentioned previously. Thus, there are no longer any fundamental uncertainties in the application of voltammetric techniques in the study of fast chemical reactions in solution.

APPROXIMATE THEORETICAL TREATMENT OF DOUBLE-LAYER EFFECTS

Although, from a practical viewpoint, a satisfactory situation had been achieved, it was desirable to attempt a detailed theoretical treatment of all the various double-layer effects on chemical reactions prior to the charge transfer step. We made a first approximate attempt[27] by treating the diffuse double layer by the Gouy–Chapman-theory[28] and the dissociation field effect according to the theory of Onsager[29]. As it was found that the dissociation field effect rapidly became a dominating influence if the ψ-potential in the outer Helmholtz plane, ψ_H, exceeded |50 mV|, for simplicity all other double-layer effects were neglected in this treatment. Also, neither the progressive decrease of the dielectric constant, ε, near the electrode nor the screening action of the supporting electrolyte ions on the reactants were accounted for. Thus, a more refined and detailed reconsideration of the whole problem seemed desirable for reasons of consistency although preliminary calculations[30] showed that no fundamental alterations in the main results were to be expected*.

(*a*) *Experimental*

The following experimental conditions will be assumed for the subsequent treatment.

The test electrode is a dropping mercury electrode. The temperature is 20°. The aqueous solution contains 1 *M* LiCl as inert supporting electrolyte. This salt also adjusts the ionic strength in the bulk of the solution and the thickness, ρ_d, of the diffuse double layer, because the reactants of the acid equilibrium (I), *i.e.*, HA, H^+ and A^-, are present in such small concentrations that in practice only LiCl is responsible for the formation of the double layer. Thus, the outer Helmholtz plane will be defined by the plane of closest approach to the electrode for the centres of the primarily hydrated

* The published treatment of the global correction for double-layer effects will not be influenced at all in the practical aspects by the present refined theoretical treatment. However, with respect to improved consistency, in the electrical equivalent circuit in Fig. 1 of ref. 27 the resistance, R_{DS}, equivalent to the total of all double-layer effects should be inserted in place of R_{fd}.

Li^+-ions. For the concentration ratio of the carboxylic acid HA and the corresponding anion A^- we shall always assume the condition:

$$c_{HA}/c_{A^-} \leqslant \tfrac{1}{10} \tag{3}$$

thus converting the recombination into a pseudo-monomolecular step of first-order. Complications due to specific adsorption of reactants, of impurities and of supporting electrolyte ions will be regarded as absent. This is a realistic assumption, because at the rather negative electrode potentials, E, in the limiting current region for the H^+-reduction at the DME, there will certainly be no specific adsorption of anions and still no specific adsorption of Li^+-ions. In fact, many of the carboxylic acids, HA, are specifically adsorbed up to E more positive than -1.2 to -1.3 V (NCE), but desorb at more negative potentials[12,13]. In this respect, the selection of an electrode material with very large hydrogen overvoltage like mercury is of importance for the feasibility of the measurements on many carboxylic acid systems.

It is presumed that a voltammetric technique is employed, where the electrode potential, E, is adjusted and the resulting current or one of its components is the signal measured (though analogous arguments could be put forward for methods of the galvanostatic or coulostatic branch). Because in chemical kinetics only the forward and backward rates of (I) are of interest, the limiting current region of the current–potential curves will be evaluated. Owing to the total irreversibility of the hydrogen evolution on mercury and the extremely short measuring intervals, t_1, in the μsec-range applied with the HLFR-technique, the limiting current region falls into the very negative potential range of -2.2 to -2.3 V (SCE), *i.e.*, about -1.6 to -1.7 V more negative than the potential of the electrocapillary zero for aqueous 1 *M* LiCl-solutions. In view of the extent and complexity of the calculations, the present treatment will be restricted to the electrode potentials mentioned, E, and the ionic strength, $I = 1.0$, in the bulk of the solution. Calculations according to the scheme to be outlined are being extended with the aid of computer programmes to a scale of electrode potentials and ionic strength values and the resulting data will be published[31] in the form of tables as guide for the design and the evaluation of further investigations.

(*b*) *Calculation of the double-layer parameters*

First, the function of the ψ-potential and the corresponding electrical field strength, ϕ, over the effective diffuse double layer have to be calculated. Empirically it has been shown[4,5,12,27] that the effective thickness of the diffuse double layer is given by:

$$\rho_{d_{eff}} = 4\,\rho_d\,, \tag{4}$$

where ρ_d is defined by eqn. (2). The calculation is based on the Gouy–Chapman-theory[28] with the modification that allowance is made for the progressive decrease of the dielectric constant, ε, towards the outer Helmholtz plane, while, on average, ε is regarded as constant within every plane parallel to the O.H.P.

There are two reasons for the decrease of ε.

(i) With decreasing distance, x, from the O.H.P. there is a progressive increase in the concentration of the supporting electrolyte cations, *i.e.*, the Li^+-ions, in our case. Thus, from the total amount of available water, the fraction bound in the

primary hydration shells of Li^+-ions, where the H_2O-dipoles are in the stage of dielectric saturation[32]*, increases the smaller the value of x.

Other authors[39,53] in their studies on other systems have allowed for the progressive decrease of the dielectric constant across the double layer. However, as their calculations contain certain approximations based on the different objectives of their investigations, for our purposes a calculation along the lines indicated in the following sections was regarded as necessary.

(ii) In addition, the effect of the progressively increasing electric field strength ϕ_x on the remaining "free" H_2O-dipoles increases with decreasing x.

The complex situation outlined required an iterative computation of the profiles of ψ, ϕ and ε over the diffuse double layer[4].

The potential-dependence of the differential double-layer capacity was determined for 1 M LiCl up to -2.0 V (SCE) with a square-wave-polarograph at a frequency of 225 Hz[4]. The curve could be extrapolated satisfactorily up to -2.4 V (SCE). By stepwise integration, the value $Q_d = 34.3\ \mu C\,cm^{-2}$ was obtained for the total charge density of the diffuse double layer at an electrode potential, $E = -2.2$ to -2.3 V (SCE). Inserting for the dielectric constant the bulk value in 1 M LiCl ($\varepsilon_{0_I} = 65$) values for ψ_H, the ψ-potential at the O.H.P., and for ρ_d were first obtained from eqn. (5).

$$Q_d = -11.72\,(\varepsilon_{0_I}/\varepsilon_{H_2O})^{\frac{1}{2}}\, c_I^{\frac{1}{2}} \cdot \sinh\{(zF/2\,RT)\psi_H\} \tag{5}$$

$\varepsilon_{H_2O} = 80$; c_I is the inert excess electrolyte concentration (LiCl in our case) in moles/l.

Curve 1 in Fig. 2 for the ψ-profile could be calculated using eqn. (6).

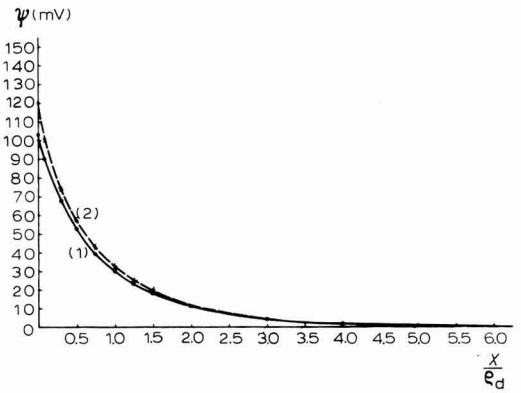

Fig. 2. ψ-potential profile across effective diffuse double layer for $Q_d = 34.3\ \mu C\ cm^{-2}$ and $I = 1.0$ with LiCl. (1), 1st iteration; (2), 2nd iteration.

$$\frac{\tanh\{(zF/4\,RT)\psi_x\}}{\tanh\{(zF/4\,RT)\psi_H\}} = \exp - \frac{x}{\rho_d} \tag{6}$$

A first result for the ϕ-profile followed (see curve 1 in Fig. 3) using eqn. (7).

* In the primary hydration shell of Li^+-ions 2.3 H_2O-dipoles are to be regarded on time average as always in the stage of total dielectric saturation[33].

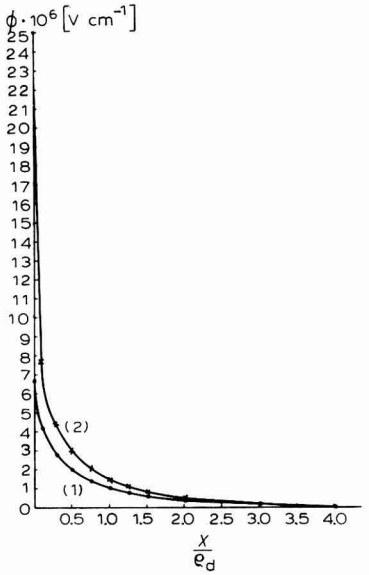

Fig. 3. Profile of electric field strength, ϕ, across effective diffuse double layer for $Q_d = 34.3\ \mu C\ cm^{-2}$ and $I = 1.0$ with LiCl. (1), 1st iteration; (2), 2nd iteration.

$$\phi_x = -\frac{2RT}{zF}\frac{1}{\rho_d}\sinh\left(\frac{zF}{2RT}\psi_x\right) \tag{7}$$

Subsequently, for each ψ_x, a first iteration value of the corresponding concentrations, $(c^*_{Li})_x$ and $(c^*_{Cl^-})_x$, within the diffuse double layer was calculated with eqn. (8).

$$(c^*)_x = {}^0c \exp -(zF/RT)\psi_x \tag{8}$$

The calculation of the distribution of the ion concentrations according to eqn. (8) is a simplifying approximation. The introduction of relations accounting for the final volume of the ions and the polarization of the solvent[21-23] would be more exact. The net result would be somewhat smaller values for $(c^*)_x$.

Generally, the decrease of the macroscopic dielectric constant of a solution due to growing ion concentrations, and the consequent increase of the amount of solvent dipoles in the dielectric saturation stage is given by[34,35]:

$$(\varepsilon_{0_I}) = \varepsilon_{H_2O} - (c_{Li^+}\delta_{Li^+}) - (c_{Cl^-}\delta_{Cl^-}) \tag{9}$$

Up to moderate salt concentrations of about 2 moles/l, the sum, $\delta_{Li^+} + \delta_{Cl^-} \approx -15$ l/mole is a constant, while at higher salt concentrations its value decreases at a progressively declining rate (see Fig. 4). From a comparison of the values for the sum, $\delta_+ + \delta_-$, for other alkali chlorides at moderate concentrations ($\leqslant 2$ moles/l) it was concluded[4] that to a first approximation:

$$\delta_{Li^+} \approx \tfrac{2}{3}(\delta_{Li^+} + \delta_{Cl^-}) \tag{10a}$$

and

$$\delta_{Cl^-} \approx \tfrac{1}{3}(\delta_{Li^+} + \delta_{Cl^-}) \tag{10b}$$

Thus, assuming that this distribution ratio for the δ-increments remains constant for all LiCl-concentrations, one can compute from the known concentration-dependence of the sum, $\delta_{Li^+} + \delta_{Cl^-}$, in symmetrical LiCl-solutions (see Fig. 4) the profile of δ_{Li^+} with respect to c_{Li^+}, which is given in Fig. 5. From this curve the $(\delta_{Li^+})_x$-value corresponding to each $(c^*_{Li^+})_x$ was interpolated, while for $(\delta_{Cl^-})_x$ the constant value -5 l/mole was taken. Inserting the respective values of the increments, $(\delta_{Li^+})_x$ and $(\delta_{Cl^-})_x$, and the corresponding concentrations, $(c^*_{Li^+})_x$ and $(c^*_{Cl^-})_x$, in eqn. (9) the profile of $(\varepsilon^*_{0_I})_x$, (*i.e.*, the decreased macroscopic dielectric constant in each solution layer at a given distance, x, due solely to the progressive increase in ion concentration and in asymmetry of ion distribution over the diffuse double layer) followed (see Fig. 6, upper curve).

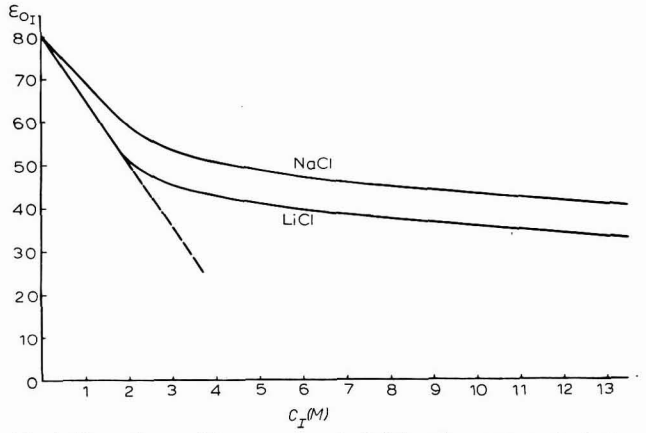

Fig. 4. Dependence of the macroscopical dielectric constant of solution on salt concn. according to ref. 35. The curves have been extrapolated for $c_I > 5$ *M*.

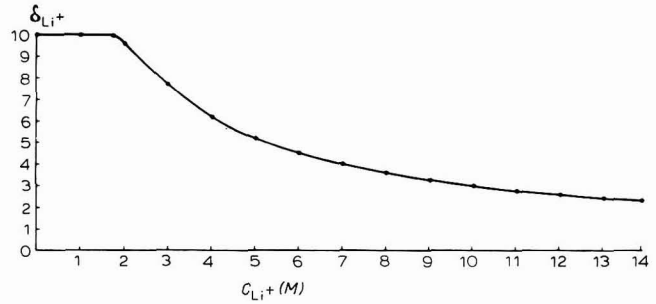

Fig. 5. Dependence of the increment δ_{Li^+} in l/mole on Li^+-concn. (*viz* eqn. (10)).

However, allowance still had to be made for the second superimposed effect of the electric field consisting in the orientation of the remaining fraction of "free" H_2O-dipoles, which leads to a further progressive decrease of the actual macroscopic dielectric constant,the smaller the value of x. If the solution in the diffuse double layer is regarded as composed of a series of layers with progressively decreasing $(\varepsilon^*_{0_I})_x$-values, the profile of $(\varepsilon_{eff})_x$ was obtained by inserting $(\varepsilon^*_{0_I})_x$ into a relation given by Grahame[36]

$$(\varepsilon_{\mathrm{eff}})_x = \{(\varepsilon^*_{0I})_x - \varepsilon_{\mathrm{lim}}\}/(1+2\,b\phi_x^2)^{\frac{1}{2}} + \varepsilon_{\mathrm{lim}} \tag{11}$$

with $\varepsilon_{\mathrm{lim}} = 3$, the value of the dielectric constant for total dielectric saturation of the solution*, and $b = 1.2 \cdot 10^{-13}$ cm^2 V^{-2}. The resulting $(\varepsilon_{\mathrm{eff}})_x$-profile is shown by the lower curve in Fig. 6. Essentially the same result would have been obtained with the equation of Booth[37], as the comparisons of various treatments in ref. 38, Fig. 3-10, show.

A further iteration step for the whole calculation of the profiles of ψ, ϕ, c^* and ε over the diffuse double layer proved to be necessary. In order to account more effectively for effects resulting from the significant decrease of the effective dielectric

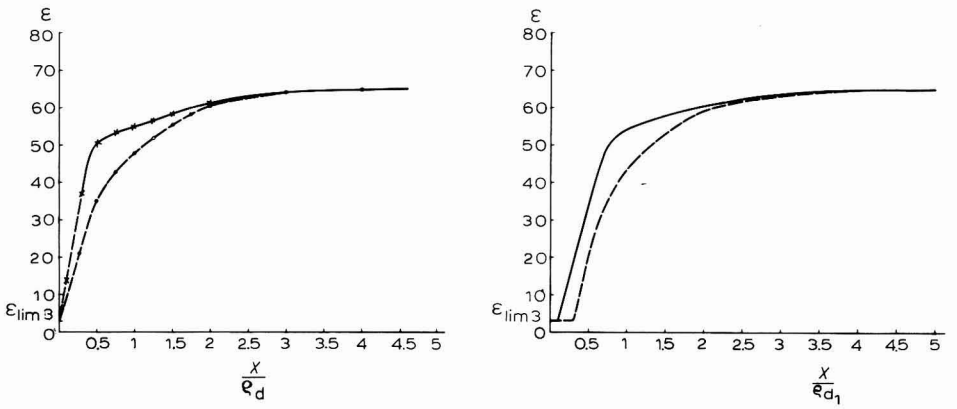

Figs. 6–7. Profile of ε^*_{0I} (upper curve) and $\varepsilon_{\mathrm{eff}}$ (lower curve) across effective diffuse double layer according to 1st iteration for $I = 1.0$ with LiCl and curves (1) for ψ and ϕ in Figs. 2 and 3 (Fig. 6); and according to 2nd iteration for $I = 1.0$ with LiCl and curves (2) for ψ and ϕ in Figs. 2 and 3 (Fig. 7).

constant in the surroundings of the O.H.P., however, the values of ψ_{H} and ϕ_{H} were now calculated from the following expression given by Grahame[36].

$$\frac{(\overline{\varepsilon^*_{0I}})_{\rho_{\mathrm{deff}}} - \varepsilon_{\mathrm{lim}}}{b}(1+2\,b\phi_{\mathrm{H}}^2)^{\frac{1}{2}} - \frac{(\overline{\varepsilon^*_{0I}})_{\rho_{\mathrm{deff}}} - \varepsilon_{\mathrm{lim}}}{b} + \varepsilon_{\mathrm{lim}}\phi_{\mathrm{H}}^2 = \frac{32\,\pi RTc_I \cdot 10^{-3}}{D_0}\sinh^2\left(\frac{zF\psi_{\mathrm{H}}}{2\,RT}\right) \tag{12}$$

$(\overline{\varepsilon^*_{0I}})_{\rho_{\mathrm{deff}}}$ is the average value of $(\varepsilon^*_{0I})_x$ over the effective diffuse double layer with thickness $\rho_{\mathrm{deff}} = 4\,\rho_{\mathrm{d}}$; $D_0 = 1.1138 \cdot 10^{-12}$ C/V cm is the diabattivity, a term defined by Grahame[36].

Also, a new value for ρ_{d} was calculated by inserting into eqn. (2) the average value of $(\varepsilon_{\mathrm{eff}})_x$ over the ρ_{deff}-value of the first iteration $(\overline{\varepsilon_{\mathrm{eff}}})_{\rho_{\mathrm{deff}}}$.

Subsequently, the second iteration followed exactly the same scheme as has been outlined for the first iteration step. Curves (2) in Figs. 2 and 3 resulted for ψ_x and ϕ_x and the curves in Fig. 7 for $(\varepsilon^*_{0I})_x$ and $(\varepsilon_{\mathrm{eff}})_x$. As expected, a rather small effect

* This situation will be not reached completely even in the first water layer at the electrode solution interface at room temperature, for which, according to the results of several authors[38–40], an $\varepsilon_{\mathrm{eff}}$-value of 6–8 is now generally assumed.

on the ψ-profile (see Fig. 2) is obtained by allowing for the progressive decrease of the macroscopic dielectric constant, caused by the two effects of the electric field mentioned, while the change in the ϕ-profile is already more pronounced (see Fig. 3). However, the ε-profile will gain significantly in importance for the dissociation field effect.

(c) *The dissociation field effect*

The treatment of the dissociation field effect is based upon the theory of Onsager[29] according to which the ratio of the dissociation rate constant enlarged by the dissociation field effect, $k^*_{d_{DF}}$, to its value at zero field strength, k_{d_0}, is a first-order Bessel function of the parameter, b.

$$(k^*_{d_{DF}}/k_{d_0})_x = F(b_x) \tag{13}$$

First the case of an uncharged acid dissociating into two oppositely charged products with $|z| = 1$ is considered. Then

$$b_x = 9.636\ \phi_x/(\varepsilon_{eff})_x\, T^2 \tag{14}$$

This expression shows that the values of the electric field strength as well as the

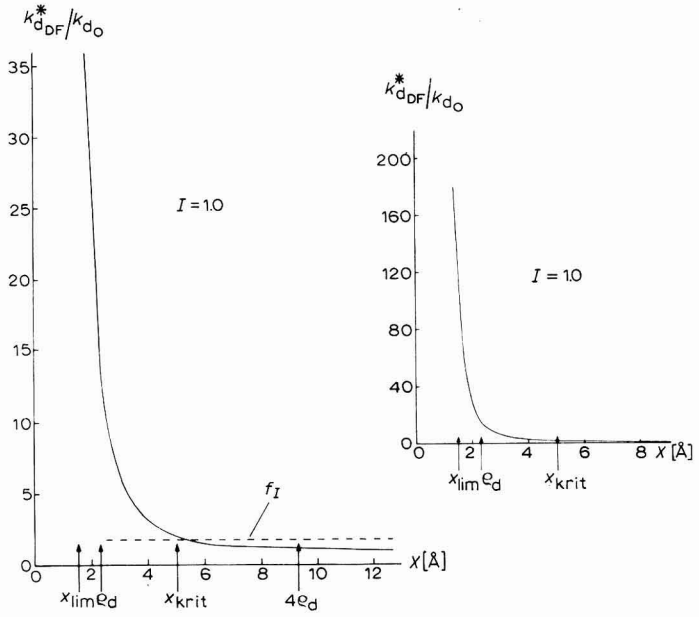

Fig. 8. Ratio $k^*_{d_{DF}}/k_{d_0}$ (*viz* eqn. (13)) as function of distance, x, from O.H.P. Dotted line corresponds to the magnitude of f_I. The right-hand part shows on reduced scale the course of $k^*_{d_{DF}}/k_{d_0}$ up to distances $x < x_{lim}$. $I = 1.0$ with LiCl; ψ, ϕ and ε_{eff} from 2nd iteration.

amount of the effective dielectric constant will determine significantly the extent of the dissociation field effect.

As ϕ_x is growing and $(\varepsilon_{eff})_x$ is becoming smaller with decreasing x, both parameters act together in producing a steeply increasing dissociation field effect in the region close to the O.H.P., as the profile in Fig. 8 shows.

The Bessel function, $F(b_x)$, can be generally developed into the following converging series.

$$F(b_x) = 1 + b_x + b_x^2/3 + b_x^3/18 + b_x^4/180 + b_x^5/2700 + b_x^6/56700 + \ldots \quad (15a)$$

For $b_x \geqslant 10$, the following asymptotic solution is a close enough approximation:

$$F(b_x) = \left(\frac{2}{\pi}\right)^{\frac{1}{2}} \frac{1}{8\, b_x^{\frac{3}{4}}} \exp(8\, b_x)^{\frac{1}{2}} \cdot \left(1 - \frac{3}{8(8\, b_x)^{\frac{1}{2}}} - \frac{15}{128.8\, b_x}\right) \quad (15b)$$

It should be noted, however, that the action of the dissociation field effect is restricted to an intermediate ion-pair stage which the dissociating acid particle passes after the breaking of the covalent bond between O and H in completing the dissociation. During this intermediate ion-pair stage, the dissociation field effect can favour dissociation by increasing the rate of the separation step of H^+ and A^- beyond the critical distance of coulombic interaction between the oppositely charged products of dissociation[29]. Obviously, in solutions of higher ionic strength there will be ion–dipole interactions or even crypto ion–ion interactions (or for charged acids, ion–ion interactions) between the dissociating acid particle and the ions of the inert excess electrolyte adjusting the ionic strength. One generally speaks of salt effects on the dissociation[41]. On the other hand, these inert excess electrolyte ions will certainly screen the dissociating acid particle to a certain extent against an external electric field. Thus, Onsager's equations can only be applied if there are no screening ion clouds around the dissociating acid particle, *i.e.*, either $I \approx 0$, or at finite ionic strength there are electric fields which are strong enough to peel off the surrounding ion cloud[29].

Therefore, we have assumed, to a first approximation, that under our experimental conditions the dissociation field effect will only operate if it is larger than the normal salt effect in 1 *M* LiCl-solutions on k_d. This salt effect, which acts also outside the diffuse double layer in the bulk of the solution, is defined by the factor (16)

$$f_I = k_{d_I}/k_{d_0}\,, \quad (16)$$

where k_{d_I} is the dissociation rate constant at ionic strength, I, adjusted with LiCl, and k_{d_0} is the value already mentioned, now more precisely defined, at zero external electrical field and zero ionic strength. The factor, f_I, depends mainly on the concentration and nature of the cations of the excess electrolyte, while f_I being due to coulombic interaction forces remains largely independent of the nature of the acid especially if this is uncharged[41]. Thus, for a given acid type the numerical value of f_I is determinable from measurements of k_d at the respective ionic strength, I, and $I \approx 0$[4,5,12,13].

At a certain distance, x_{crit}, from the O.H.P. for given experimental conditions, f_I and $(k^*_{d_{DF}}/k_{d_0})_x$ will reach the same order of magnitude. Thus, the range where only the dissociation field effect is effective but the salt effect disappears owing to the peeling off of the ion cloud formed by the excess electrolyte ions, will be restricted to distances, $x \leqslant x_{crit}$, approximately (see Figs. 8 and 1)[4].

(d) The case of charged acid particles

An analogous treatment is to be applied if the acid particle carries a charge[27]. The parameter, b_x, is defined by the following more general expression[29]:

$$b_x = \frac{|z_{A^+}^2||z_{A^-}^2|(\Lambda_{H^+} + \Lambda_{A^-})}{|z_{A^-}||\Lambda_{H^+}| + |z_{H^+}|\Lambda_{A^-}} \cdot 9.636 \frac{\phi_x}{(\varepsilon_{eff})_x T^2} \tag{17}$$

Λ is the ionic conductivity. Since for the effective range of the dissociation field effect a complete disappearance of the ionic cloud around HA^{z-} is presumed, known values at $I=0$ may be inserted for Λ.

Further, the stationary concentration profile of the (charged) acid across the reaction layer* will be shifted by a static ψ-effect in that part of the reaction layer that is coinciding with the diffuse double layer (see also Fig. 1). Thus, the more general eqn. (18) has to be applied instead of eqn. (13).

$$(k_{d_{DF}}^*/k_{d_0})_x = F(b_x) \exp(-z_{HA}F/RT)\psi_x \tag{18}$$

Important examples for this case of charged acids are the higher dissociation stages of multi-basic-acids where z_{HA} has a negative sign. Then there is an antagonistic action of dissociation field effect and static ψ-effect on the acid particle.

(e) *Comparison between theoretical and experimental results*

When the results of the theoretical treatment are compared with the experimental observations one has to take note of the fact that the voltammetric measurements always determine the average value over the whole reaction layer of an effective dissociation rate constant, $(\overline{k_d^*})_\mu$. This entity is related to the value of the dissociation rate constant, k_{d_I}, operating in the bulk at a given ionic strength, I, adjusted by a certain excess electrolyte (for instance LiCl), by the following equation:

$$(\overline{k_d^*})_\mu/k_{d_I} = \frac{f_\psi}{f_I \mu_{eff}} \left[\int_{x_{lim}}^{x_{crit}} \frac{k_{d_{DF}}^*}{k_{d_0}} \, dx + \int_{x_{crit}}^{\mu_{eff}} \frac{k_{d_I}}{k_{d_0}} \, dx \right] \tag{19}$$

In chemical kinetics one is mainly interested in k_{d_I}, the value free from any double-layer effects.

The first integral within the brackets refers to the dissociation field effect restricted to the range, $x \leqslant x_{crit}$, of the diffuse double layer, while the second integral corresponds to the salt effect acting on the dissociation rate in the remaining part of the reaction layer as outlined above, *i.e.*, for all distances $x_{crit} \leqslant x \leqslant \mu_{eff}$ (see also Fig. 1). As k_{d_I} and k_{d_0} are independent of x for this range, the second integral reduces to the product, $f_I(\mu_{eff} - x_{crit})$.

The factor f_ψ, to be discussed in the next section, allows for the influence of the electric field on the recombination rate averaged over the effective reaction layer. These effects lead in total to a decrease of the recombination rate. Thus, they can also be treated as if they cause an equivalent increase in $(\overline{k_d^*})_\mu$, the effective dissociation rate constant directly accessible by experiment.

The ratio $(\overline{k_d^*})_\mu/k_{d_I}$ follows in the course of the evaluation, directly from experiment before application of the empirical correction for the total of the double-layer effects[4,5,12,27]. The curve of the dependence of this ratio on the corresponding μ-values has the same shape as the theoretical curve defined by eqn. (19) regardless of the numerical value inserted for x_{lim} (see Fig. 9). If the right value for x_{lim} is selected,

* The basic condition[42] for a stationary acid concentration across the reaction layer is $\delta_D \geqslant 3\,\mu$, where δ_D is the diffusion layer thickness given, in the case of linear diffusion, by $\delta_D = \sqrt{\pi D_{HA} t}$.

the experimental and theoretical curves coincide. For the reaction type treated and the assumed experimental conditions, x_{lim}-values between 1.4 and 1.5 Å have to be inserted in eqn. (19) to reach this coincidence. As these x_{lim}-values have to be interpreted as the average values for the distance of closest approach to the O.H.P. of the carboxylic groups of the acid particles, their magnitude seems plausible. The

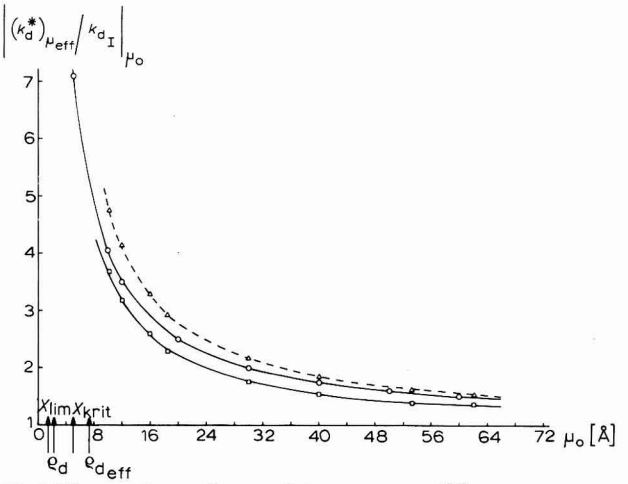

Fig. 9. The experimentally accessible average ratio $(\overline{k_d^*})_\mu/k_{d_I}$ as function of the formal reaction layer thickness, μ_0, for the same conditions as in Fig. 8. (○), Computed curve for $x_{lim} = 1.45$ Å; (△), expl. curve for benzoic acid ($x_{lim} = 1.375$ Å); (□), expl. curve for acetic acid ($x_{lim} = 1.50$ Å).

centres of the acid particles can approach the O.H.P. closer, on average, than x_{lim}. The sum of the diameter of the compact double layer plus x_{lim} then defines the distance of closest approach for the carboxylic function of HA to the electrode[27]. Since the O.H.P. was defined by the average value of closest approach to the electrode for the centres of the hydrated Li^+-ions, a complete coincidence of O.H.P. and x_{lim}, *i.e.*, $x_{lim} = 0$, was not to be expected. At first glance there might seem difficulties in accounting for the length of the acid particles. However, despite the dipole moment of HA and the high electric field strength, only a certain diagonal orientation of the HA-particles in the distance of closest approach is possible, on average, at room temperature and not a position completely normal to the electrode surface.

(f) Influences on the recombination

Following the discussion of the influences of the electric field in the effective diffuse double layer acting directly or indirectly on the dissociation step of importance for the reaction type treated under the applied experimental conditions, the effects on the recombination step will now be considered. Here, the recombination of A^- and H^+ to HA is usually regarded as a totally diffusion-controlled reaction[4-7]. For this reaction type it follows that[45,46]:

$$k_r = \gamma 4\pi N_L \cdot 10^{-3} aP(D_{H^+} + D_{A^-}) \tag{20}$$

with

$$p = \frac{z_{H^+} z_{A^-} e_0^2}{\varepsilon \kappa T a} \cdot \frac{1}{\left(\exp \frac{z_{H^+} z_{A^-} e_0^2}{\varepsilon \kappa T a}\right) - 1} \tag{21}$$

Equation (21) refers to a situation, where shielding by ion clouds is absent. γ is a yield factor determined mainly by steric requirements[43], which has a value of about 0.6 for normally behaving[4,5,11,12] carboxylic acids; N_L is Avogadro's number; $e_0 = 4.8 \cdot 10^{-10}$ electrostatic units; $\kappa = 1.38 \cdot 10^{-16}$ erg deg^{-1} is Boltzmann's constant; ε is the respective effective value $(\varepsilon_{eff})_x$ of the macroscopical dielectric constant of the solution and a is the critical encounter distance of the hydrated H^+- and A^--ions.

If H^+ and A^- have approached each other by diffusion up to the distance a, an intermediate stage has been formed, which we term a "latent ion-pair"[4,5,11-13]

$$H^+ \cdot aq. + A^- \cdot aq. + (n-2)\,aq. \rightleftarrows [H^+(aq.)_n A^-] \rightleftarrows HA + n \cdot aq. \tag{IV}$$

In this stage, an intermolecular hydrogen bridge system reaching over n water molecules (aq.) couples H^+ and A^- and a very rapid proton transfer by the special proton-"jump"-mechanism to A^- becomes possible. This completing step of recombination to HA (or HA^z) proceeds by orders of magnitude faster than the diffusion-controlled approach of (hydrated) H^+ and A^- to the critical distance a. A preliminary partial dehydration of the reactants is not necessary, because a water dipole in each of the primary hydration shells around H^+ and A^- participates in the intermolecular H-bridge system going over n H_2O-molecules[44].

The electric field across the diffuse double layer will affect this type of recombination in principle in three different ways, of which only one proves to be of significance. All three effects act in the evaluation of the measured limiting current *via* the value of the effective thickness of the reaction layer, μ_{eff}. This quantity is defined by eqn. (22).

$$\mu_{eff} = \left(\frac{D_{H^+}}{(\overline{k_r^* \cdot c_{A^-}^*})_{\mu_{eff}}}\right)^{\frac{1}{2}} = \left(\frac{D_{H^+}}{k_{r_I}(\overline{c_{A^-}^*})_{\mu_{eff}}}\right)^{\frac{1}{2}} \cdot \left(\frac{k_{r_I}}{(\overline{k_r^*})_{\mu_{eff}}}\right)^{\frac{1}{2}} \tag{22}$$

(i) By the disintegration of the ion clouds the electric field causes an increase of the mass transfer rate of H^+ and A^- in the diffuse double layer. For $x \leqslant x_{crit}$, this effect, well known from conductivity studies as the first Wien-effect, reaches a limiting value. On k_r it acts *via* the sum, $(D_{H^+} + D_{A^-})$, in eqn. (19). As D_{H^+} dominates the sum, because $D_{H^+} \gg D_{A^-}$, its influence on μ_{eff} largely compensates according to eqn. (22)[27].

(ii) A further effect of the electric field on k_r results from its influence on ε_{eff} and a (see eqns. (20) and (21)). If for $x \leqslant x_{crit}$, a total disintegration of the ionic clouds around H^+ and A^- is assumed the value $a^* \approx 7.5 \cdot 10^{-8}$ cm valid for $I \approx 0$, must be inserted in eqns. (20) and (21)[43], while for ε the respective $(\varepsilon_{eff})_x$-value is relevant. On the other hand, assuming for $x \geqslant x_{crit}$ complete shielding of H^+ and A^- by surrounding excess electrolyte ion clouds, $p_I \approx 1$ and $a_I \approx 13.5 \cdot 10^{-8}$ cm, valid for $I = 1.0$ adjusted with 1 M LiCl must be inserted in eqns. (20) and (21)[4,5]. Then for the increase of k_r in the range, $x \leqslant x_{crit}$:

$$(k_r^*)_x / k_{r_I} = p_x^* a^* / a_I \tag{23}$$

The profile of this ratio across the diffuse double layer is given in Fig. 10.

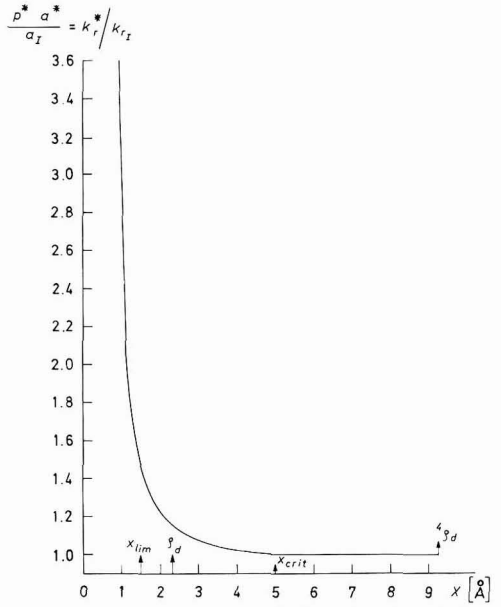

Fig. 10. Ratio k_r^*/k_I (*viz* eqn. (23)) as function of distance x from O.H.P. $I = 1.0$ with LiCl; $\rho_d = 2.32$ Å; $a^* = 7.5 \cdot 10^{-8}$ cm; $a_I = 13.5 \cdot 10^{-8}$ cm; $P_I \approx 1$.

Also, for recombination the average value of the smallest distance for the reactants from the O.H.P. equals $x_{\lim}$. Thus, the mean value of the ratio defined by eqn. (23) which affects μ_{eff} is:

$$(\overline{k_r^*/k_{r_I}})_{\mu_{\text{eff}}} = \frac{1}{\mu_{\text{eff}}} \int_{x_{\lim}}^{\mu_{\text{eff}}} \frac{(k_r^*)_x}{k_{r_I}} \, dx = \frac{1}{\mu_{\text{eff}}} \int_{x_{\lim}}^{\mu_{\text{eff}}} \frac{p_x^* a^*}{a_I} \, dx \tag{24}$$

Table 1 shows that for $\mu_{\text{eff}} \geqslant 4 \, \rho_d$, the experimental condition usually adjusted, the

TABLE 1

μ_0 (Å)	μ_{eff} (Å)	$(\overline{k_r^*/k_{r_I}})_{\mu_{\text{eff}}}$	$\{(k_{r_I}/\overline{k_r^*})_{\mu_{\text{eff}}}\}^{\frac{1}{2}}$
2	5.25	1.097	0.955
5	7.35	1.055	0.974
10	12.60	1.030	0.985
20	22.20	1.015	0.995

effect expressed by eqns. (23) and (24) remains negligible. Therefore it was not taken into account in our previous publications[4,5,12,13,27].

(iii) Of some significance for μ_{eff}, and thus for the total of all double-layer effects on chemical reactions, there remains the third influence of the electric field on the recombination rate[4,5], *i.e.*, the static ψ-effect on the stationary profile of c_A- across the reaction layer, and thus also its part coinciding with the diffuse double

layer. Figure 11 shows the profile across the reaction layer for the ratio defined by eqn. (25).

$$({}^{*}c_{A^-})_x/{}^{0}c_{A^-} = \exp(-z_{A^-}F/RT)\,\psi_x\,, \tag{25}$$

where ${}^{0}c_{A^-}$ is the anion concentration at $\psi_x = 0$, and is in practice a constant if condition (3) has been regarded. For ψ_x, the values of the second iteration (curve 2 in Fig. 2) have been taken.

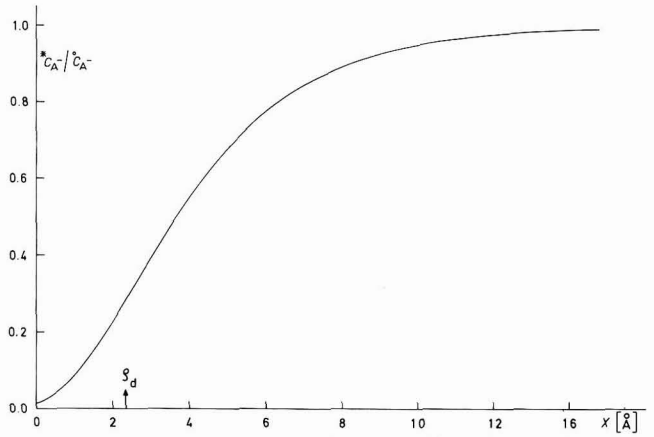

Fig. 11. Profile of the concn. ratio of the carboxylate anions A^- (*viz* eqn. (25)) across effective diffuse double layer for $I = 1.0$ with LiCl and ψ_x from curve (2) in Fig. 2.

Equations (1), (22), (23), (24) and (25) give:

$$\mu_{\text{eff}} = \mu_0 f_\psi \tag{26}$$

and

$$\mu_{\text{eff}} = \left(D_{H^+} \Big/ \frac{k_{r_I}\,{}^{0}c_{A^-}\,a^*}{\mu_{\text{eff}}\,a_I} \int_{x_{\text{lim}}}^{\mu_{\text{eff}}} p_x^* \mathrm{d}x \int_0^{\mu_{\text{eff}}} \exp - \frac{z_{A^-}F}{RT}\,\psi_x \mathrm{d}x \right)^{\frac{1}{2}} \tag{27}$$

Thus

$$f_\psi = \left(k_{r_I}\mu_{\text{eff}} \Big/ (\overline{k_r^*})_{\mu_{\text{eff}}} \int_0^{\mu_{\text{eff}}} \exp - \frac{z_{A^-}F}{RT}\,\psi_x \mathrm{d}x \right)^{\frac{1}{2}} \tag{28}$$

For $\mu_{\text{eff}} \geqslant 4\,\rho_d$, however, $0.97 < k_{r_I}/(\overline{k_r^*})_{\mu_{\text{eff}}} < 1.0$ and eqn. (28) reduces to:

$$f_\psi \approx \left(\mu_{\text{eff}} \Big/ \int_0^{\mu_{\text{eff}}} \exp - \frac{z_{A^-}F}{RT}\,\psi_x \mathrm{d}x \right)^{\frac{1}{2}} \tag{28a}$$

As eqns. (28) and (28a) contain μ_{eff} as factor and as upper integration limit, f_ψ has to be computed by iterations until convergence is reached.

The dependence of f_ψ on the ratio ρ_d/μ_{eff} is shown in Fig. 12 for the ψ-potentials operating under the conditions of our measurements and the curves obtained for our conditions with the expressions given by other authors[18,20] are included for

comparison. Generally, the agreement is fair and becomes excellent for the condition, $\mu \gtrsim 4\ \rho_d$ usually adjusted in such measurements*.

As has already been mentioned in section (e), although in reality the influence reflected in f_ψ causes a decrease of the recombination rate, f_ψ acts virtually according to the evaluation of the measured limiting current as if it were responsible for an equivalent increase of the effective average dissociation rate constant, $(k_d^*)_\mu$. Thus, f_ψ has to enter eqn. (19) as a factor.

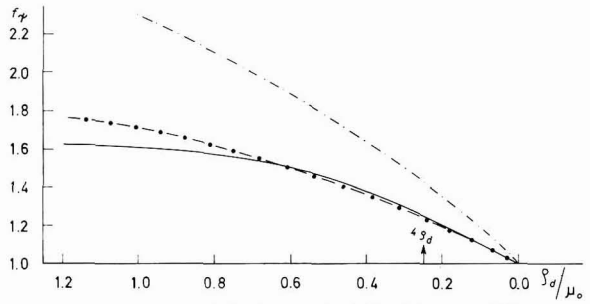

Fig. 12. Dependence of the factor, f_ψ, defined by eqn. (28), on the ratio of the diameters of diffuse double layer (ρ_d) and formal reaction layer (μ_0) for $I = 1.0$ with LiCl and ψ_x-values of curve (2) in Fig. 2 according to the relations of different authors: (— · —) Albery; (— • —) Matsuda; (——) Nürnberg.

DISCUSSION

(a) *General aspects*

The good agreement between the experimental observations and the final results of the theoretical treatment (see Fig. 9) shows that the main aspects of the complex problem of double-layer effects on homogeneous chemical reactions are theoretically accessible in the manner described. This is at least true for the type of homogeneous chemical reactions considered and the assumed experimental conditions, while for the more general case a somewhat more extended approach including a further double-layer effect, discussed later, might become necessary.

It is of interest that the modified Gouy-Chapman-theory which has been applied, is obviously a sufficient model to describe the behaviour of the diffuse double layer and the profile of its parameters (ψ, ϕ, ε_{eff}) across it, although this theoretical approach reduces what is in reality a 3-dimensional problem to a 1-dimensional one. A homogeneous value of the double-layer parameters within the planes parallel to the electrode surface is presumed in the Gouy–Chapman-theory. Although the reality is almost certainly different, it can be concluded that, on average, the degree of homogeneity in each of those planes is large enough to avoid disagreements between the theoretical and the experimental results obtainable at present. In other words, although the Gouy–Chapman-theory is certainly not an exact and complete

* The equation relevant to the reaction type treated here is eqn. (25) in ref. 18 for the case $p \neq 0$ and $-q$. The treatment of Gierst and Hurwitz[17] should lead to the same final results as the relation of Matsuda[18], because for our conditions ($K_c \ll 1$ and large $|\psi_H|$-values) the treatments of all the authors mentioned lead to the same final equations.

model of the diffuse double layer, it reflects sufficiently well the major trends and aspects with respect to their present experimental accessibility.

A further general conclusion is that the double-layer effects on the kinetics of fast homogeneous chemical reactions with respect to the error limits of ± 20–$30\,\%$ now obtainable with advanced voltammetric techniques[3-5] demand consideration and correction if $|\psi_H| \geqslant 50$ mV, even if a relatively large reaction layer thickness of $40\,\text{Å} < \mu < 60\,\text{Å}$ and quite a small thickness, ρ_d, of the diffuse double layer are obtained by adding 0.1–1 M inert excess electrolyte to the solution[27].

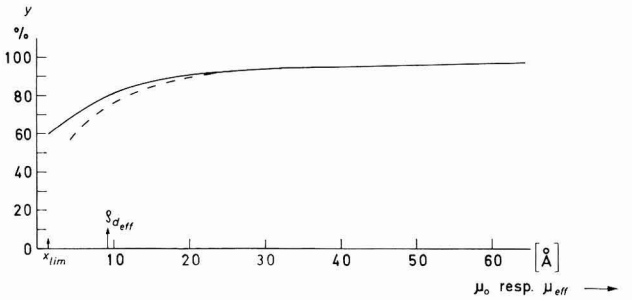

Fig. 13. Percentage, y, of dissociation field effect contribution to the experimentally accessible ratio $(\overline{k_d^*})_\mu/k_{d_r}$ (*viz* Fig. 9) as function of the formal (—— μ_0) and the effective (------- μ_{eff}) reaction layer thickness. For $\mu > 22$ Å both curves coincide.

Another general result is the fact, reflected by Fig. 13, that for large $|\psi_H|$-values ($\geqslant 100$ mV) and small diameters, $\rho_{d_{eff}}$, for the effective diffuse double layer corresponding to larger ionic strength values in the bulk of the solution (between 0.1 and 1.0, or higher) the dissociation field effect will be the dominant double-layer effect, especially if the condition, $\mu_{eff} \geqslant \rho_{d_{eff}}$, holds as is usual. Then the dissociation field effect corresponds, according to the amount of μ_{eff}, to 80–95 % of the global double-layer effect. In this respect, the neglect of other double-layer effects in our previous paper[27] appears as a not impermissible crude approximation for the reaction type treated under the assumed experimental conditions.

(*b*) *Restrictive effects on dissociation in the double layer*

During the last ten years a series of papers[21-24] have dealt with effects in the double layer especially on the dissociation of acids and more generally on the dissociation of chemical compounds into charged products according to relation (III). At first attention was limited mainly to the consequences of the polarization of the solvent caused by the electric field and by all sorts of solute particles present in the solution. The external electric field, as well as the solute components, contribute to the decrease of the macroscopic dielectric constant of the solution. For thermodynamic reasons, the stage of uncharged (or less charged) compounds (as acid molecules, HA, or more generally ion-pairs) will be more favoured than the stage of ions in a medium of low dielectric constant (ε_{eff}), *i.e.*, for instance the polarized aqueous solution in the diffuse double layer. Thus it was concluded at first[21,22] that generally the net result on chemical reactions in the double-layer region would always be a restriction of dissociation.

Obviously, this general postulation is in contradiction to our experimental results, which show unequivocally that, at least under our experimental conditions, the action of the electric field in the diffuse double layer leads to a significant increase of dissociation[4,5,10,12,13,27]. Furthermore, it has been shown in the preceding sections of this paper that our experimental observations can be satisfactorily interpreted in terms of Onsager's theory of the dissociation field effect besides additional rather small effects. Equations (14), (15), (17) and (18) stress the point that also the progressive decrease of ε_{eff} near the electrode, as well as the progressively growing field strength, ϕ, contribute considerably to the progressive increase in dissociation rate. It is the joint action of both parameters, ϕ_x and $(\varepsilon_{\text{eff}})_x$, that is responsible for the very steep increase of the ratio, $k^*_{\text{d}_{\text{DF}}}/k_{\text{d}_0}$, near x_{lim} (see Fig. 8).

On the other hand, thermodynamically the ion stage is doubtless less favoured in the same region of low $(\varepsilon_{\text{eff}})_x$-values where the dissociation field effect is strong and thus, *via* the polarization of the solvent, the electric field should indirectly exert also a restricting influence on dissociation, because the unfavourable solvent conditions cause an increase in the value of the free activation enthalpy, ΔG^*_{d}, of dissociation. Yet this restrictive influence is obviously largely overruled by the dissociation field effect under our experimental conditions. Consequently, the earlier theoretical postulation[21,22] that the sole result of the electric field in the double-layer region is (with respect to dissociation) its restriction *via* the polarization of the solvent, can no longer be accepted, as has been recently admitted by the same authors[23,24].

However, there is also experimental evidence[47] pointing more to the decrease of dissociation in the double-layer region with the solvent progressively more polarized nearer the electrode. In a number of cases, additional interactions, such as specific adsorption at the electrode or water structure induced association of relative large ions with a considerable degree of hydrophobic character (an association type termed also "cavity sharing"[48]) seem to be largely responsible for the restriction of dissociation. However, there remain examples where ion-pairs are primarily due to coulombic interactions and our following considerations are restricted to this type.

At first it must be concluded that the complete problem of the double-layer effects on chemical reactions is more complicated than previously anticipated and that it seems to depend significantly on the respective conditions whose influence on dissociation becomes dominant.

In a recent paper, Sanfeld and Steinchen-Sanfeld[24] attempted to show that their theory could also explain the enhancement of dissociation, provided the following conditions are fulfilled:

(i) The dielectric constant has to decrease with the concentration of the uncharged acid particle, *i.e.*, $-(\partial\varepsilon/\partial c_{\text{HA}})$.

(ii) The numerical value of this entity has to be larger than the sum $-[(\partial\varepsilon/\partial c_+)+(\partial\varepsilon/\partial c_-)]$, which refers to the influence of the ionic components of the solute. As a consequence of the significant dielectric saturation of the water dipoles belonging to the primary hydration shells around the ions, this sum is assumed to have always a negative sign for salt concentrations above 10^{-2} M. Also, a negative sign for $\partial\varepsilon/\partial c_{\text{HA}}$ seems not implausible with respect to the increased order of the water immediately surrounding the HA-particles resulting from hydration of the second kind[49,50] (*i.e.*, water structure with non-tetrahedral H-bridges) around their hydrophobic part and the usual hydration, more similar to that around charged sites, at the carboxylic

group of the acid particles. However, the resulting degrees of the enhancement in dissociation are rather small and throw severe doubts on the authors' suggestion that this might be a treatment equivalent to the application of Onsager's relation[29] for the dissociation field effect. On the contrary, in our opinion a further but small contribution to an enhancement in dissociation of second order magnitude is treated here, operating if the assumed conditions are given.

Furthermore, the treatment just discussed certainly provides no explanation at all for the enhanced dissociation observed under our experimental conditions, which are characterized in this respect by a large excess of supporting electrolyte (*viz* 1 *M* LiCl in the bulk of the solution). In this case, the influence of the solute components on the polarization of the solvent is, in practice, caused entirely by the supporting electrolyte ions, *i.e.*, for negatively charged electrodes, largely by the cations, which are Li^+-ions in our study.

A more promising comprehensive theoretical treatment of the whole complex problem has quite recently been published by Jenard and Hurwitz[51]. Their approach accounts both for the enhancement of dissociation *via* the Onsager relation for the dissociation field effect[29]* and for the decrease of dissociation *via* a factor referring to the polarization of the solvent which alone was considered in earlier papers[21,22].

The calculations of Jenard and Hurwitz[51] show that up to an electric field strength, ϕ_x, of $2\text{–}3 \cdot 10^6$ $V cm^{-1}$, the dissociation field effect is dominant, while at higher fields, under certain conditions, the decrease of dissociation due to the polarization of the solvent might begin to overrule. However, if eventually ϕ_x reaches values that cause, under the respective other conditions, total dielectric saturation of the solvent, the dissociation field effect again breaks through and operates solely for further increasing ϕ_x.

We have also considered a similar approach[52], which has not so far been published because for our conditions, the modifications invoked by the decrease of dissociation due to polarization of the solvent remain rather small as is shown below.

Our experimental conditions are characterized by large negative ψ_H-values (due to the very negative range of electrode potential, E, for the limiting current region in our HLFR-measurements) and a high ionic strength, adjusted to $I = 1.0$ with LiCl in the bulk of the solution. Allowance for the decrease of dissociation arising from polarization of the solvent can be made by correcting the ratio, $k^*_{d_{DF}}/k_{d_0}$, defined by eqns. (13) or (18), with the factor, f_δ. This gives:

$$(k^*_{d_{DF}}/k_{d_0})'_x = (k^*_{d_{DF}}/k_{d_0})_x \cdot f_\delta \tag{29}$$

with

$$f_\delta = \exp(-\delta_\varepsilon \phi_x^2 / 8\,\pi RT) \tag{30}$$

For ϕ_x, the values from curve 2 in Fig. 3 (after conversion to c.g.s.-units (!)) were inserted and for δ_ε the constant amount, $-1.5 \cdot 10^4$ cm^3/mole. The progressive increase of the Li^+-concentration and of the asymmetry of the ionic strength over the diffuse double layer probably causes some corresponding decrease in δ_ε. However,

* An exact calculation is only possible for selected x-values by inserting into the Onsager function the respective value $(\varepsilon_{eff})_x$. This demand has been met only approximately in ref. 51 for the case where $\varepsilon_{eff} \approx 10$ was inserted.

the easily accessible value for δ_ε was employed as a sufficient approximation for the calculation of limiting cases.

Figure 14 shows a logarithmic plot of the resulting dependence for the ratios $(k^*_{d_{DF}}/k_{d_0})_x$, defined by eqn. (13), and $(k^*_{d_{DF}}/k_{d_0})'_x f_\delta$, defined by eqn. (29), on the electric field strength, ϕ_x, for two values ($I=1.0$ and $I=0.1$) of the ionic strength in the bulk of the solution (adjusted with LiCl) and the ψ_H-value referring to the very negative electrode potentials ($E=-2.2$ to -2.3 V *vs.* SCE) in the limiting current region of our HLFR-polarograms[4,5,12,13].

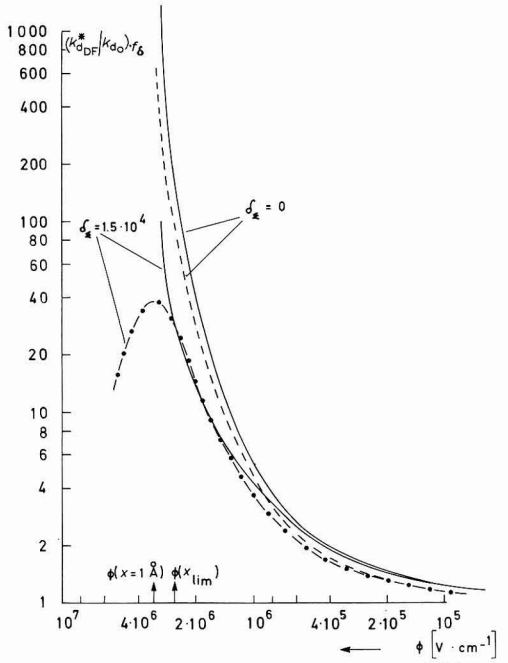

Fig. 14. Logarithmic plot of the dependence of $(k^*_{d_{DF}}/k_{d_0})_x \cdot f_{\delta_\varepsilon}$ on the electrical field strength, ϕ_x, for I: (——), 1.0; (– – –), 0.1. The ϕ_x-values corresponding to $x_{lim}=1.45$ Å and $x=1.0$ Å are indicated by arrows.

For the bulk value $I=1.0$, the situation corresponding to our conditions of measurement, the effect of f_δ to account for the decrease of dissociation due to the polarization of the solvent, remains very marginal and furthermore, constitutes an upper limiting case, as in reality δ_ε should not be constant but decrease somewhat with ϕ_x. No minimum indicating the occurrence of a dominating f_δ-effect appears, because, owing to the high ionic strength for $\phi_x > 3\cdot10^6$ V cm^{-1}, the stage of total dielectric saturation of the solvent is already approached and, on the other hand, for $\phi_x = 2\text{–}3\cdot10^6$ V cm^{-1} the distance, $x=x_{lim}$, is reached. In the stage of complete dielectric saturation of the solvent, the dielectric constant cannot be altered further and for $(\varepsilon_{eff})_x=\varepsilon_{lim}$, $\delta_\varepsilon=0$. Thus, the whole effect of the decrease of dissociation represented by the influence of f_δ in eqn. (29) is limited for the conditions of our studies on the dissociation and recombination of carboxylic acids, to a very small decrease of x_{lim} from 1.45 Å to maximal 1.05 Å (see Fig. 14).

A somewhat more pronounced effect of f_δ is to be expected, if the bulk ionic strength is reduced to $I=0.1$*. For $x \geqslant x_{\text{lim}}$, corresponding to $\phi_x \leqslant 2.5 \cdot 10^6$ V cm^{-1}, a decrease into a minimum is also not yet observed. However, the minimum appears if smaller x-values and higher ϕ_x-values are considered because even for x-values somewhat smaller than x_{lim} the solvent has not yet reached complete dielectric saturation since the concentration of supporting electrolyte ions is now lower and, consequently, also their corresponding contribution to the decrease of $(\varepsilon_{\text{eff}})_x$ (see eqn. (9)). Under these circumstances, the square of the electrical field strength entering the exponential in eqn. (30) defining f_δ can display for high ϕ_x-values its full influence and may lead to an overruling of the dissociation field effect. Thus, a dominant effect of the decrease of dissociation due to polarization of the solvent seems possible for reactions with smaller x_{lim}-values and the same, or larger, amounts of δ_ε. In this way, the stabilisation of ion-pairs in the double layer, emerging from the investigations of Gierst and Hurwitz[17] for various cases where special additional interactions as "cavity sharing" or specific adsorption can be excluded, might find a theoretical explanation.

In general, one may conclude that by the joint efforts of various investigators the main contours of the rather complex influences on homogeneous chemical reactions in the double layer have now been clarified and brought to at least an approximate quantitative theoretical interpretation. Further progress in this direction is not only important for electrode kinetics but has also considerable biological interest with respect to the mechanism of the "active" transport of alkali ions through cell membranes. Also, for this process, chemical reactions which proceed under the action of rather high electric fields in a double layer of the system, cell membrane/aqueous alkali salt solution, are of great significance.

ACKNOWLEDGEMENTS

The authors thank Dr. W. J. Albery, Oxford; Dr. H. D. Hurwitz, Dr. A. Sanfeld and Dr. A. Jenard, Brussels, for various stimulating and clarifying discussions during the last few years.

SUMMARY

An approximate theoretical treatment of the various influences on homogeneous chemical reactions in the diffuse double layer is given and compared with experimental results. The dissociation and recombination of carboxylic acids prior to the charge transfer step of the hydrogen evolution at a mercury electrode is taken as an example.

On the basis of a modified Gouy–Chapman-theory the profiles of the various double-layer parameters across the effective diffuse double layer are computed and the profile of the dissociation field effect is then obtained with Onsager's theory. The double-layer effects on the recombination rate are also discussed. Good agreement between the experimentally accessible global effect of the double-layer effects and the

* It should be mentioned that so far an experimentally confirmed curve for $(k^*_{d_{DF}}/k_{d_0})_x$ does not exist for our systems in the case, $I=0.1$.

overall theoretical result developed, is achieved. Under the conditions assumed, the dissociation field effect proves to be the dominant double-layer influence on the reaction type considered. Finally, decrease of dissociation for thermodynamic reasons caused by the polarization of the solvent is discussed. It is shown that these restrictions remain very marginal for the reaction type treated under the assumed conditions, although they might be of more importance for other cases.

REFERENCES

1 B. BREYER AND H. H. BAUER, *Alternating Current Polarography and Tensammetry* in *Chemical Analysis*, Vol. XIII, edited by P. J. ELVING AND I. M. KOLTHOFF, Interscience Publishers, New York, 1963.
2 P. DELAHAY, *Advan. Electrochem. Electrochem. Eng.* 1 (1961) 233.
3 H. W. NÜRNBERG AND G. WOLFF, *Chem. Ing.-Tech.*, 37 (1965) 977; 38 (1966) 160.
4 H. W. NÜRNBERG, *Ber. Kernforschungsanlage Jülich, Jül-475-CA*, December, 1967.
5 H. W. NÜRNBERG, *Fortschr. Chem. Forsch.*, 8 (1967) 241.
6 M. EIGEN AND L. DE MAEYER, *Technique of Organic Chemistry*, Part II, edited by A. WEISSBERGER, Interscience Publishers, New York, 2nd ed., 1963, chap. 18; E. F. CALDIN, *Fast Reactions in Solution*, Blackwell, Oxford, 1964.
7 M. EIGEN, *Angew. Chem.*, 75 (1963) 489.
8 A. WELLER, *Progress in Reaction Kinetics*, Vol. I, edited by G. PORTER, Pergamon Press, Oxford, 1961, p. 187.
9 H. STREHLOW AND M. BECKER, *Z. Elektrochem.*, 63 (1959) 457.
10 H. W. NÜRNBERG AND G. C. BARKER, *Naturwissenschaften*, 51 (1964) 191.
11 H. W. NÜRNBERG AND H. W. DÜRBECK, *Z. Anal. Chem.*, 205 (1964) 217.
12 H. W. NÜRNBERG, *Polarography 1964, Proc. 3rd Intern. Congr. Polarography, 1964*, edited by G. J. HILLS, MacMillan, London, 1966, p. 149.
13 H. W. NÜRNBERG, H. W. DÜRBECK AND G. WOLFF, *Z. Phys. Chem. NF*, 52 (1967) 144.
14 G. C. BARKER AND H. W. NÜRNBERG, *Naturwissenschaften*, 51 (1964) 191.
15 G. C. BARKER, H. W. NÜRNBERG AND J. A. BOLZAN, 14th CITCE-Meeting Moscow, 1963; *Ber. Kernforschungsanlage Jülich, Jül-137-CA*, September, 1963.
16 W. A. BROCKE AND H. W. NÜRNBERG, *Z. Instrumentenk.*, 75 (1967) 355.
17 L. GIERST AND H. D. HURWITZ, *Z. Elektrochem.*, 64 (1960) 36; H. D. HURWITZ, *ibid.*, 65 (1961) 178.
18 H. MATSUDA, *J. Phys. Chem.*, 64 (1960) 336.
19 M. SENDA AND P. DELAHAY, *J. Phys. Chem.*, 65 (1961) 1580.
20 W. J. ALBERY, *Trans. Faraday Soc.*, 61 (1965) 2063; *Discussions Faraday Soc.*, 39 (1965) 159, 162.
21 A. SANFELD, A. STEINCHEN-SANFELD, H. HURWITZ AND R. DEFAY, *J. Chim. Phys.*, 58 (1962) 139.
22 H. D. HURWITZ, A. SANFELD AND A. STEINCHEN-SANFELD, *Electrochim. Acta*, 9 (1964) 929.
23 A. STEINCHEN-SANFELD, A. SANFELD AND H. HURWITZ, *Konink. Vlaam. Acad. Wetenschap. Letter. Schone Kunsten, Belg. Colloq.*, (1966) 41.
24 A. SANFELD AND A. STEINCHEN-SANFELD, *Trans. Faraday Soc.*, 62 (1966) 1907.
25 P. DELAHAY AND W. VIELSTICH, *J. Am. Chem. Soc.*, 77 (1955) 4955.
26 G. C. BARKER, private communication.
27 H. W. NÜRNBERG, *Discussions Faraday Soc.*, 39 (1965) 136.
28 G. GOUY, *J. Phys. (Paris)*, 9 (1910) 457; D. CHAPMAN, *Phil. Mag.*, 25 (1913) 475; see also R. PARSONS *Modern Aspects of Electrochemistry*, Vol. 1, edited by J. O'M. BOCKRIS AND B. E. CONWAY, Butterworth, London, 1954, p. 103.
29 L. ONSAGER, *J. Chem. Phys.*, 2 (1934) 599.
30 H. W. NÜRNBERG, *Discussions Faraday Soc.*, 39 (1965) 160.
31 H. W. NÜRNBERG AND CH. FREIBURG, *J. Electroanal. Interfacial Chem.*, in preparation.
32 D. M. RITSON AND J. B. HASTED, *J. Chem. Phys.*, 16 (1948) 11.
33 E. GLUECKAUF, *Trans. Faraday Soc.*, 60 (1964) 914.
34 J. B. HASTED, D. M. RITSON AND C. H. COLLIE, *J. Chem. Phys.*, 16 (1948) 1, 11; G. H. HAGGIS, J. B. HASTED AND C. H. COLLIE, *ibid.*, 20 (1952) 1452.
35 G. KORTÜM, *Elektrochemie*, Verlag Chemie, Weinheim/Bergstr., 1962, p. 128.
36 D. C. GRAHAME, *J. Chem. Phys.*, 18 (1950) 903.

37 F. BOOTH, *J. Chem. Phys.*, 19 (1951) 391.
38 P. DELAHAY, *Double Layer and Electrode Kinetics*, Interscience Publishers, New York, 1965.
39 B. E. CONWAY, J. O'. M. BOCKRIS AND I. A. AMMAR, *Trans. Faraday Soc.*, 47 (1951) 755.
40 J. O'. M. BOCKRIS, M. A. V. DEVANATHAN AND K. MÜLLER, *Proc. Roy. Soc. (London)*, A 274 (1963) 55.
41 H. S. HARNED AND B. B. OWEN, *The Physical Chemistry of Electrolytic Solutions*, Reinhold, New York, 3rd ed., 1963, chap. 15/8.
42 J. KORYTA, *Z. Elektrochem.*, 64 (1960) 23.
43 A. WELLER, *Discussions Faraday Soc.*, 27 (1959) 28.
44 M. EIGEN, *Z. Phys. Chem. NF*, 1 (1954) 154.
45 M. v. SMOLUCHOWSKI, *Z. Physik.*, 15 (1916) 555, 585; *Z. Physik. Chem.*, 92 (1917) 129.
46 P. DEBYE, *Trans. Electrochem. Soc.*, 82 (1942) 2916.
47 L. GIERST, L. VANDENBERGHEN, E. NICOLAS AND A. FRABONI, *J. Electrochem. Soc.*, 113 (1966) 1025.
48 R. M. DIAMOND, *J. Phys. Chem.*, 67 (1963) 2513.
49 E. WICKE, *Angew. Chem.*, 78 (1966) 1.
50 H. G. HERTZ AND W. SPALTHOFF, *Z. Elektrochem.*, 63 (1959) 1096.
51 A. JENARD AND H. D. HURWITZ, *J. Electroanal. Interfacial Chem.*, 19 (1968) 441.
52 H. W. NÜRNBERG, unpublished work, Harwell, 1963.
53 H. BRODOWSKY AND H. STREHLOW, *Z. Elektrochem.*, 63 (1959) 262.

ELECTROANALYTICAL CHEMISTRY AND INTERFACIAL ELECTROCHEMISTRY
Elsevier Sequoia S.A., Lausanne – Printed in The Netherlands

APPLICATION OF AN ENFORCED LINEAR IMPEDANCE BRIDGE TO A.C. POLAROGRAPHIC MEASUREMENTS

REITA TAMAMUSHI AND KIYOSHI MATSUDA
The Institute of Physical and Chemical Research, Yamato-machi, Kita-adachi-gun, Saitama (Japan)
(Received October 24th, 1968)

The measurement of impedances of electrode–solution interfaces as a function of the d.c. potential of the electrode provides useful information on the mechanism of the electrode process. The conventional a.c. polarograph is a most practicable instrument suitable for routine work; most of the accurate work over a wide range of frequencies, however, has been carried out by bridge techniques similar to that of Grahame[1]. When the bridge technique is applied to the a.c. polarographic measurement, one meets difficulties in connecting a direct voltage source to the cell. These difficulties, which are more important at lower frequencies, were thoroughly discussed by Britz and Bauer[2]. Modifying the instruments used by Randles[3] and by Bauer and Elving[4], Britz and Bauer proposed an apparatus capable of high accuracy over a wide range of frequencies, including frequencies as low as 5 Hz[2].

Recently, the present authors examined the utility of a deviation-linear bridge[5], in which two operational amplifiers enforce the linearity, in the accurate measurement of faradaic impedances and a.c. polarograms including tensammetric waves. The technique proposed in this paper eliminates the difficulties in applying a direct voltage to the cell, and proved to be very useful for electrochemical studies.

The basic circuit of the apparatus is shown in Fig. 1.

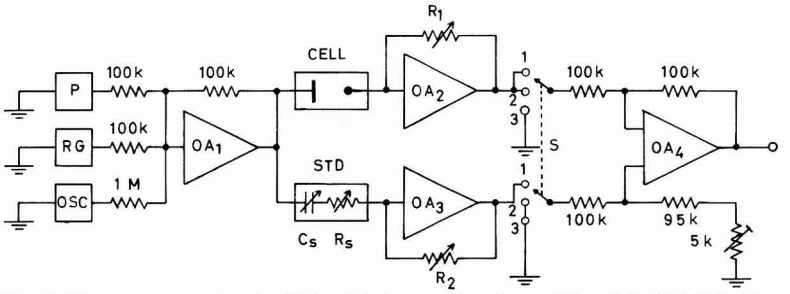

Fig. 1. The measuring circuit: (OA_1–OA_4), operational amplifiers (Model 9814, Aiko Denki Co., Ltd., Tokyo); (P), d.c. potentiometer; (RG), ramp generator; (OSC), oscillator.

The alternating voltage generated by the oscillator (OSC) was added by the operational amplifier (OA_1) to the direct voltage supplied from the potentiometer (P) and/or the ramp generator (RG); the output voltage of OA_1 was applied both to the cell and the variable standard impedance (STD) consisting of a decade resistance (R_s) and a

decade capacitance (C_s) in series. The voltage across the cell and STD is practically equal to the output voltage of OA_1, because the voltage between the summing points of operational amplifiers, OA_2 and OA_3, and ground is virtually zero within the error signal of the amplifiers (usually less than 0.1 mV). The currents flowing through the cell and STD were amplified by OA_2 and OA_3, respectively.

In impedance measurements by the bridge technique, the difference between the output voltages of OA_2 and OA_3 was detected by the operational amplifier, OA_4, with switch S in position 1; the output signal of OA_4 was then introduced to a cathode-ray oscilloscope equipped with a tuned amplifier. Simple calculation shows that the following conditions should be satisfied when the alternating voltage at the output of OA_4 is made equal to zero by adjusting R_s and C_s,

$$R_x = R_s \frac{R_1}{R_2} \quad \text{and} \quad C_x = C_s \frac{R_2}{R_1}$$

where R_x and C_x are the series resistance and capacitance, respectively, of the cell impedance.

The accuracy and sensitivity of the bridge were examined with a dummy cell consisting of a known resistance (500 Ω) and capacitance (1 μF) in series at various

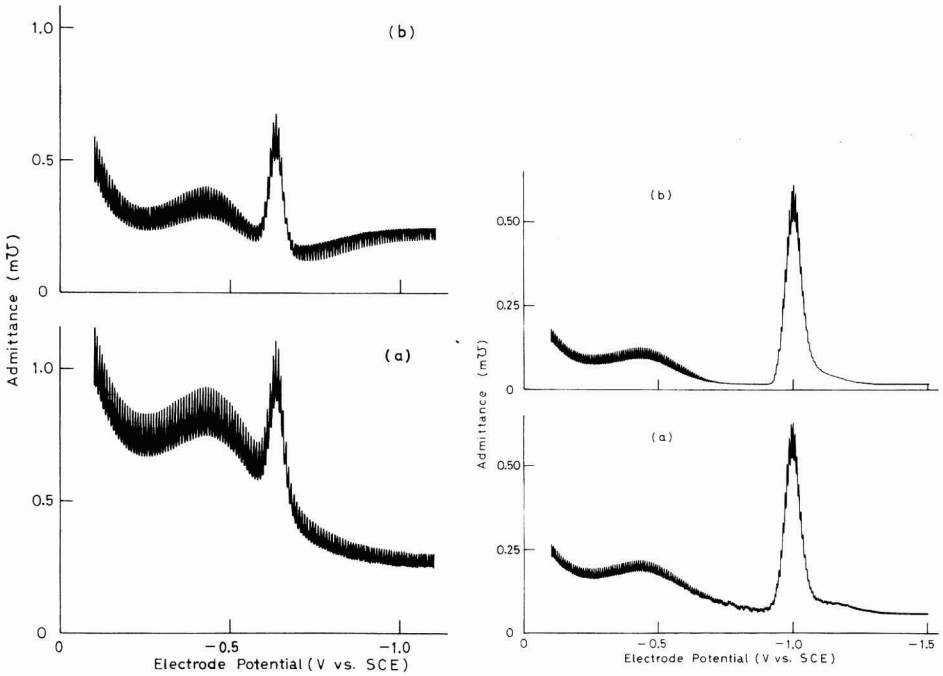

Fig. 2. A.c. polarograms of 0.1 m*M* $Cd(NO_3)_2$ in 1 *M* KCl measured at 140 Hz and at 25° (time constant of the damping circuit, *ca.* 3 sec): (a), without base-current compensation; (b), with base-current compensation ($R_s = 50\ \Omega$, $C_s = 0.6\ \mu F$).

Fig. 3. A.c. polarograms of 1 m*M* $Zn(NO_3)_2$ in 1 *M* KCl measured at 35 Hz and at 25° (time constant of the damping circuit, *ca.* 3 sec): (a), without base-current compensation; (b), with base-current compensation ($R_s = 60\ \Omega$, $C_s = 0.4\ \mu F$).

frequencies of 40–2,000 Hz and at various settings of R_1 and R_2. When the amplitude of the alternating voltage applied to the bridge was about 15 mV, the accuracy of R- and C-measurements was proved to be better than 0.5%, and the deviation as small as 0.2% was easily detected except for the resistance measurements at frequencies lower than 100 Hz. The performance of this bridge at higher frequencies is determined mainly by the "roll-off" characteristics of the operational amplifiers with frequency; a careful control of the closed-loop gains of OA_2 and OA_3 was required in order to operate the bridge at frequencies higher than 1 kHz.

Conventional a.c. polarographic measurements at various frequencies can also be made by this apparatus with switch S in position 2 and by connecting a suitable recorder with an a.c.-to-d.c. converter to the output of OA_4; the output signal was proved to be directly proportional to the alternating current flowing through the cell.

Because of the enforced linearity of the bridge, the proposed circuit is effective in suppressing the base-current in a.c. polarography. When switch S is set in position 1 and the values of C_s and R_s are properly adjusted, the contribution of the double-layer capacity and the resistance of solution can be eliminated from the total impedance of the cell at the output of OA_4. A reasonable suppression of the base-current was achieved in this way as shown in Figs. 2 and 3. Under the ideal conditions that the resistance of solution is zero and the value of C_s is exactly equal to the double-layer capacity, the instrument response is expected to be determined only by the faradaic impedance of the system.

SUMMARY

The circuit of a deviation-linear bridge for the measurement of faradaic impedances is described. Examples of a.c. polarograms obtained with the bridge are given.

REFERENCES

1 D. C. GRAHAME, *J. Am. Chem. Soc.*, 63 (1941) 1207.
2 D. BRITZ AND H. H. BAUER, *J. Sci. Instr.*, 44 (1967) 843.
3 J. E. B. RANDLES, *Discussions Faraday Soc.*, 1 (1947) 11.
4 H. H. BAUER AND P. J. ELVING, *J. Am. Chem. Soc.*, 82 (1960) 2091.
5 C. F. MORRISON, *Anal. Chem.*, 35 (1963) 1820.

ELECTROANALYTICAL CHEMISTRY AND INTERFACIAL ELECTROCHEMISTRY
Elsevier Sequoia S.A., Lausanne – Printed in The Netherlands

NOISE CONNECTED WITH ELECTRODE PROCESSES

G. C. BARKER
Atomic Energy Research Establishment, Harwell, Berks. (England)
(Received October 18th, 1968)

Shot noise[1] in electronic devices is dependent on the charge of the current carrier as well as on the current flowing and it is to be expected that electrical noise connected with statistical fluctuations in the rate of an irreversible electrochemical charge transfer process will also depend on the size of individual charge transfer events. This possibility, which seems not to have been discussed previously, is considered in this paper. Noise arising in electrochemical systems at equilibrium is also discussed.

HIGHLY IRREVERSIBLE CHARGE TRANSFER REACTION

Noise associated with the ideal highly irreversible charge transfer process

$$O + n\varepsilon \rightarrow R$$

is considered first. The *simultaneous* transfer of n electrons to species O is supposed to form R which does not participate in any other electrode process. Ideality in this case implies complete kinetic control of the reaction rate and the absence of catalysis by ions or other species present at the interface. Charge transfer is regarded as a completely random process which occurs with equal probability at all points on the surface. The faradaic current has a small fluctuating component analogous to the shot noise component of the current flowing in a temperature limited (no space charge of electrons close to the cathode) thermionic diode. The mean square noise current, $\overline{\Delta i^2}$, at constant interfacial potential within a small frequency band, df, is given by the analogue of the Shottky expression[1] for shot noise and

$$\overline{\Delta i^2} = 2|n\varepsilon\, i|\, df \qquad (1)$$

where i is the average faradaic current, ε the specific electronic charge and n the number of electrons which cross the electrode–solution interface simultaneously when the process occurs once. The current noise is dependent on n and, in principle, n can be determined directly if the noise *at constant interfacial potential* can be measured. The noise per unit bandwidth is independent of frequency and such noise may be termed "white noise" to distinguish it from noise considered later that lacks this frequency-independence.

In practice, owing to the finite internal resistance of the cell and the finite double-layer capacity of the electrode it may not be feasible to hold the interfacial potential even approximately constant, and only fluctuations in interfacial potential may be measurable. In such circumstances, the current noise can still be evaluated

with the aid of the equivalent electrical circuit for the cell. This takes the form shown in Fig. 1(a) if the counter-electrode is sufficiently large to be regarded as noiseless and unpolarizable. In this circuit C_{dl} is the differential capacity of the electrode (assumed to be virtually noiseless), R_c is the internal resistance of the cell and R_{ct} the apparent charge transfer resistance $(\partial E/\partial i)$ connected with the dependence of i on the interfacial potential, E. As charge transfer is taken to be entirely kinetically controlled, noise due to random variations in the surface concentration of O is unimportant. The noise component of i is represented in the circuit by an infinite-impedance current generator supplying a current defined by (1) which shunts the differential capacity. Noise due to thermal agitation of the ions in the solution is allowed for by inserting a zero-impedance voltage generator in series with R_c, the voltage supplied by this generator being defined by the Nyquist equation[2]

$$\overline{\Delta V^2} = 4kTR_c\,df \tag{2}$$

where k is Boltzmann's constant and T is the absolute temperature. Strictly, this equation is only applicable to a resistance through which no current flows steadily, but

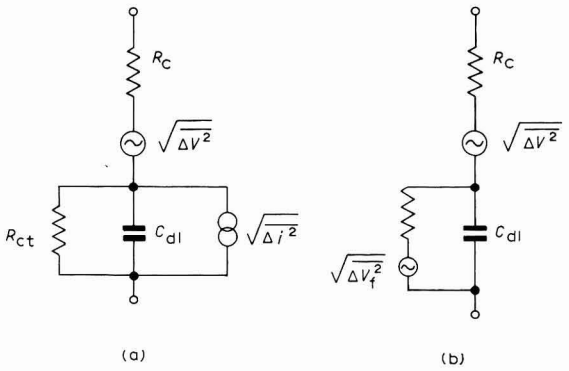

Fig. 1. Equivalent electrical circuits when the faradaic current associated with a highly irreversible charge transfer reaction has a noise component.

for a solution of a strong electrolyte and fields of normal magnitude, (2) should still accurately define noise connected with thermal agitation of the current carriers in the solution.

In the circuit in Fig. 1(a), the charge transfer resistance is treated as a noiseless component but in an alternative form of the circuit (Fig. 1(b)) the noise current generator is replaced by a zero-impedance noise voltage generator connected in series with R_{ct}, the voltage supplied by the latter being given by

$$\overline{\Delta V_f^2} = \overline{\Delta i^2} R_{ct}^2 \tag{3}$$

This noise voltage, it should be noted, only equals the "thermodynamic" voltage due to thermal agitation of the current carriers in a real resistance of value R_{ct} when the transfer coefficient for the charge transfer process is 0.5. The significance (if any) of this fact is not obvious.

It is evident from the circuits in Fig. 1 that both the internal resistance of the cell and the double-layer capacity of the test electrode will hamper the measurement

of noise components of the faradaic current and interfacial potential, especially at high frequencies. However, elementary calculations suggest that using modern electronic techniques, noise measurements should be feasible at frequencies up to at least 100 kHz in the case of a mercury electrode in contact with a highly conducting solution. At high frequencies, although the contribution of the charge transfer process to the noise voltage developed between the two electrodes of a cell may fall rather rapidly with increasing frequency, adventitious noise such as that due to mechanical vibration almost certainly will become unimportant at frequencies above 100 kHz. The actual noise voltages or currents will usually be minute compared with the potential and current variations when conventional relaxation techniques are used to study electrode processes, but this is only a trivial difficulty as with available solid state amplifying devices, noise factors below 6 dbs can be achieved at frequencies above 1 kHz with source impedances down to a few ohms if transformers are used to match the cell impedance to the input impedance of the measuring equipment.

Possible complications

No systematic measurements of noise associated with an irreversible charge transfer process have yet been made and it would be premature to discuss at length the consequences of deviations of real charge transfer processes from ideality. There are, however, three possible complications which should be mentioned. The first of these is concerned with the size of the individual charge transfer events. It is doubtful whether in any multi-electron irreversible reduction more than one electron crosses the electrode–solution interface at a time, though it is possible that the delay between the transfer of the first and subsequent electrons may often be extremely small. Thus, when considering the noise associated with a two electron reduction it may be necessary to regard the reduction as a two-step reaction

$$O + \varepsilon \rightarrow OR \qquad OR + \varepsilon \rightarrow R$$

where OR is an unstable intermediate which possibly exists only at the interface. The noise component of the total faradaic current in such a case may depend on whether the frequency is large or small compared with the reciprocal of τ, the half-life of species OR. Clearly, if τ is relatively small and OR is largely converted to R, the system will behave as though O is converted directly to R and the appropriate value of n to be substituted into (1) is then 2. At frequencies large compared with the reciprocal of τ, the correlation between the two charge transfer processes tends to vanish and then the mean square noise component of the total current, i, presumably tends to become the sum of the noise currents associated with two independent currents, each of magnitude $i/2$. Thus, remembering that noise currents and voltages must be summed vectorially, the mean square noise per unit frequency interval at high frequencies should fall to half the low frequency value. Information about the average life of unstable intermediates thus might be obtained by studying the distribution of noise energy throughout the frequency spectrum.

The second important complication is catalysis of charge transfer by species adsorbed at the interface. The reduction of nitrate ions at a mercury electrode is known to be catalysed by certain polyvalent cations and even the reduction of the hydrogen ion often takes place more readily at a mercury surface contaminated with organic matter. Although in such cases the exact mechanism of the catalysis usually is

not known, it is clear that the rate of charge transfer will depend on the surface concentration of the catalyst and the current thus may contain additional noise due to variations in the number of catalytic centres. In an extreme case the mean square noise current may be given approximately by

$$\overline{\Delta i^2} = \frac{\overline{\Delta m^2}}{m^2} i^2 \tag{4}$$

where m is the total number of catalytic centres and $\overline{\Delta m^2}$ is the mean square variation in m. It will be shown later that if the catalyst is an organic molecule or an inorganic ion it is possible to evaluate $\overline{\Delta m^2}/m^2$ with the aid of the equivalent circuit for the interface if certain electro-capillary data are available. Alternatively, if the frequency is sufficiently low for equilibrium to exist between the interface and the solution as regards the adsorption of the catalytic ion or molecule, it follows from an equation derived later (11) that if the surface density of catalytic centres is low

$$\frac{\overline{\Delta m^2}}{m^2} = \frac{4\mathrm{d}f}{ANC_c(2\omega D_c)^{\frac{1}{2}}} \tag{5}$$

where C_c is the catalyst concentration in the solution (mole cm^{-3}), D_c the diffusion coefficient of the catalyst, ω the angular frequency, N Avogadro's number and A the electrode surface area. From (4) and (5) it is clear that as the frequency decreases catalytic noise increases progressively in size. Such "red" noise may be likened to flicker noise in thermionic valves which, although not well understood, is probably due to variations with time in the emissive characteristics of the thermionic cathode.

The last complication to be mentioned is thermal agitation of the surface of a mercury electrode. Normally, the electrical energy stored in the double layer at the interface does not very greatly exceed the total kinetic energy of the mercury ions in the surface and it is clear that the occurrence of short-lived surface irregularities with dimensions comparable with or larger than the thickness of the discrete part of the double layer may be quite frequent. Whether or not such irregularities appreciably influence the rate of charge transfer and introduce another type of noise is far from clear. It is certain from arguments presented later that the electrical double layer at an electrode in contact with a concentrated aqueous solution of a strong electrolyte is not normally a very noisy part of the electrochemical system, but reasoning connected with a system in equilibrium gives no certain indication of the possible effect of thermal agitation of the surface (which is linked with variations in energy stored in the double layer) on the rate of an irreversible charge transfer process. Intuitively, one expects that heterogeneity in the surface will not make charge transfer more random than random but the matter requires detailed theoretical study.

SYSTEMS AT EQUILIBRIUM

It was first shown by Nyquist[2] that the mean square noise voltage developed across an isolated resistance is:

$$\overline{\Delta V^2} = 4kTR\mathrm{d}f \tag{2a}$$

where R is the value of the resistance. The noise voltage is thus not dependent on the mechanism of current conduction or on the charge and mobility of the current car-

riers if the resistance is unpolarized. This simple equation was derived by considering the noise power transferred between two identical resistances linked by a transmission line the characteristic impedance of which equals the two terminating resistances. Invoking the second law of thermodynamics, the noise energy transferred from one resistance to the terminated line must equal that transferred from the other resistance to the line and (2a) readily follows from a consideration of noise energy stored within the line.

The derivation of expressions for noise voltages and currents in an electrochemical system at equilibrium is even more straightforward if an equivalent electrical circuit for the system is available. Again, invoking the second law of thermodynamics, there can be no steady loss or gain of energy by the electrochemical system if it is connected to its equivalent circuit. It is obvious that a zero-impedance noise voltage generator satisfying (2a) must be inserted in series with each resistance in the equivalent electrical circuit if this thermodynamic requirement is not to be violated. It is also clear that any reactive elements in the equivalent circuit must be treated as noiseless components as any actual reactance is a noiseless component. The calculation of noise in an electrochemical system at equilibrium is thus, in principle, a trivial problem.

One further fact is also clear. Measurement of the frequency-dependence of noise associated with a system at equilibrium at the best can only give information about the frequency dispersion of the resistive and reactive parts of the equivalent circuit for the system, information that usually can more readily be obtained by a conventional perturbation method. In the remainder of the paper noise in equilibrium systems is discussed in greater detail mainly to clarify the causes of the noise or to obtain results needed for the calculation of noise associated with a faradaic current that is influenced by parts of the system which are virtually at equilibrium.

Simple redox reaction

In the absence of reactant adsorption at the interface, the equivalent electrical circuit for the faradaic impedance[3] associated with the reaction

$$O + n \rightleftharpoons R$$

consists of a charge transfer resistance, R_{ct}, in series with the diffusion impedances for the two reactants. If the system is at equilibrium the potential of the open-circuited electrode contains a noise component due to noise defined by (2a) originating in R_{ct} and in the resistive parts of the diffusion impedances for reactants O and R. In the complete equivalent circuit for the interface, this noise is represented by noise voltages supplied by three generators inserted directly in series with the three sources of noise. The observed noise component of potential may of course be smaller than the vectorial sum of these noise voltages if, at the frequency in question, the impedance of the double-layer capacity is not very much larger than the faradaic impedance.

As $R_{ct} = RT/nFi_0$, where i_0 is the exchange current at equilibrium, the noise voltage associated with the two opposing charge transfer processes is

$$\overline{\Delta V^2} = \frac{4(RT)^2}{nFNi_0} \cdot df \tag{6}$$

If by some means R_{ct} could be short-circuited, the noise current flowing through the short-circuit would be:

$$\overline{\Delta i}^2 = 4(n\varepsilon i_0)\mathrm{d}f \tag{7}$$

This is the noise current predicted by the Shottky equation[1] for two opposing and independent currents, each of magnitude i_0, and each composed of randomly occurring charge transfer events of size $n\varepsilon$. A clear and not unexpected link between statistical noise and noise due to thermal agitation is thus found in the case of noise connected with a charge transfer resistance. Charge transfer resistance noise is dependent on the size of the charge transfer events but unfortunately the evaluation of n demands a knowledge of i_0 which invariably presupposes a knowledge of n. Measurements of charge transfer resistance noise consequently provide no unique information about the mechanism of charge transfer. All that can be determined experimentally is ni_0 and this quantity usually can be readily obtained by more conventional methods[3,4].

Diffusion impedance noise

If in the case of a simple redox reaction the reactants move to and from the electrode only by linear diffusion it is known[5] that the diffusion impedance for each reactant can best be represented in the equivalent circuit for the faradaic impedance by a resistive transmission line with uniform series resistance and shunt capacity. This circuit is only valid if the deviation of the line voltage from the equilibrium value (normally zero) is minute compared with RT/nF and it is also implicitly assumed that the standard free energy of formation of the reactant is the same at all points in the solution and that the inner potential of the solution is absolutely constant. It is,

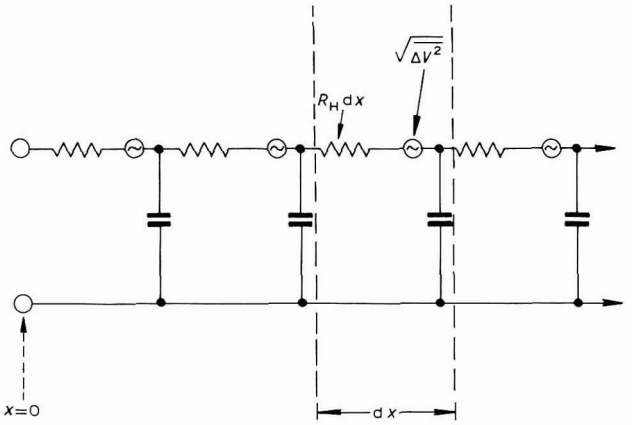

Fig. 2. Equivalent electrical circuit for a diffusion impedance when account is taken of thermal agitation.

consequently, a circuit without precise thermodynamic meaning but its electrical characteristics are consistent with known experimental facts and it can be employed to clarify the physical significance of a noise component of potential connected with the resistive part of a diffusion impedance.

To allow for the effects of thermal agitation, noise voltage generators must be distributed along the length of the resistive conductor of the transmission line as shown in Fig. 2. The resistance per unit length of this conductor is:

$$R_{tl} = RT/n^2F^2AC_lD_l \tag{8}$$

if the line represents the linear diffusion of reactant I and this reactant participates in a charge transfer reaction (apparently) involving n electrons[5]. Thus, diffusion across a layer of solution of thickness, dx, is represented in the circuit by the diffusion of charge through a resistance of value, $(RT/n^2F^2AC_1D_1)\mathrm{d}x$. Using the Nyquist equation the noise voltage developed across this small element of series resistance is found to be

$$\overline{\mathrm{d}V^2} = 4(RT/F)^2\,\mathrm{d}f\mathrm{d}x/An^2NC_1D_1$$

and as a change in line voltage, dV, represents a change in reactant concentration, $(nFC_1/RT)\mathrm{d}V$, the mean square variation in reactant concentration across a thin layer of solution of thickness, dx, *due to thermal agitation within the layer* is

$$\overline{\mathrm{d}C_i^2} = 4C_1\mathrm{d}f\mathrm{d}x/AND_1 \tag{9}$$

This result can be used to calculate non-equilibrium noise connected with the diffusion of a reactant through a diffusion layer at a polarized electrode.

However the validity of (9) will first be checked by using (9) to calculate the variations in the concentration of the reactant at the electrode surface ($x=0$) when no electrode reaction takes place. Use is made of the well-known expression for the temperature in a semi-infinite medium when the temperature at the plane $x=0$ varies sinusoidally with time[6], remembering that random variations in concentration in a small frequency band, df, can be regarded as the vectorial sum of a large number of minute *sustained* sinusoidal variations having frequencies within this band. Also, it has to be borne in mind that concentration variations across a thin layer of solution tend to be propagated towards $x=\infty$ as well as towards $x=0$, and that the actual variations in concentration at $x=0$ are the vectorial sum of concentration variations originating in solution laminae from $x=0$ to $x=|\infty|$. It readily follows that for an infinite medium ($x=-\infty$ to $x=+\infty$) the mean square variation in reactant concentration at $x=0$ is

$$\begin{aligned}\overline{\Delta C_I^2} &= 2\int_0^{\infty} \frac{\overline{\mathrm{d}C_I^2}}{4} \exp\left[-x\left\{\frac{2\omega}{D_1}\right\}^{\frac{1}{2}}\right]\cdot \mathrm{d}x \\ &= \frac{2C_1\mathrm{d}f}{AN(2\omega D_1)^{\frac{1}{2}}}\end{aligned} \tag{10}$$

For a semi-infinite medium extending from the plane of the electrode surface to infinity, the mean square noise component of concentration will be twice the value for an infinite medium and thus the concentration variations at the electrode surface when the reactant is not reduced or oxidised by the electrode are:

$$\overline{\Delta C_I^2} = \frac{4C_1\mathrm{d}f}{AN(2\omega D_1)^{\frac{1}{2}}} \tag{11}$$

The same result can be obtained more directly by the application of the Nyquist equation to the resistive part of the diffusion impedance[3] $\{RT/n^2F^2C_1(2\omega D_1)^{\frac{1}{2}}\}$ and replacing line voltage by concentration using the conversion factor employed earlier. The noise component of potential in the case of a completely reversible redox reaction is clearly due to fluctuations in the concentrations of the reactants at the electrode surface induced by thermal agitation in the entire body of solution, although,

of course, solution near the surface contributes most of the noise. Diffusion impedance noise, it will be noted, increases progressively as the frequency decreases and becomes relatively more important with decreasing reactant concentration.

Diffusion current noise

Equation (9) should still hold for a system which, although microscopically at equilibrium, is macroscopically not at equilibrium and, in the case where reactant I is reduced at the electrode surface and a diffusion layer of appreciable thickness, δ, is established at the surface, the concentration variation across a thin layer of solution within the diffusion layer now is

$$\overline{\mathrm{d}C_{\mathrm{I}}^2} = 4C_{\mathrm{I}} \frac{x}{\delta} \mathrm{d}f\mathrm{d}x/AND_{\mathrm{I}} \tag{12}$$

A linear concentration gradient for $0 < x < \delta$ and zero concentration at the electrode surface are assumed. The noise component of the diffusion current can be calculated with the aid of the solution of the previously mentioned problem in heat conduction[6] introducing positive and negative images of the concentration sources within the semi-infinite medium in order to satisfy the boundary condition, $C_{\mathrm{I}} = 0$ at $x = 0$. The solution for frequencies large compared with $\pi D_{\mathrm{I}}/\delta^2$ is found to be:

$$\overline{\Delta i_{\mathrm{d}}^2} = \left| \frac{nF}{N} i_{\mathrm{d}} \right| \mathrm{d}f \sum_{m=0}^{\infty} \frac{1}{(2m+1)^2} = 1.23 |n\varepsilon i_{\mathrm{d}}| \, \mathrm{d}f \tag{13}$$

where i_{d} is the limiting diffusion current. The mean square noise component of the limiting diffusion current is thus about two-thirds of the noise for an equal current composed of randomly occurring charge transfer events of size, $n\varepsilon$. The space cloud of diffusing reactant reduces the noise in much the same way as the electronic space charge that surrounds the cathode of a thermionic valve reduces the shot noise. It is somewhat surprising that the reduction is almost identical in the two cases, the factor to be applied in the thermionic emission case[7] being also approximately $\frac{2}{3}$.

It is assumed in the derivation of (13) that the reactant is reduced (or oxidised) instantaneously on arrival at the electrode surface and that the reaction takes place with equal probability at all points on the surface. Clearly, the noise might change in size somewhat if reduction, although apparently diffusion-controlled, only takes place close to ions adsorbed at the interface. The noise might conceivably exceed that predicted by (13) if, for example, the reduction of a hydrated metallic ion were to be catalysed by adsorbed (halide) ions. Another case in which excessive noise might well be observed is when the dynamic ψ-effect[8] markedly affects the rate of an intrinsically fast charge transfer process. It is possible that noise measurements might serve to clarify such phenomena.

Non-faradaic noise

Although few measurements have yet been made of the impedance at high frequencies[9] of the electrical double layer at the interface between a mercury electrode and a moderately concentrated aqueous solution of a single electrolyte, there is no evidence indicating that the differential capacity is not an aperiodic quantity up to frequencies of at least 1 MHz. The resistive part of the double-layer impedance at such frequencies must be very small and noise due to thermal agitation will usually be small

compared with that due to thermal agitation of the ions in the bulk of the solution. Often, therefore, it is justifiable to regard the double-layer capacity as a noiseless component.

Non-faradaic noise should, however, be observed when a minor organic or inorganic component of a concentrated electrolyte solution is strongly adsorbed at the interface. It is known that the equivalent circuit for the double layer[5,10] then takes the form shown in Fig. 3. The capacity, C_∞, the differential capacity at infinite frequency (ignoring small effects[11] due to the change in the transport numbers of the ions of the main electrolyte at the interface) is shunted by an adsorption capacity, C_a, in series with a resistive transmission line. The latter circuit component is connected with the linear diffusion of the strongly adsorbed component in the solution and is responsible for the non-faradaic noise. As with other electrochemical systems at equilibrium, thermal agitation is allowed for in the circuit by introducing a noise voltage generator in series with the resistive part of the circuit. The input impedance of the transmission line is known to be[12]

$$Z_a = -\left(\frac{\partial E}{\partial C_A}\right)_{\Gamma_A} \left(1 + \frac{1}{j}\right) \Big/ \left(\frac{\partial q}{\partial \Gamma_A}\right)_E A(2\omega D_A)^{\frac{1}{2}} \tag{14}$$

where Γ_A is the surface excess of the strongly adsorbed minor component A, q is the double layer charge density and C_A the concentration of A in the solution. Application of the Nyquist equation to the real part of this impedance gives the noise voltage and it is a simple matter to calculate the noise component of Γ_A if the derivatives in (14) and the derivatives defining $C_\infty[A(\partial q/\partial E)_{\Gamma_A}]$ and $C_a[A(\partial \Gamma_A/\partial E)_{C_A} \cdot (\partial q/\partial \Gamma_A)_E]$ are known.

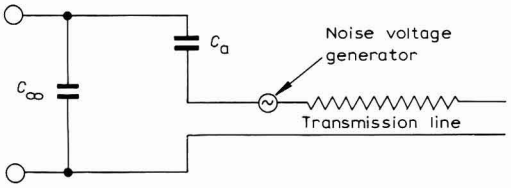

Fig. 3. Equivalent electrical circuit for the interface when a minor component is strongly adsorbed and account is taken of thermal agitation.

Although appreciable non-faradaic noise might sometimes be observed, it seems likely that studies of such noise cannot yield any information that cannot more easily be obtained by other experimental routes. However, as mentioned earlier, the circuit of Fig. 3 may be needed to account for noise in a polarized system when charge transfer is catalysed by species adsorbed at the interface which in some way facilitate the passage of electrons or charged ions across the interface. Catalysis in systems at equilibrium does not influence the noise other than by its effect on the exchange current, this being a consequence of the principle of microscopic reversibility.

Tentatively, it can be concluded that while it would seem a profitless task to study noise in electrochemical systems at equilibrium, it is possible that noise measurements made on non-equilibrium systems might, together with more conventional kinetic measurements, help to establish the mechanism of charge transfer in certain cases.

SUMMARY

Electrical noise in electrochemical systems at equilibrium, and in a non-equilibrium state, is discussed. It is shown that although little is to be gained from studies of noise in equilibrium systems connected with thermal agitation and the finite size of charge transfer events, experiments with systems far from equilibrium may cast some light on the mechanism of charge transfer. Noise measurements are most likely to prove informative when charge transfer is catalysed by a minor component of the interface.

REFERENCES

1 W. SCHOTTKY, *Ann. Physik*, 57 (1918) 541.
2 H. NYQUIST, *Phys. Rev.*, 32 (1938) 110.
3 J. E. B. RANDLES, *Discussions Faraday Soc.*, 1 (1947) 11.
4 P. DELAHAY, *Adv. Electrochem. Electrochem. Eng.*, 1 (1961) 233.
5 G. C. BARKER, *Pure Appl. Chem.*, 15 (1967) 239.
6 H. S. CARSLAW AND J. C. JAEGER, *Conduction of Heat in Solids*, Clarendon Press, Oxford, 1948, p. 48.
7 F. E. TERMAN, *Radio Engineers' Handbook*, McGraw-Hill, New York, 1943, p. 293.
8 L. GIERST, *Transactions Symposium on Electrode Processes*, edited by E. YEAGER, Wiley, New York, 1961, p. 109.
9 G. C. BARKER, *Transactions Symposium on Electrode Processes*, edited by E. YEAGER, Wiley, New York, 1961, p. 325; W. LORENZ AND G. KRÜGER, *Z. Physik. Chem. Leipzig*, 221 (1962) 231; W. LORENZ, *Z. Physik. Chem. Leipzig*, 224 (1963) 145; G. C. BARKER, *Polarography 1964*, edited by G. J. HILLS, Macmillan, London, 1966, p. 25.
10 G. C. BARKER AND A. W. GARDNER, AERE-C/R 1606, 1955.
11 G. C. BARKER, *J. Electroanal. Chem.*, 12 (1966) 495; F. C. ANSON, *J. Phys. Chem.*, 71 (1967) 3605.
12 A. N. FRUMKIN AND V. I. MELIK-GAIKAZYAN, *Dokl. Akad. Nauk, SSSR*, 78 (1951) 855; W. LORENZ AND F. MOCKEL, *Z. Elektrochem.*, 60 (1956) 507.

ELECTROANALYTICAL CHEMISTRY AND INTERFACIAL ELECTROCHEMISTRY
Elsevier Sequoia S.A., Lausanne – Printed in The Netherlands

ON THE IMPEDANCE OF GALVANIC CELLS

XXV. THE DOUBLE-LAYER CAPACITANCE OF THE DROPPING MERCURY ELECTRODE IN 1 *M* HCl, 7.5 *M* HCl AND 5.2 *M* $HClO_4$ AND THE KINETIC PARAMETERS OF THE HYDROGEN ELECTRODE REACTION AS A FUNCTION OF TEMPERATURE IN THESE SOLUTIONS

B. G. DEKKER, M. SLUYTERS-REHBACH AND J. H. SLUYTERS
Laboratory of Analytical Chemistry, State University, Utrecht (The Netherlands)

(Received June 26th, 1968)

INTRODUCTION

One of the interesting problems in electrochemistry is the theoretical interpretation of the kinetic parameters of electrode reactions. The most studied subject in this respect is probably the hydrogen evolution reaction on mercury. For example, the relation between overvoltage and double-layer structure has been investigated by Frumkin[1], and various attempts have been made to assess a scheme for the reaction mechanism (for a review, see Vetter[2]). Parsons and Bockris[3] have given a calculation of the theoretical energy of activation based on the model of the so-called discharge reaction[2], the result of which compares favourably with experimental values. From this and also from other work[4–10] it appears worthwhile to study the temperature-dependence of the exchange current density, i_O, and the transfer coefficient, β.

Unfortunately, the inconsistencies of the abundance of experimental data[11] available for the hydrogen electrode make it difficult to draw decisive conclusions. Also, anomalous results are often reported, and need further investigation. Most of this work has been concerned with the determination of the Tafel[12] parameters by direct current methods.

As part of a general programme for the study of the effect of temperature on the parameters of electrode reactions, and the properties of the electrode–solution interface, we investigated the impedance of the dropping mercury electrode in concentrated acid solutions at different temperatures. The advantage of the impedance method is that it contains information both on the electrode reaction and the double-layer capacitance, even in the potential region where the faradaic process occurs[13,14]. As the rate of an electrode reaction is closely related to the structure of the double layer, this may be a valuable parameter.

Moreover, the $H^+/H_2(Hg)$ reaction appears to be a suitable system for the demonstration of the applicability of the impedance method to the study of irreversible systems, as postulated recently[15].

In this paper, we report the results of measurements in aqueous 1 *M* HCl, in the eutectic mixtures of composition, 7.5 *M* HCl, and 5.2 *M* $HClO_4$. The eutectic compositions were chosen because they have very low freezing points.

A critical discussion will be given in the light of the existing literature, especially as regards the temperature-dependence of the transfer coefficient, which for 7.5 *M* HCl was observed by Bockris and Matthews[10] to be anomalous.

EXPERIMENTAL

The cell consisted of two sections, one for the dropping mercury electrode (cathode) and a mercury pool counter electrode (anode), and the other for a reversible hydrogen reference electrode. The latter consisted of a short piece of coiled platinum wire coated with platinum black. The two compartments were connected by a short capillary, the top of which was near the DME. The whole system was saturated with hydrogen gas, which was deoxygenated (by passing it through a column filled with reduced copper oxide in a very active form, BTS-Katalysator, BASF at a temperature of 50°) and then equilibrated with a solution of the same composition and temperature as in the measuring cell.

Care was taken to eliminate impurities from the solutions: reagent-grade HCl and $HClO_4$ were used, and water was distilled twice, successively from acid and alkaline permanganate solution. The mercury was doubly-distilled.

All glassware was cleaned with dichromic acid and steamed out for a few hours. Immediately before use it was rinsed with doubly-distilled water.

For some experiments, the solution was pre-electrolyzed overnight at 5 mA/cm^2 using an auxiliary Pt cathode which was removed shortly before the measurements. However, as we found no difference in the results for the same experiment with and without pre-electrolysis, this was omitted.

The impedance measurements were carried out at potentials as far cathodic as possible, *i.e.*, until the rapid evolution of hydrogen bubbles disturbed the regular dropping of the mercury, which was mechanically controlled. The impedance and d.c. potential measurements were made with the a.c. bridge and additional set-up as described elsewhere[13].

A special provision was made for temperature control. The cell was surrounded by two jackets; the outer jacket was evacuated, and through the inner one methanol or water was circulated from a cryostat or thermostat, depending on the temperature range desired. In this way the accuracy was better than 0.1°.

RESULTS

Interpretation of impedance measurements

Since the $H^+/H_2(Hg)$ electrode reaction is extremely irreversible, polarization to fairly negative potentials is required to obtain a substantial faradaic current, both for d.c. and a.c. At more positive potentials, the measured impedance yielded directly the values of the ohmic resistance, R_Ω, and the double-layer capacity, C_d. In the faradaic region itself, the components Z' and Z'' of the cell impedance were determined as a function of frequency (420–3000 Hz) and analyzed according to the complex plane method[13,14]. As in our present investigations the double-layer capacitance is not *a priori* known (no indifferent electrolyte added), the so-called frequency variation method had to be applied, *i.e.*, we considered the frequency-dependence of the components Y'_{el} and Y''_{el}, of the electrode admittance, calculated from

$$Y'_{el} = \frac{Z' - R_\Omega}{(Z' - R_\Omega)^2 + Z''^2} \tag{1a}$$

$$Y''_{el} = \frac{Z''}{(Z' - R_\Omega)^2 + Z''^2} \tag{1b}$$

In all cases, Y'_{el} and Y''_{el}/ω were independent of frequency, indicating that diffusion polarization is negligible, as would be expected for the H^+/H_2(Hg) electrode at the foot of the reduction wave. Thus, the impedance data enable the calculation[16] of the transfer resistance, $\theta = 1/Y'_{el}$, and the double-layer capacitance, $C_d = Y''_{el}/\omega$.

Potential-dependence of the transfer resistance

A general equation for the potential-dependence of θ has been given by Timmer *et al.*[16]. Since in the present case $E \ll E_O$, the simplified equation may be considered:

$$\theta = \frac{RT}{n^2F^2k^a_{sh}} \cdot \frac{a_O + \exp\left[-(\beta nF/RT)(E-E_O)\right]}{\beta a_O C^*_O \exp\left[-(\beta nF/RT)(E-E_O)\right]} \tag{2}$$

in which C^*_O is the H^+ concentration, k^a_{sh} the apparent standard heterogeneous rate constant, β the cathodic transfer coefficient and $a_O = (7D_O/3\pi t)^{\frac{1}{2}}k_{sh}^{-1}$ for a DME. If k_{sh} is sufficiently small, $a_O \gg \exp\left[-(\beta nF/RT)(E-E_O)\right]$, leading to

$$\theta = \frac{RT}{n^2F^2k^a_{sh}\beta C^*_O} \exp\left[\frac{\beta nF}{RT}(E-E_O)\right] \tag{3}$$

For a comparison with literature data it is more convenient to count the potential, E, from the reversible equilibrium potential, E_{eq}, and to consider values of i_O, the exchange current density, at E_{eq}:

$$i_O = nFk^a_{sh} C^{*\alpha}_O C^{*\beta}_R . \tag{4}$$

With eqn. (4) and $E - E_{eq} = \eta$, eqn. (3) can be transformed into

$$\theta = \frac{RT}{nF\beta i_O} \exp\frac{\beta nF}{RT}\eta \tag{5}$$

or

$$\ln\theta = \ln\frac{RT}{nF\beta i_O} + \frac{\beta nF}{RT}\eta \tag{6}$$

As in all cases of the present study $\log\theta$ *vs.* η plots were linear, it can be concluded that the conditions for eqn. (3) are fulfilled. The values of β and i_O can be calculated from the slope and the intercept of such a plot. The slope is, in fact, the reciprocal of the Tafel[12] parameter, b.

Temperature-dependence of i_O and β

i. 1 M HCl. The measurements with this solution were carried out at 0°, 15°, 25° and 45°. At each temperature, θ was determined at about 10 potentials in a range of about 200 mV. The value of θ never exceeded 1000 Ω cm^2 (higher values cannot be determined accurately[13]). The reproducibility was good. The equations of the $\log\theta$ *vs.* η plots were assessed by the method of least squares. The results are presented in Table 1, together with the values for β and $\log i_O$. The averaged errors are, ± 0.02 in β and ± 0.30 in $\log i_O$.

In order to make a direct comparison with d.c. measurements, a Tafel line was also recorded at 25°. The result was in excellent agreement with that of the impedance method, confirming the applicability of the latter. Our results are in reasonable agree-

ment with those of Jofa and Stepanova[5] (log $i_0 = -11.7$ and $\beta = 0.49$ at 20°) and of De Béthune[17] (log $i_0 = -11.53 \pm 0.05$ and $\beta = 0.50$ at 25°).

An important conclusion from Table 1 is that the transfer coefficient does not vary significantly with temperature in the range investigated. This is in agreement with the experience of Jofa and Stepanova[5] and also of Post and Hiskey[8] for 0.1 *M* HCl, although the latter authors observed above 35° an increase in β from 0.50 to

TABLE 1

DATA FOR 1.0 *M* HCl

Temp. (°C)	*Eqns. of log θ vs. overpotential, η* (θ *in* Ω cm^2, η *in volts*)	β	*log* i_0 (i_0 *in A* cm^{-2})
0	$\log \theta = 12.30 + 9.59\,\eta$	0.52	−13.65
+15	$\log \theta = 11.74 + 9.36\,\eta$	0.53	−13.08
+25	$\log \theta = 10.68 + 8.64\,\eta$	0.51	−11.98
+45	$\log \theta = 9.99 + 8.43\,\eta$	0.53	−11.28

0.55 at 91.3°. However, Bockris and Parsons[7] reported a significant temperature-dependency of β, for 0.1 *M* HCl solution. As these authors found identical Tafel lines for HCl solutions on changing the acid concentration from 0.01 *M* to 1 *M*, a comparison with our results seems to be justified and the disagreement has to be considered.

The apparent heat of activation at the reversible potential, ΔH, can be obtained from a plot of log i_0 *vs.* $1/T$. Figure 1 shows that our plot for 1 *M* HCl (curve 1)

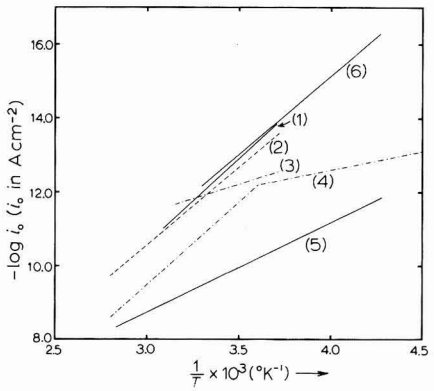

Fig. 1. Dependence of i_0 on temp.: (1), 1.0 *M* HCl (this work); (2), 0.1 *M* HCl (Post and Hiskey[8]); (3), 0.1 *M* HCl (Bockris and Parsons[7]); (4), 7.5 *M* HCl (Bockris and Matthews[10]); (5), 7.5 *M* HCl (this work); (6), 5.2 *M* $HClO_4$ (this work).

agrees satisfactorily with that derived from the data of Post and Hiskey[8] for 0.1 *M* HCl (curve 2). The ΔH-values are 21.1 ± 2.0 kcal $mole^{-1}$ for curve 1 and 19.3 kcal $mole^{-1}$ for curve 2. A similar treatment of the data of Bockris and Parsons[7], however, produces a deviating plot (curve 3) with a ΔH-value of 7.2 kcal $mole^{-1}$. On the other hand, the authors report an apparent heat of activation of 21.1 kcal $mole^{-1}$, calculated from $(\partial\eta/\partial T)_i$ in a way which theoretically should give the same result as the calcula-

tion from Fig. 1. The discrepancy is caused by the temperature-dependency of β, found by Bockris and Parsons and which, in our opinion, is incorrect.

ii. 7.5 M HCl. The measurements in 7.5 *M* HCl have been made in a temperature range, $-35°$ to $+72°$. The equations for the log θ *vs.* η lines, the values of β, and of log i_0 are given in Table 2. The averaged errors are, ± 0.01 in β and ± 0.20 in log i_0. Again, an excellent agreement was found with a d.c. Tafel line recorded at 25°.

TABLE 2

DATA FOR 7.5 *M* HCl

Temp. (°C)	*Eqns. of log* θ *vs. overpotential,* η (θ *in* Ω cm^2, η *in volts*)	β	*log* i_0 (i_0 *in A* cm^{-2})
−35	$\log \theta = 10.39 + 8.24\ \eta$	0.389	−11.66
−25	$\log \theta = 9.96 + 8.14\ \eta$	0.400	−11.23
−15	$\log \theta = 9.30 + 7.78\ \eta$	0.398	−10.55
− 5	$\log \theta = 9.42 + 8.21\ \eta$	0.436	−10.70
+ 5	$\log \theta = 9.10 + 8.19\ \eta$	0.452	−10.38
+10	$\log \theta = 8.74 + 7.97\ \eta$	0.447	−10.00
+15	$\log \theta = 8.61 + 7.97\ \eta$	0.455	− 9.88
+20	$\log \theta = 8.50 + 7.99\ \eta$	0.464	− 9.77
+25	$\log \theta = 8.53 + 8.17\ \eta$	0.483	− 9.80
+35	$\log \theta = 8.06 + 8.03\ \eta$	0.491	− 9.33
+45	$\log \theta = 7.89 + 8.14\ \eta$	0.514	− 9.16
+50	$\log \theta = 7.58 + 7.91\ \eta$	0.507	− 8.85
+55	$\log \theta = 7.61 + 8.14\ \eta$	0.530	− 8.88
+65	$\log \theta = 7.25 + 7.99\ \eta$	0.536	− 8.52
+72	$\log \theta = 7.13 + 8.04\ \eta$	0.550	− 8.40

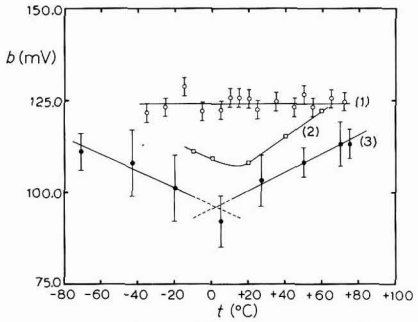

Fig. 2. Dependence of Tafel parameter, *b*, on temp.: (1), 7.5 *M* HCl (this work); (2), 7.0 *M* HCl (Jofa and Stepanova[5]); (3), 7.5 *M* HCl (Bockris and Matthews[10]).

The most remarkable result of these measurements is the very marked temperature-dependence of β in Table 2. To our knowledge, such a significant trend of the transfer coefficient with temperature has not previously been published. Bockris and Matthews[10] also studied the H^+/H_2(Hg) reaction in 7.5 *M* HCl and observed an anomalous temperature-dependence of the Tafel slope *b*, with a minimum at $+5°$. For comparison, we calculated *b* from our measurements and plotted it against temperature in Fig. 2, together with the results of Bockris and Matthews[10], and of Jofa and Stepanova[5] for 7 *M* HCl, which cover a smaller temperature range.

It can be seen that the minimum found by Bockris and Matthews is not very significant, whereas our results indicate quite significantly that the Tafel slope is independent of temperature. In other words, we find β to be proportional to the absolute temperature, with a temperature coefficient, $1.56 \cdot 10^{-3}$ degree^{-1}.

Our values for the exchange current density are also in disagreement with those of Bockris and Matthews[10] (see Fig. 1) who report two values for the apparent heat of activation, ΔH_0, at the reversible potential: $\Delta H_0 = 21.0$ kcal mole^{-1} for $t = +5°$ to $+60°$ and $\Delta H_0 = 5$ kcal mole^{-1} for $t = +5°$ to $-71°$, with a sharp discoptinuity at $+5°$. We find $\Delta H_0 = 11.1 \pm 0.5$ kcal mole^{-1} for the whole temperature range ($-35°$ to $+72°$).

iii. 5.2 *M* $HClO_4$. The measurements in this medium were carried out to compare the behaviour of the H^+/H_2(Hg) electrode in 7.5 *M* HCl (where specific adsorption of chloride may play a role) with that in a concentrated acid solution with no (or anyway less) specific anion adsorption.

The results, obtained as before, are presented in Table 3. The averaged errors are, ± 0.02 in β and ± 0.50 in log i_0.

TABLE 3

DATA FOR 5.2 *M* $HClO_4$

Temp. (°C)	*Eqns. of log* θ *vs. overpotential,* η (θ *in* Ω cm^2, η *in volts*)	β	*log* i_0 (i_0 *in A* cm^{-2})
−39	$\log \theta = 15.11 + 11.20\ \eta$	0.52	−16.52
−35	$\log \theta = 14.17 + 10.50\ \eta$	0.50	−15.56
−25	$\log \theta = 14.25 + 10.80\ \eta$	0.53	−15.64
− 5	$\log \theta = 12.90 + 10.10\ \eta$	0.54	−14.26
0	$\log \theta = 11.74 + 9.19\ \eta$	0.50	−13.07
+ 5	$\log \theta = 11.71 + 9.26\ \eta$	0.50	−13.03
+10	$\log \theta = 12.23 + 9.80\ \eta$	0.55	−13.58
+15	$\log \theta = 11.93 + 9.62\ \eta$	0.55	−13.28
+25	$\log \theta = 10.86 + 8.82\ \eta$	0.52	−12.17

The transfer coefficient is clearly not significantly temperature-dependent within the range investigated. The apparent heat of activation at the reversible potential, calculated from the Arrhenius plot (Fig. 1) is 19.5 ± 2.2 kcal mole^{-1}.

To our knowledge, the effect of temperature on this system has not previously been investigated.

Temperature-dependence of the double-layer capacity in 1 *M HCl,* 7.5 *M HCl and* 5.2 *M* $HClO_4$

The data on C_d, obtained in the region of H^+ reduction from Y''_{el}/ω (eqn. 1b), were extended to more positive potentials by direct measurements of the electrode capacitance. The results for 1 *M* HCl, 7.5 *M* HCl and 5.2 *M* $HClO_4$ are shown in Figs. 3, 4 and 5.

The dashed portions of the curves indicate the region where the hydrogen evolution reaction occurs and form a quite logical prolongation of the more positive parts, which might suggest that effects of coupling between the faradaic admittance

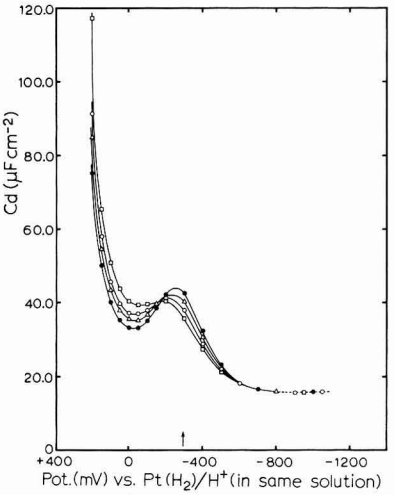

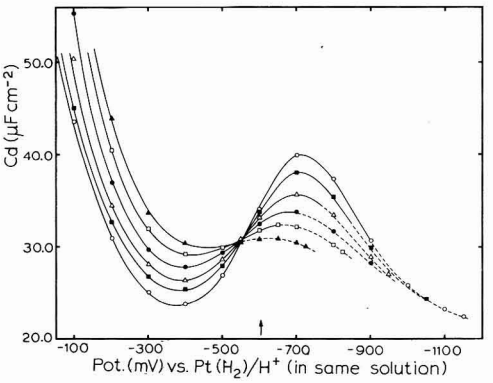

Figs. 3–4. Capacity–potential curves for mercury. (3) in 1.0 *M* HCl at: (□), +45°; (○), +25°; (△), +15°; (●), 0°. (4) in 7.5 *M* HCl at: (▲), +65°; (□), +45°; (●), +25°; (△), +5°; (■), −15°; (○), −35°. The dashed part in the curves indicates the region of the hydrogen evolution reaction. The vertical arrow indicates the position of the p.z.c. at 25°.

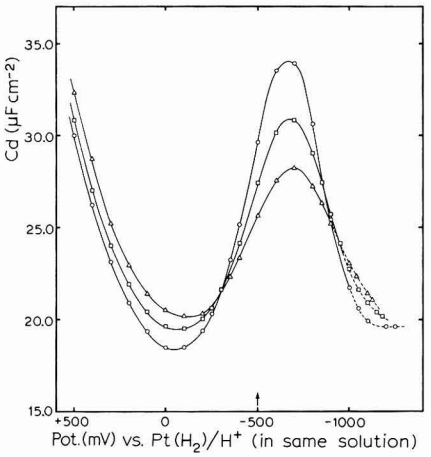

Fig. 5. Capacity–potential curves for mercury in 5.2 *M* $HClO_4$ at several temps.: (△), +25°; (□), −5°; (○), −35°. The dashed part in the curves indicates the region of the hydrogen evolution reaction. The vertical arrow indicates the position of the p.z.c. at 25°.

and (specific) adsorption of electroactive species are negligible[18]. For 1 *M* HCl the capacity minimum in the negative potential region is 16 $\mu F/cm^2$.

In all cases, the capacity–potential curves pass through a common point, situated on the left-hand side of the so-called "hump". This behaviour is similar to that of plots of the inner-layer capacity *vs.* electrode charge, published by Grahame[19] for 0.8 *M* NaF. Because of the high electrolyte concentrations, our capacities may also be considered as approximately equal to the inner layer capacities. A comparison

with Grahame's data suggests that specific adsorption of chloride has little effect on the general shape of the curves, except that the hump seems to be somewhat more pronounced.

In contrast with the case of hydrochloric acid, where the curves tend to coincide in the negative potential region, the capacity–potential curves for 5.2 *M* $HClO_4$ have a second common intersection point which is situated in the potential region where the hydrogen evolution reaction begins. (Fig. 5).

In Figs. 3, 4 and 5 the potentials of zero charge, p.z.c., at 25° are also indicated. The p.z.c. was determined by means of drop-time measurements and was found to be in agreement with literature values[20]. Only a slight temperature-dependence of the p.z.c. was found, in accordance with the measurements of Paik *et al.*[21] in 1 *M* KCl solution. In Fig. 3 it can be seen that the maximum of the hump in 1 *M* HCl is observed at a potential positive to the p.z.c., similar to the fluoride case. This was ascribed by Mott and Watts-Tobin[22] to specific anion adsorption, although this is rather unlikely for fluoride[23]. The position of the hump appears to be an important feature in the development of theories for explaining its occurrence[24]. Satisfactory explanations for all phenomena have not yet been given, especially for the fact that in some solvents (water, dimethylsulfoxyde[24], sulfolane[25]) the hump is found anodic to the p.z.c., and in other solvents (formamide, N-methylformamide) on the cathodic side. Our experiments in concentrated acids have revealed a new phenomenon, which, as far as we know, has not been previously observed: in 7.5 *M* aqueous HCl and 5.2 *M* aqueous $HClO_4$ the humps are situated at potentials negative to the p.z.c. This suggests that the effect of increasing the electrolyte concentration has also to be considered.

DISCUSSION

It has been stated that the temperature-dependence of the transfer coefficient of the hydrogen electrode reaction might be of diagnostic value, especially with respect to the so-called proton-tunnelling mechanism[26]. However, Conway and Salomon[9] showed that the occurrence of tunnelling at a mercury electrode is improbable. Instead, they support the view of Bockris and Parsons[7], that "a satisfactory account of the variation of β with temperature could be given on the basis of the variation of the thickness of the double layer with temperature, deduced from the temperature dependence of the double-layer capacitance." As, according to Parsons and Bockris[3], β is an inverse function of the double-layer thickness, the observed decrease of β with decreasing temperature should correspond to a decrease in capacity. However, our capacity measurements in 7.5 *M* HCl show an increase in capacity with decreasing temperature in the potential region of the hydrogen reduction. As this region coincides with the hump region, where dielectric saturation may be incomplete, it is quite reasonable to ascribe this trend to the variation of the dielectric constant with temperature[22]. In the far negative potential region, the capacity–potential curves clearly tend to coincide, so that no evidence for the temperature-dependence of the double-layer thickness can be deduced from our experiments. On the other hand, the capacity in 5.2 *M* $HClO_4$ shows a decrease with decreasing temperature in the "hydrogen region", but in this case β is found to be independent of temperature.

In our opinion, the explanation must be sought, anyway in the first instance,

in considering that the experimentally-determined value of β is not necessarily a "real" transfer coefficient. It has been shown recently[27], that the rate constant, k_{sh}, and thus i_O, can be a function of potential. In that case the slope of the log θ *vs.* η plot (see eqn. 6) becomes

$$\left(\frac{\partial \ln \theta}{\partial \eta}\right)_T = \frac{\beta nF}{RT} - \left(\frac{\partial \ln i_O}{\partial \eta}\right)_T \tag{7}$$

A similar expression may be derived for the slope of the d.c. current–voltage curve:

$$\ln i = \ln i_O - \frac{\beta nF}{RT}\,\eta \tag{8}$$

giving

$$\left(\frac{\partial \ln i}{\partial \eta}\right)_T = -\frac{\beta nF}{RT} + \left(\frac{\partial \ln i_O}{\partial \eta}\right)_T \tag{9}$$

The "apparent transfer coefficient" β_{app}, calculated with (7) or (9) is equal to

$$\beta_{app} = \frac{RT}{nF}\left(\frac{\partial \ln \theta}{\partial \eta}\right)_T = -\frac{RT}{nF}\left(\frac{\partial \ln i}{\partial \eta}\right)_T = \beta - \frac{RT}{nF}\left(\frac{\partial \ln i_O}{\partial \eta}\right)_T = \beta - g \tag{10}$$

If β is considered as a fundamental constant (independent of η and T) the following conclusions can be drawn from the results reported in this paper: (a) For 1 *M* HCl and 5.2 *M* $HClO_4$ solutions, g in eqn. (10) is probably negligible, because β_{app} is independent of temperature. (b) For the 7.5 *M* HCl solution, g has a substantial value: as β_{app} is found to be independent of potential and a linear function of temperature, $\partial \ln i_O/\partial \eta$ is not significantly dependent on η and T in the range investigated.

Bockris and Matthews[10] developed a similar idea, ascribing their anomalous Tafel slopes for 7.5 *M* and 3 *M* HCl to the fact that k_{sh}^a in eqn. (4) contains the Frumkin correction term, in which the outer Helmholtz plane potential, ϕ_2, is potential-dependent. However, this effect is not, as the authors suggest, characteristic for a solution from which anions (*i.e.*, chloride ions) are specifically adsorbed. Moreover, it is too small for a quantitative explanation of the anomalous β-values. Recently[28,29], we showed that the presence of specifically adsorbed anions, itself can have a considerable influence on the rate constant of the $Zn^{2+}/Zn(Hg)$ electrode reaction, in decreasing the activation energy of the charge transfer. It seems reasonable to apply this view also to the $H^+/H_2(Hg)$ reaction. This means that, if specific adsorption is significant, the change of the specifically adsorbed amount with potential causes the activation energy, and thus i_O, to be potential-dependent. As specific adsorption increases with decreasing temperature, it can be expected that the heat of activation is temperature-dependent also, and consequently the ΔH-value, calculated for 7.5 *M* HCl, will be the mean value of the ΔH-values pertaining to the temperatures in the range investigated. It may be noted that the temperature and potential range of the measurements is obviously very important to the results obtained and this may explain the discrepancies between the results of different investigators, *e.g.* between the work of Bockris and Matthews and ours.

The present results are unsuitable for more quantitative considerations, but we hope to make further investigations in that direction.

ACKNOWLEDGEMENT

This investigation was supported in part by the Netherlands Foundation for Chemical Research (SON) with financial aid from the Netherlands Organisation for the Advancement of Pure Research (ZWO).

SUMMARY

The impedance of the dropping mercury electrode in aqueous solutions in 1 *M* HCl, 7.5 *M* HCl and 5.2 *M* $HClO_4$, saturated with hydrogen at one atmosphere was measured at temperatures between $-39°$ and $+72°$ both in and outside the potential region where the electrode reaction, $e+H^+ \rightleftarrows \frac{1}{2}H_2$, proceeds.

Analysis of the impedance data gave information about both the kinetics of the electrode reaction and the double-layer capacity. Exchange current densities and transfer coefficients are reported. The apparent heat of activation is 21.1 kcal $mole^{-1}$ for 1 *M* HCl, 19.5 kcal $mole^{-1}$ for 5.2 *M* $HClO_4$, and 11.1 kcal $mole^{-1}$ for 7.5 *M* HCl. In the latter solution the transfer coefficient is found to be a linear function of temperature. In 1 *M* HCl and 5.2 *M* $HClO_4$ the transfer coefficient is virtually independent of temperature.

In 1 *M* HCl the hump in the capacity curve is situated anodically to the potential of zero charge but in 7.5 *M* HCl and 5.2 *M* $HClO_4$ this is reversed.

In both 1 *M* HCl and 7.5 *M* HCl the capacity–potential curves show one potential where the double-layer capacitance is independent of temperature. In the case of 5.2 *M* $HClO_4$, this occurs at two potentials, situated at either side of the potential of zero charge.

REFERENCES

1 A. N. Frumkin, *Z. Physik. Chem.*, 164A (1933) 121.
2 K. J. Vetter, *Elektrochemische Kinetik*, Springer-Verlag, Berlin, 1961, pp. 410-497.
3 R. Parsons and J. O'M. Bockris, *Trans. Faraday Soc.*, 47 (1951) 914.
4 F. P. Bowden, *Proc. Roy. Soc. (London)*, A126 (1929) 107.
5 Z. A. Jofa and V. Stepanova, *J. Phys. Chem. USSR*, 19 (1945) 125.
6 J. N. Agar, *Discussions Faraday Soc.*, 1 (1947) 81.
7 J. O'M. Bockris and R. Parsons, *Trans. Faraday Soc.*, 45 (1949) 916.
8 B. Post and C. F. Hiskey, *J. Am. Chem. Soc.*, 72 (1950) 4203.
9 B. E. Conway and M. Salomon, *J. Chem. Phys.*, 41 (1964) 3169.
10 J. O'M. Bockris and D. B. Matthews, *Electrochim. Acta*, 11 (1966) 143.
11 *Gmelins Handbuch der Anorganischen Chemie, Quecksilber*, Teil A, Verlag Chemie, Weinheim, 1962, p. 706.
12 J. Tafel, *Z. Physik. Chem.*, 50 (1905) 641.
13 M. Sluyters-Rehbach and J. H. Sluyters, *Rec. Trav. Chim.*, 82 (1963) 525, 535.
14 M. Sluyters-Rehbach, D. J. Kooyman and J. H. Sluyters, *Polarography (1964)*, edited by G. J. Hills, Macmillan, London, p. 135.
15 M. Sluyters-Rehbach and J. H. Sluyters, *Rec. Trav. Chim.*, 83 (1964) 581.
16 B. Timmer, M. Sluyters-Rehbach and J. H. Sluyters, *J. Electroanal. Chem.*, 14 (1967) 169, 181.
17 A. J. De Béthune, *J. Am. Chem. Soc.*, 71 (1949) 1556.
18 B. Timmer, M. Sluyters-Rehbach and J. H. Sluyters, *J. Electroanal. Chem.*, 19 (1968) 73.
19 D. C. Grahame, *J. Am. Chem. Soc.*, 79 (1957) 2093.
20 *Gmelins Handbuch der Anorganischen Chemie, Quecksilber*, Teil A, Verlag Chemie, Weinheim, 1962, p. 607.

21 W. PAIK, T. N. ANDERSON AND H. EYRING, *J. Phys. Chem.*, 71 (1967) 1891.
22 N. F. MOTT AND R. J. WATTS-TOBIN, *Electrochim. Acta*, 4 (1961) 79.
23 J. LAWRENCE, R. PARSONS AND R. PAYNE, *J. Electroanal. Chem.*, 16 (1968) 193.
24 R. PAYNE, *J. Am. Chem. Soc.*, 89 (1967) 489.
25 J. LAWRENCE AND R. PARSONS, *Trans. Faraday Soc.*, 64 (1968) 751.
26 B. E. CONWAY, *Can. J. Chem.*, 37 (1959) 178.
27 M. SLUYTERS-REHBACH, B. TIMMER AND J. H. SLUYTERS, *Z. Physik. Chem. N.F.*, 52 (1967) 89.
28 P. TEPPEMA, M. SLUYTERS-REHBACH AND J. H. SLUYTERS, *J. Electroanal. Chem.*, 16 (1968) 165.
29 M. SLUYTERS-REHBACH, J. S. M. C. BREUKEL AND J. H. SLUYTERS, *J. Electroanal. Chem.*, 19 (1968) 85.

ELECTROANALYTICAL CHEMISTRY AND INTERFACIAL ELECTROCHEMISTRY
Elsevier Sequoia S.A., Lausanne – Printed in The Netherlands

MODEL OF MERCURY/SOLUTION INTERFACE IN THE PRESENCE OF ORGANIC COMPOUNDS ADSORBED IN TWO DIFFERENT POSITIONS

B. B. DAMASKIN

Chemical Faculty, Moscow State University, Moscow V-234 (USSR)

(Received October 29th, 1968)

As was shown in a number of papers[1-3], adsorption of various aliphatic compounds at the mercury/solution interface is quantitatively described by means of a two parallel capacitors model[4,5] if a small additional correction is introduced to take into account the discrete nature of adsorbed organic dipoles[6]. In the general case, this model proves to be inapplicable for the description of adsorption of aromatic or heterocyclic compounds (see, *e.g.* ref. 7), since owing to π-electronic interaction, molecules of these compounds can be adsorbed in two different positions: flat and vertical. The ratio between the number of molecules oriented flat and vertically can change, both with the electrode potential, E, and with increasing organic substance concentration, c. To describe such adsorption phenomena, a system of isotherms of the type;

$$\left.\begin{aligned} B_1 c &= \{\theta_1/n_1(1-\theta_1-\theta_2)^{n_1}\} \exp(g_{11}\theta_1+g_{12}\theta_2) \\ B_2 c &= \{\theta_2/n_2(1-\theta_1-\theta_2)^{n_2}\} \exp(g_{21}\theta_1+g_{22}\theta_2) \end{aligned}\right\} \quad (1)$$

was proposed[8], in which the adsorption equilibrium constants, B_1 and B_2, were considered as some functions of the electrode charge, q. In eqns. (1), θ_i is the surface coverage, n_i the ratio of the area occupied by an adsorbate molecule to that of a cluster of adsorbed water molecules (see refs. 9, 10), and g_{ij} parameters of intermolecular interaction of adsorbed particles; indices 1 and 2 in our notation refer to vertical and flat orientation of adsorbate molecules, respectively.

The aim of the present paper is to fit the system of isotherms (1) to the model of three parallel capacitors which physically must correspond to the electrode/solution interface in the presence of organic substance adsorbed in two different positions.

The basic equation of this model can be written as:

$$q = q_0(1-\theta_1-\theta_2) + C_1(E-E_{N1})\theta_1 + C_2(E-E_{N2})\theta_2 \quad (2)$$

where q_0 is the electrode charge in pure supporting electrolyte solution, C_1 and C_2 the double-layer capacities at $\theta=1$ and $\theta_2=1$, respectively, and E_{N1} and E_{N2} the shifts of the point of zero charge (p.z.c.) upon transition from $\theta_1=\theta_2=0$ to $\theta_1=1$ and $\theta_2=1$, respectively; the potential, E, is read from p.z.c. in supporting electrolyte solution.

Equation (1) can be related to eqn. (2) by means of the basic equation of electrocapillarity, which at $E=$ const., for such systems can be written as:

$$\mathrm{d}\sigma = -(A/n_1)\theta_1 \,\mathrm{d}\log c - (A/n_2)\theta_2 \,\mathrm{d}\log c \quad (3)$$

where σ is the interfacial tension, $A=n_1RT\,\Gamma_\infty^{(1)}=n_2RT\Gamma_\infty^{(2)}$ and $\Gamma_\infty^{(i)}$ the limiting ad-

sorption. Let us show that system (1) agrees with eqns. (2) and (3) under the following conditions: $B_1 = B_1(E)$; $B_2 = B_2(E)$; $g_{11} = -2n_1a_1$; $g_{12} = -2n_1a_3$; $g_{21} = -2n_2a_3$ and $g_{22} = -2n_2a_2$, where a_i are attraction constants for the following orientations of adsorbate molecules: a_1—vertical/vertical, a_2—flat/flat and a_3—vertical/flat. If these conditions are fulfilled, system (1) assumes the form:

$$\left.\begin{aligned} B_1(E)c &= \{\theta_1/n_1(1-\theta_1-\theta_2)^{n_1}\}\exp(-2n_1a_1\theta_1-2n_1a_3\theta_2)\\ B_2(E)c &= \{\theta_2/n_2(1-\theta_1-\theta_2)^{n_2}\}\exp(-2n_2a_2\theta_2-2n_2a_3\theta_1)\end{aligned}\right\} \tag{4}$$

which gives at $E = \text{const.}$

$$\left.\begin{aligned} \mathrm{d}\log c &= \frac{\mathrm{d}\theta_1}{\theta_1} + \frac{n_1\mathrm{d}\theta}{1-\theta} - 2n_1a_1\mathrm{d}\theta_1 - 2n_1a_3\mathrm{d}\theta_2\\ \mathrm{d}\log c &= \frac{\mathrm{d}\theta_2}{\theta_2} + \frac{n_2\mathrm{d}\theta}{1-\theta} - 2n_2a_2\mathrm{d}\theta_2 - 2n_2a_3\mathrm{d}\theta_1\end{aligned}\right\} \tag{5}$$

where $\theta = \theta_1 + \theta_2$. Introducing (5) into (3), after integration we obtain

$$\sigma = \sigma_0 + A\left[\log(1-\theta) + \frac{n_1-1}{n_1}\theta_1 + \frac{n_2-1}{n_2}\theta_2 + a_1\theta_1^2 + a_2\theta_2^2 + 2a_3\theta_1\theta_2\right] \tag{6}$$

where σ_0 is the value of σ in supporting electrolyte solution, since at $\theta_1 = \theta_2 = 0$, $\sigma = \sigma_0$. Equation (6) can be used as a basis for calculating the σ, E-curves, provided that the dependence of surface coverages, θ_1 and θ_2, on the potential is known.

Since it is assumed that eqn. (6) is valid at all potentials, its differentiation with respect to E gives for the electrode charge:

$$\begin{aligned} q = -\frac{\mathrm{d}\sigma}{\mathrm{d}E} = q_0 + A\Bigg(&\frac{1}{1-\theta}\frac{\mathrm{d}\theta}{\mathrm{d}E} - \frac{n_1-1}{n_1}\frac{\mathrm{d}\theta_1}{\mathrm{d}E} - \frac{n_2-1}{n_2}\frac{\mathrm{d}\theta_2}{\mathrm{d}E} -\\ &- 2a_1\theta_1\frac{\mathrm{d}\theta_1}{\mathrm{d}E} - 2a_2\theta_2\frac{\mathrm{d}\theta_2}{\mathrm{d}E} - 2a_3\theta_1\frac{\mathrm{d}\theta_2}{\mathrm{d}E} - 2a_3\theta_2\frac{\mathrm{d}\theta_1}{\mathrm{d}E}\Bigg)\end{aligned} \tag{7}$$

If we introduce the symbols $P_1 = \mathrm{d}\log B_1/\mathrm{d}E$ and $P_2 = \mathrm{d}\log B_2/\mathrm{d}E$, we obtain from eqn. (4)

$$\left.\begin{aligned} P_1 &= \frac{1}{\theta_1}\frac{\mathrm{d}\theta_1}{\mathrm{d}E} + \frac{n_1}{1-\theta}\frac{\mathrm{d}\theta}{\mathrm{d}E} - 2n_1a_1\frac{\mathrm{d}\theta_1}{\mathrm{d}E} - 2n_1a_3\frac{\mathrm{d}\theta_2}{\mathrm{d}E}\\ P_2 &= \frac{1}{\theta_2}\frac{\mathrm{d}\theta_2}{\mathrm{d}E} + \frac{n_2}{1-\theta}\frac{\mathrm{d}\theta}{\mathrm{d}E} - 2n_2a_2\frac{\mathrm{d}\theta_2}{\mathrm{d}E} - 2n_2a_3\frac{\mathrm{d}\theta_1}{\mathrm{d}E}\end{aligned}\right\} \tag{8}$$

Using (8) we can readily see that the expression in the brackets of eqn. (7) is equal to $P_1\theta_1/n_1 + P_2\theta_2/n_2$, and hence

$$q = q_0 + A\left(\frac{P_1\theta_1}{n_1} + \frac{P_2\theta_2}{n_2}\right) \tag{9}$$

Equations (2) and (9) coincide under the condition

$$P_1 = -\frac{n_1[q_0 + C_1(E_{N1} - E)]}{A} \qquad P_2 = -\frac{n_2[q_0 + C_2(E_{N2} - E)]}{A} \tag{10}$$

Integration of (10) gives

$$B_1 = B_{01} \exp\left[-\frac{\int_0^E q_0 dE + C_1 E(E_{N1} - E/2)}{A/n_1}\right]$$
$$B_2 = B_{02} \exp\left[-\frac{\int_0^E q_0 dE + C_2 E(E_{N2} - E/2)}{A/n_2}\right] \quad (11)$$

where B_{01} and B_{02} are the values of B_1 and B_2 at $E = 0$. Equation (11) defines concretely the $B_1(E)$- and $B_2(E)$-dependences contained in the system of isotherms (4).

Now let us find the expression for the differential capacity, C, in the presence of organic substances adsorbed in two different positions. Differentiating (9) with respect to E, we find

$$C = \frac{dq}{dE} = C_0 + A\left(\frac{\theta_1}{n_1}\frac{dP_1}{dE} + \frac{\theta_2}{n_2}\frac{dP_2}{dE}\right) + A\left(\frac{P_1}{n_1}\frac{d\theta_1}{dE} + \frac{P_2}{n_2}\frac{d\theta_2}{dE}\right) \quad (12)$$

The derivatives, dP_1/dE and dP_2/dE, contained in this equation are found from (10) and the derivatives, $d\theta_1/dE$ and $d\theta_2/dE$, by solving a linear system of eqns. (8), in which the sum, $d\theta_1/dE + d\theta_2/dE$, should be substituted for $d\theta/dE$. After substitution of these derivatives into eqn. (12), we obtain

$$C = C_0(1-\theta_1-\theta_2) + C_1\theta_2 + C_2\theta_2 + A\frac{\frac{P_1^2}{n_1^2}\left(\frac{1}{n_2\theta_2} + \frac{1}{1-\theta} - 2a_2\right) - 2\frac{P_1P_2}{n_1n_2}\left(\frac{1}{1-\theta} - 2a_3\right) + \frac{P_2^2}{n_2^2}\left(\frac{1}{n_1\theta_1} + \frac{1}{1-\theta} - 2a_1\right)}{\left(\frac{1}{n_1\theta_1} + \frac{1}{1-\theta} - 2a_1\right)\left(\frac{1}{n_2\theta_2} + \frac{1}{1-\theta} - 2a_2\right) - \left(\frac{1}{1-\theta} - 2a_3\right)^2} \quad (13)$$

In principle, eqn. (13) with a known dependence of θ_1 and θ_2 on E permits the complete calculation of the C, E-curve in the presence of organic substances adsorbed in two different positions. From a practical point of view, however, the use of this equation is inconvenient, since at $\theta_1 \to 0$, $\theta_2 \to 0$ or $\theta \to 1$, the terms in the numerator and denominator tend to infinity. To avoid these difficulties eqn. (13) can be transformed to the form

$$C = C_0(1-\theta) + C_1\theta_1 + C_2\theta_2 + \frac{1}{A} \times \frac{M_1^2 x_1[x_2 + (1-\theta)(1-2a_2x_2)] - 2M_1M_2x_1x_2[1-2a_3(1-\theta)] + M_2^2x_2[x_1 + (1-\theta)(1-2a_1x_1)]}{(x_1+x_2) + (1-\theta)[1-2a_1x_1 - 2a_2x_2 + 4x_1x_2(a_1a_2 - a_3^2)] - 2x_1x_2(a_1 + a_2 - 2a_3)} \quad (14)$$

where $x_1 = n_1\theta_1$; $x_2 = n_2\theta_2$; $M_1 = q_0 + C_1(E_{N1} - E)$; $M_2 = q_0 + C_2(E_{N2} - E)$.

The dependence of θ_1 and θ_2 on E, necessary for the determination of the theoretical σ, E- and C, E-curves from eqns. (6) and (14), can be calculated as follows. First, from eqn. (4) at given values of n_1, n_2, a_1, a_2 and a_3 are plotted the dependences of $\log(B_1c)$ on θ_1 for different θ_2 and of $\log(B_2c)$ on θ_2 for different θ_1 (Fig. 1). Then, the potential is given and from eqn. (11) the values of B_1 and B_2 are calculated for this potential. Thus, with a chosen concentration, c, we now have the values of $\log(B_1c)$ and $\log(B_2c)$. With these values known, two dependences of θ_2 on θ_1 are plotted by

means of the plots shown in Fig. 1. For the values $\log(B_1 c) = -0.5$ and $\log(B_2 c) = +0.5$ (see Fig. 1) such dependences of θ_2 on θ_1 are given in Fig. 2. The intersection of these two curves determines the values of θ_1 and θ_2 at given E. Then a new potential value is given and the values of θ_1 and θ_2 are found for it in a similar way, etc. In a particular case, when $a_1 = a_2 = a_3 = 0$, $n_1 = 1$ and $n_2 = 2$, the solution of system (4) is greatly simplified, since in this case eqn. (4) gives a quadratic equation for θ (see ref. 11).

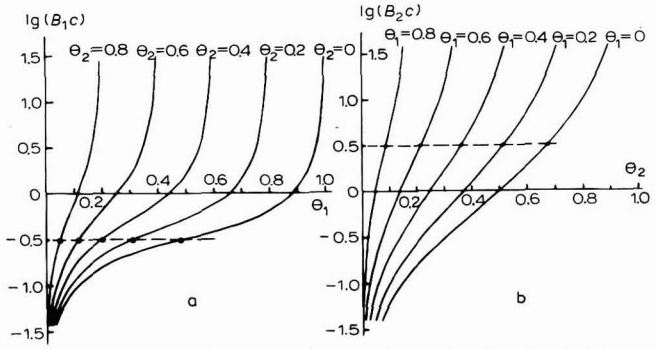

Fig. 1. Dependence of (a), $\log(B_1 c)$ on θ_1; (b), $\log(B_2 c)$ on θ_2 calcd. by means of eqn. (4) with $n_1 = 1$; $n_2 = 2$; $a_1 = 1.15$ and $a_2 = a_3 = 0$.

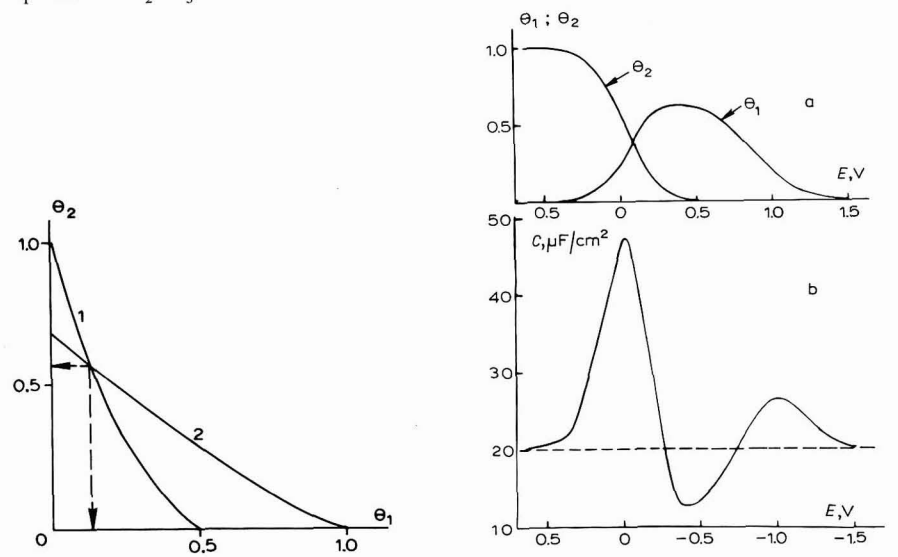

Fig. 2. Dependence of θ_2 on θ_1 obtained by means of the plots in Fig. 1 under the condition: (1), $\log(B_1 c) = -0.5$; (2), $\log(B_2 c) = +0.5$.

Fig. 3. Dependence of (a), coverages θ_1 and θ_2; (b), differential capacity on the electrode potential calculated for case (1) under the following additional conditions: $C_0 = 20\ \mu F/cm^2$; $C_1 = 7\ \mu F/cm^2$; $A = 1.6\ \mu J/cm^2$; $E_{N1} = 0.5$ V; $E_{N2} = -0.5$ V; $B_{01} c = 2$ and $B_{02} c = 5$.

We have calculated the curves of the potential-dependence of θ_1 and θ_2, as well as the differential capacity curves for the following particular cases:

(1) $n_1=1$; $n_2=2$; $a_1=a_2=a_3=0$; $C_2=C_0=$const.;
(2) $n_1=1$; $n_2=2$; $a_1=a_2=a_3=0$; $C_2\neq C_0=$const.;
(3) $n_1=1$; $n_2=2$; $a_2=a_3=0$; $a_1\neq 0$; $C_2\neq C_0=$const;
(4) $n_1=1$; $n_2=2$; $a_2=0$; $a_1\neq 0$; $a_3\neq 0$; $C_2\neq C_0=$const.

The results obtained are given in Figs. 3–7. It follows from the figures, that owing to the condition, $C_2=C_0$, the organic substance is not desorbed with increasing positive charge, whereas at $C_2<C_0$ and $C_1<C_0$ it is desorbed and both the curves θ_1–E and θ_2–E are bell-shaped. In both cases, at large $q>0$, the C,E-curves in solu-

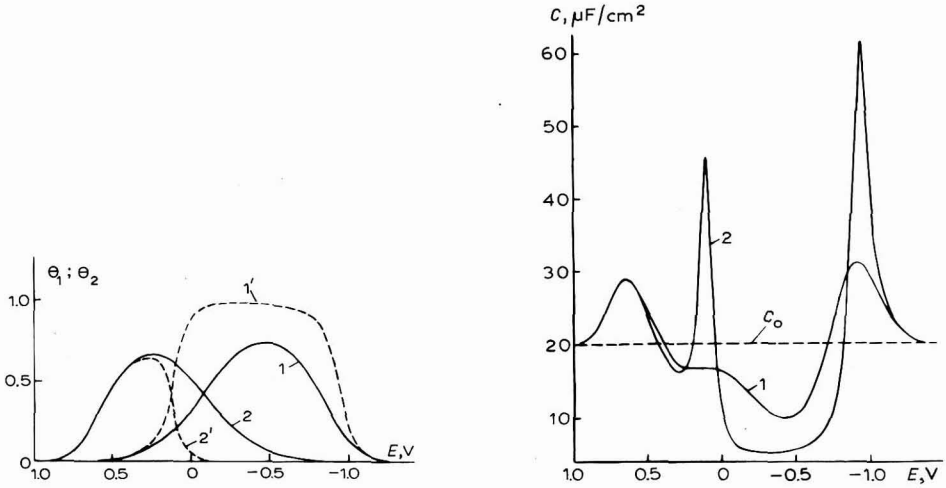

Fig. 4. Dependence of (1 and 1'), coverages θ_1; (2 and 2'), θ_2 on the potential calcd. for cases (2) and (3) under the following additional conditions: $C_0=20$ μF/cm^2; $C_1=5$ μF/cm^2; $C_2=10$ μF/cm^2; $A=1$ μJ/cm^2; $E_{N1}=1$ V; $E_{N2}=0$; $B_{01}c=2$; $B_{02}c=10$. (1 and 2), case (2); (1' and 2'), case (3) at $a_1=1.15$.

Fig. 5. Differential capacity curves calcd. for the conditions of Fig. 4. (1), case (2); (2), case (3) at $a_1=1.15$.

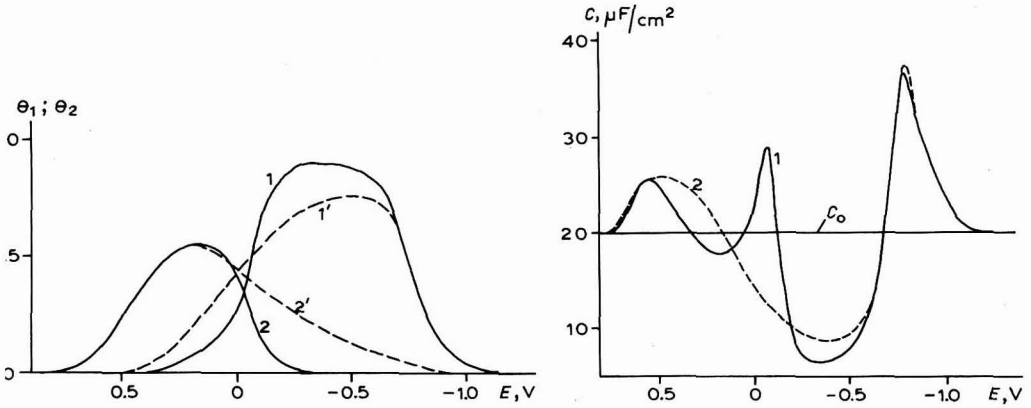

Fig. 6. Dependence of (1 and 1'), coverages θ_1; (2 and 2'), θ_2 on the potential calcd. for cases (3) and (4) under the following additional conditions: $C_0=20$ μF/cm^2; $C_1=5$ μF/cm^2; $C_2=10$ μF/cm^2; $A=1$ μJ/cm^2; $E_{N1}=1$ V; $E_{N2}=0$; $B_{01}c=0.5$; $B_{02}c=2.5$. Curves (1 and 2), case (3); at $a_1=1.15$; (1' and 2'), case (4) at $a_1=a_3=1.15$.

Fig. 7. Differential capacity curves calcd. for the conditions of Fig. 6. (1), case (3) at $a_1=1.15$; (2), case (4) at $a_1=a_3=1.15$.

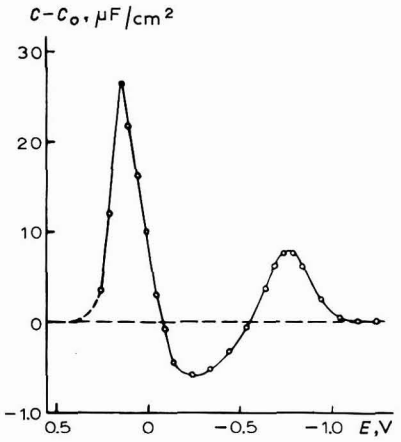

Fig. 8. Differential capacity curve for the system, 1 *M* KCl + 0.02 *M* *p*-phenylenediamine; 25°, 400 c/sec. For ease of comparison with the theoretically calcd. *C*, *E*-curves, the difference between capacities in solution with the organic addition and in the supporting electrolyte soln. is plotted along the ordinate axis. The potential is measured against p.z.c. in supporting electrolyte soln.

tions with organic substance additions coincide with the *C*, *E*-curve of the supporting electrolyte. Taking account of the attractive interaction between adsorbate molecules in the first position ($a_1 > 0$) leads to the widening of the corresponding adsorption region and to the reduction of the adsorption region for the second position (Fig 4). Moreover, the transition from one adsorbate orientation to the other at $a_1 > 0$ is more abrupt, which results in the appearance of pronounced reorientation peaks on the *C*, *E*-curves (Fig. 5). On the contrary, the attraction interaction between adsorbate molecules in two different positions ($a_3 > 0$) leads to widening of the co-adsorption region (Fig. 6) and to the disappearance of the reorientation peak (Fig. 7).

Case (1) considered by us corresponds qualitatively to the adsorption on mercury of aniline molecules[7], as well as of *o*- and *p*-phenylenediamines[11] (*cf.* Figs. 3a and 8). Case (3) is realized for coumarin adsorption on mercury. The *C*, *E*-curves for this case are given in Fig. 9. The cathodic adsorption–desorption peak is not realized here owing to electroreduction of coumarin[12,13]. *C*, *E*-curves of a similar shape with a peak in the middle were obtained also for some other compounds[14,15].

If the two positions in which organic molecules can be adsorbed differ only in the values of the adsorption potential drops ($E_{N1} \neq E_{N2}$), and the adsorption energy at $E = 0$ changes linearly with the total coverage, θ, it is possible to use formally for the description of such systems (as shown in ref. 16) the two parallel capacitors model with account taken of the linear dependence of the attraction constant, a, in Frumkin's isotherm on the potential ($da/dE = \text{const.} < 0$). This gives theoretical substantiation to the results obtained by us earlier in the investigation of adsorption on mercury of pyridine[17] and phenol[18].

Thus, the three parallel capacitors model can be used as a satisfactory basis for the description of the behaviour of the electrode/solution interface in the presence of organic compounds adsorbed in two different positions. It should be noted that all the relations obtained here are valid also for co-adsorption of two organic compounds, if only their molecules lie within the adsorption monolayer. Some particular cases of

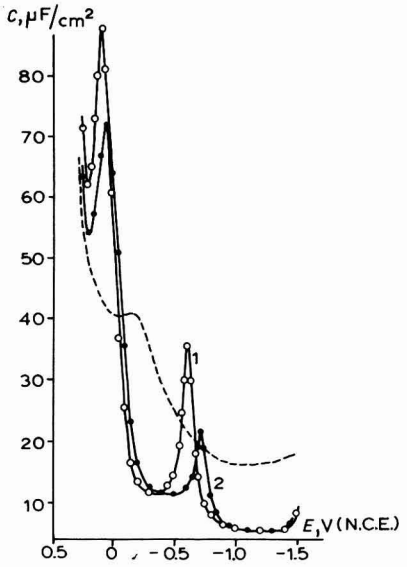

Fig. 9. Differential capacity curves of 1 *N* Na_2SO_4 (dashed) and of 1 *N* Na_2SO_4 with additions of coumarin: (1), $5 \cdot 10^{-3}$ *M*; (2), $2 \cdot 10^{-3}$ *M*; 25°; 400 c/sec.

the three parallel capacitors model have been considered for the case of co-adsorption of two organic compounds[19].

SUMMARY

The capacity of the mercury–solution interface is calculated on the basis of a model of three capacitors in parallel representing the surface with no adsorbed species and the surface with adsorbed species oriented in two ways. The calculated curves are compared with experimental data on the adsorption of *p*-phenylenediamine and coumarin.

REFERENCES

1 B. B. DAMASKIN, *Electrochim. Acta*, 9 (1964) 231.
2 R. LERKH AND B. B. DAMASKIN, *Zh. Fiz. Khim.*, 38 (1964) 1154; 39 (1965) 211, 495.
3 B. B. DAMASKIN, A. A. SURVILA AND L. E. RYBALKA, *Elektrokhimiya*, 3 (1967) 146, 927, 1138.
4 A. N. FRUMKIN, *Z. Physik*, 35 (1926) 792.
5 A. N. FRUMKIN AND B. B. DAMASKIN, *Modern Aspects of Electrochemistry*, edited by J. O'M. BOCKRIS, Butterworths, London, 1964, p. 149, Vol. 3.
6 B. B. DAMASKIN, *Elektrokhimiya*, 1 (1965) 1123.
7 B. B. DAMASKIN, I. P. MISHUTUSHKINA, V. M. GEROVICH AND R. I. KAGANOVICH, *Zh. Fiz. Khim.*, 38 (1964) 1797.
8 J. M. PARRY AND R. PARSONS, *J. Electrochem. Soc.*, 113 (1966) 992.
9 B. B. DAMASKIN, *Elektrokhimiya*, 1 (1965) 63.
10 R. PARSONS, *J. Electroanal. Chem.*, 8 (1964) 93.
11 B. B. DAMASKIN, A. N. FRUMKIN AND S. L. DYATKINA, *Izv. Akad. Nauk, Ser. Khim.*, (1967) 2171.
12 A. J. HARLE AND L. E. LYONS, *J. Chem. Soc.*, (1950) 1575.
13 O. ČAPKA, *Collection Czech. Chem. Commun.*, 15 (1950) 965.

14 Z. OSTROWSKI AND H. FISCHER, *Electrochim. Acta*, 8 (1963) 1, 37.
15 H. FISCHER AND W. SEILER, *Corrosion Sci.*, 6 (1966) 159.
16 B. B. DAMASKIN, *Elektrokhimiya*, 4 (1968) 675.
17 L. D. KLYUKINA AND B. B. DAMASKIN, *Izv. Akad. Nauk, Ser. Khim.*, (1963) 1022.
18 B. B. DAMASKIN, V. M. GEROVICH, I. P. GLADKIKH AND R. I. KAGANOVICH, *Zh. Fiz. Khim.*, 38 (1964) 2495.
19 G. A. TEDORADZE, R. A. ARAKELYAN AND E. D. BELOKOLOS, *Elektrokhimiya*, 2 (1966) 563.

ELECTROANALYTICAL CHEMISTRY AND INTERFACIAL ELECTROCHEMISTRY
Elsevier Sequoia S.A., Lausanne – Printed in The Netherlands

INTERPRETATION OF THE POLAROGRAPHIC BEHAVIOUR OF METAL–SOLOCHROME VIOLET RS COMPLEXES

T. M. FLORENCE AND W. L. BELEW*

Chemistry Division, Australian Atomic Energy Commission Research Establishment, Lucas Heights, N.S.W. (Australia)

(Received October 24th, 1968)

INTRODUCTION

The ability of certain di-*o*-hydroxyazo dyes to form discrete polarographic reduction waves in the presence of metal ions was first observed by Willard and Dean[1], who used the dye, solochrome violet RS (5-sulfo-2-hydroxybenzene-azo-2-naphthol, also known as pontachrome violet SW, and eriochrome violet B; C.I. 15670, mordant violet 5) for the determination of traces of aluminium. Later workers used solochrome violet RS and other di-*o*-hydroxyazo dyes to determine a wide range of metals. Developments in this field up to the end of 1966 have been reviewed by Latimer[2], who pointed out that analytical applications have far out-stripped the understanding of the solution and electrode mechanisms that lead to the production of a discrete metal–dye complex wave.

The mechanism of reduction of a di-*o*-hydroxyazo compound at a mercury electrode has been established with reasonable certainty[3–7]. The reduction path involves a potential-determining 2-electron step yielding an unstable hydrazo intermediate which disproportionates within the lifetime of a mercury drop. Disproportionation yields the amines and the original azo compound, leading to a total *n*-value of four.

$$-N{=}N + 2\,H^+ + 2e \rightleftarrows -NH{-}NH- \qquad (1)$$

$$2\ -NH{-}NH- \longrightarrow -N{=}N- + -NH_2 + -NH_2 \qquad (2)$$

Kinetic parameters have been measured for the disproportionation of a simple hydrazo compound, 4-aminohydrazobenzene-4′-sulfonic acid[6].

Several theories have been proposed to explain why the metal complex of a di-*o*-hydroxyazo dye is reduced at a more negative potential than the free dye. Willard and Dean originally suggested[1] that the effect is due to stabilization of one of the geometrical isomers of the dye, but this explanation can be discounted on structural grounds[8,9]. Also, the magnitude of the half-wave potential shift ($\Delta E_{\frac{1}{2}}$) of the dye on complexing with a metal is not constant, but shows a wide variation with metal ion present. If isomer-stabilization were the explanation, $\Delta E_{\frac{1}{2}}$-values would be independent of the nature of the metal ion. Dean and Bryan[9] later attempted to explain $\Delta E_{\frac{1}{2}}$-values on the basis of the "rigidity" of the metal–dye complex, and, in

* On attachment from Oak Ridge National Laboratories, Oak Ridge, Tenn., U.S.A.

support of this theory, showed that a correlation existed between $\Delta E_{\frac{1}{2}}$ and ionic radius of the metal ion. Our present work using more accurate $\Delta E_{\frac{1}{2}}$-values shows, however, that there is no apparent correlation between $\Delta E_{\frac{1}{2}}$ and ionic radius.

The most obvious explanation of the polarographic activity of these dyes towards metal ions is that the half-wave potential shift is caused by metal–dye chelate formation, and that the azo group is involved in the coordination. The $\Delta E_{\frac{1}{2}}$-values should then be related to the relevant metal–dye stability constants. Drew and Fairbairn[10] and Coates and Rigg[11,12] have shown conclusively that di-*o*-hydroxyazo dyes normally act as tridentate ligands, with the azo nitrogen group forming a co-ordinate link with the metal ion. Dean and Bryan[9] rejected azo co-ordination as the cause of half-wave potential shifts, since their data showed that some metals with a maximum co-ordination number of six formed 1:3 metal–dye complexes. This implied that the dye was acting only as a bidentate ligand, with no metal–azo group co-ordinate bonding. However Coates and Rigg[12] using high-purity solochrome violet RS and precise titration techniques could find no indication of 1:3 complexes, and it is very doubtful if metal–dye complexes higher than 1:2 do exist.

Latimer[2] pointed out that if the half-wave potential shift is caused by azo co-ordination, there are many apparent anomalies in the relationship between $\Delta E_{\frac{1}{2}}$ and stability constant of the metal–dye complex. In the present paper we have shown that these apparent anomalies can be resolved if the potential-determining step in the reduction of metal–solochrome violet RS complexes is considered to be a redox reaction involving the metal complexes of both the azo- and hydrazo-derivatives. The $\Delta E_{\frac{1}{2}}$-values are then related not simply to the stability of the metal–solochrome violet RS complexes, but to the *ratio* of the stability constants of the metal ion with the azo- and hydrazo-derivatives of solochrome violet RS.

EXPERIMENTAL

Apparatus and reagents

Solochrome violet RS (SVRS). The dye was synthesized by coupling diazotized *o*-aminophenol-*p*-sulfonic acid (recrystallized from 7 *M* HCl) with 2-naphthol in alkaline solution. The crude azo compound was recrystallized twice from 50% aqueous ethanol to yield the pure crystalline monosodium salt of 5-sulfo-2-hydroxybenzene-azo-2-naphthol. The dye was dried overnight at 70° in a vacuum oven, then allowed to equilibrate for a week in a desiccator over silica gel. The product was analyzed using potentiometric titration with NaOH, controlled-potential coulometric titration, and determination of sodium content. All these methods gave a purity of $100 \pm 2\%$ as $C_{16}H_{11}N_2O_5SNa \cdot 2H_2O$.

Polarograph. The polarograph used for this work was an ORNL model Q-2792 solid-state controlled-potential d.c. polarograph[13]. This instrument uses active first and second derivative networks which give accurate derivative waves, independent of scan rate, on precisely calibrated scales. An ORNL-Q-2942 polarographic drop time controller[14] was incorporated in the dropping mercury electrode stand, and enabled highly precise drop times of 0.25, 0.5, 1.0, or 2.0 sec to be used.

The polarographic cell was water-jacketted, and utilized a fibre-type saturated calomel reference electrode. Solutions were purged with argon, which was also passed over the solution during recording of the polarograms. The cell was completely

sealed from the atmosphere by means of an O-ring to prevent any possibility of oxygen interfering with the electrode reactions. The dropping mercury electrode had a mercury flow rate of 1.643 mg/sec.

Streaming mercury electrode. The streaming mercury electrode has been described previously[15]. It was used in conjunction with the ORNL-Q-2792 polarograph.

Experimental procedures

Measurement of $\Delta E_{\frac{1}{2}}$-values. The difference between the half-wave potentials of the metal–SVRS complex and the free SVRS waves ($\Delta E_{\frac{1}{2}}$) was determined for each metal using a total SVRS concentration of $2 \cdot 10^{-5}$ *M*. This was a sufficiently high concentration to produce well-formed and easily measured waves with the ORNL-Q-2792 polarograph, yet was low enough to avoid significant dimerization of the free dye in acid media[16]. Also, previous work with azo compounds[15] has shown that complete surface coverage of the mercury drop by adsorption takes place at dye concentrations greater than $2 \cdot 10^{-5}$ *M*. It was desirable to eliminate, as far as possible, adsorption effects affecting the $\Delta E_{\frac{1}{2}}$-values.

In acetic acid–sodium acetate buffers the metal–SVRS complex was formed by heating the solutions in a water bath at 70° for 1 h. In ammonia–ammonium nitrate buffers the solutions were allowed to stand for 1 h at room temperature before measurement. Ionic strength was adjusted with sodium nitrate. From the derivative waves, half-wave potentials could be measured to ± 2 mV, so that $\Delta E_{\frac{1}{2}}$-values are considered accurate to ± 5 mV.

Unless otherwise stated, all polarographic measurements were made at $30.0 \pm 0.1°$.

Determination of stability constants. Spectrophotometric stability constants were determined using the method of Coates and Rigg[12]. To avoid metal impurities in the buffer constituents interfering with the spectrophotometric measurements, an ionic strength of 0.002 *M* was used throughout. The stability constants were corrected to zero ionic strength using a modified Debye–Huckel equation[12]. Stability constants for several metals were also checked using a potentiometric titration technique[17].

RESULTS

$\Delta E_{\frac{1}{2}}$-values

Tables 1 and 2 contain the $\Delta E_{\frac{1}{2}}$-data for various metal ions in acetic acid–sodium acetate and ammonia–ammonium nitrate buffers. Some metals are discussed below in more detail. The experimental conditions were those given in Tables 1 and 2, with equal concentrations of metal and SVRS.

Cadmium. In an ammonia buffer of pH 9.2, Cd^{2+} is reduced with an $E_{\frac{1}{2}}$ of -0.598 V. In the presence of SVRS a composite wave is obtained at the same potential, consisting of the simultaneous reduction of cadmium and SVRS in the Cd–SVRS complex. Since free SVRS is reduced with an $E_{\frac{1}{2}}$ of -0.573 V (Table 2), the $\Delta E_{\frac{1}{2}}$-value is at least 25 mV, but may be limited by reduction of cadmium in the complex.

Copper. Cupric ions in an acetate buffer of pH 4.2 have an $E_{\frac{1}{2}}$ of $+0.024$ V. The Cu^{2+}–SVRS complex exhibits two waves, at -0.178 V and -0.280 V, corresponding to reduction of Cu^{2+} and free dye, respectively. So, although there is no shift in the reduction potential of SVRS because copper in the complex is reduced

TABLE 1

$\Delta E_{\frac{1}{2}}$-VALUES IN ACETIC ACID–SODIUM ACETATE BUFFER pH 4.30

(Total SVRS = $2 \cdot 10^{-5}$ *M*, buffer = 0.04 *M*, μ = 0.04 *M*, t = 30°)

Metal ion	*Concn.* ($M \cdot 10^4$)	$-\Delta E_{\frac{1}{2}}$ (*mV*)[a]	$w_{\frac{1}{2}}$ (*mV*)[b]	i_d (μA)[c]	
				Free dye	*Complex wave*
—	—	—	—	0.130	—
Al^{3+}	0.2	141	65	0.016	0.115
	1	141	64	0.005	0.131
Co^{2+}	0.2	237	—	0.083	0.038
	2	242	—	0.060	0.050
Cr^{3+}	0.2	170	—	0.018	0.110[d]
Cu^{2+}	0.2	—	—	0.128	—
Fe^{3+}	0.2	268	45	0.011	0.120
	1	265	45	0.008	0.125
Ga^{3+}	0.2	84	54	0.014	0.117
	1	86	54	nil	0.131
In^{3+}	0.2	130	—	0.120	0.010
Ni^{2+}	0.2	270	59	0.117	0.010
	2	273	55	0.073	0.054
Sc^{3+}	0.2	251	—	0.094	0.034
	1	251	54	0.035	0.075
Ti^{4+}	0.2	75	45	0.015	0.097
UO_2^{2+}	0.2	180	80	—	0.065
V^{4+}	0.2	90	55	nil	—
V^{5+}	0.2	90	53	nil	—
	1	88	52	nil	—

[a] $E_{\frac{1}{2}}$ free SVRS = −0.278 V

[b] $w_{\frac{1}{2}}$ = width of derivative wave at half-peak height; for free dye $w_{\frac{1}{2}}$ = 58 mV

[c] drop time = 0.5 sec, m = 1.643 mg/sec

[d] after heating for 20 h at 70°

first, there is a negative shift of 202 mV in the reduction of cupric ions.

Iron. Polarograms of the Fe^{3+}–SVRS complex show, in addition to the usual free dye and iron–dye complex waves, a third wave with an $E_{\frac{1}{2}}$ of +0.050 V. The height of this wave corresponds to a 1-electron reduction process, and the same wave is observed at the rotating pyrolytic graphite, and the streaming mercury electrodes. Investigations are continuing to elucidate the electrode process that gives rise to this third wave.

Manganese. Manganese(II) is reduced in an ammonia buffer of pH 9.2 at a potential of 1.479 V. Addition of SVRS has no effect on the half-wave potential of the Mn(II)–Mn(O) reduction.

Nickel. In an ammonia buffer, reduction of the Ni^{2+}–SVRS complex involves the simultaneous reduction of Ni^{2+} and SVRS at a potential of −0.842 V. The wave height corresponds to a 6-electron reduction.

Vanadium. Table 1 shows that both V(IV) and V(V) produce $\Delta E_{\frac{1}{2}}$-values of 90 mV. The height of the vanadium–SVRS complex wave, however, corresponds to a 5-, rather than a 4-electron reduction. It appears that V(IV), in the presence of SVRS, is oxidized to V(V) by dissolved oxygen. The observed reduction wave then involves the simultaneous reduction of SVRS, and V(V) to V(IV).

TABLE 2

$\Delta E_{\frac{1}{2}}$-VALUES IN AMMONIA–AMMONIUM NITRATE BUFFER pH 9.20

(Total SVRS $= 2 \cdot 10^{-5}$ *M*, buffer = 0.04 *M*, $\mu = 0.04$ *M*, $t = 30°$)

Metal ion	*Concn.* ($M \cdot 10^5$)	$-\Delta E_{\frac{1}{2}}$ (*mV*)[a]	$w_{\frac{1}{2}}$ (*mV*)[b]	i_d (μA)[c]	
				Free dye	*Complex wave*
—	—	—	—	0.158	—
Al^{3+}	2	92	—	0.080	0.070
Co^{2+}	2	262	49	0.048	0.095
Ga^{3+}	2	—	—	0.157	—
In^{3+}	2	80	—	0.125	0.020
Mn^{2+}	2	145	65	0.042	0.110
Ni^{2+}	2	260	—	0.006	—
Sc^{3+}	2	175	112	0.014	0.117
Zn^{2+}	2	170	77	0.011	0.144
	4	170	79	0.004	0.151
La^{3+}	2	215	—	0.118	0.010
Pr^{3+}	2	232	130	0.080	0.043
Nd^{3+}	2	237	125	0.077	0.047
Eu^{3+}	2	225	104	0.060	0.070
Dy^{3+}	2	225	100	0.058	0.060
Tm^{3+}	2	204	95	0.058	0.068
Lu^{3+}	2	198	80	0.040	0.080

[a] $E_{\frac{1}{2}}$ free SVRS $= -0.573$

[b] $w_{\frac{1}{2}}$ = width of derivative wave at half-peak height; for free dye $w_{\frac{1}{2}} = 45$ mV

[c] drop time = 0.5 sec, $m = 1.643$ mg/sec

Streaming mercury electrode

To eliminate the possibility that adsorption effects are the sole cause of the phenomenon of discrete metal–dye complex reduction waves, some systems were investigated using the streaming mercury electrode (Table 3). Because of the rapid rate of renewal of the electrode surface, currents at the streaming mercury electrode

TABLE 3

$\Delta E_{\frac{1}{2}}$-VALUES AT THE STREAMING MERCURY ELECTRODE, pH 4.30

(Total SVRS $= 2 \cdot 10^{-4}$ *M*, total metal $= 2 \cdot 10^{-4}$ *M*, acetate buffer = 0.4 *M*, $\mu = 0.4$ *M*, $t = 30°$)

Metal ion	$-\Delta E_{\frac{1}{2}}$ (*mV*)[a]	$w_{\frac{1}{2}}$ (*mV*)[b]	i_l (μA)		$-\Delta E_{\frac{1}{2}}$ (*mV*) *DME*
			Free dye	*Complex wave*	
—	—	—	46	—	—
Al^{3+}	55	110	—	46	145
Fe^{3+}	180	44	nil	40	265
Ga^{3+}	25	130	—	44	80
Ni^{2+}	205	—	28	10	261
V^{4+}	100	100	23	23	108

[a] $E_{\frac{1}{2}}$ free SVRS $= -0.445$ V

[b] $w_{\frac{1}{2}}$ for free dye = 90 mV

are affected very little by adsorption of the depolarizer[15]. Table 3 shows that although $\Delta E_{\frac{1}{2}}$-values at the streaming mercury electrode are in general smaller than those recorded at the DME, a separate wave for the metal complex is still observed. The reduction of SVRS at the streaming mercury electrode involves only 2 electrons[15], because the rate of disproportionation of the hydrazo derivative is not fast enough to contribute regenerated azo compound to the electrode reaction. For this reason, and because of the irreversible nature of the electrode processes involved, $\Delta E_{\frac{1}{2}}$-values recorded at the two electrodes are unlikely to be equal.

Stability constants

Table 4 is a summary of the stability constant data obtained using spectrophotometric and potentiometric techniques. Ionic radii and $\Delta E_{\frac{1}{2}}$-values are included

TABLE 4

THERMODYNAMIC STABILITY CONSTANTS FOR METAL–SOLOCHROME VIOLET RS COMPLEXES

($t = 25°$, zero ionic strength)

Metal ion	*Spectrophotometric* $\log \beta_1$	*Potentiometric*		$-\Delta E_{\frac{1}{2}}$ *(mV)*		*Ionic radius (Å)*
		$\log \beta_1$	$\log \beta_2$	*pH* 4.3	*pH* 9.2	
Al^{3+}	19.5	19.4	35.4	141	92	0.50
	18.4[a]	18.4[a]	31.6[a]			
Cd^{2+}	—	9.45	—[b]	—	25	0.97
Co^{2+}	16.6	16.8	34.2	237	—	0.78
Fe^{3+}	22.9	—	36.0	268	—	0.64
Ga^{3+}	21.6	—	—	84	—	0.62
La^{3+}	—	10.84	19.9	—	215	1.15
Mg^{2+}	—	7.43	—[b]	—	227[c]	0.65
		8.6[a]	5.0[a]			
Mn^{2+}	—	11.45	23.1	—	145	0.80
Ni^{2+}	—	15.86	27.5	260	270	0.78
	16.0[a]	15.9[a]	26.4[a]			
Sc^{3+}	19.0	—	—	251	175	0.81
UO_2^{2+}	18.8	—	—	180	—	—
V^{5+}	21.2	—	—	90	—	0.59
Zn^{2+}	—	12.7	21.5	—	170	0.74
		13.5[a]	20.9[a]			

[a] data from ref. 12

[b] no evidence of 1:2 metal–SVRS complex

[c] diethylamine buffer, pH 11.1

in the Table for comparison. In an acetate buffer of pH 4.3, and with the solution conditions given in Table 1, only the 1:1 metal–SVRS complexes are formed.

It is interesting to note that the Co^{2+}–SVRS complexes are more stable than the corresponding nickel complexes. This is the reverse of the normal order, and it was suspected that cobalt may be oxidized to Co^{3+} in its complexes with SVRS. However, the polarograms showed no evidence of a Co(III)–Co(II) reduction wave.

Kinetic studies

The kinetics of formation of the 1:1 complexes of SVRS with Al^{3+} and Fe^{3+} were studied in an attempt to gain further insight into the nature of the complexes.

Formation of the complexes was followed spectrophotometrically in buffered solutions, using several different pH-values. The concentration of complex produced after each time interval could be calculated from the absorbance data[18]. The results were found to adhere closely to the rate equation for a second-order reaction, and at constant acidity the reaction rate was first-order with respect to both metal ion and SVRS. The pseudo-second order rate constant, k_0, is defined by[19],

$$-\frac{d[M^{3+}]}{dt} = -\frac{d[SVRS]}{dt} = k_0[M^{3+}][SVRS]$$

where $k_0 = k' \cdot [H^+]^{-n}$.
The experimental values of k_0 are given in Table 5. From a plot of log k_0 *vs.* pH, the

TABLE 5

KINETIC STUDIES

(SVRS $= 1 \cdot 10^{-5}$ *M*, $\mu = 0.002$ *M*, $t = 25°$)

pH	k_0 (*l mole*$^{-1}$ *sec*$^{-1}$)[a]		*pH*	k_0 (*l mole*$^{-1}$ *sec*$^{-1}$)[a]	
	Al^{3+}	Fe^{3+}		Al^{3+}	Fe^{3+}
2.07	—	$6.72 \cdot 10^2$	4.38	28.5	—
2.37	—	$1.38 \cdot 10^3$	4.63	90.8	—
2.82	—	$3.17 \cdot 10^3$	4.77	$2.28 \cdot 10^2$	—
3.20	—	$5.90 \cdot 10^3$	5.00	$5.51 \cdot 10^2$	—

[a] k_0 is the pseudo-second order rate constant

values of k' and n for aluminium were found to be $1.6 \cdot 10^{-8}$ l mole^{-1} sec^{-1} and 2.1, respectively, at 25°. For iron, the corresponding values were 15.1 l mole^{-1} sec^{-1} and 0.85.

Measurement of the variation of the conditional stability constants of the aluminium– and iron–SVRS complexes with pH showed that in both cases two protons are released on co-ordination[18]. It appears that in the pH-range studied the reaction between aluminium and SVRS proceeds *via* a hydroxy intermediate, the main reaction being,

$$Al(OH)_2^+ + H_2D \rightleftarrows AlD^+ + 2H_2O$$

And for iron,

$$Fe(OH)^{2+} + H_2D \rightleftarrows FeD^+ + H_3O^+$$

where D represents SVRS with both hydroxyl groups ionized, and the charge on the sulfonic acid group is neglected.

DISCUSSION

The potential-determining step in the reduction of SVRS involves a 2-electron reduction to the hydrazo derivative. In acid media,

$$H_2D + 2H^+ + 2e \rightleftarrows H_2D^*$$

where D is SVRS with both phenolic hydrogens ionized, and D* is the corresponding hydrazo derivative. If the electrode reaction is reversible, the potential of the DME is given by,

$$E_d = E^0 - \frac{RT}{2F} \ln \frac{[H_2D^*]_0}{[H_2D]_0} + \frac{RT}{F} \ln [H^+] \quad (1)$$

The reduction of a metal–SVRS complex may conceivably proceed *via* one of two reaction paths,

Case 1

The azo group in the metal–SVRS complex is reduced, but the metal remains complexed to the hydrazo derivative.

$$MD + 2H^+ + 2e \rightleftarrows MD^*$$

If

$$\beta_1 = \frac{[MD]}{[M][D]} \quad \text{and} \quad \beta_1^* = \frac{[MD^*]}{[M][D^*]},$$

and

$$K_{a1} = \frac{[HD][H^+]}{[H_2D]}, \qquad K_{a2} = \frac{[D][H^+]}{[HD]},$$

and K_{a1}^* and K_{a2}^* are the corresponding acid dissociation constants for the hydrazo derivative,

$$\frac{[H_2D^*]}{[H_2D]} = \frac{[MD^*]}{[MD]} \cdot \frac{\beta_1 K_{a1} K_{a2}}{\beta_1^* K_{a1}^* K_{a2}^*}$$

Substituting in (1),

$$E_c = E^0 - \frac{RT}{2F} \ln \frac{[MD^*]_0}{[MD]_0} - \frac{RT}{2F} \ln \frac{\beta_1 K_{a1} K_{a2}}{\beta_1^* K_{a1}^* K_{a2}^*} + \frac{RT}{F} \ln [H^+] \quad (2)$$

At the half-wave potential, $[H_2D^*]_0 = [H_2D]_0$, and $[MD^*]_0 = [MD]_0$. Thus,

$$E_{\frac{1}{2}}(\text{complex}) - E_{\frac{1}{2}}(\text{dye}) = \Delta E_{\frac{1}{2}} = -\frac{RT}{2F} \ln \frac{\beta_1 K_{a1} K_{a2}}{\beta_1^* K_{a1}^* K_{a2}^*} \quad (3)$$

In this case, the $\Delta E_{\frac{1}{2}}$-value is independent of pH and metal concentration, and depends only on the ratio of the relevant stability constants and acid dissociation constants.

Case 2

The metal–SVRS complex dissociates at the electrode surface prior to reduction. The electrode reaction then involves free dye only.

$$MD \rightleftarrows M + D$$

$$D + 2H^+ \rightleftarrows H_2D$$

$$H_2D + 2H^+ + 2e \rightleftarrows H_2D^*$$

Substituting

$$[H_2D]_0 = \frac{[MD]_0[H^+]^2}{[M]_0\beta_1 K_{a1} K_{a2}} \text{ in eqn. (1),}$$

$$E_c = E_0 - \frac{RT}{2F}\ln\frac{[H_2D^*]_0}{[MD]_0} - \frac{RT}{2F}\ln[M]_0 -$$

$$- \frac{RT}{2F}\ln\beta_1 K_{a1} K_{a2} + \frac{2RT}{F}\ln[H^+] \qquad (4)$$

When $E_c = E_{\frac{1}{2}}$, $[H_2D^*]_0 = [MD]_0$,
Therefore,

$$E_{\frac{1}{2}}(\text{complex}) = E_0 - \frac{RT}{2F}\ln[M]_0 - \frac{RT}{2F}\ln\beta_1 K_{a1} K_{a2} + \frac{2RT}{F}\ln[H^+]$$

and

$$E_{\frac{1}{2}}(\text{complex}) - E_{\frac{1}{2}}(\text{dye}) = \Delta E_{\frac{1}{2}}$$

$$= -\frac{RT}{2F}\ln[M]_0 - \frac{RT}{2F}\ln\beta_1 K_{a1} K_{a2} + \frac{RT}{F}\ln[H^+] \qquad (5)$$

When the concentration of free metal in the solution is sufficiently high so that $[M]_0 = [M]$, at constant pH a plot of $\Delta E_{\frac{1}{2}}$ *vs.* $\log_{10}[M]$ should have a slope of 30 mV. With constant metal concentration, $\Delta E_{\frac{1}{2}}$ *vs.* pH should produce a straight line with a slope of 60 mV.

To determine whether Case 1 or Case 2 (eqns. (3) or (5)) is applicable to the polarographic behaviour of metal–SVRS complexes, the nickel system in acetate buffer was chosen for more detailed study. A possible complication is that the reduction of neither the free dye nor the nickel–dye complex is completely reversible at pH 4.3. The width of the derivative wave at half-peak height should be equal to $90/n$ mV, or 45 mV for a reversible 2-electron reaction. Both the dye and its nickel complex have half-peak height widths of 55–60 mV, indicating that the reductions are not reversible. However, since the degree of irreversibility is about the same for both waves, it is unlikely that the $\Delta E_{\frac{1}{2}}$-value would be greatly affected. Plots of $\log_{10}[i/(i_d - i)]$ *vs.* E were constructed for free SVRS and Ni–SVRS at pH 4.3. Both plots exhibited slight curvature, and the values of $E_{\frac{1}{2}}$(reversible) were estimated by extrapolation of the lower straight-line portion of the curves to zero ordinate[20]. The estimated values of $E_{\frac{1}{2}}$(reversible) obtained in this manner were only 5–10 mV more positive than the $E_{\frac{1}{2}}$-values measured from the polarogram, and $\Delta E_{\frac{1}{2}}$ was unchanged. It appears that most of the $\Delta E_{\frac{1}{2}}$-values listed in Table 1 can be compared with one another without considering ambiguities arising from irreversibility.

Table 6 shows that pH and nickel concentration have no effect on the Ni^{2+}–SVRS $\Delta E_{\frac{1}{2}}$-value, which is remarkably constant within experimental accuracy over a wide range of solution conditions. Variation of metal concentration also had little or no effect on several other metal–SVRS systems studied (Table 1). These results

TABLE 6

$\Delta E_{\frac{1}{2}}$-VALUES FOR THE NICKEL–SVRS COMPLEX

(Total SVRS $= 2 \cdot 10^{-5}$ M, 0.04 M acetate buffer, $\mu = 0.04$ M, $t = 30°$)

$Ni^{2+}(M \cdot 10^3)$	pH	$-\Delta E_{\frac{1}{2}}$ (mV)[a]	$Ni^{2+}(M \cdot 10^3)$	pH	$-\Delta E_{\frac{1}{2}}$ (mV)[a]
0.02	4.28	270	5	4.32	268
0.2	4.22	273	2	3.90	272
0.5	4.32	268	2	4.72	269
1	4.32	268	2	5.35	273
2	4.31	272	0.02	9.20[b]	260

[a] drop time = 0.5 sec, $m = 1.643$ mg/sec
[b] 0.04 M ammonia–ammonium nitrate buffer

strongly indicate that Case 1 is applicable, *i.e.*, that the metal remains bonded to the dye after reduction and the $\Delta E_{\frac{1}{2}}$-value depends only on the ratio of the relevant stability constants and acid dissociation constants. Unfortunately, because of the instability of the hydrazo derivative of SVRS, no direct determination could be made of the acid dissociation constants or metal–hydrazo dye stability constants.

Other explanations previously put forward for the formation of discrete metal–SVRS reduction waves are not supported by this study. Table 4 shows that the $\Delta E_{\frac{1}{2}}$-values are apparently unrelated to either ionic radius or the stability constant of the metal–SVRS complex. Since half-wave potential shifts are produced at the streaming mercury electrode as well as at the dropping mercury electrode, adsorption cannot be the sole cause of the potential shift. With dye concentrations above $1 \cdot 10^{-4}$ M, however, adsorption does seem to have a marked effect on $\Delta E_{\frac{1}{2}}$-values in some cases. Using $2 \cdot 10^{-5}$ M SVRS, $\Delta E_{\frac{1}{2}}$ for the lanthanides is essentially constant, particularly if change in reversibility is taken into account, and has a value of about 200 mV in an ammonia buffer (Table 2). This is the situation one would expect if Case 1 were applicable, since because of the chemical similarity of the lanthanides, the *ratio* of the stability constants of the lanthanide azo– and hydrazo–dye complexes would be very similar for each member of the series. However, with a SVRS concentration of $2 \cdot 10^{-4}$ M, lanthanide $\Delta E_{\frac{1}{2}}$-values in ammonia buffer vary from 45 mV for lanthanum to 234 mV for lutetium[4]. The complexes of the lighter lanthanides with SVRS are known to be more strongly adsorbed at the DME than those of the heavy lanthanides[21], so adsorption may well be the cause of the wide variation in $\Delta E_{\frac{1}{2}}$-values for the lanthanides at high dye concentrations. In support of this conclusion it has been shown[4] that in buffers of the strongly surface-active base, piperidine, $\Delta E_{\frac{1}{2}}$ is constant (180 mV) for all lanthanides, even with SVRS concentrations of $2 \cdot 10^{-4}$ M.

SUMMARY

A detailed investigation has been carried out to elucidate the electrode and solution phenomena that produce two discrete polarographic reduction waves when the azo dye, solochrome violet RS (5-sulfo-2-hydroxybenzene-azo-2-naphthol), is complexed with metals. Previous explanations put forward to explain the polarographic activity of di-*o*-hydroxyazo compounds towards certain metals were shown

to be invalid. It is proposed that the half-wave potential shift ($\Delta E_{\frac{1}{2}}$) results from the metal remaining bonded to the reduced form of the dye (hydrazo derivative), the potential of the DME being controlled by the metal–azo/metal–hydrazo redox couple. The $\Delta E_{\frac{1}{2}}$-values are then independent of pH and metal concentration, and depend only on the relevant stability constants and acid dissociation constants.

The rates of reaction of Al^{3+} and Fe^{3+} with solochrome violet RS have been measured, and both reactions were shown to proceed *via* metal hydroxy complexes.

REFERENCES

1 H. H. WILLARD AND J. A. DEAN, *Anal. Chem.*, 22 (1950) 1264.
2 G. W. LATIMER, *Talanta*, 15 (1968) 1.
3 H. A. LAITINEN AND T. J. KNEIP, *J. Am. Chem. Soc.*, 78 (1956) 736.
4 T. M. FLORENCE AND G. H. AYLWARD, *Australian J. Chem.*, 15 (1962) 65.
5 T. M. FLORENCE AND G. H. AYLWARD, *Australian J. Chem.*, 15 (1962) 416.
6 T. M. FLORENCE, *Australian J. Chem.*, 18 (1965) 609.
7 T. M. FLORENCE, *Australian J. Chem.*, 18 (1965) 619.
8 M. PERKINS AND G. F. REYNOLDS, *Anal. Chim. Acta*, 19 (1958) 194.
9 J. A. DEAN AND H. A. BRYAN, *Anal. Chim. Acta*, 16 (1957) 94.
10 H. D. DREW AND R. E. FAIRBAIRN, *J. Chem. Soc.*, (1939) 823.
11 E. COATES AND B. RIGG, *Trans. Faraday Soc.*, 58 (1962) 88.
12 E. COATES AND B. RIGG, *Trans. Faraday Soc.*, 58 (1962) 1.
13 M. T. KELLEY, U.S.A.E.C. rept. ORNL-3750 (1965).
14 M. T. KELLEY, U.S.A.E.C. rept. ORNL-4039 (1966).
15 T. M. FLORENCE AND Y. J. FARRAR, *Australian J. Chem.*, 17 (1964) 1085.
16 E. COATES AND B. RIGG, *Trans. Faraday Soc.*, 57 (1961) 1088.
17 H. IRVING AND H. S. ROSSOTTI, *J. Chem. Soc.*, (1954) 2904.
18 H. E. ZITTEL AND T. M. FLORENCE, *Anal. Chem.*, 39 (1967) 320.
19 T. M. FLORENCE AND P. J. SHIRVINGTON, *Anal. Chem.*, 37 (1965) 950.
20 J. HEYROVSKÝ AND J. KŮTA, *Principles of Polarography*, Academic Press, New York, 1st ed., 1966, p. 214.
21 T. M. FLORENCE, thesis, University of N.S.W., 1961.

ELECTROANALYTICAL CHEMISTRY AND INTERFACIAL ELECTROCHEMISTRY
Elsevier Sequoia S.A., Lausanne – Printed in The Netherlands

ALTERNATING CURRENT POLAROGRAPHIC BEHAVIOR OF PYRIMIDINE IN AQUEOUS MEDIA

JAMES E. O'REILLY AND PHILIP J. ELVING
The University of Michigan, Ann Arbor, Mich. (U.S.A.)
(Received November 21st, 1968)

INTRODUCTION

Pyrimidine is a key compound in understanding the electrochemical behavior of pyrimidines and purines, including those of biological importance which are the essential bases of the nucleic acids, *e.g.*, the electrochemical reduction of purines occurs in the pyrimidine ring[1,2]. The polarography of pyrimidine and its derivatives at the dropping mercury electrode (DME) has been studied by several investigators[2], the most detailed study being that of Smith and Elving[3]. The latter included controlled-potential electrolysis and coulometry as well as d.c. polarography and resulted in the following mechanism being postulated for the electrochemical reduction of pyrimidine at the DME, which results in five polarographic waves appearing over the pH-range, 0.5–13.

In highly acid media, pH-dependent one-electron (1*e*) wave I is seen. At about pH 3, pH-independent 1*e* wave II emerges from back-ground discharge. These two waves merge near pH 5 to form pH-dependent 2*e* wave III. Near pH 7.2, pH-independent 2*e* wave IV emerges from background and, at pH 9.2, merges with wave III to form pH-dependent 4*e* wave V. Wave I is postulated to be the 1*e* reduction of pyrimidine to the neutral radical; wave II is the 1*e* reduction of the latter to a dihydropyrimidine with wave III being the composite of these two steps. Wave IV is the 2*e* reduction of the dihydro species to a tetrahydropyrimidine with wave V being the composite of waves III and IV.

Recently, Timmer *et al.* presented a theoretical treatment[4] and an experimental verification[5] of a.c. polarographic waves for irreversible electrode reactions, which have done much to dispel the belief that only "reversible" polarographic waves exhibit a.c. polarographic peaks, and which should, therefore, promote the use of a.c. polarography in the elucidation of organic oxidation–reduction paths and the determination of kinetic parameters; the latter have not been as well studied as those of inorganic systems probably because of the generally irreversible nature of organic polarographic reactions. We have been prompted by these studies to investigate the a.c. polarographic behavior of pyrimidine in aqueous media in an effort to obtain further evidence for the proposed pyrimidine reduction mechanism (particularly in respect to the controlling step in each process) and to evaluate the various theoretical predictions for a rather complicated organic system.

EXPERIMENTAL

Chemicals

Pyrimidine (Mann Research Laboratories) was of chromatographic grade; its polarographic pattern afforded no evidence of any electroactive impurity. Buffer solutions (Table 1) were prepared from analytical reagent-grade chemicals; ionic strength was kept constant at 0.5 *M*. Nitrogen used for deoxygenating (Liquid Carbonic, O.P.) was purified and equilibrated by bubbling it successively through two acidic vanadous solutions, saturated calcium hydroxide, and distilled water. Triply-distilled mercury was used.

TABLE 1

BUFFER AND BACKGROUND ELECTROLYTE SOLUTIONS[a]

Buffer No.	*pH range*	*Composition*
1	0.5– 2.5	$HCl + KCl$
2	2.2– 8.0	$Na_2HPO_4 \cdot 7\,H_2O$ + citric acid monohydrate + KCl
3	8.0–10.2	$H_3BO_3 + KOH + KCl$
4	10.5–13.0	$KOH + KCl$
5	11.0–13.0	$(C_2H_5)_4NOH + (C_2H_5)_4NClO_4$

[a] All buffers used were 0.5 *M* ionic strength

Apparatus

The water-jacketted (thermostatted at $25.0 \pm 0.1°$), three-compartment polarographic cell employed was previously described[6]. The counter electrode was a coil of platinum wire dipped into a 0.5 *M* KCl solution; the reference was an aqueous saturated calomel electrode, to which all potentials are referred. The capillary (marine barometer tubing) had the following *m*-values (mg/sec) in 0.5 *M* KCl at 25° and open circuit: 1.326 at 52.7 cm of mercury, corrected for back pressure; 1.577 (62.7 cm); and 1.833 (72.7 cm). Drop-times, measured at potentials of interest, were generally between 3 and 10 sec; drop-times greater than 6 sec were encountered only at heights of 22 and 32 cm during height-variation experiments, where the response was normal.

Slow, single-scan d.c. polarography, used to check $E_{\frac{1}{2}}$-values previously obtained[3], was performed with a Sargeant Model XV polarograph.

A.c. polarograms were obtained with a potentiostatic control loop of conventional design using Philbrick K2-XA and K2-P operational amplifiers and a precision rectifier previously described by Smith[7]; they were recorded with a Moseley 7035A X-Y recorder. The d.c. ramp voltage was supplied by a utility integrator constructed using a Philbrick UPA-2 amplifier and a step-function module consisting of a mercury battery and a resistive voltage divider. Scan rate was constant at 1.0 mV/sec. The superimposed sine wave was supplied by a Hewlett-Packard 202A low frequency function generator, whose output was regulated to between 5 and 60 mV peak-to-peak by means of an external voltage divider.

The output of the precision rectifier was calibrated using a sine wave of known r.m.s. amplitude and a dummy cell of resistive components; the output was linear from about 100 mV to over 30 V. The performance of this unit was tested by examining

the ferrous/ferric couple in 0.25 *M* potassium oxalate–0.25 *M* oxalic acid buffer. The response was identical with that previously reported for this system and with that expected for a reversible system[8]: The alternating current was independent of mercury column height, linearly proportional to the amplitude of the superimposed alternating voltage, and proportional to the square root of frequency to about 65 Hz; the summit potential was identical with the $E_{\frac{1}{2}}$, within experimental error. The alternating current, Δi_s, for 0.969 m*M* Fe(III) in oxalate background was 8.29 μA; the calculated, theoretically expected value[8] is 11.37 μA ($A = 3.38 \cdot 10^{-2}$ cm^2, $V = 8.46$ mV r.m.s., $f = 50$ Hz, $D_0 = 5.70 \cdot 10^{-6}$ cm^2/sec). The difference is due primarily to the attenuation by the damping capacitor in the precision rectifier.

A Beckman Model G pH-meter was used to measure the pH of buffer and test solutions.

Procedures

Stock solutions of background buffers and pyrimidine were prepared by dissolving weighed quantities and diluting to known volume. Test solutions were prepared by pipetting appropriate amounts of stock solutions into 10- or 50-ml volumetric flasks and diluting to volume with distilled water. Nitrogen was bubbled through the test solution in the polarographic cell for 5 min; the DME was then inserted and voltammograms were recorded with nitrogen passing over the test solution.

The summit potential, E_s, for a.c. voltammograms, was taken as that potential at which the total alternating current due to the electroactive species, Δi_s, reached a maximum; Δi_s was measured as the difference in current at E_s between solutions containing the background buffer plus electroactive species, and the buffer only.

The error in Δi_s is estimated to be $\pm 5\%$ for moderate to large currents, *i.e.*, above 0.5 μA; with smaller currents, the error is larger owing to the problem of subtracting a large base current.

A. C. POTENTIAL BEHAVIOR

Wave pattern

Over the pH-range 0.5–13, pyrimidine gives five recognizable, if distorted, a.c. polarographic waves, which correspond to the five observed d.c. polarographic waves (*cf.* Fig. 1 for examples). At low pH, a single pH-dependent wave is observed (wave I). At about pH 2.8, pH-independent wave II, whose current is much less than that for wave I, emerges from background. At about pH 4.8, waves I and II merge to form pH-dependent wave III, whose peak current is close to that observed for wave I. At about pH 7.0, wave IV emerges from background and merges with wave III at about pH 8.3 to form pH-dependent wave V. Above pH 9, wave V is observed only as an inflection on background discharge in KCl/KOH buffer; point-by-point subtraction of background is necessary to obtain even a distorted wave. In Et_4NClO_4/Et_4NOH buffer, the background discharge is sufficiently removed from E_s that reproducible measurements can be made. E_s does not shift with change of background electrolyte from KCl to Et_4NClO_4, as has been seen in some systems.

The linear E_s *vs.* pH relationships presented in Table 2 were obtained by a least-squares analysis of the experimental data.

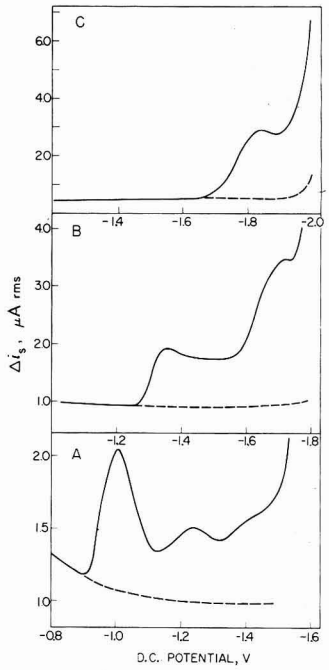

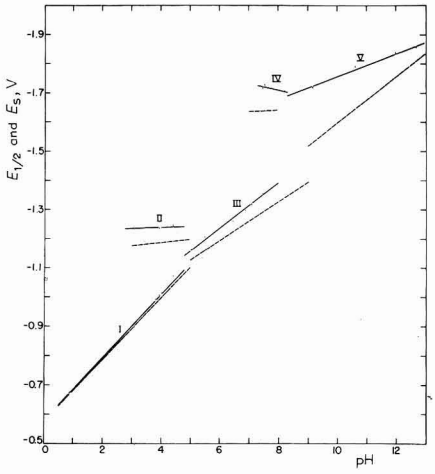

Fig. 1. Alternating current polarograms of 0.954 m*M* pyrimidine (——) and background alone (– – – –). (A), Waves I and II, pH 3.96 (buffer 2); (B), waves III and IV, pH 7.48 (buffer 2); (C), wave V, pH 12.00 (buffer 5). Conditions: 62.7 cm mercury (corr.); 50 Hz applied frequency; 8.46 mV applied voltage. Only the peaks of drop oscillations are indicated.

Fig. 2. Linear E_s (——) and $E_{\frac{1}{2}}$ (– – – –) *vs.* pH relationships for pyrimidine. Each E_s-value is the average of two or more measurements (with an estimated uncertainty of ±5 mV) for the following conditions: 0.954 m*M* pyrimidine concn.; 62.7 cm mercury (corr.); 50 Hz applied frequency; 8.46 mV r.m.s. applied voltage. $E_{\frac{1}{2}}$-data taken from ref. 3.

TABLE 2

LINEAR E_s *vs.* pH RELATIONSHIPS FOR PYRIMIDINE[a]

Wave	*pH range*	E_s^b (*V*)
I	0.5– 4.8	−0.575 − 0.108 pH
II	2.8– 4.8	−1.226 − 0.003 pH
III	4.8– 8.0	−0.766 − 0.078 pH
IV	7.0– 8.3	−1.982 + 0.023 pH
V	8.3–13.0	−1.365 − 0.039 pH

[a] Conditions: 0.954 m*M* pyrimidine; 50 Hz; 62.7 cm mercury (corr.); 8.46 mV r.m.s. applied voltage.
[b] The equations given indicate the E_s, when extrapolated to zero pH, and the variation of E_s with pH.

Relations of E_s and $E_{\frac{1}{2}}$

As can be seen from Fig. 2, the a.c. polarographic behavior of pyrimidine over the pH-range closely parallels the d.c. behavior at the DME. The deviation of E_s from $E_{\frac{1}{2}}$ can be considered as a measure of the reversibility of the originating electrode reaction[8]. E_s for waves II, IV and V, all corresponding to the direct formation of a

stable molecular species, are more negative than their corresponding $E_{\frac{1}{2}}$-values by 60 to 200 mV. Wave I, on the other hand, which corresponds to a 1*e* addition to pyrimidine to form a radical species, shows little difference in E_s and $E_{\frac{1}{2}}$; this is, however, not to be taken in itself as an indication of the reversibility of the wave, as the observed alternating current is less than that theoretically expected for a 1*e* reversible system[8]. The derived linear E_s *vs.* pH relationships are only approximations to the true behavior of the system, *e.g.*, a considerable departure from linearity is observable near the merging of two waves, which is particularly evident in the wave III data.

Effect of experimental conditions

E_s does not shift with amplitude of the applied alternating voltage (2–15 mV r.m.s.) or mercury column heights (drop-time), *e.g.*, E_s for wave V is -1.836 ± 0.003 V (average deviation) for twelve different applied voltages and column heights. E_s for all five waves, however, shifts to more negative potential with increasing frequency of applied alternating voltage (Table 3), as expected for irreversible reactions. Plots of E_s *vs.* $\log f$ are approximately linear; however, the uncertainty of an individual datum (about ± 5 mV) is relatively large compared to the magnitude of the potential shift and precludes quantitative appraisal of the effect.

The width of the a.c. wave at half-height, $\Delta E_{s/2}$, for wave I at pH 0.92 and 3.96 does not vary, within experimental error, with changes in mercury column height or in magnitude of applied alternating voltage within the ranges studied; it is 124 ± 6 mV, as compared to the 90.5 mV predicted for a reversible, diffusion-controlled 1*e* reaction[8]. The a.c. wave is not symmetrical about E_s: $E_{(s/2)_1} - E_s = 52 \pm 3$ mV and $E_s - E_{(s/2)_2} = 72 \pm 3$ mV. In the frequency range, 5–100 Hz, $\Delta E_{s/2}$ appears to follow the same curvilinear trend as does the total current for change in frequency (*vide infra*), increasing from 106 mV at 5 Hz to 125 mV at 50 Hz and then decreasing to 118 mV at 100 Hz. The $\Delta E_{s/2}$-values for the other waves cannot be determined because the current does not drop to one-half the peak value on the negative potential side of the a.c. wave.

TABLE 3

VARIATION OF E_s WITH FREQUENCY FOR PYRIMIDINE[a]

Frequency (*Hz*)	*Wave*				
	I	*II*	*III*	*IV*	*V*
1	—	—	1.359	—	—
5	0.986	1.231	—	—	1.812
10	0.991	1.232	1.372	1.712	1.824
20	—	—	1.363	1.706	—
25	0.996	1.239	—	—	1.831
50	1.005	1.236	1.372	1.724	1.836
75	1.011	1.244	—	—	1.841
100	1.020	1.245	1.389	1.765	1.851

[a] Conditions: Waves I and II, pH 3.96 (buffer 2); waves III and IV, pH 7.55 (buffer 2); wave V, pH 12.00 (buffer 5). Pyrimidine concn., 0.954 m*M*; 8.46 mV r.m.s. applied voltage; 62.7 cm (corr.). E_s-values are in negative volts *vs.* SCE. Dash indicates measurement not made.

A. C. CURRENT BEHAVIOR

Over the pH-range, the presence of pyrimidine shows no tendency to elevate or depress the a.c. base current before a reduction peak, regardless of the nature of the buffer; under all conditions, the base current was identical, within experimental error, with that observed in the absence of pyrimidine. This would seem to indicate that little or no adsorption of pyrimidine occurs, since a.c. polarography is a very sensitive technique for detecting adsorption. There does appear to be, however, some increase in base current after a reduction peak, *e.g.*, at low pH, the current after wave I does not return to the base-line even though there is sufficient potential span before background discharge (*ca.* 0.35 V) to permit this, which would seem to indicate some adsorption of the pyrimidine reduction product(s). The presence of pyrimidine does shift the background discharge to more positive potential; the magnitude is irregular but continues across the pH-range; the cause of this effect is not known but may be due to the pyrimidine reduction products.

Effect of alternating voltage

The alternating current observed for all five waves is a linear function of the applied alternating voltage from 2 to 15 mV r.m.s. (Fig. 3); none of the plots intersects at the origin. With waves II and IV, part of this effect may be explained by the proximity of these two waves to the previously occurring wave; thus, a residual current

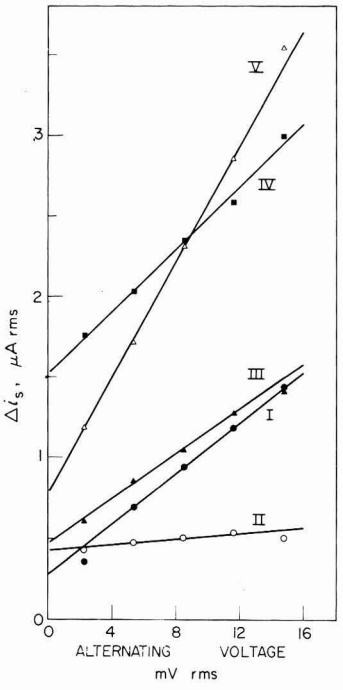

Fig. 3. Variation of alternating current, Δi_s, with amplitude of applied a.c. voltage: Waves I and II, pH 3.96 (buffer 2); waves III and IV, pH 7.48 (buffer 2); wave V, pH 12.00 (buffer 5). Conditions: 0.954 m*M* pyrimidine concn.; 50 Hz applied frequency; 62.7 cm mercury (corr.).

element may be incorporated. In addition, the apparent increased base current after a reduction wave, noted previously, may account for part of the increased current. The fact that plots for waves I, III and V also do not intersect the origin, however, indicates that other factors must be operative.

Effect of drop-time

Early theoretical treatments[8] indicated that the faradaic alternating current for reversible and quasi-reversible electrode reactions should be independent of drop-time. Recently, several workers[9-12] have commented on the drop-time dependence of a.c. polarographic current with the general conclusion that such dependence will be exhibited whenever some rate process other than diffusion is kinetically influencing the faradaic process[11]. Experimental evidence was presented on the drop-time dependence for (a) the quasi-reversible electron-transfer process and (b) reductions and oxidations involving coupled chemical reactions, rate limited surface coverage, and amalgam formation[9]. Timmer *et al.*[4] supported their theoretical predictions that a.c. peak heights should be proportional to $t^{-\frac{1}{2}}$ for highly irreversible electrode reactions, with the experimental data of Aylward and Hayes[9] on the reduction of the cadmium–EDTA complex.

In the case of pyrimidine, all five a.c. waves exhibit a considerable linear increase of current with $t^{-\frac{1}{2}}$. The relations for waves I, III, IV and V intersect near the origin (infinitely long drop-time) (Fig. 4); the small values of the intercepts can be attributed to experimental error. The relatively large positive intercept for wave II, as

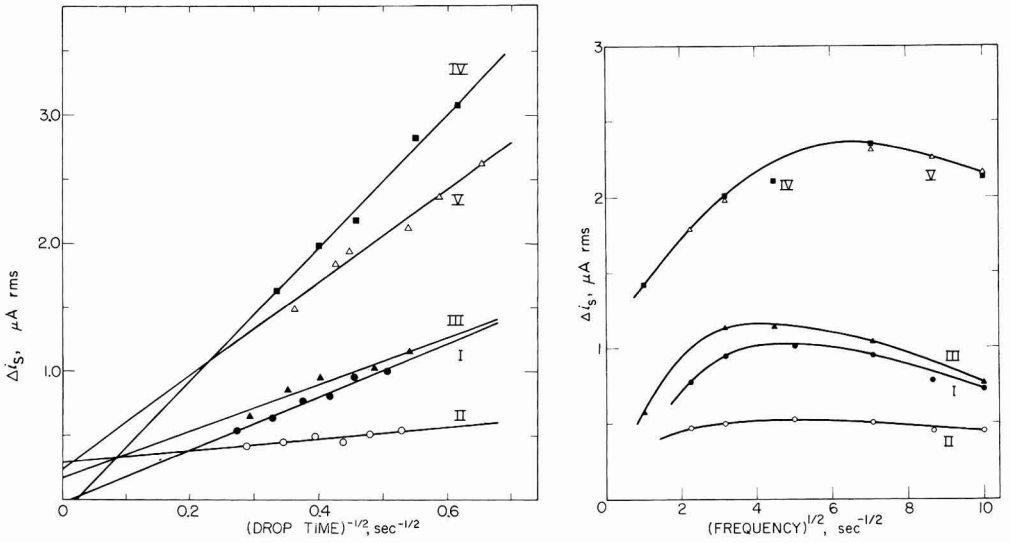

Fig. 4. Variation of alternating current, Δi_s, with drop-time, expressed as $t^{-\frac{1}{2}}$: Waves I and II, pH 3.96 (buffer 2); waves III and IV, pH 7.48 (buffer 2); wave V, pH 12.00 (buffer 5). Conditions: 0.954 m*M* pyrimidine concn.; 8.46 mV r.m.s. applied alternating voltage; 50 Hz applied frequency.

Fig. 5. Variation of alternating current, Δi_s, with the square root of applied frequency: Waves I and II, pH 3.96 (buffer 2); waves III and IV, pH 7.48 (buffer 2); wave V, pH 12.00 (buffer 5). Conditions: 0.954 m*M* pyrimidine concn.; 8.46 mV r.m.s. applied voltage; 62.7 cm mercury (corr.).

compared to the magnitude of the current observed, may be attributed to a residual current or capacitive current element from wave I, as mentioned previously. That waves IV and V exhibit such a relationship, despite the complexity of their electrode reactions, is significant.

Frequency-dependence

The frequency-dependence of the five waves (Fig. 5) shows the behavior generally expected for semi-reversible systems: increase in current to a maximum and then decrease. Wave II shows only a very small frequency-dependence, as would be expected with a highly irreversible wave. The almost identical response to frequency change shown by waves IV and V probably indicates that both waves involve a single rate-determining step, although a contributing factor may be their having almost identical currents at the applied voltage (8.46 mV) (Fig. 3).

Effect of concentration

The alternating current for wave I is linear with concentration in the range, 0.5–10 mM, with a small but definite change in slope at *ca.* 5 mM (Fig. 6). There seems to be a "toeing" below 0.5 mM.

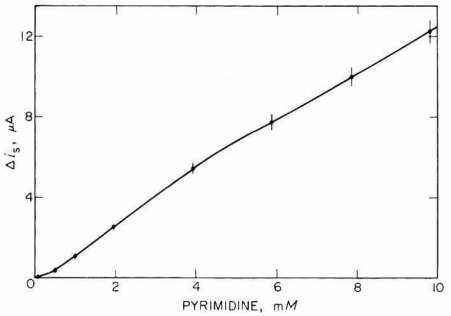

Fig. 6. Variation of alternating current, Δi_s, with pyrimidine concn. for wave I. Conditions: pH 0.92 (buffer 1); 50 Hz applied frequency; 8.46 mV r.m.s. applied voltage; 62.7 cm mercury (corr.).

REDUCTION MECHANISM FOR PYRIMIDINE

The a.c. polarographic behavior of pyrimidine generally substantiates the proposed reduction mechanism as outlined in Fig. 7. Wave I, associated with a 1e, one-proton addition to pyrimidine to produce a neutral radical, is the most reversible of the pyrimidine waves on the basis of proximity of the $E_{\frac{1}{2}}$- and E_s-values, and a general consideration of alternating current magnitudes. Furthermore, the increased proximity of $E_{\frac{1}{2}}$- and E_s-values with increased hydrogen ion concentration (Fig. 2) supports the postulate that proton addition is part of the overall first step; as more of the pyrimidine is protonated, the coupled chemical reaction of protonation becomes less critical in determining the rate of the first step. (pK_a for protonation of pyrimidine is 1.30.) Owing to the relative simplicity of wave I, lack of preceding reactions and near-reversibility, it would be most amenable to analysis of kinetic parameters, particularly in highly acid media.

Wave II, associated with 1e addition to the neutral radical to form a dihydro-

pyrimidine, appears to be the most irreversible of the pyrimidine waves, as might be expected because of the stability of the dihydro species and the extreme difficulty of reoxidizing an aliphatic carbon site. The alternating current for this wave shows very little change with variation in applied voltage, drop-time or frequency; this behavior is expected since, once a reaction appears to be very irreversible under a given set of conditions, relatively small changes in variables would only slightly affect

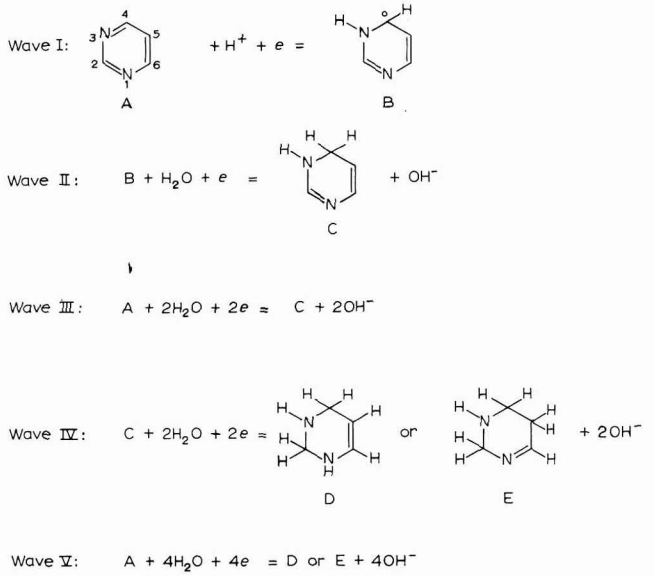

Fig. 7. Reactions producing the five polarographic waves observed in the electrochemical reduction of pyrimidine (compound A).

this irreversibility. Wave II differs most from the other waves of the reduction path in that its first step involves attack on a neutral radical, whereas the initial step for waves I, III and V presumable involves initial attack of the 3,4-carbon–nitrogen double bond, and that for wave IV on the 1,2-carbon–nitrogen double bond. This difference would account for the difference in electrochemical properties relative to the other waves.

The very similar characteristics of waves I and III are attributable to the fact that wave III involves the same initial step as wave I, *i.e.*, a 1*e* attack on the 3,4-N=C bond. Thus, although wave III should have four times the alternating current of wave I (for both reversible and irreversible reactions, Δi_s should vary as n^2), its current is actually only slightly larger. However, wave III is somewhat less reversible than wave I, as attested to by the larger deviation of E_s from $E_{\frac{1}{2}}$ and the fact that its maximum current is reached at a lower frequency (15 Hz; 25 Hz for wave I).

Waves IV and V, associated with the formation of a tetrahydropyrimidine species known to be unstable under the alkaline conditions of its formation, are highly irreversible. The similarity in their behavior with variation in drop-time, applied voltage and frequency, mentioned earlier, is probably due to the composite nature of wave V. Waves III and IV both involve a 2*e* attack on a double bond. The current for wave IV, as a function of applied alternating voltage, is about twice that for wave

III; since the shape of the a.c. wave (Fig. 1B) indicates that wave IV sits on top of wave III, the doubling of the current could indicate approximately equal contributions from the two waves.

CONCLUSIONS

The present state of the art does not permit quantitative evaluation of kinetic parameters or detailed specification of the pyrimidine reduction mechanism. For example, since there have been no theoretical nor—to our knowledge—experimental treatments of a system as complicated as pyrimidine, which has five discrete reduction waves and numerous intermediate chemical reactions, the magnitude of the "expected" currents for waves III—V are really not known and the reversibilities of the pyrimidine waves cannot be assessed by comparison of the magnitudes of alternating current. However, the qualitative application of a.c. polarography to the understanding of a complicated, quasi-reversible organic reduction series has been shown to be possible, *i.e.*, a.c. polarography has yielded interpretable results for the five-wave reduction pattern of pyrimidine. The qualitative correspondence of the five pyrimidine reduction waves with theoretical predictions for irreversible waves (effect of drop-time, frequency, applied voltage, and concentration) indicates the validity of contemporary theory and the possibility that further theoretical and experimental work on more complicated reaction mechanisms may be fruitful.

Use of phase-sensitive a.c. polarography, useful for suppression of the base current which becomes a problem with small faradaic currents, and a more detailed examination of wave I under highly acid conditions would probably be most useful in further clarifying the pyrimidine reduction mechanism. Phase angle measurements under a variety of conditions may yield more easily interpretable results for the more complicated waves, II–V.

ACKNOWLEDGEMENTS

The authors thank the National Science Foundation for helping to support the work described. One of the authors (JEO) thanks the Department of Health, Education and Welfare, and the Michigan Department of Chemistry for an NDEA Fellowship.

SUMMARY

The electrochemical reduction of pyrimidine in aqueous media was studied using alternating current (a.c.) polarography. Over the pH-range, 0.5–13, five moderately to highly irreversible a.c. waves were observed, which corresponded to the five waves observed on d.c. polarography. Although the electrochemical reduction path of pyrimidine is complex and only partially understood, good qualitative agreement between the features of the mechanism and various polarographic parameters was achieved, providing further support for the proposed mechanism, and indicating the validity of current theoretical and experimental results in the area of the a.c. polarography of quasi-reversible electrode reactions. Summit potentials for the five waves, which vary linearly with pH, are independent of applied alternating voltage, mercury

column height (drop-time) and concentration, but shift to more negative potential with increasing frequency. Total alternating current for all waves increases linearly with amplitude of applied alternating voltage and the negative square root of drop-time; plots of total alternating current *vs.* square root of applied frequency exhibit curvilinear trends with a maximum in the range, 15–50 Hz.

REFERENCES

1 B. JANIK AND P. J. ELVING, *Chem. Rev.*, 68 (1968) 295.
2 P. J. ELVING, W. A. STRUCK AND D. L. SMITH, *Mises Point Chim. Anal. Org. Pharm. Bromatol.*, 14 (1965) 141.
3 D. L. SMITH AND P. J. ELVING, *J. Am. Chem. Soc.*, 84 (1962) 2741.
4 B. TIMMER, M. SLUYTERS-REHBACH AND J. H. SLUYTERS, *J. Electroanal. Chem.*, 14 (1967) 169.
5 B. TIMMER, M. SLUYTERS-REHBACH AND J. H. SLUYTERS, *J. Electroanal. Chem.*, 14 (1967) 181.
6 J. E. HICKEY, M. S. SPRITZER AND P. J. ELVING, *Anal. Chim. Acta*, 35 (1966) 277.
7 D. E. SMITH, *Anal. Chem.*, 35 (1963) 1181.
8 H. BREYER AND H. H. BAUER, *Alternating Current Polarography and Tensammetry*, Interscience Publishers, New York, 1963.
9 G. H. AYLWARD AND J. W. HAYES, *J. Electroanal. Chem.*, 8 (1964) 442.
10 G. H. AYLWARD AND J. W. HAYES, *Anal. Chem.*, 36 (1964) 2218.
11 H. L. HUNG AND D. E. SMITH, *Anal. Chem.*, 36 (1964) 922.
12 D. E. SMITH AND H. L. HUNG, *Anal. Chem.*, 36 (1964) 2219.

ELECTROANALYTICAL CHEMISTRY AND INTERFACIAL ELECTROCHEMISTRY
Elsevier Sequoia S.A., Lausanne – Printed in The Netherlands

BREYER-WECHSELSTROMPOLAROGRAPHIE VON DESOXYRIBONUCLEINSÄURE

H. BERG, D. TRESSELT, J. FLEMMING, H. BÄR UND G. HORN
Institut für Mikrobiologie und experimentelle Therapie, Jena, Abteilung Biophysikochemie, Deutsche Akademie der Wissenschaften zu Berlin (DDR)
(Eingegangen am 29 Oktober, 1968)

EINLEITUNG

Unter den verbreiteten elektrochemischen Varianten erwies sich die Breyer-Wechselstrompolarographie für das Studium von Nucleinsäuren besonders aussichtsreich, nachdem wir charakteristische Veränderungen im Wechselstrompolarogramm[1,2] während der DNS-Denaturierung registrieren konnten. Daneben verursachen auch Hefe-RNS, Poly-A, Poly-G, Poly-C und Poly-U, sowie einige der Nucleotide und Basen mehr oder minder ausgeprägte Peaks[3-9] auf dem negativen Ast der Elektrokapillarkurve. Da andererseits im Gleichspannungspolarogramm auch kathodische Stufen der protonisierten Formen[10] im gleichen Potentialgebiet auftreten, erhebt sich die Frage nach der Ursache der a.c.-Peaks.

Noch in seinen letzten Monaten hat Breyer unsere Versuche zur Klärung mit grossem Interesse verfolgt und schon damals aus seinen reichen Erfahrungen den Denaturierungspeak als tensammetrische Welle gedeutet.

Demgegenüber glaubt Palecek[6,8] insbesondere aus Abhängigkeiten der d.c.-Stufe, des a.c.-Peaks und des Pulse-Polarogramms auf eine Elektronenaufnahme bestimmter Basen als Peakursache schliessen zu können. Hiernach spiele die Übereinstimmung der Potentiallage von d.c.-Stufe und a.c.-Peak als Hinweis auf gleichartige Elektrodenreaktionen eine gewichtige Rolle.

Wir möchten nun die Ergebnisse weiterer entscheidender Experimente diskutieren.

Die früheren experimentellen Bedingungen[3] wurden beibehalten; Einzelheiten enthalten die Bildlegenden.

ERGEBNISSE

Vorangestellt seien in Abb. 1 zwei Ausschnitte von a.c.-Polarogrammen vor und nach alkalischer Denaturierung. Ebenso wie bei thermischer Denaturierung wächst auf der negativen Seite des runden Peaks der nativen DNS ein hoher spitzer Peak heraus, der ein Mass für den Denaturierungsgrad darstellt. Zunächst prüften wir sein Ansprechen auf Phasenwinkeländerung.

1. *Die Phasenwinkelabhängigkeit*

Mit einer phasenempfindlichen Torstufe kann die unterschiedliche Phasenlage

von Kapazitäts- und Durchtrittsstrom nachgewiesen werden. Dabei wird der durch die Zelle fliessende Wechselstrom nur dann unvermindert registriert, wenn er phasenrichtig zu einer Referenzspannung liegt, deren Phasenlage vorgegeben werden kann.

Registriert man ein Wechselstrompolarogramm mehrmals bei verschieden eingestellten Phasenwinkeln der Referenzspannung, so werden die im Polarogramm zu untersuchenden Wechselstrompeaks bei unterschiedlichem Phasenwinkel, φ, ihre volle Höhe erreichen, je nachdem, ob sie durch einen Kapazitäts-, einen Durchtrittsstrom oder eine Superposition aus beiden verursacht werden. In Abb. 2 zeigen die Kurven der Vergleichssubstanzen Thallium Tl^+ (Durchtrittspeak) und Zyklohexanol

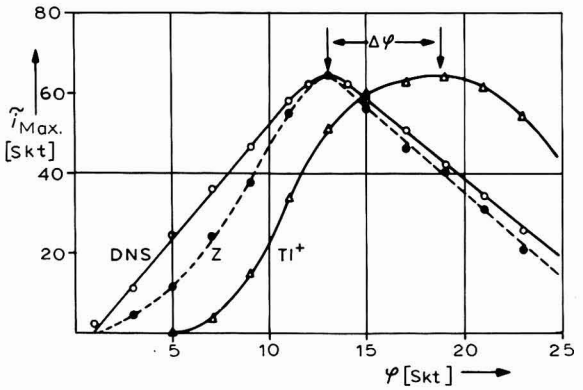

Abb. 1. Ausschnitte von a.c.-Polarogrammen (ab −0.8 V gegen NCE; mit 0.1 V/cm, Amplitude 20 mV, Frequenz 78 Hz registriert) von Kalbsthymus-DNS ($5 \cdot 10^{-4}$ g/ml in Phosphatpuffer 0.16 *M*, 25°), untere Kurve: native KT-DNS bei pH 7; obere Kurve: alk. denaturierte KT-DNS bei pH 11.8.

Abb. 2. Phasenwinkelabhängigkeit von Durchtritts- und Adsorptionspeaks bei 85°, in Standardphosphatpuffer von pH 7; Amplitude 20 mV, Frequenz 78 Hz. (○), KT-DNS; (●), Zyklohexanol; (△), Thalliumsulfat.

Z (Desorptionspeak) eine Differenz: $\Delta\varphi = 5.75$ Skalteile $\triangleq 35°$. Der unter gleichen apparativen Bedingungen gemessene zweite Wechselstrompeak denaturierter KT-DNS (Standardphosphatpuffer pH 7, 85°) weist die gleiche Phasenlage auf wie der Desorptionspeak des Zyklohexanols.

Analoge Messungen in alkalischer Lösung führten zu dem gleichen Ergebnis.

Auch frequenzabhängige Messungen der Peakhöhe denaturierter DNS bestätigen seinen kapazitiven Charakter. Es zeigte sich, dass die Peakhöhe in gleicher Weise von der Frequenz der überlagerten Wechselspannung abhängt, wie die der Desorptionspeaks z.B. von Tylose, Zyklohexanol, d.h. sehr steiler Anstieg mit steigender Frequenz bis weit über 400 Hz, während Durchtrittsströme ohne merkliche Adsorption einen völlig anderen Frequenzgang (flacher Anstieg mit steigender Frequenz, Abfall schon ab 300–400 Hz) aufweisen.

2. *pH-Einflüsse*

Der sigmoide Verlauf[10] der d.c.-Stufenhöhe über dem pH-Wert von Nukleinsäurebasen zeigt die Nichtreduzierbarkeit der neutralen und dissoziierten Formen nach höheren pH-Werten. Daraus ist zu schliessen, dass der DNS–Denaturierungspeak (Abb. 1) ebenso wie die zugehörige d.c.-Reststufe im Alkalischen Desorptionen des DNS-Knäuels mit flexiblen Einzelsträngen anzeigen.

Wie verhält sich demgegenüber DNS in neutraler und saurer Lösung? In dem entscheidenden pH-Bereich der verstärkten Protonisierung nimmt der Peak sehr stark ab (Abb. 3). Umgekehrt steigt gemäss der fortschreitenden Protonisierung

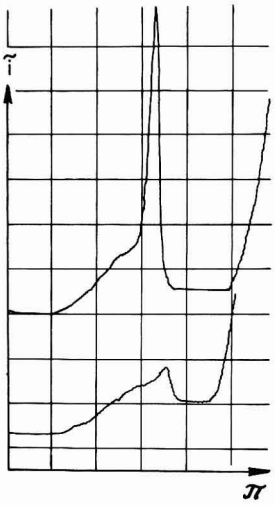

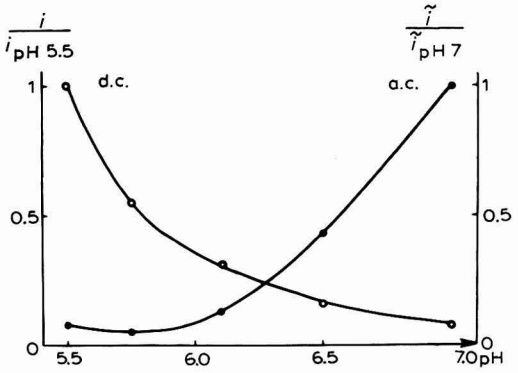

Abb. 3. Ausschnitte von a.c.-Polarogrammen (ab −0.8 V gegen 0.2 *M* CEC; mit 0.1 V/cm, Amplitude 10 mV, Frequenz 78 Hz, Tropfzeit 1.5 sec registriert) von thermisch denaturierter KT–DNS ($5 \cdot 10^{-4}$ g/ml in 0.04 *M* Phosphatpuffer, 0.11 *M* NaCl, 63°). untere Kurve: pH 6.1; obere Kurve: pH 7.

Abb. 4. pH-Abhängigkeit der d.c.-Stufe und des a.c.-Peaks (normiert auf die Höhe der Stufe bei pH 5.5 bzw. des Peaks bei pH 7) von thermisch denaturierter KT–DNS ($5 \cdot 10^{-4}$ g/ml in 0.04 *M* Phosphatpuffer, 0.11 *M* NaCl, 63°).

die d.c.-Stufe exponentiell an, so dass die pH-Abhängigkeiten der normierten Höhen von a.c.-Peak und d.c.-Stufe einen Schnittpunkt aufweisen (Abb. 4).

3. *Präparative Elektrolyse*

Als experimentum crucis war danach die präparative Elektroreduktion der elektronenaufnehmenden Basen in der denaturierten DNS anzusehen, wodurch eine Abnahme der Reduktionsstufe und eine annähernde Konstanz des Desorptionspeaks zu erwarten war. Eine mehrstündige Elektrolyse bei pH 7 (Phosphatpuffer, 60°) entsprach dieser Voraussage.

Zur Sicherung wurde die Elektrolyse bei pH 6 wiederholt, um eine noch grössere Anzahl protonisierter Nukleinsäurebausteine zu reduzieren. Das Resultat verdeutlicht Abb. 5 einschliesslich der weiteren Tests auf Peakkonstanz. Gemäss Abb. 4

ist die Veränderung des Peaks bei saurer Lösung nicht so empfindlich zu registrieren wie die Abnahme der d.c.-Stufe (obere Kurven). Daher wurde die elektrolysierte Lösung in zwei Richtungen im Vergleich zu der nichtelektrolysierten DNS-Lösung mit folgendem Ergebnis getestet (untere Kurven):

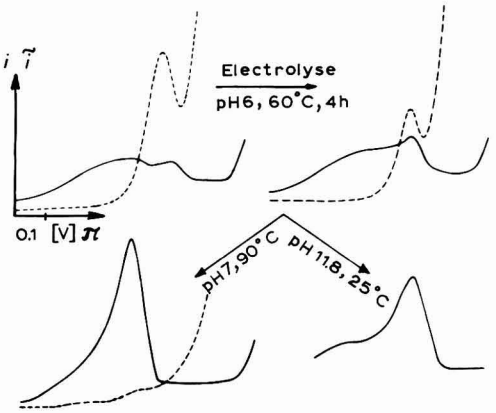

Abb. 5. Elektrolyse thermisch denaturierter KT–DNS ($5 \cdot 10^{-4}$ g/ml in Phosphatpuffer pH 6 bei 60°). (—), a.c.-Polarogramme: ab −1.0 V gegen NCE, bei 78 Hz und 20 mV Amplitude; (---), d.c.-Polarogramme: ab −1.0 V gegen NCE. oben: vor und nach der Elektrolyse registriert; unten: Anteil der Elektrolysenlösung überführt in pH 7, 90° (links); Anteil der Elektrolysenlösung überführt in pH 11.8, 25° (rechts).

(a) bei pH 7 und 90° stimmen die Peakhöhen elektrolysierter und nichtelektrolysierter DNS praktisch überein.

(b) bei pH 11.8 und 25° lassen sich die Peaks beider Proben ebenfalls kaum unterscheiden.

DISKUSSION

Unsere drei verschiedenartigen Versuchsanordnungen basierten auf dem Grundgedanken gleichsinniger Abhängigkeiten elektrochemischer Messgrössen bei gleicher Ursache bzw. umgekehrt. Dazu muss betont werden, dass die Breyer-Wechselstrompolarographie empfindlich anspricht auf reversible Durchtrittsreaktionen und tensammetrische Wellen, jedoch schwach auf irreversible Elektronenaufnahmen, wie sie bei Nukleinsäurebasen[10] festgestellt wurden. Daher ist Vorsicht geboten mit Schlussfolgerungen aus einfachen Vergleichen zwischen Kurven der a.c.-, der d.c.-Polarographie, der Pulse-Polarographie und der Oszillopolarographie. Wir möchten deshalb nun die eingangs gestellte Frage beantworten, womit auch unsere künftigen Untersuchungen des Helix-Coil-Übergangs gefördert werden:

Wodurch wird der spitze DNS-Denaturierungspeak in der Breyer–Wechselstrompolarographie verursacht?

Teilantworten darauf geben

Experiment 1: kapazitiver Effekt,

Experiment 2: a.c.-Peak und d.c.-Stufe haben verschiedene Ursachen,

Experiment 3: der a.c.-Peak bleibt nach DNS-Reduktion praktisch erhalten.

Aus all dem folgt, dass der spitze DNS-Denaturierungspeak durch Adsorp-

tions – Desorptions – Effekte hervorgerufen wird, d.h. eine tensammetrische Welle im Sinne Breyers darstellt, ebenso wie der runde Peak, der allein bei der nativen DNS vorkommt. Demgemäss gleicht die Konzentrationsabhängigkeit der Peakhöhe einer Langmuir-Adsorptions-Isotherme[11].

Überschaut man das bisherige polarographische Studium hochmolekularer Nukleinsäuren, dessen Beginn[12] in das Jahr 1957 zurückreicht, darf behauptet werden, dass unter allen Bedingungen die Adsorption eine wesentliche Rolle spielt.

Nur in solchen Fällen, wo protonisierte Basen—entgegen sterischen Hinderungen—der Elektrodenoberfläche genügend nahe kommen können, erfolgt ausserdem Elektronenübergang. Da die d.c.-Stufenhöhe eines Biopolymeren von mehreren Molekülparametern bestimmt wird, ist die klassische Ilkovič-Gleichung allerdings nicht mehr anwendbar. Hinzu kommt, dass in saurer Grundlösung sich katalytische Wasserstoffwellen überlagern können.

Damit sind keineswegs alle Fragen nach der Natur der DNS-Desorptionswellen beantwortet. Von wesentlicher praktischer Bedeutung ist z.B. die Klärung des Zusammenhanges zwischen Peakhöhe und Denaturierungsgrad, wobei die zugehörigen Adsorptionsisothermen berücksichtigt werden müssen. Von speziellem Interesse für die physikalische Chemie der Nukleinsäuren versprechen die Ergebnisse der Breyer-Wechselstrompolarographie zu werden, wenn sich die bestehenden Unterschiede zu spektroskopischen Daten aus konformativen Ursachen erklären lassen.

SUMMARY

In contrast to native DNA, denatured DNA gives a new sharp peak in the Breyer-a.c.-polarogram. It was shown by means of three different polarographic techniques: phase angle-dependence of a.c.-peak height; pH-effect on a.c.-peak in comparison to the d.c.-step height; electrolysis of denatured DNA in acidic solution, that this peak is capacitive in origin; in other words, denatured DNA causes tensammetric waves also according to the terminology of Breyer.

ZUSAMMENFASSUNG

Im Gegensatz zu nativer DNS verursacht denaturierte einen neuen spitzen Peak im Wechselstrompolarogramm nach Breyer. Mit Hilfe von drei polarographischen Kriterien: (i) Phasenwinkelabhängigkeit dieser Peakhöhe, (ii) pH-Einfluss auf die Peakhöhe im Vergleich zur Höhe der Gleichspannungsstufe, (iii) Elektrolyse thermisch denaturierter DNS in schwach saurer Lösung, wurde gezeigt, dass dieser a.c.-Peak kapazitativen Ursprungs ist, d.h. in der Terminologie von Breyer verursachen denaturierte und native DNS tensammetrische Wellen.

Demgegenüber gibt es andersartige polarographische Methoden, die neben katalytischen Wellen weitere irreversible Durchtrittsreaktionen protonisierter Basen in der DNS anzuzeigen vermögen.

LITERATUR

1 H. BERG UND H. BÄR, *Monatsber. Deut. Akad. Wiss. Berlin*, 7 (1965) 210; Preprint P. 178, Symp. Makromolec. Chem., Prag, 1965.
2 H. BERG UND F. A. GOLLMICK, *III. Jena. Symp., 1965: Elektrochemische Methoden und Prinzipien in der Molekularbiologie*, Akad. Verlag, Berlin, 1966, S.533.
3 H. BERG, H. BÄR UND F. A. GOLLMICK, *Biopolymers*, 5 (1967) 61.
4 H. BERG UND H. BÄR, *IV. Jena. Symp., 1967: Molekulare Mechanismen photodynamischer Effekte, Studia Biophysica*, 3 (1967) 133.
5 E. PALEČEK, *Biochim. Biophys. Acta*, 145 (1967) 410.
6 E. PALEČEK, *Arch. Biochem. Biophys.*, 125 (1968) 142.
7 H. BERG, *J. Chim. Phys.*, 65 (1968) 54; Preprint 10, 17. Réunion annuelles de la Société de Chimie Physique: Macromolecules Helicoïdales en Solution, Paris, Mai, 1967.
8 E. PALEČEK UND V. VETTERL, *Biopolymers*, 6 (1968) 917.
9 H. BERG, JU. JEWDOKIMOW, H. BÄR UND JA. WARSCHAWSKY, *Molekul. Biol. (Russ.)*, 2 (1968) 830.
10 B. JANIK UND P. ELVING, *Chem. Rev.*, 68 (1968) 295.
11 JU. JEWDOKIMOW, JA. WARSCHAWSKIJ, H. BERG UND H. BÄR, in Vorbereitung.
12 H. BERG, *Biochem. Z.*, 329 (1957) 274.

ELECTROANALYTICAL CHEMISTRY AND INTERFACIAL ELECTROCHEMISTRY
Elsevier Sequoia S.A., Lausanne – Printed in The Netherlands

A.C. POLAROGRAPHIC STUDIES OF OXINE AND ITS DERIVATIVES

TAITIRO FUJINAGA, KOSUKE IZUTSU, SATOSHI OKAZAKI AND HIROMITI SAWAMOTO
Chemistry Institute, Faculty of Science, University of Kyoto, Sakyo-ku, Kyoto (Japan)
(Received November 1st, 1968)

INTRODUCTION

The study of adsorption processes by alternating current measurements was introduced independently by Breyer and Hacobian[1] and by Doss and Kalyanasundaram[2]. Breyer and Hacobian called their method tensammetry and many tensammetric investigations have been reported since their work[3]. Breyer and Hacobian[4] also found well-defined a.c. waves of halide ions at positive potentials. As these waves were different in nature from that of a tensammetric wave, they proposed to call this type of wave a transition wave[5]. Takemori and Tachi[6], and Biegler[7] also studied this type of wave, but even now it is not fully understood.

Breyer and his coworkers[8,9] in their study of the a.c. polarographic behaviour of oxine found no a.c. polarographic wave corresponding to the reduction of oxine, but obtained two a.c. waves at positive potentials — the wave at the more positive potential will be called wave I and the one at the more negative potential, wave II. From the experimental results it was concluded that wave I is a transition wave, and wave II a tensammetric wave. Certain metal ions when added to very dilute oxine solutions lowered wave II by forming metal oxinates and this could be used to detect the end-point of titrations of several metal ions; the method was called tensammetric titration[9,10].

The present paper deals with the study of the a.c. polarographic behaviour of oxine and its derivatives and their application to tensammetric titrations. Oxine-5-sulphonic acid, ferron and 2-methyloxine were the chosen oxine derivatives.

EXPERIMENTAL

Polarograms were recorded with the Shimadzu polarograph RP-2 with an a.c. attachment, BF-1. An alternating voltage of frequency 60 c/sec and an amplitude of 20 mV r.m.s. was used. The capillary characteristics of the dropping mercury electrode were: $t = 3.38$ sec and $m = 1.11$ mg/sec at 0 V *vs.* SCE in 0.2 *M* sodium nitrate solutions.

Oxine (8-hydroxyquinoline) was purified by steam distillation. Oxine-5-sulphonic acid (8-hydroxyquinoline-5-sulphonic acid) was prepared by adding fuming sulfuric acid to oxine, and recrystallizing the product twice from 1 *M* hydrochloric acid. Ferron (7-iodo-8-hydroxyquinoline-5-sulphonic acid) was recrystallized twice from water. 2-Methyloxine (2-methyl-8-hydroxyquinoline) was recrystallized twice from aqueous ethanol. All other chemicals were of analytical-reagent grade, and twice

distilled water was used throughout the work. The pH of the electrolytic solution was adjusted with perchloric acid, acetic acid, ammonium acetate, ammonia or sodium hydroxide, or their mixtures; in all cases, their total concentration was kept at 0.1 *M* in the final solution. Sodium nitrate (0.2 *M*) was added to all solutions to keep the electrical conductivity of the solution at a suitable level.

RESULTS AND DISCUSSION

1. *Polarographic waves of oxine and its derivatives at positive polarization*

The a.c. and d.c. polarograms of oxine, oxine-5-sulphonic acid, ferron and 2-methyloxine are shown in Figs. 1 and 2. All compounds investigated yield waves

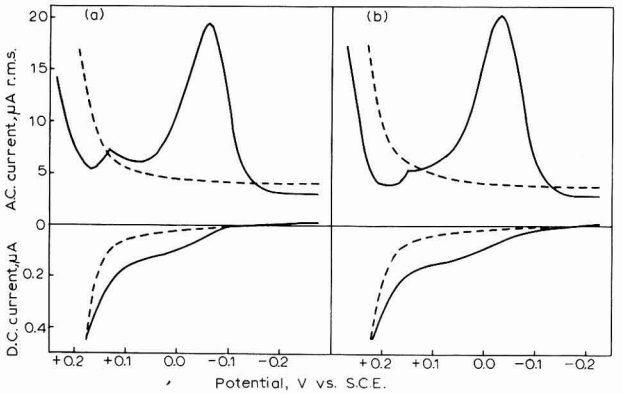

Fig. 1. A.c. and d.c. polarographic waves of: (a), $1.4 \cdot 10^{-4}$ *M* oxine in 0.1 *M* $CH_3COONH_4 + 0.2$ *M* $NaNO_3$, pH 6.6 (solid lines) and 0.1 *M* $CH_3COONH_4 + 0.2$ *M* $NaNO_3$, pH 6.5 (dotted lines); (b), $1.4 \cdot 10^{-4}$ *M* oxine-5-sulphonic acid in 0.1 *M* $CH_3COONH_4 + 0.2$ *M* $NaNO_3$, pH 5.3 (solid lines) and 0.1 *M* CH_3COOH–$CH_3COONH_4 + 0.2$ *M* $NaNO_3$, pH 5.2 (dotted lines).

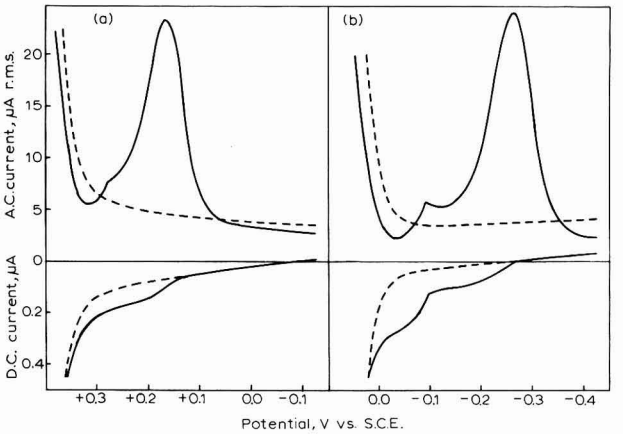

Fig. 2. A.c. and d.c. polarographic waves of: (a), $1.4 \cdot 10^{-4}$ *M* ferron in 0.1 *M* $HClO_4 + 0.2$ *M* $NaNO_3$, pH 1.1 (solid lines) and 0.1 *M* $HClO_4 + 0.2$ *M* $NaNO_3$, pH 1.1 (dotted lines); (b), $1.4 \cdot 10^{-4}$ *M* 2-methyloxine in 0.1 *M* CH_3COONH_4–$NH_4OH + 0.2$ *M* $NaNO_3$, pH 9.0 (solid lines) and 0.1 *M* CH_3COONH_4–$NH_4OH + 0.2$ *M* $NaNO_3$, pH 8.9 (dotted lines).

similar to wave II of oxine at concentrations above *ca.* $3 \cdot 10^{-6}$ *M*. Oxine and 2-methyloxine gave wave I at concentrations above *ca.* $8 \cdot 10^{-5}$ *M*, but oxine-5-sulphonic acid and ferron did not show such a well-defined wave I. The a.c. base current at more positive potentials than wave I is considerably depressed by the presence of oxine and its derivatives, indicating adsorption of a surface-active substance which is assumed to be mercury oxinate formed at the electrode by the dissolution of mercury. Therefore, wave I is a transition wave. The a.c. base current at more negative potentials than wave II was also depressed considerably by the presence of oxine and its derivatives, probably as a result of their adsorption on the electrode surface. From the dependence of wave II on the concentration and temperature, this wave seems to be a tensammetric wave. α-Naphthol and quinoline were tested by a.c. polarography under the same conditions, and no difference was observed in the base current. Therefore, for oxine and its derivatives to adsorb on to the mercury electrode, both phenol and pyridyl radicals must be present.

2. *Effect of concentration and temperature*

Oxine and its derivatives yield wave II at concentrations as low as $3 \cdot 10^{-6}$ *M*. In the concentration range up to $2\text{–}3 \cdot 10^{-5}$ *M*, the height of the wave increases almost linearly with concentration. Above this concentration region, the calibration curve begins to deviate from linearity. The results obtained are shown in Fig. 3.

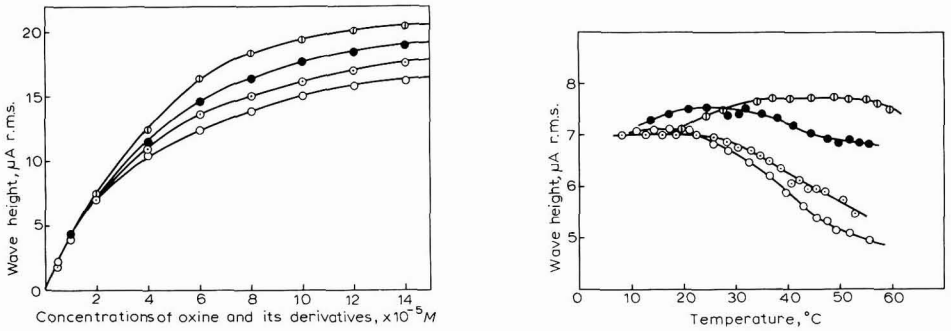

Fig. 3. Effect of concn. of oxine and its derivatives on wave height: (–○–), Oxine in 0.1 *M* CH_3COONH_4 + 0.2 *M* $NaNO_3$, pH 6.0; (–⊙–), oxine-5-sulphonic acid in 0.1 *M* CH_3COONH_4 + 0.2 *M* $NaNO_3$, pH 5.8; (–●–), ferron in 0.1 *M* $HClO_4$ + 0.2 *M* $NaNO_3$, pH 1.1; (–⊕–), 2-methyloxine in 0.1 *M* CH_3COONH_4–NH_4OH + 0.2 *M* $NaNO_3$, pH 8.8.

Fig. 4. Effect of temp. on wave height: (–○–), $2 \cdot 10^{-5}$ *M* oxine in 0.1 *M* CH_3COONH_4 + 0.2 *M* $NaNO_3$, pH 6.0; (–⊙–), $2 \cdot 10^{-5}$ *M* oxine-5-sulphonic acid in 0.1 *M* CH_3COONH_4 + 0.2 *M* $NaNO_3$, pH 5.8; (–●–), $2 \cdot 10^{-5}$ *M* ferron in 0.1 *M* $HClO_4$ + 0.2 *M* $NaNO_3$, pH 1.1; (–⊕–), $2 \cdot 10^{-5}$ *M* 2-methyloxine in 0.1 *M* CH_3COONH_4–NH_4OH + 0.2 *M* $NaNO_3$, pH 8.8.

The summit potential does not change appreciably at concentrations above $4 \cdot 10^{-5}$ *M*.

The temperature effect on the height of wave II is shown in Fig. 4. At lower temperatures, an increase in temperature results in an increase in the height of wave II and the diffusion of oxine and its derivatives towards the electrode seems to control the wave height. On the other hand, at higher temperatures, an increase in temperature results in a decrease in the height of the wave; this is a characteristic trend for a tensammetric wave.

3. *Effect of pH*

The effect of pH on the height and summit potential of wave II are summarized in Figs. 5–8. The wave heights are markedly dependent on pH, and the regions of maximum wave height are in a limited pH interval. The pH at which the maximum wave height appears shifts towards the acidic side in the order: 2-methyloxine, oxine, oxine-5-sulphonic acid and ferron. The pk_1- and pk_2- values of these substances change in the same order (Table 1).

TABLE 1

VALUES OF pk_1 AND pk_2[11]

	pk_1	pk_2		pk_1	pk_2
2-Methyloxine	5.70	10.31	Oxine-5-sulphonic acid	4.07	8.35
Oxine	5.16	9.63	Ferron	2.50	7.05

Oxine and its derivatives (HOx) are mostly amphoteric, and the following equilibria can be considered:

$$H_2Ox^+ \rightleftharpoons H^+ + HOx$$

$$k_1 = (H^+)[HOx]/[H_2Ox^+] \quad (1)$$

$$HOx \rightleftharpoons H^+ + Ox^-$$

$$k_2 = (H^+)[Ox^-]/[HOx] \quad (2)$$

where k_1 and k_2 are primary and secondary dissociation constants of the acid, H_2Ox^+, in which hydrogen ion is measured by its activity and other species in terms of their concentration.

When the values of k_1, k_2 and (H^+) are known, the ratio of concentration of these three species can be calculated from eqns. (1) and (2). The concentration of the neutral form, HOx, thus obtained is shown in Figs. 5–8 as dotted lines. These Figures show that, except in the acidic region of ferron, the dotted lines coincide fairly well with the solid lines that show the heights of wave II. Therefore, it may be concluded that the neutral species of oxine, oxine-5-sulphonic acid and 2-methyloxine mainly contribute to the tensammetric wave II, while for ferron both acidic and neutral species may give wave II.

Summit potentials of wave II move in the negative direction with increase in pH. At pH-values near pk_1 and pk_2, discontinuous changes of summit potentials are observed; the discontinuity is marked at a pH near pk_2, but not at pk_1, especially in the case of ferron.

4. *Tensammetric titrations*

Certain metal ions when added to a solution of oxine or its derivative lower wave II until the equivalence point is attained. Conversely, when oxine or its derivative is added to solutions of certain metal ions, wave II begins to appear after the equivalence point and increases almost linearly. Tensammetric titration uses this phenomena to detect the end-point of titrations.

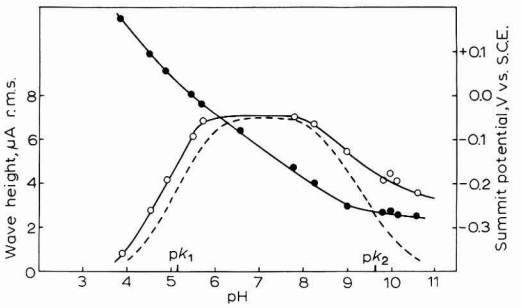

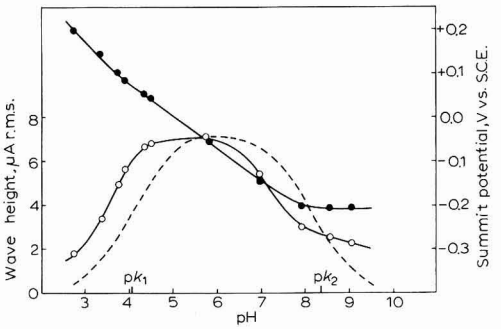

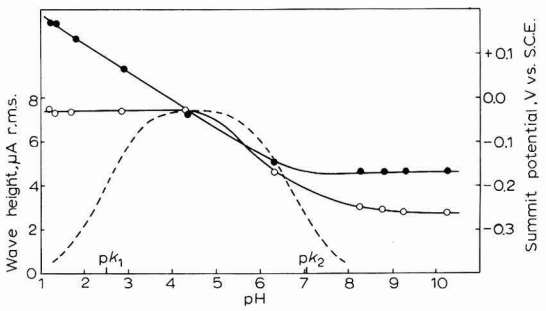

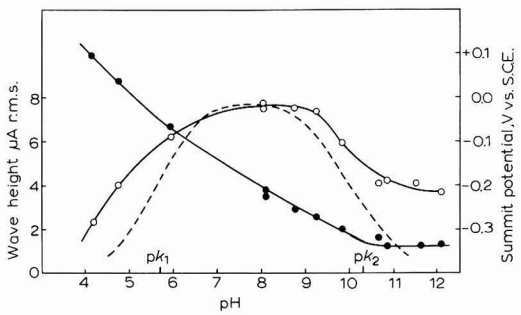

Figs. 5–8. Effect of pH on the waves of $2 \cdot 10^{-5}$ *M* solns. of: (5) oxine, (6) oxine-5-sulphonic acid, (7) ferron, (8) 2-methyloxine. (○) wave height; (●) summit potential; (---) quantity of neutral molecule present.

TABLE 2

TITRATION OF COPPER WITH OXINE

No.	*Titration of* Cu^{2+} (1 *ml* $1 \cdot 10^{-3}$ *M* Cu^{2+} *in* 50 *ml* 0.1 *M* CH_3COONH_4) *with* $1 \cdot 10^{-3}$ *M oxine*	*Titration of oxine* (2 *ml* $1 \cdot 10^{-3}$ *M oxine in* 50 *ml* 0.1 *M* CH_3COONH_4) *with* 10^{-3} *M* Cu^{2+}
	Oxine used (*ml*)	Cu^{2+} *used* (*ml*)
1	2.080	0.944
2	2.090	0.910
3	2.045	0.888
4	2.079	0.920
5.	2.055	0.926
mean	2.070 with 0.8 % Rel. S.D.	0.918 with 2 % Rel. S.D.

The titration curves of copper with oxine and of oxine with copper are shown in Fig. 9. Although the titrations were carried out in very dilute solutions, the end-point could be obtained fairly accurately and the results were satisfactory (see Table 2).

The titration curves of ferron with copper are shown in Fig. 10; it can be seen that ferric ion present in an equivalent amount with ferron does not affect the height of wave II of ferron. The addition of 10^{-3} *M* of ferric iron, however, decreases wave II of ferron to some extent, but does not affect the end-point. Table 3 shows the possi-

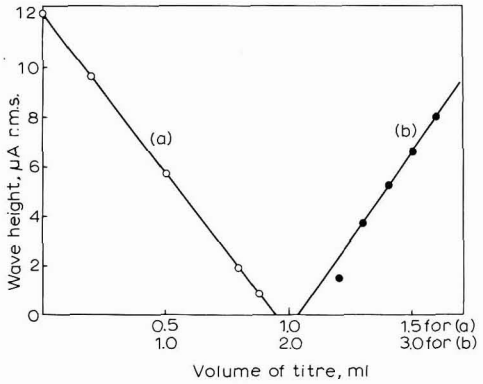

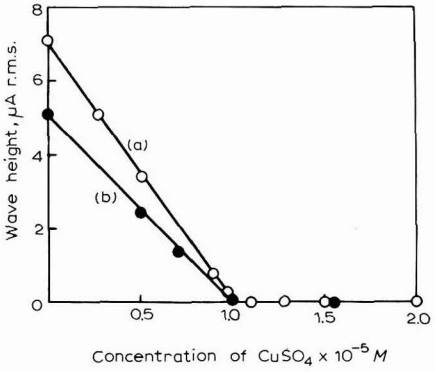

Fig. 9. Titration curves of copper with oxine: (a), oxine ($4 \cdot 10^{-5}$ *M*) with Cu^{2+} (10^{-3} *M*); (b), Cu^{2+} ($2 \cdot 10^{-5}$ *M*) with oxine (10^{-3} *M*).

Fig. 10. Titration curves of iron with ferron: (a), ferron ($2 \cdot 10^{-5}$ *M*) with Cu^{2+}; (b), ferron ($2 \cdot 10^{-5}$ *M*) with Cu^{2+} in the presence of Fe^{3+} (10^{-3} *M*).

bilities for the tensammetric titrations of $2 \cdot 10^{-5}$ *M* metal ions. In the Table, mark ○ indicates that the addition of metal ions decreases the height of wave II quantitatively; mark △ shows that the height of wave II is decreased but that the reaction is not quantitative and mark × that the addition of metal ion does not decrease the height of wave II.

Although the tensammetric wave is observable only above *ca.* $3 \cdot 10^{-6}$ *M* oxine

TABLE 3

RESULT OF TENSAMMETRIC TITRATION

Metal ions	*Oxine and its derivatives*			
	Oxine	*Oxine-5-sulphonic acid*	*Ferron*	*2-Methyl-oxine*
Cu^{2+}	○	○	○	○
Zn^{2+}	○	○	×	△
Ni^{2+}	○	○	×	○
UO_2^{2+}	○	○	△	×
Cd^{2+}	△	△	×	○
Pb^{2+}	△	△	×	△
Mg^{2+}	×	×	×	×
Ca^{2+}	×	×	×	×
Fe^{3+}	○	△	×	×
In^{3+}	○	△	△	×
Th^{4+}	×	△	×	×
pH	6.5	5.9	2.7	8.5

Total concn. of oxine or its derivatives, $2 \cdot 10^{-5}$ *M*.

or its derivatives, the end-point obtained by extrapolating the titration curve agrees within a few percent with the value calculated by the stoichiometric relation.

The applicability of the tensammetric titration was considered using the stability constants of metal ions with oxine and its derivatives. When metal ion, M^{n+}, is titrated with oxine or its derivative, the following relationship holds all the way through the titration step. To simplify the discussion, the volume change in the titration procedure and other sub-reactions were neglected.

$$M(Ox)_{i-1}^{(n-i+1)+} + Ox^- \rightleftharpoons M(Ox)_i^{(n-i)+}$$

$$K_i = \frac{[M(Ox)_i^{(n-i)+}]}{[M(Ox)_{i-1}^{(n-i+1)}][Ox^-]} \tag{3}$$

If the total concentrations of metal ions and of oxine or its derivative are c_M and c_{Ox}, respectively, then

$$c_M = \sum_{i=0}^{n} [M(Ox)_i^{(n-i)+}] \quad (M(Ox)_0^{n+} = M^{n+}) \tag{4}$$

$$c_{Ox} = \sum_{i=0}^{n} \{i[M(Ox)_i^{(n-i)+}]\} + [Ox^-] + [HOx] + [H_2Ox^+] \tag{5}$$

As in these equations $[HOx] \equiv x$ contributes to wave II, elimination of $[M(Ox)_i^{(n-i)+}]$, $[Ox^-]$, and $[H_2Ox^+]$ from eqns. (1)–(5) finally leads to

$$f(x) = \sum_{i=0}^{n} \left[\beta^{n-i} \kappa_i \left\{ x^{i+1} + \frac{\beta}{\alpha} (ic_M - c_{Ox}) x^i \right\} \right] = 0 \tag{6}$$

where $\kappa_i = \prod_{j=0}^{i} K_j$, $K_0 = 1$, $[Ox^-]^0 = 1$, $\alpha = 1 + (H^+)/k_2 + (H^+)^2/k_1k_2$ and $x/\beta = [HOx] \cdot k_2/(H^+) = [Ox^-]$. As the metal ions used in the titration were di-, tri- and

tetra-valent, eqn. (6) is difficult to solve algebraically. As the approximate solution was sufficient for present purposes, the following relationship was used, *i.e.*, when $f(a) \cdot f(b) < 0$, the root, x, of eqn. (6) lies between a and b. The results thus calculated are shown in the last columns of Tables 4–7. Metal species that can be determined by tensammetric titration are rather limited by the fact that the reaction of metal ions with oxine or its derivative is not always quantitative in these dilute solutions. However, if the concentration of the neutral molecule present at the equivalence point is below $3 \cdot 10^{-6}$ M, the titration is possible, except in the cases of titrations of Th^{4+} with oxine, Fe^{3+} and Th^{4+} with oxine-5-sulphonic acid, and Zn^{2+}, UO_2^{2+} and Pb^{2+} with 2-methyloxine. In these cases, side reactions, such as with hydroxyl ion, may interfere with the titration.

TABLE 4

APPLICABILITY OF THE TENSAMMETRIC TITRATION, AND THE CALCULATED CONCENTRATION OF NEUTRAL MOLECULES AT THE EQUIVALENT POINT (OXINE)

Metal ions	*Possibility of titration*	*Stability constant*[1,2]				*Concn. of neutral molecules (M)*
		log K_1	*log* K_2	*log* K_3	*log* K_4	
Cu^{2+}	○	13.5	12.7			10^{-8}–10^{-7}
Zn^{2+}	○	10.0	8.9			$3 \cdot 10^{-6}$–$4 \cdot 10^{-6}$
Ni^{2+}	○	11.4	9.9			10^{-6}–$2 \cdot 10^{-6}$
UO_2^{2+}	○	11.3	9.6			$2 \cdot 10^{-6}$–$3 \cdot 10^{-6}$
Cd^{2+}	△	9.4	7.7			$7 \cdot 10^{-6}$–$8 \cdot 10^{-6}$
Pb^{2+}	△	10.6	8.1			$5 \cdot 10^{-6}$–$6 \cdot 10^{-6}$
Mg^{2+}	×	6.4	5.4			$1.9 \cdot 10^{-5}$–$2 \cdot 10^{-5}$
Ca^{2+}	×	3.5				$1.9 \cdot 10^{-5}$–$2 \cdot 10^{-5}$
Fe^{3+}	○	12.3	11.3	10.3		10^{-7}–10^{-6}
Th^{4+}	×	10.5	10.0	9.5	9.0	$2 \cdot 10^{-6}$–$3 \cdot 10^{-6}$

Total concn. of oxine, $2 \cdot 10^{-5}$ M.

TABLE 5

APPLICABILITY OF THE TENSAMMETRIC TITRATION, AND THE CALCULATED CONCENTRATION OF NEUTRAL MOLECULES AT THE EQUIVALENT POINT (OXINE-5-SULPHONIC ACID)

Metal ions	*Possibility of titration*	*Stability constant*[1,2]				*Concn. of neutral molecules (M)*
		log K_1	*log* K_2	*log* K_3	*log* K_4	
Cu^{2+}	○	13.3	11.7			10^{-8}–10^{-7}
Zn^{2+}	○	8.7	7.5			$6 \cdot 10^{-6}$–$7 \cdot 10^{-6}$
Ni^{2+}	○	10.0	8.1			$4 \cdot 10^{-6}$–$5 \cdot 10^{-6}$
UO_2^{2+}	○	8.5	7.2			$6 \cdot 10^{-6}$–$7 \cdot 10^{-6}$
Cd^{2+}	△	7.7	6.5			$1.3 \cdot 10^{-5}$–$1.4 \cdot 10^{-6}$
Pb^{2+}	△	8.5	7.6			$6 \cdot 10^{-6}$–$7 \cdot 10^{-6}$
Mg^{2+}	×	4.8	3.4			$1.9 \cdot 10^{-5}$–$2 \cdot 10^{-5}$
Ca^{2+}	×	3.5				$1.9 \cdot 10^{-5}$–$2 \cdot 10^{-5}$
Fe^{3+}	△	11.6	11.2	12.8		10^{-8}–10^{-7}
Th^{4+}	△	9.6	8.7	7.6	6.1	$6 \cdot 10^{-6}$–$7 \cdot 10^{-6}$

Total concn. of oxine-5-sulphonic acid, $2 \cdot 10^{-5}$ M.

TABLE 6

APPLICABILITY OF THE TENSAMMETRIC TITRATION, AND THE CALCULATED CONCENTRATION OF NEUTRAL MOLECULES AT THE EQUIVALENT POINT (FERRON)

Metal ions	*Possibility of titration*	*Stability constants*[1,2]			*Concn. of neutral molecules (M)*
		log K_1	*log* K_2	*log* K_3	
Mg^{2+}	×	3.8	6.2		$1.9 \cdot 10^{-5}$–2 $\cdot 10^{-5}$
Ca^{2+}	×	3.1	4.0		$1.9 \cdot 10^{-5}$–2 $\cdot 10^{-5}$
Fe^{3+}	×	8.9	8.4	7.9	$1.8 \cdot 10^{-5}$–$1.9 \cdot 10^{-5}$

Total concn. of ferron, $2 \cdot 10^{-5}$ *M*.

TABLE 7

APPLICABILITY OF THE TENSAMMETRIC TITRATION, AND THE CALCULATED CONCENTRATION OF NEUTRAL MOLECULES AT THE EQUIVALENT POINT (2-METHYLOXINE)

Metal ions	*Possibility of titration*	*Stability constants*[1,2]		*Concn. of neutral molecules (M)*
		log K_1	*log* K_2	
Cu^{2+}	○	12.5	11.5	10^{-8}–10^{-7}
Zn^{2+}	△	8.7	8.1	$2 \cdot 10^{-6}$–$3 \cdot 10^{-6}$
Ni^{2+}	○	9.4	8.4	10^{-6}–$2 \cdot 10^{-6}$
UO_2^{2+}	×	9.4	8.0	10^{-6}–$2 \cdot 10^{-6}$
Cd^{2+}	○	9.0	7.6	$3 \cdot 10^{-6}$–$4 \cdot 10^{-6}$
Pb^{2+}	△	10.3	8.2	10^{-7}–10^{-6}
Mg^{2+}	△	5.2	4.4	$1.9 \cdot 10^{-5}$–$2 \cdot 10^{-5}$

Total concn. of 2-methyloxine, $2 \cdot 10^{-5}$ *M*.

ACKNOWLEDGEMENT

The authors are especially grateful to the late Professor Breyer, who initiated this work during a stay as visiting professor at the University of Kyoto in 1963–64.

SUMMARY

Oxine and its derivatives, oxine-5-sulphonic acid, ferron and 2-methyloxine, yield two a.c. waves at the positive region of the dropping mercury electrode. Wave I at more positive polarization, although ill-defined in the cases of oxine-5-sulphonic acid and ferron, is the so-called transition wave, and wave II at more negative potentials is a tensammetric wave. The height of wave II is dependent on pH, and the pH-region at which maximum wave height is obtained is specific to the compound, depending on its p*k*-value. Oxine and its derivatives can exist as three species according to the pH of the solution: *i.e.*, acidic, neutral and basic forms. The neutral species of oxine, oxine-5-sulphonic acid and 2-methyloxine mainly contribute to wave II, while for ferron, both acidic and neutral species can contribute to wave II. The addition of certain metal ions that form chelates with oxine or its derivatives quantitatively depress wave II. This fact can be used to detect the end-point of titrations of metal ion in very dilute concentrations. The theoretical possibility of the titration has been considered.

REFERENCES

1 B. BREYER AND S. HACOBIAN, *Australian J. Sci. Res.*, A5 (1952) 500.
2 K. S. G. DOSS AND A. KALYANASUNDARAM, *Proc. Indian. Acad. Sci.*, 35A (1952) 27.
3 B. BREYER AND H. H. BAUER, *Alternating Current Polarography and Tensammetry*, Interscience Publishers, New York, 1963.
4 B. BREYER AND S. HACOBIAN, *Australian J. Sci. Res.*, A4 (1951) 610.
5 B. BREYER, *Australian J. Chem.*, 6 (1953) 186.
6 Y. TAKEMORI AND I. TACHI, *Bull. Chem. Soc. Japan*, 28 (1955) 151
7 T. BIEGLER, *J. Electroanal. Chem.*, 6 (1963) 357, 365, 373.
8 B. BREYER, *Australian J. Sci.*, 23 (1961) 225.
9 B. BREYER, J. W. HAYES, T. FUJINAGA, C. TAKAGI AND S. OKAZAKI, *Bunseki Kagaku*, 14 (1965) 1023.
10 B. BREYER, T. FUJINAGA AND H. SAWAMOTO, *Bunseki Kogaku*, 15 (1966) 487.
11 R. G. W. HOLLINGSHEAD, *Oxine and its Derivatives*, Butterworths Scientific Publications, London, 1954.
12 L. G. SILLÉN AND A. E. MARTELL, *Stability Constants of Metal–Ion Complexes*, *Chem. Soc. (London)*, *Spec. Publ.*, 17 (1964).

ELECTROANALYTICAL CHEMISTRY AND INTERFACIAL ELECTROCHEMISTRY
Elsevier Sequoia S.A., Lausanne – Printed in The Netherlands

POLAROGRAPHIC REDUCTION OF ALDEHYDES AND KETONES

VIII. POLAROGRAPHIC BEHAVIOUR OF CHALCONE AND DIHYDROCHALCONE*

A. RYVOLOVÁ-KEJHAROVÁ
J. Heyrovský Institute of Polarography, Czechoslovak Academy of Science, Prague (Czechoslovakia)

P. ZUMAN
Department of Chemistry, The University, Birmingham 15 (Great Britain)

(Received November 25th, 1968)

Polarographic reduction of α,β-unsaturated ketones of type $C_6H_5COCH=CHR$ takes place in a two-electron step (i_I), followed at higher pH-values by a further reduction wave, (i_{II}). The first two-electron process is split at lower pH-values into two one-electron steps, $(i_I)_1$ and $(i_I)_2$ (Fig. 1). These three waves were observed by Pasternak[1], who correctly assigned the first two-electron process to the reduction of the ethylenic bond, basing his deduction on comparison of half-wave potentials of wave i_{II} with those of aryl–alkyl ketones. The same author carried out also controlled-potential electrolysis by means of a mercury pool electrode. At pH 1.3, apart

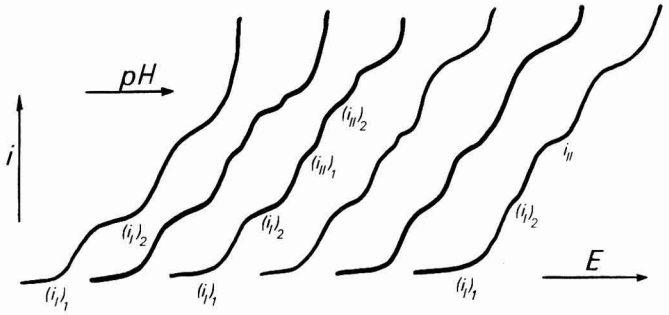

Fig. 1. pH-Dependence of the reduction waves of chalcone (schematical).

from a non-crystalline side-product, a crystalline substance was isolated as the predominating product to which "probably the structure of dimer(I)" was attributed[1]. At pH 8.6 at the limiting current of $(i_I)_1 + (i_I)_2$ corresponding to the transfer of 1.7 electrons, a mixture of the product obtained in acidic media, and benzylacetophenone was isolated[1].

$$\begin{matrix} C_6H_5COCH_2CHR \\ | \\ C_6H_5COCH_2CHR \end{matrix} \quad (I)$$

Part VII: *Trans. Faraday Soc.*, in the press.

This interpretation of consecutive reduction of the ethylenic linkage and carbonyl group has been adopted by most of the subsequent authors[2-8], usually without experimental proof other than the ratio of wave-heights. More recently, the pH-dependence of the wave-height and of the half-wave potentials of the more negative wave of phenyl vinyl ketone was used[9] to prove that saturated ketone results from the acceptance of the first two electrons. A similar approach was used also in the interpretation of the reduction process of *o*-hydroxychalcone and its heterocyclic analogues[10]. For the quinoline analogue of chalcone with the heterocyclic group adjacent to the carbonyl group[11], the first reduction step was reported to take place in one two-electron step at pH < 10. Saturated ketone formation was detected among the products of controlled-potential electrolysis on a mercury pool electrode. At pH 13, where the height of the first wave decreased and corresponded to an approximately one-electron process, the mercury pool electrolysis gave rise to a red amorphous solid for which a M.W. of 536 was found cryoscopically in benzene. The product, which gave a strong infrared band at 1680 cm^{-1}, was assumed to be a mixture of various dimeric products.

A polymer was obtained also by electrolysis of chalcone in anhydrous dimethylformamide[12], in which the formation of a radical anion and radical dianion was proved by reaction with carbon dioxide. It was assumed[12] that the more complicated course of reduction in non-aqueous media in the absence of carbon dioxide compared with that in aqueous solutions, is due to the stability of the radical anions formed and their reaction with the parent compound.

On the other hand, Russian authors[13,14] maintain that the first electron attack takes place on the carbonyl group and[14] "that the free radical formed undergoes isomerization* into another free radical which is further reduced in the second wave" or can be converted into a dimer of structure I. Formation of dimer I was postulated from the M.W. of the electrolysis product obtained in acidic media, determined by the Rast method[13], or from a doubtful shape of the wave and from half-wave potentials at unspecified pH (*cf.* Figs. 10 and 12, ref. 14). The latter authors[14] also applied to the wave-shape a treatment derived[15] for an electrode process accompanied by dimerization, under the assumption that the first electron uptake is a reversible process.

This complex situation indicates a need for revision. In connection with our previous work on unsaturated ketones[9,16] and our present work on α,β-unsaturated aldehydes[17-19], in which it was confirmed[9,17,18] that the ethylenic linkage undergoes reduction prior to the carbonyl group, a further investigation of the electroreduction of the α,β-unsaturated ketones was carried out. These studies were prompted by the fact that α,β-unsaturated ketones were either used as reactant[20-22] or formed as products[23,24] in homogeneous reactions—such as hydrolysis of the double bond or elimination reactions of Mannich bases and similar compounds—that we have studied recently.

Chalcone was used as a model substance for our investigation because it was often used in our kinetic studies, because its reactivity towards hydroxyl ions is relatively low and its polarographic behaviour can be studied up to relatively high pH-values, and, finally, because for this compound the reduction product of the first

* The authors[14] do not distinguish between isomers and electromers.

two-electron step, dihydrochalcone, is a stable compound. This makes it possible to study its polarographic behaviour, to compare it with that of the more negative waves of chalcone and so investigate the reactions[9,10] by which the primary product of the two-electron reduction is transformed into dihydrochalcone, reducible in the consecutive step.

EXPERIMENTAL

Apparatus

Polarographic curves were recorded by means of the polarograph LP 60 (Laboratorní Přístroje, Prague) in connection with the recorder EZ2. Polarographic electrolyses were carried out in a Kalousek vessel with a separated saturated calomel electrode (SCE). Controlled-potential electrolyses were carried out in a H-type vessel according to Manoušek[25] for small volumes, enabling work in 0.5–1.0 ml of solution with an SCE separated by an agar bridge. The two capillaries used had out-flow velocities, $m = 3.2$ mg/sec and 1.34 mg/sec, and drop-times, $t_1 = 2.7$ sec and 5.0 sec at mercury pressure $h = 60$ cm in 0.1 M potassium chloride at the potential of SCE.

pH-values were measured with a glass electrode, type G 200B on a pH-meter PHM4 (Radiometer, København). The concentration of mercury vapours was measured by the Mercury Vapour Concentration Meter, type E 3472 (Hendray Relays Ltd.).

Substances and solutions

Chalcone used was a commercial product (Laboratorní Potřeby, Prague) recrystallised from ethanol. Dihydrochalcone (m.p. 71°) was prepared by B. Uchytil. Stock solutions of the electroactive species (0.002 M) were prepared by dissolving the substances in 96% ethanol. Buffers and supporting electrolytes used were prepared from AnalaR-grade chemicals.

Techniques of polarographic investigations

For polarographic examinations, 4 ml of the buffer were mixed with 0.5 ml of ethanol, and oxygen removed by a nitrogen stream; 0.5 ml of the 0.002 M stock solution of the electroactive compound was added to this solution and nitrogen was introduced for a short time and the polarographic curve recorded. In alkaline solutions, where hydration of chalcone takes place[20,21,23] and causes a change in polarographic curves with time, the recording of the curves was started within 20 sec after mixing.

Techniques of controlled potential electrolyses

Controlled-potential electrolysis was carried out with both a mercury pool electrode in about 50 ml of the solution, and a dropping mercury electrode in 0.5–1.0 ml of the solution. Because the results obtained with the mercury pool electrode differed from those obtained with the dropping mercury electrode and because current–voltage curves recorded with a mercury pool electrode were different from those obtained polarographically, further attention was restricted to electrolytic reductions with the dropping mercury electrode.

For electrolysis, 0.5–1.0 ml of $1–2 \cdot 10^{-4}$ M solution in the buffer solution

chosen were placed into the electrolytic cell and deaerated. To prevent re-diffusion of oxygen, nitrogen was introduced during electrolysis above the solution surface. To prevent contact of the dropped-off mercury with the electrolysed solution, the part of the electrolytic vessel above the vessel was narrowed. The level of the dropped-off mercury was kept constant by connecting the bottom of the cell with a mercury reservoir. Separation of the dropped-off mercury by means of a layer of chloroform or tetrachloromethane did not prove satisfactory, because chalcone dissolved in this layer and its wave-height in the aqueous phase altered.

The electrolysis was carried out at conditions (dropping electrode, reference electrode, concentrations) identical with those in polarography at the potentials of limiting currents at various pH-values. After chosen time-intervals, during electrolysis polarographic curves were recorded and the change in the wave-heights and their ratio measured.

The electrolysis products were identified polarographically. In these solutions, in which dihydrochalcone shows well-defined waves, it was possible to compare waves obtained directly in the electrolytic cell with those of dihydrochalcone under the same conditions. The electrolysis was carried out in solutions containing $5 \cdot 10^{-4}$ M chalcone until at least 90% conversion, in particular at pH < 7, where the waves of dihydrochalcone were ill-defined. The resulting solution was transferred into alkaline buffers and at several pH-values between pH 7 and 10 the waves of the electrolysis product were compared with those of dihydrochalcone.

To detect the presence of any product with a 1,2-diol grouping, the solution after electrolysis was treated with periodic acid. The time-change of periodate concentration was followed polarographically[26] by adjusting the pH of the solution to pH 4.7–5.0, and adding periodate solution so that its final concentration was twice to three times that of the original chalcone concentration. The decrease of the limiting current of periodic acid with time was followed in a darkened cell to eliminate the effect of light on the reaction. Dropped-off mercury was separated by a narrow part of the electrolytic cell and by a chloroform layer, which in this case does not interfere. No difference was found between the decrease in the height of the periodate wave in the presence of the electrolysed solution and in a blank without chalcone.

The precipitate, obtained in the electrolysis carried out at the potential of the limiting current of the first wave $(i_l)_1$ in solutions containing a higher concentration of chalcone ($1 \cdot 10^{-3}$ M) in 0.1 M hydrochloric acid with 50% ethanol, was separated and heated in a test tube. The vapours evolved were introduced into the inlet of the Mercury Vapour Concentration Meter. Alternatively, it was possible to heat the solution after electrolysis to boiling and to analyze the vapour.

RESULTS

Polarographic behaviour of chalcone

The first two-electron reduction step of chalcone is split into two one-electron steps, $(i_l)_1$ and $(i_l)_2$ (Figs. 1 and 2). The half-wave potential of wave $(i_l)_1$ is shifted to more negative values at pH < 10.6 by some 60 mV/pH; at pH > 10.6 it is pH-independent (Fig. 3).

Logarithmic analysis of the first one-electron wave, $(i_l)_1$, between pH 9 and 11 indicates that the wave is composed of two steps. The plot of $\log[(i_d - i)/i] - E$

shows two linear parts, the more negative increasing with increasing pH. Hence, of the two steps which in this region coalesce to form wave $(i_I)_1$, the more positive decreases and the more negative increases with increasing pH, but their half-wave potentials are so close that a separation of the two waves is not observed.

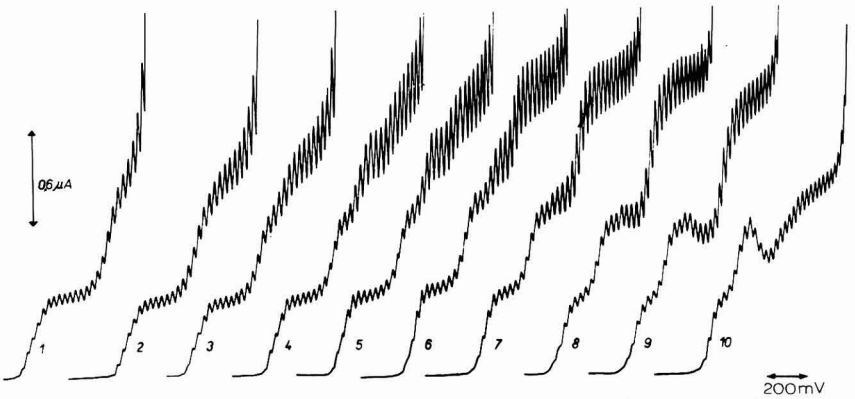

Fig. 2. Dependence of the reduction waves of chalcone on pH. $2 \cdot 10^{-4}$ *M* chalcone in Britton–Robinson buffers containing 20% ethanol. pH-values: (1), 2.37; (2), 5.2; (3), 5.93; (4), 6.88; (5), 7.2; (6), 7.82; (7), 8.42; (8), 9.57; (9), 10.3; (10), 12.1. Curves starting at: (1–2), −0.4; (3–7), −0.6; (8–10), −0.8 V *vs.* SCE capillary II.

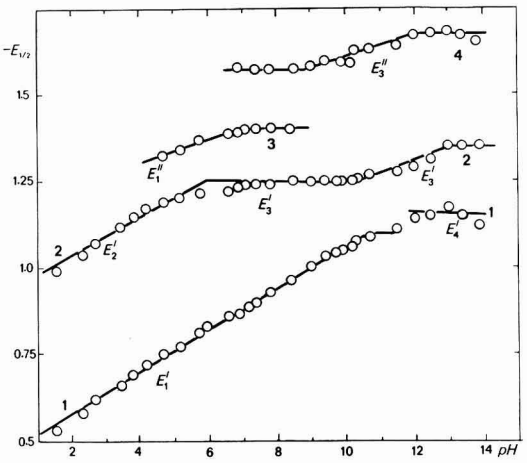

Fig. 3. Dependence of half-wave potentials of chalcone waves on pH. (1), $(i_I)_1$; (2), $(i_I)_2$; (3), $(i_{II})_1$; (4), $(i_{II})_2$.

The half-wave potentials of the second one-electron wave, $(i_I)_2$, is shifted at pH < 6 by some 60 mV/pH, and becomes pH-independent between pH 6 and 10.2. At pH > 10.2, the half-wave potential is shifted again by 40 mV/pH to more negative values (Fig. 3). The difference of about 450 mV between the half-wave potentials of waves $(i_I)_1$ and $(i_I)_2$ in acidic media (Table 1), and the pH-independence of wave $(i_I)_1$ at pH > 10.6 explain the separation of the two one-electron steps over the whole pH-range. Such a separation is rarely observed with other carbonyl compounds.

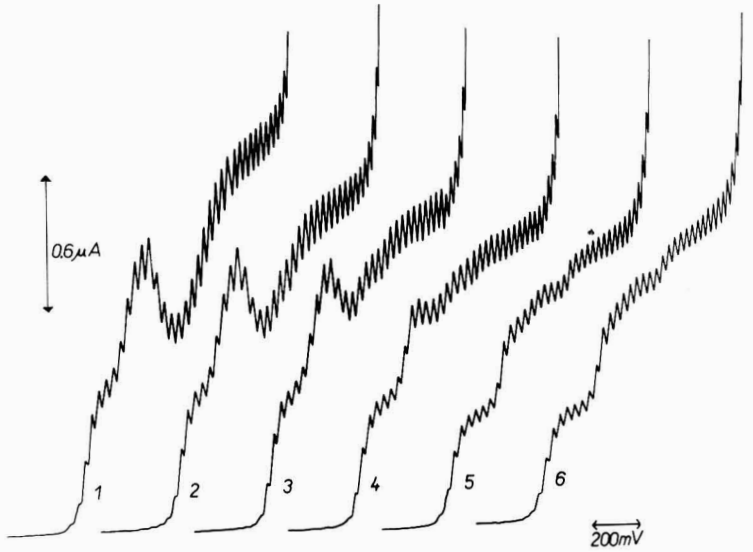

Fig. 4. Effect of hydroxide ions concn. on reduction waves of chalcone. $2 \cdot 10^{-4}$ *M* chalcone in LiOH containing 20% ethanol. (1), 0.01; (2), 0.03; (3), 0.08; (4), 0.2; (5), 0.5; (6), 0.8 *N* LiOH. Curves starting at −0.8 V *vs.* SCE capillary II.

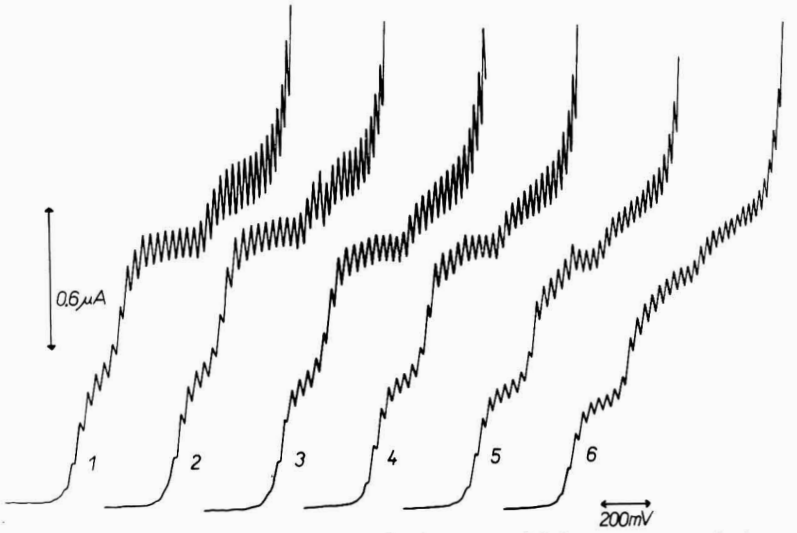

Fig. 5. Effect of hydroxide ions concn. on reduction waves of chalcone at constant ionic strength. $2 \cdot 10^{-4}$ *M* chalcone in LiOH and LiCl with $\mu = 0.8$, containing 20% ethanol. (1), 0.01; (2), 0.05; (3), 0.08; (4), 0.2; (5), 0.5; (6), 0.8 *N* LiOH. Curves starting at −0.8 V *vs.* SCE capillary II.

Above pH 11, the second reduction wave, $(i_l)_2$, shows a decrease (trough) on the limiting current, when the ionic strength is low (curve 10, Fig. 2, Fig. 4). When the ionic strength is adjusted to 0.8 by the addition of lithium or potassium chloride (Fig. 5), this decrease is eliminated. Above pH 13, the height of wave $(i_l)_2$ decreases with increasing pH, even when the ionic strength is kept constant.

TABLE 1

DEPENDENCE OF HALF-WAVE POTENTIALS OF CHALCONE WAVES ON pH

pH	$-E_{\frac{1}{2}}/V$ (SCE)				pH	$-E_{\frac{1}{2}}/V$ (SCE)			
	$(i_I)_1$	$(i_I)_2$	$(i_{II})_1$	$(i_{II})_2$		$(i_I)_1$	$(i_I)_2$	$(i_{II})_1$	$(i_{II})_2$
1.5	0.53	0.99	—	—	9.9	1.05	1.24	—	1.59
3.1	0.66	1.12	—	—	11.5	1.11	1.27	—	1.64
4.7	0.74	1.19	1.32	—	12	1.14	1.29	—	1.67
6.6	0.86	1.22	1.38	—	13	1.17	1.35	—	1.67
7.4	0.90	1.24	1.4	1.57	14	1.12	1.35	—	1.65
8.4	0.96	1.24	1.4	1.57					

At ionic strength 0.5 and higher, the ratio of wave heights, $(i_I)_1 : (i_I)_2$, is not strictly equal to one, wave $(i_I)_2$ being higher. This is due to maxima of the second kind at these high electrolyte concentrations at the limiting current of $(i_I)_2$.

The reduction that takes place in excess of the uptake of the first two electrons occurs also in two waves, $(i_{II})_1$ and $(i_{II})_2$. At pH < 4.6, wave $(i_{II})_1$ was not observed; at higher pH the total height of waves, $i_{II} = (i_{II})_1 + (i_{II})_2$, increases with increasing pH (Fig. 6). When i_{II} was less than 25% of the value corresponding to the two-electron

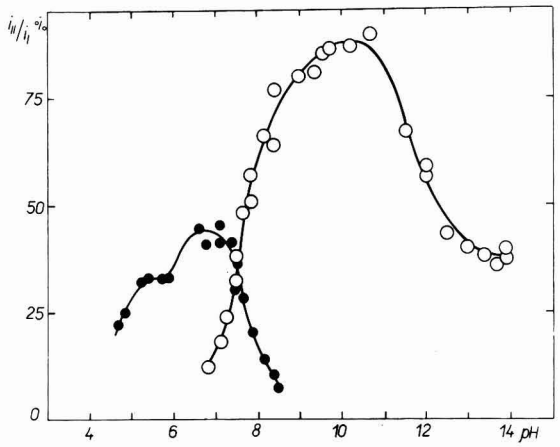

Fig. 6. Dependence of the limiting currents $(i_{II})_1$ and $(i_{II})_2$ of chalcone on pH. (●), $(i_{II})_1$; (○), $(i_{II})_2$. The limiting current i_I is 100%.

diffusion-governed process, its height was found to be independent of mercury pressure. This indicates that the total height of wave i_{II} is governed by the rate of an interposed chemical reaction. In the pH-region in which wave i_{II} was smaller than a two-electron diffusion current, its height increased with increasing buffer concentration. Furthermore, the shape of the plot of the dependence of the total limiting current of i_{II} on pH depends on the buffer kind and composition.

The ratio of waves, $(i_{II})_1 : i_{II}$, changes with increasing pH in the shape of a dissociation curve (Fig. 7); simultaneously, the height of wave $(i_{II})_2$ (expressed as a fraction of the total height, i_{II}) increases in the shape of a dissociation curve. The shape,

position and dependence on buffer composition for the $(i_{II})_1/i_{II}$–pH plot is exa the same as for the $i_1/(i_1+i_2)$–pH plot for dihydrochalcone and, similarly, the p of $(i_{II})_2/i_{II}$–pH for the chalcone wave is identical with the $i_2/(i_1+i_2)$–pH plot for hydrochalcone (p. 200). The shape of the observed dissociation curve depends ethanol concentration (Fig. 7). Measurements of wave-heights at various merc pressures indicated that the decrease of wave $(i_{II})_1$ and increase of $(i_{II})_2$ are gover by the rate of protonation reaction.

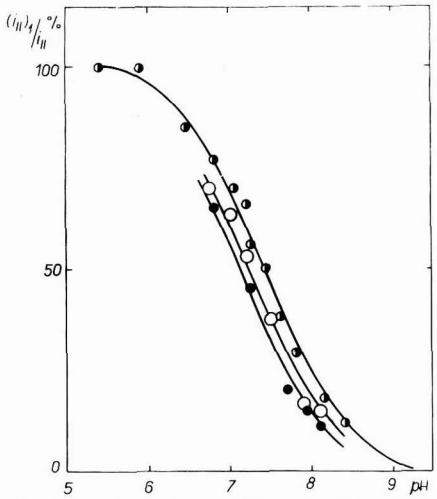

Fig. 7. pH-dependence of the ratio $(i_{II})_1 : i_{II}$, for the third wave of chalcone at various ethanol co (◑), 20; (○), 30; (●), 40% of ethanol.

The height of wave $(i_{II})_2$ reaches its limiting value corresponding to a t electron diffusion-controlled process at about pH 10. At pH > 11 the height of wave decreases in the shape of a dissociation curve until it reaches the value (corresponding to a one-electron process. Because the height of wave $(i_{II})'_2$ depend addition to pH, also on the kind and concentration of the cation in the suppor electrolytes, it proved best to use solutions containing lithium ions to obtain height $(i_{II})'_2$ approaching most closely at sufficiently high pH-values to the one-electron w All the changes in height with increasing pH and other properties of wave $(i_{II})_2$ w fully parallel to the variations observed for wave i_2 of dihydrochalcone in these alka media.

The half-wave potentials of wave $(i_{II})_1$ are shifted at pH < 6.9 by 35 mV/ and are pH-independent at higher pH-values. The half-wave potentials of wave (are pH-independent below pH 8.75 and shift at higher pH-values with increasing to more negative potentials by 37.5 mV/pH, and become pH-independent at pH > The half-wave potential of wave $(i_{II})_2$ is independent of ethanol concentration whe that of wave $(i_{II})_1$ is shifted at increasing ethanol concentrations to more nega potentials so that at concentrations higher than about 50% ethanol, waves $(i_{II})_1$ $(i_{II})_2$ coalesce. In the presence of 20% dimethylformamide, wave $(i_{II})_1$ was not obser and the height of wave $(i_{II})_2$ shows a less steep increase with increasing pH than in presence of 20% ethanol.

Controlled potential electrolysis of chalcone

When the electrolysis was carried out at the potential of the limiting current of the first wave, $(i_I)_1$, the logarithm of the limiting current was a linear function of time over the whole pH-range studied (pH 1–9.5) (Fig. 8). Decrease of wave $(i_I)_2$ was parallel to that of $(i_I)_1$. The change in the height of the wave of the second two-electron step, $i_{II} = (i_{II})_1 + (i_{II})_2$, depends on the pH-range in which the electrolysis at the limiting current $(i_I)_1$ was carried out. When the electrolysis was carried out at pH 9.2 where wave i_{II} is limited by diffusion, the height of wave i_{II} decreases regularly and the ratio, $i_I : i_{II}$, remains unchanged during electrolysis (where $i_I = (i_I)_1 + (i_I)_2$) (Fig. 9). When, on the other hand, the electrolysis was carried out at the potential of wave $(i_I)_1$ at pH 7.4

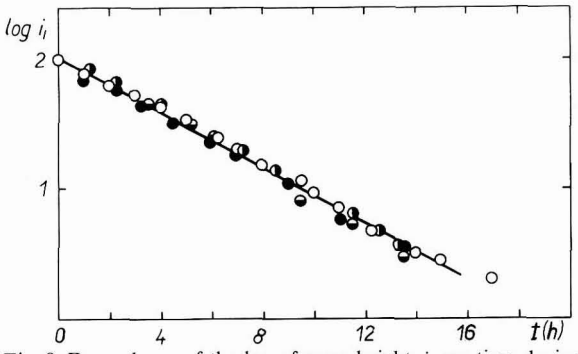

Fig. 8. Dependence of the log of wave height, i_l, on time during electrolysis of chalcone at various pH. (○), 0.1 *N* HCl; (◒), acetate buffer, pH 5; (◑), 0.1 *N* H_2SO_4; (●), borate buffer, pH 9.5. The wave height i_l before electrolysis is 100%.

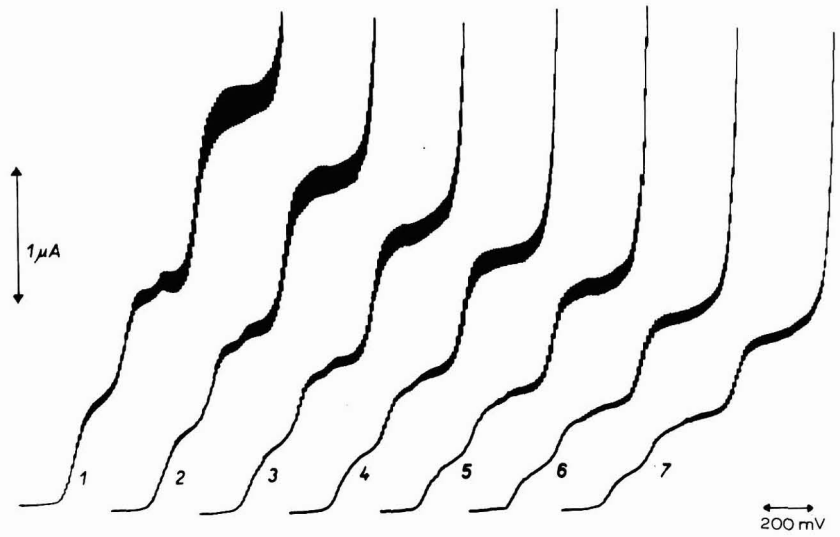

Fig. 9. Change in wave heights of chalcone during electrolysis. 1 ml $2 \cdot 10^{-4}$ *M* chalcone in borate buffer, pH 9.2, containing 20% ethanol. Electrolysed at the potential, −1.1 V corresponding to the limiting current of the first wave $(i_I)_1$. Time of electrolysis: (1), 0; (2), 1; (3), 2; (4), 3; (5), 4; (6), 5; (7), 6 h. Curves starting at −0.8 V *vs.* SCE capillary I.

where the height of wave i_{II} is kinetically-controlled, the height of wave i_{II} decreases in the course of electrolysis, but the ratio, $i_{II} : i_I$, increases with time (Fig. 10) as the proportion of wave i_{II} increases.

Apart from the electrolyses of chalcone described above in which the changes of polarographic waves during some few hours were followed, the controlled-potential

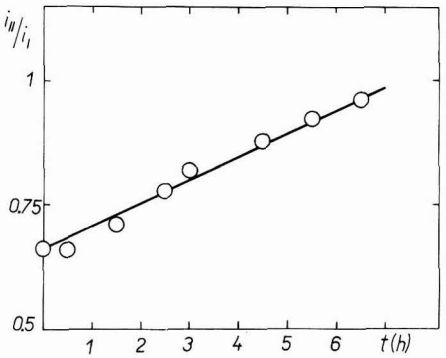

Fig. 10. Depencence of the ratio, $i_{II} : i_I$, for chalcone waves on time during electrolysis. Phosphate buffer, pH 7.4, containing 20% ethanol. Electrolysed at the potential, −1.0 V on the limiting current of the first one-electron wave $(i_I)_1$.

electrolysis using a dropping mercury electrode at the potential of the limiting current of $(i_I)_1$ was carried out also over prolonged periods, of thirty or more hours, until the height of wave $(i_I)_1$ decreased to less than 10% of the original height. Such electrolyses were carried out in 0.1 *M* hydrochloric acid and in acetate buffer pH 5. Because wave i_{II} was not apparent in any of these solutions, the solution after electrolysis was transferred into buffers pH 7–13, but in none of these solutions was any wave of the reduction product found, apart from the residual chalcone waves. This excludes the possibility of formation of (I) or (II):

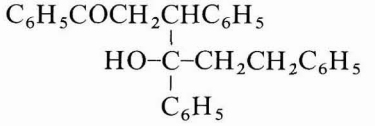

(II)

since the benzoyl grouping in compounds I and II would give a reduction wave, similar to that of acetophenone.

An aliquot of the solution after electrolysis was transferred into a periodate solution pH 4.7 and the change in the periodate limiting current with time was followed polarographically[26]. No difference was observed when compared with a blank. This excludes the possibility of formation of dimer III:

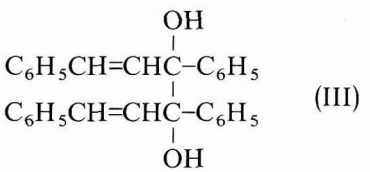

(III)

When the electrolysis at the potential of the limiting current of the first wave $(i_l)_1$ was carried out at a higher concentration of chalcone ($1 \cdot 10^{-3}$ *M*) in 0.1 *M* hydrochloric acid containing 50% ethanol (to increase the solubility of chalcone), the height of wave $(i_l)_1$ decreased with time. Simultaneously, a new wave, increasing directly from the dissolution of mercury, was formed the height of which increased with time only to a certain value and then remained constant. After prolonged electrolysis, a white precipitate was formed in the electrolysis cell. This precipitate was insoluble in ethanol, but soluble in ethyl cellosolve, where it gave a reduction wave increasing at positive potentials directly from the mercury dissolution, and small waves at more negative potentials attributed to residual chalcone absorbed on the precipitate.

The precipitate was separated and heated in a test tube. The vapours evolved were brought to the inlet of the Mercury Vapour Concentration Meter. The deflection corresponded to 200 μg of mercury/1 m^3 of air; the blank was below 10 μg of mercury/1 m^3 of air. The precipitate need not be separated, the detection of mercury is possible even when the solution after electrolysis is heated to boiling and the vapour analyzed. In all cases of solutions between pH 1 and 9.2 electrolysed at the limiting current of wave $(i_l)_1$, 150–200 μg mercury/1 m^3 was observed; only for acetate buffer pH 5.0 was 100 μg mercury/1 m^3 obtained. Electrolysis at the limiting current of the two-electron wave $(i_l)_2$ used as blank, gave a value below 10 μg/1 m^3. These results indicate the formation of an organomercury compound in the reaction between the radical and metallic mercury.

When the electrolysis was carried out at the limiting current of wave $(i_l)_2$, decrease of waves $(i_l)_1$ and $(i_l)_2$ was regular. The change in the height of wave i_{II} was found to depend on the process governing the height of this wave. At pH 9.9, where wave i_{II} is governed by diffusion and its height is the same as that of an equimolar solution of dihydrochalcone at the same conditions, the height of wave i_{II} does not change during the electrolysis. On the other hand, when the electrolysis was carried out in the pH-region in which the overall height of wave i_{II} is controlled by the rate of the interposed chemical reaction, such as at pH 5.8 (Fig. 11) or pH 7.4, an increase

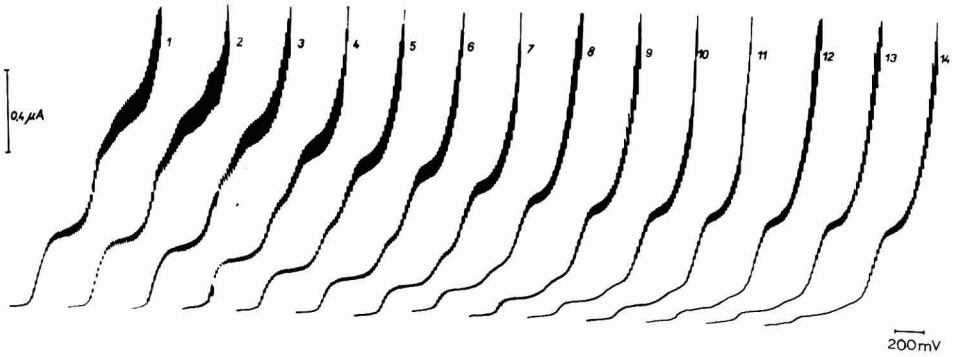

Fig. 11. Change of wave heights of chalcone during electrolysis. 1 ml $2 \cdot 10^{-4}$ *M* chalcone in Britton–Robinson buffer, pH 5.8, containing 20% ethanol. Electrolysed at the potential, −1.24 V corresponding to the potential of the second one-electron wave $(i_l)_2$. Time of electrolysis: (1), 0; (2), 0.5; (3), 1; (4), 2; (5), 3; (6), 4; (7), 5; (8), 6; (9), 7; (10), 8; (11), 9; (12), 10; (13), 11; (14), 12 h. Curves starting at −0.6 V *vs.* SCE capillary I.

in the height of dihydrochalcone i_{II} was observed in the course of electrolysis. Wave i_{II}, which before the electrolysis was considerably smaller than the corresponding wave of dihydrochalcone, practically reached its height after the electrolysis had been carried out to more than 90% conversion.

The controlled-potential electrolysis product of the two-electron step has been proved to be dihydrochalcone (IV) over the whole pH-range.

When the electrolysis was carried out at the limiting current of wave $(i_{II})_1$ at pH 5.8, the total wave-height, similarly as in the previous case, decreased with the time of electrolysis, and also the height of $(i_{II})_1$ increased relative to i_I (Fig. 12). Comparison of Figs. 11 and 12 indicates that when the electrolysis is carried out at the limiting current of $(i_{II})_1$, wave i_{II} does not remain constant, but shows a decrease with time until it finally disappears. An analogous picture was observed when the electro-

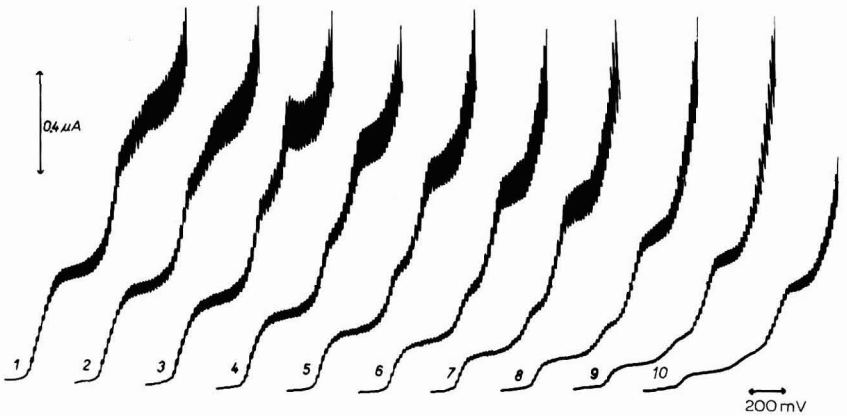

Fig. 12. Change of wave heights of chalcone during electrolysis. 1 ml $2 \cdot 10^{-4}$ *M* chalcone in Britton–Robinson buffer, pH 5.8, containing 20% ethanol. Electrolysed at the potential -1.5 V at the final limiting current $(i_{II})_1$. Time of electrolysis: (1), 0; (2), 0.5; (3), 1; (4), 2; (5), 3; (6), 4; (7), 5; (8), 6; (9), 8; (10), 10 h. Curves starting at -0.6 V *vs.* SCE capillary I.

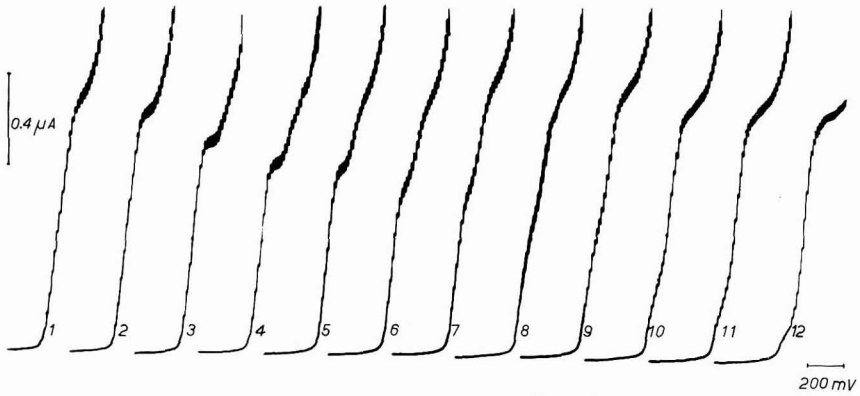

Fig. 13. pH-dependence of wave of dihydrochalcone. $2 \cdot 10^{-4}$ *M* dihydrochalcone in phosphate buffer of constant ionic strength, $\mu = 0.15$, containing 20% ethanol. pH-values: (1), 5.37; (2), 5.93; (3), 6.17; (4), 6.5; (5), 6.75; (6), 6.96; (7), 7.13; (8), 7.3; (9), 7.5; (10), 7.7; (11), 8.07; (12), 8.6. Curves starting at -1.0 V *vs.* SCE capillary I.

lysis was carried out at pH 7.2, where waves $(i_{II})_1$ and $(i_{II})_2$ coexist. For the observed change in the polarographic waves during electrolysis under these conditions it was of little importance whether the electrolysis was carried out at the limiting current of wave $(i_{II})_1$ or $(i_{II})_2$.

The electrolysis at the potential of the limiting current of $(i_{II})_2$ at pH 10 has shown a simple decrease of all waves i_I and i_{II} in a practically constant ratio.

Polarographic reduction of dihydrochalcone(IV)

Polarographic reduction of dihydrochalcone(IV) follows the reduction paths described for aryl–aryl ketones in Part I of this series[27] and shows in acidic media two separated one-electron reduction waves, $(i_1)_a$ and $(i_1)_b$, which merge into a two-electron wave, i_1, at about pH 5 (as shown schematically in Fig. 2. ref. 27). Simultaneously, the total height of wave i_1 starts to decrease with increasing pH and another more negative wave, i_2, appears (Fig. 13). Decrease of wave i_1 (or increase of wave i_2) has the shape of a dissociation curve, provided that in buffer series the concentration of the base component of the buffer is kept constant. Moreover, the position of the dissociation curve on the pH-axis depends on the concentration of the base buffer component chosen, in a similar way as was found for deoxybenzoins and as was predicted by the theory[28].

At pH >9 a decrease in the height of wave i_2 with increasing pH was observed until at about pH 12 the height of wave i_2 reached the value corresponding to a one-electron diffusion process. The wave at higher pH-values was accompanied by a pre-wave which was shown[29] to correspond to a change in the capacity current,

$C_6H_5COCH_2CH_2C_6H_5$ (IV)

caused by desorption of the oxidized form of the ketone (IV). This change in the capacity current occurs in the potential region in which the decrease (a trough) was observed at pH >9 on the limiting current of $(i_I)_2$ of chalcone (p. 202). At pH 10.2, an increase in ethanol concentration suppressed the pre-wave (because of competitive adsorption) and increased wave i_2 (Fig. 14).

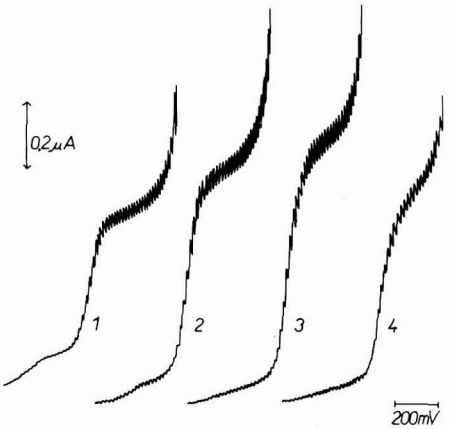

Fig. 14. Dependence of wave height of dihydrochalcone on ethanol concn. $2 \cdot 10^{-4}$ *M* dihydrochalcone in borate buffer, pH 10.2, containing: (1), 20; (2), 30 (3), 40; (4), 50% ethanol. Curves starting at -1.2 V *vs.* SCE capillary I.

TABLE 2

DEPENDENCE OF HALF-WAVE POTENTIALS OF DIHYDROCHALCONE WAVES ON pH

pH	$-E_{\frac{1}{2}}/V$ (SCE)			pH	$-E_{\frac{1}{2}}/V$ (SCE)		
	$(i_1)_a$	$(i_1)_b$	i_2		$(i_1)_a$	$(i_1)_b$	i_2
2.5	1.11	—	—	9.4			1.58
4.7	1.25	1.38	—	10.0			1.60
5.4	1.33		—	11.5			1.64
6.5	1.38		1.56	12			1.65
7.5	1.42		1.56	13			1.65
8.6	1.42		1.56	14			1.65

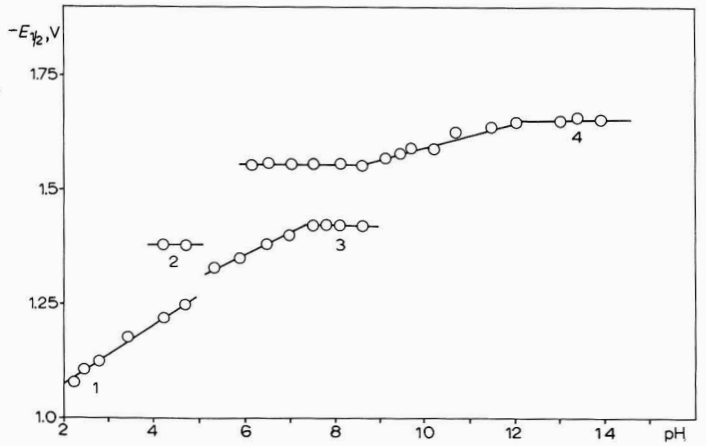

Fig. 15. Dependence of half-wave potentials of dihydrochalcone waves on pH. (1), $(i_1)_a$; (2), $(i_1)_b$; (3), i_1; (4), i_2.

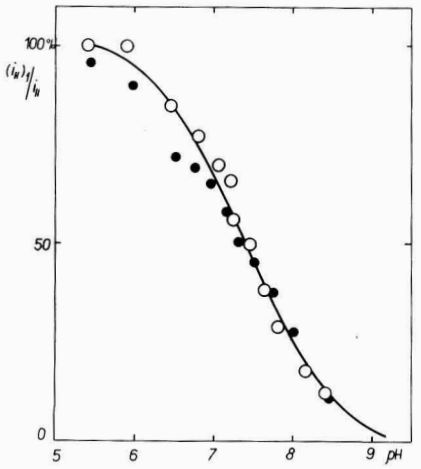

Fig. 16. Comparison of the dissociation curves of third wave of chalcone, $(i_{II})_1$ and the first wave of dihydrochalcone, i_1. (○), chalcone; (●), dihydrochalcone.

The half-wave potentials (Table 2) of the first one-electron wave $(i_1)_a$ were shifted to more negative potentials by some 60 mV/pH; those of wave $(i_1)_b$ were pH-independent. The half-wave potentials of the combined wave, i_1, are shifted between pH 5.2 and 7.0 by some 40 mV/pH and are pH-independent at pH > 7. The half-wave potentials of wave i_2 are pH-independent at pH 6–8.75 (Fig. 15) and are shifted to more negative potentials between pH 8.75 and 12 by some 30 mV/pH; at pH > 12 they are pH-independent.

The half-wave potentials of wave i_1 for dihydrochalcone were found identical, within ± 10 mV, in their value and pH-dependence with that observed for wave $(i_{II})_1$ of chalcone, and those of wave i_2 of ketone IV with that of wave $(i_{II})_2$ of chalcone (comparison of Figs. 3 and 15). In all instances where dihydrochalcone was added to chalcone solutions, waves $(i_{II})_1$ and $(i_{II})_2$ increased in the expected proportions. The plot of the change in the ratio, $i_1 : i_2$, with increasing pH (in a series of buffers with constant base buffer component concentration) was identical with the dissociation curve obtained with chalcone for the ratio, $(i_{II})_1 : (i_{II})_2$, in the same series of buffers (Fig. 16).

DISCUSSION

Polarographic reduction of chalcone occurs in principle in two two-electron steps, i_I and i_{II}. The overall process can be formulated by scheme (A)–(U):

$\underbrace{\mathrm{ArCOCH{=}CHAr}}_{\mathrm{H^+}}$	$\overset{k_1}{\underset{k_{-1}}{\rightleftharpoons}}$	$\mathrm{ArCOCH{=}CHAr + H^+}$	$\mathrm{p}K_1$	(A)
$\underbrace{\mathrm{ArCOCH{=}CHAr} + e}_{\mathrm{H^+}}$	$\xrightarrow{E_2^1}$	$\mathrm{ArCO\dot{C}HCH_2Ar}$	$(i_I)_1$	(B)
$\mathrm{ArC(OH^+)\dot{C}HCH_2Ar}$	$\overset{k_2}{\underset{k_{-2}}{\rightleftharpoons}}$	$\mathrm{ArCO\dot{C}HCH_2Ar + H^+}$	$\mathrm{p}K_2$	(C)
$2\,\mathrm{ArC(OH^+)\dot{C}HCH_2Ar}$	$\xrightarrow{k_3}$	Dimer		(Da)
$2\,\mathrm{ArCO\dot{C}HCH_2Ar}$	$\xrightarrow{k_4}$	Dimer		(Db)
$\mathrm{ArC(OH^+)\dot{C}HCH_2Ar + Hg}$	$\longrightarrow$	Mercury compound		(Dc)
$\mathrm{ArCO\dot{C}HCH_2Ar + Hg}$	$\longrightarrow$	Mercury compound		(Dd)
$\mathrm{ArC(OH^+)\dot{C}HCH_2Ar + solvent}$	$\longrightarrow$	Product		(De)
$\mathrm{ArCO\dot{C}HCH_2Ar + solvent}$	$\longrightarrow$	Product		(Df)
$\mathrm{ArC(OH^+)\dot{C}HCH_2Ar} + e$	$\xrightarrow{E_2^1}$	$\mathrm{ArC(OH^+)\bar{C}HCH_2Ar}$	$(i_I)_2$	(E)
$\mathrm{ArCO\dot{C}HCH_2Ar} + e$	$\xrightarrow{E_3^1}$	$\mathrm{ArC(O)\bar{C}HCH_2Ar}$	$(i_I)_2$	(F)

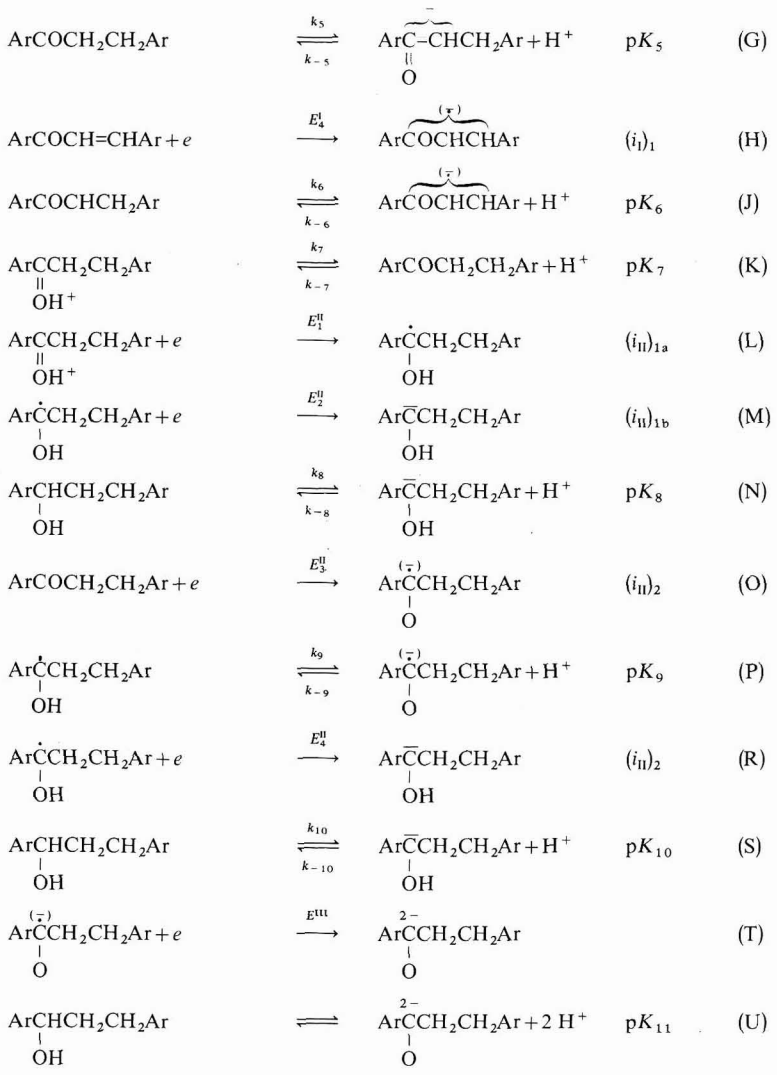

The reaction of chalcone in the first two-electron step, $(i_I)_1 + (i_I)_2$, produces as the final product a saturated ketone, dihydrochalcone (IV). This has been proved by comparison of the half-wave potentials of waves $(i_{II})_1$ and $(i_{II})_2$ (Fig. 3) over a wide pH-range with those (i_1, i_2) of authentic dihydrochalcone (Fig. 15). Half-wave potentials of wave $(i_{II})_1$ were found identical in values and pH-dependence with those of wave i_1, and those of wave $(i_{II})_2$ with those of i_2. Furthermore, the change of wave-heights with pH were analogous: the ratio $i_1 : i_2$ changed with pH exactly in the same way as $(i_{II})_1 : (i_{II})_2$ (Fig. 16).

Further evidence for the formation of dihydrochalcone was obtained from the controlled-potential electrolysis at the potential corresponding to the limiting current of wave $(i_I)_2$. No side products were detected and all identification techniques used indicated that the final product of the two-electron reduction step is dihydro-

chalcone. The conversion of chalcone to dihydrochalcone was found to be quantitative during prolonged electrolysis even under conditions (pH 4.5–8) where chalcone gave waves $(i_{II})_1$ and $(i_{II})_2$ at the same potentials and showing the same ratio of wave-heights as the dihydrochalcone waves i_1 and i_2, but where the wave $(i_{II})_1$ and $(i_{II})_2$ were considerably smaller. This behaviour indicates that, over this pH-region, dihydrochalcone is not the primary electrolysis product, but is formed from the primary product by a chemical reaction in the solution.

In acidic media, the reduction of chalcone in the first two-electron step at pH < 5 follows the sequence: proton, electron, proton, electron (H^+, e, H^+, e), as described by the scheme (A)–(E). This is indicated by the shift of both waves, $(i_I)_1$ and $(i_I)_2$, at potentials E^I_1 and E^I_2, with pH in this region, corresponding to acid–base equilibrium (A) and (C) (with $pK''_2 = 6.0$) preceding the electron transfers (B) and (E). The pre-protonation equilibrium (A) is rapidly established over this entire pH-range and equilibrium (C) below pH 4. In the pH-range 4–6, where the rate of establishment of equilibrium (C) is lower, separation of the two waves was not observed, because the potentials of the protonated form, E^I_2, and of the unprotonated radical, E^I_3, lie so close together that no separation of waves is observed.

At present it is not clear whether the protonation in step (A) takes place preferentially on the carbonyl group or on the ethylenic bond. For the sake of simplicity, the latter was chosen in the formulation of the product of reaction (B); nevertheless, the radical, $ArCO\dot{C}HCH_2Ar$, cannot be distinguished from $Ar\dot{C}(OH)CH{=}CHAr$, which would participate in reactions (Db), (Dd), (Df) and (F). If the protonation (A) takes place preferentially on the carbonyl group, equilibrium (C) would be considered in the form (Ca) followed by analogous reactions (D) and (Ea):

$$Ar\dot{C}\underbrace{CH{=}CHAr}_{OH \quad H^+} \rightleftharpoons Ar\dot{C}\underset{OH}{CH{=}CHAr} + H^+ \qquad pK_{2a} \qquad (Ca)$$

$$Ar\dot{C}\underbrace{CH{=}CHAr}_{OH \quad H^+} + e \xrightarrow{E^I_{2a}} Ar\underbrace{C{=}CH{=}CHAr}_{OH \quad H^+} \qquad (i_I)_2 \qquad (E_a)$$

Since the saturated ketone is obtained as the final product, this path seems to be less probable.

In the pH-region between pH 7 and 9, the reduction in the first two-electron step follows the sequence: proton, electron, electron, proton (H^+, e, e, H^+). This corresponds to the scheme: (A), (B), (D), (F), in accordance with the pH-dependence of wave $(i_I)_1$ at potential E^I_1 caused by the protonation (A) antecedent to the electron transfer (B). The pH-independence of the half-wave potential of the second wave $(i_I)_2$, here denoted as E^I_3, indicates that no proton transfer takes place between the acceptance of the first electron in (B) and of the second in (F).

In the pH-region between 11 and 13, the reduction is considered to follow the sequence: electron, proton, electron, proton (e, H^+, e, H^+) corresponding to the scheme: (H), (J), (F), (G). This is indicated by the pH-independence of the half-wave potential, E^I_4, the change in the logarithmic analysis of wave $(i_I)_1$ (p. 200) and by the change in the slope of the half-wave potential of wave $(i_I)_2$.

Above pH 8, the rate of the surface protonation (A) with rate constant, k_{-1}, becomes too slow to transform all of the chalcone into the protonated form. At pH

9–11, simultaneous reduction of the protonated and unprotonated form of chalcone occurs, with the proportion of the unprotonated increasing with increasing pH, as shown by the trend in the logarithmic analysis. At pH > 11.5, practically only the unprotonated form is reduced. Nevertheless, because potentials E_1^{I} of the protonated form, and E_4^{I} of the unprotonated form in this pH-range are little different, a separation of two waves, $(i_{\mathrm{l}})_{1\mathrm{a}}$ and $(i_{\mathrm{l}})_{1\mathrm{b}}$, cannot be observed even when the pH-dependence of the half-wave potentials indicates two waves. Intersection on the E_1–pH plot ($\mathrm{p}K_1'' =$ 10.6) and the value of pH, at which both linear parts on the logarithmic plot were equal ($\mathrm{p}K_1' = 10$) lie close together.

Intersection of the two linear parts on the E_3^{I}-pH plot for the second one-electron wave $(i_{\mathrm{l}})_2$ was found at pH = 10.2. This wave, $(i_{\mathrm{l}})_2$, corresponds to the reduction of the radical, $\mathrm{ArCO\dot{C}HCH_2Ar}$, in step (F) which is formed from the radical anion in the rapidly established equilibrium (J). The inverted L-shaped dependence indicates that the intersection at pH 10.2 corresponds to the true value of the dissociation constant, $\mathrm{p}K_6 = 10.2$.

According to the scheme (A)–(J), the half-wave potential of wave $(i_{\mathrm{l}})_1$ at pH > 11.6 should be pH-independent, (E_4^{I}). Small variations observed experimentally are attributed to specific cation effects on the double-layer composition, as with the small shifts of the theoretically pH-independent half-wave potentials of wave $(i_{\mathrm{l}})_2$ at pH 5–7.

As has been proved in detail for cinnamaldehyde[17,18], where the waves of the radical, $\mathrm{HCO\dot{C}HCH_2Ar}$, and the ketyl, $[\mathrm{HCOCHCHAr}]\dot{\mathrm{M}}\mathrm{e}$ (where Me is a metal cation), are separated, the radical anion formed in reduction (H) can react not only with hydronium ions, but also with alkali metal cations, according to the reaction (Ja):

$$\mathrm{Ar}\underbrace{\overbrace{\mathrm{COCHCH}}^{\cdot}}_{\mathrm{Me}}\mathrm{Ar} \underset{k_{-\mathrm{M}}}{\overset{k_{\mathrm{M}}}{\rightleftharpoons}} \mathrm{Ar}\overbrace{\mathrm{COCHCH}}^{(\dot{-})}\mathrm{Ar} + \mathrm{Me}^+ \qquad \mathrm{p}K_{\mathrm{M}} \qquad \text{(Ja)}$$

$$\mathrm{Ar}\underbrace{\overbrace{\mathrm{COCHCH}}^{\cdot}}_{\mathrm{Me}}\mathrm{Ar} + e \xrightarrow{E_{\mathrm{M}}} \mathrm{Ar}\overbrace{\underset{\underset{\mathrm{O}}{\|}}{\mathrm{C}}{=}\mathrm{CH}{=}\mathrm{CH}}^{2-}\mathrm{Ar} + \mathrm{Me}^+ \qquad i_{\mathrm{M}} \qquad \text{(Fa)}$$

In the case of chalcone, potentials E_3^{I} and E_{M} are so close together that no separate wave, i_{M}, is formed and only one wave, $(i_{\mathrm{l}})_2$, is observed. With increasing metal ion concentration, as follows from a comparison of Figs. 4 and 5, the height of wave $(i_{\mathrm{l}})_2$ at a given hydroxyl ion concentration increases with metal cation concentration. The impossibility of separating currents $(i_{\mathrm{l}})_2$ and i_{M} prevented quantitative treatment of equilibrium (Ja). The effect of the cation increased with increasing cation size.

With increasing concentration of lithium hydroxide, a decrease of the height of wave $(i_{\mathrm{l}})_2$ was observed at constant ionic strength, above pH 13. In this pH-region, the conversion of the radical anion into both the radical and ketyl was no longer fast enough to convert all the radical anion into the more easily reducible form. The reduction waves of the radical anion at more negative potentials $(i_{\mathrm{l}})_3$ are usually ill-developed (Figs. 4, 5) and correspond to process (Ha), (Hb):

$$\overbrace{\mathrm{ArCOCHCHAr}}^{(\dot{-})} + e \rightarrow \overbrace{\mathrm{ArCOCHCHAr}}^{2-} \qquad (i_l)_3 \qquad \text{(Ha)}$$

$$\mathrm{ArCOCH_2CH_2Ar} \rightleftharpoons \overbrace{\mathrm{ArCOCHCHAr}}^{2-} + 2\,\mathrm{H^+} \qquad \text{(Hb)}$$

The dip on the limiting current of $(i_l)_2$ indicates that the reactions (J) and (Ja) with rate constants K_{-6} and K_{-M} furnishing the radical or ketyl, are surface rather than volume reactions[30]. The dip depends on the double-layer composition, as is shown by its elimination with increasing neutral salt concentration (Figs. 4 and 5). The rate of formation of the radical or ketyl is decreased with increasingly negative potential. This can be interpreted either by desorption of the reacting radical anion from the electrode surface or by the effect of double-layer on the rate constant. The effect of adsorption–desorption phenomena seems to be indicated by the fact that the dip on the limiting current of wave $(i_l)_2$ occurs in the potential region in which desorption of dihydrochalcone (*i.e.*, the product formed in wave $(i_l)_2$) occurs[29].

The radical formed in the reduction at the limiting current of wave $(i_l)_1$ can undergo various chemical reactions, some of them indicated as (Da)–(Df). Dimerisation was assumed to take place in earlier studies[1-8,10] either without any proof or by means of mercury pool electrolysis. Of the three main types of possible dimers, (I)–(III), compounds I and II contain a benzoyl grouping and can be expected to be electroactive and give reduction waves not too different from dihydrochalcone (*i.e.*, at potentials similar to those of waves $(i_{II})_1$ and $(i_{II})_2$). The third dimer III, on the other hand, can be expected to be electroinactive in the potential range available.

When controlled-potential electrolysis is carried out at the potential corresponding to the limiting current of wave $(i_l)_1$, the formation of dimers of type I or II would be expressed either by the formation of a new wave or by the total height of wave i_{II} remaining unchanged. No formation of a new wave was observed and in the pH-range where the height of wave i_{II} was limited by diffusion, its height decreased regularly (Fig. 9). Hence, the formation of dimers I and II as the path for deactivation of the radical formed can be ruled out.

The absence of reactivity of the product formed at the limiting current of wave $(i_l)_1$ at the dropping mercury electrode in the periodate reaction excludes the formation of dimer III.

Increase in current at positive potentials and the proof of mercury in the product isolated and in the solution after electrolysis, indicate that an organomercury compound is formed. Limited solubility and reduction at positive potentials offer an explanation why this product was not observed from the change in polarographic waves. It can be concluded that formation of an organomercury compound of type (Dc) and (Dd) is the predominant path for deactivation of the electrolytically-formed radical in the first reduction step of chalcone, similarly as has been proved for methyl vinyl ketone[31] and for cinnamaldehyde[17,18].

The reduction of dihydrochalcone formed in the first two-electron step takes place in two waves, $(i_{II})_1$ and $(i_{II})_2$, and follows scheme (L)–(U) and is preceded by two chemical reactions, the rate of which is pH-dependent. First, the overall height of the second two-electron process, $(i_{II})_1 + (i_{II})_2$, is governed by the rate of the general acid–base catalysed reaction (G) in which the carbanion-enolate formed in the first two-electron step is transformed into dihydrochalcone. Secondly, the ratio of waves,

$(i_{II})_1 : (i_{II})_2$, is governed by the rate of protonation of dihydrochalcone in reaction (K) with rate constant k_{-7}.

The increase of wave i_{II} during the electrolysis at potentials of the limiting currents of wave $(i_I)_2$ or $(i_{II})_1$ (Figs. 11 and 12) indicates the presence of a chemical reaction interposed between electrolytic steps (F) and (L) or (O). The same interpretation was supported by the kinetic character of wave i_{II} when small. It is assumed that the rate-governing step is the formation of dihydrochalcone from the carbanion-enolate in step* (G) with rate constant, k_{-5}. The application of theoretical treatments**[32,33] for calculation of rate constant, k_{-5}, from the dependence of wave i_{II} on pH, buffer kind and concentration, was only partly successful. A good agreement was found between the theoretical and experimental shape of the pH-dependence of the total wave-height, i_{II}. At a given pH, the formal rate constant found has shown the predicted dependence on buffer concentration. The specific rate constants obtained have shown a dependence on the nature of the base buffer component corresponding to the Brønsted equation, but the calculated value of the rate constant changed with drop-time showing that the theoretical treatment is incomplete. As analogous behaviour was observed for other systems involving interposed reactions, such as *p*-nitrophenol[34], *p*-diacetylbenzene[34] and cinnamaldehyde[18], it seems that the theoretical treatment of interposed reactions needs a general revision.

The rate of protonation (K) with rate constant k_{-7} governs the ratio of wave-heights, $(i_{II})_1 : (i_{II})_2$, in a similar way as it governs the ratio, $i_1 : i_2$, in dihydrochalcone (Fig. 16). Thus, rate of protonation of dihydrochalcone (K) is not affected by the previous reduction and the transformation of the ambident carbanion-enolate ion into dihydrochalcone.

Reduction of the protonated form of dihydrochalcone below pH 4 in waves $(i_I)_{1a}$ and $(i_I)_{1b}$ (or i_{1a} and i_{2a}) follows the sequence: (G), (K)–(N). In this region, the potential of wave i_{1a} is shifted with pH because reduction (L) is preceded by protonation (K); that of wave i_{1b} is pH-independent, showing that between electron-transfers (L) and (M) no proton transfer takes place. The sequence of steps in this pH-range therefore corresponds to: proton, electron, electron, proton (H^+, e, e, H^+). Above pH 5, the half-wave potentials of waves i_{1a} and i_{1b} are so close together that only one, two-electron wave is observed, corresponding to the scheme (G), (K)–(N).

At about pH 8, the rate of protonation (K) is small and the rate of ketone

---

* Enol formation is a competitive reaction with the formation of dihydrochalcone. No quantitative information is available about the keto–enol equilibrium in the system:

$$\mathrm{ArCOCH_2CH_2Ar} \underset{k_{-5}}{\overset{k_5}{\rightleftharpoons}} \mathrm{Ar\widetilde{C(O)-CH}CH_2Ar} + \mathrm{H^+} \qquad pK_5 \qquad \text{(G)}$$

$$\mathrm{ArC(OH)=CHCH_2Ar} \underset{k_{-E}}{\overset{k_E}{\rightleftharpoons}} \mathrm{Ar\widetilde{C(O)-CH}CH_2Ar} + \mathrm{H^+} \qquad pK_E \qquad \text{(Ga)}$$

Nevertheless, it can be assumed that the keto–enol equilibrium is shifted in favour of the keto form and thus $pK_5 \gg pK_E$. Consequently, the competitive enol formation can be expected to play a role, particularly at lower pH-values.

** Both treatments by Kastening[32] and Nicholson[33] give exactly the same shape for the pH-dependence of the limiting current.

formation (G) is large. Reduction in the step $(i_{II})_2$ or i_2 follows the sequence (O)–(S). The half-wave potential of E_4^{II} is more positive or equal to E_3^{II} and hence only one, two-electron wave, i_2, is observed. Below pH 8.75, the half-wave potential of wave i_2 is independent and hence either reaction (O) is potential-determining or equilibrium (P) is in this pH-range completely shifted to the left-hand side.

In the intermediate range between pH 6 and 8, processes (K)–(N) and (O)–(S) are competitive and two waves, i_1 and i_2, are observed on the polarographic curves of dihydrochalcone. Their ratio is governed by the rate of reaction (K) with rate constant k_{-7}. The inflexion point of the pH-dependence of wave i_1 ($pK'_7 = 6.6$) is in good agreement with the intersection of the two linear parts of the E^{II}–pH plot ($pK'' = 6.9$). The thermodynamic constant, K_7, is not accessible and therefore the calculation of the rate constant, k_{-7}, from polarographic data is not possible. Because it can be assumed that $pK_7 < 0$, it can be deduced that reaction (K) occurs predominantly as a surface reaction.

Acids other than hydronium ion can participate in the protonation (K). This was shown by the shape of the pH-dependence of the limiting current of i_1 which was in agreement with the theory[28], and by its dependence on buffer kind and concentration.

The shifts of half-wave potentials of wave i_2 at pH > 8.75 indicate the presence of an acid–base equilibrium which is rapidly established at pH < 11, and comparable with the rate of electrolysis at pH > 11. This indicates participation of an acid–base equilibrium with a thermodynamic $pK_9 = 8.75$ antecedent to the potential-determining step. The reaction involved can be either dissociation of dihydrochalcone to form the carbanion, $ArCOCHCH_2Ar^-$, antecedent to the uptake of the first electron, or equilibrium (P) antecedent to the uptake of the second electron. The pK-value of the carbanion formation would be expected at pH > 12, but not at pK 8.75. On the other hand, pK-values of other radical anions are observed at pH < 10, therefore the attribution of $pK_9 = 8.75$ and the potential-determining step to (R) seems plausible.

Above pH 11, a decrease in the height of wave i_2 is observed and this decrease from a two-electron to a one-electron wave has the shape of a dissociation curve. The inflexion point of this curve is in agreement with the break-point on the E_3^{II}-pH plot ($pK'' = 11.8$). The current i_2 is, in this pH-region, governed by the rate of protonation (P) with rate constant k_{-9}. This interpretation is in accordance with the explanation of the shifts of half-wave potentials of wave i_2 given in the preceding paragraph. The reduction of the radical anion in steps (T) and (U) occurs at such negative potentials (E^{III}) that the corresponding reduction wave (i_3) was not distinguished.

α,β-Unsaturated ketones, that bear a phenyl group adjacent to the carbonyl group (such as phenyl vinyl ketone[9]) or those which have neutral heterocyclic ring[5,10] adjacent to the carbonyl group are expected to behave in an analogous manner to chalcone. Also, those chalcone derivatives that have a substituent which is electroinactive and does not undergo protonation (NH_2 or OH groups) are expected to behave similarly.

Information on acid–base reactions in system (A)–(U) are summarised in Table 3.

On the other hand, differences are shown by those α,β-unsaturated ketones that have a basic heterocyclic ring (such as pyridine[10,35] or quinoline[11]) or an alkyl group (as in benzalacetone[20]) adjacent to the carbonyl group. Consecutive reductions

TABLE 3

SUMMARY OF DATA ON ACID–BASE REACTIONS

Acid form	*Process*	pK^a	pK'^b	pK''^c
$ArCOCH{=}CHAr$ (under H^+)	(A)	—	$pK'_1 = 10$	$pK''_1 = 10.6$
$ArC(OH^+)CHCH_2Ar$	(C)	—	—	$pK''_2 = 6.0$
$ArCOCH_2CH_2Ar$	(G)	—	general catalysis	
$ArCOCHCH_2Ar$	(J)	$pK_6 = 10.2$	$pK'_6 = 13$	$pK''_6 = 13.0$
$ArC(OH)CH_2CH_2Ar$	(K)	—	$pK'_7 = 6.6^d$	$pK''_7 = 6.9$
$ArCHCH_2CH_2Ar$ (OH)	(P)	$pK_9 = 8.75$	$pK'_9 = 11$	$pK''_9 = 11.8$

[a] Value obtained from $E_{\frac{1}{2}}$–pH plot corresponding to equilibrium conditions. [b] Value numerically equal to pH at which the heights of polarographic kinetic waves of acid and base forms are equal. [c] Value numerically equal to the pH at which intersection of two linear sections on the $E_{\frac{1}{2}}$–pH plot was observed. [d] Value depends on buffer composition and concentration.

in unsaturated ketones such as dibenzalacetone and benzalcinnamalacetone are more complicated[36] and indicate interactions of the intermediates formed.

Inconsistencies reported in the literature[2–8,13,14] are partly due to insufficiently detailed investigations, to improper choice of buffer (*e.g.*, containing surface-active phenol[14]) and, in particular, to the transfer of the results of mercury pool electrolysis to those obtained with the dropping mercury electrode. Scheme (A)–(U) presented seems to be consistent with the experimental results obtained and is related to processes observed for other carbonyl compounds[18–20,27,28] and can be considered to describe the individual steps in the reduction of chalcone in solutions containing 20% ethanol.

SUMMARY

Individual steps in the reduction of chalcone at the dropping mercury electrode are expressed by scheme (A)–(U). The product of the first two-electron step is dihydrochalcone; in the second, alcohol is formed. Reduction of dihydrochalcone is governed by the rate of its general acid–base catalysed formation from the carbanion-enolate which is the primary electrolytic product. In the first one-electron step, an organomercury compound is formed. Reduction processes are accompanied by antecedent and interposed proton transfers. For the protonation of the radical anion, $[ArCOCHCHAr]^{(\cdot-)}$, resulting in the chalcone reduction, an approximate value, $pK_6 = 10.2$ was found and for that of the radical anion, $[ArCOCH_2CH_2Ar]^{(\cdot-)}$, resulting in the dihydrochalcone reduction, an approximate value, $pK_9 = 8.75$ was found. Radical

anions react with alkali metal cations, but the waves of ketyls formed are not separated from those of radicals, resulting in analogous reactions with hydronium ions. The importance of using results obtained with controlled-potential electrolysis by means of a dropping mercury electrode rather than with a mercury pool electrode, for elucidation of polarographic processes, was stressed.

REFERENCES

1 R. PASTERNAK, *Helv. Chim. Acta*, 31 (1948) 753.
2 T. A. GEISSMAN AND S. L. FRIESS, *J. Am. Chem. Soc.*, 71 (1949) 3893.
3 CH. PREVOST, P. SOUCHAY AND J. CHAUVELIER, *Bull. Soc. Chim. France*, 18 (1951) 715.
4 D. M. COULSON AND W. R. CROWELL, *J. Am. Chem. Soc.*, 74 (1952) 1290, 1294.
5 J. E. CASSIDY AND W. J. WHITCHER, *J. Phys. Chem.*, 63 (1959) 1824.
6 C. W. JOHNSON, C. G. OVERBERGER AND W. J. SEAGERS, *J. Am. Chem. Soc.*, 75 (1953) 1495.
7 J. TIROUFLET AND A. CORVAISIER, *Bull. Soc. Chim. France*, (1962) 535.
8 J. TIROUFLET, E. LAVIRON, J. METZGER AND J. BOICHARD, *Collection Czech. Chem. Commun.*, 25 (1960) 3277.
9 P. ZUMAN AND J. MICHL, *Nature*, 192 (1961) 655.
10 J. M. MEUNIER, M. PERSON AND P. FOURNARI, *Bull. Soc. Chim. France*, (1967) 2872.
11 Z. S. ARIYAN, B. MOONEY AND H. I. STONEHILL, *J. Chem. Soc.*, (1962) 2239.
12 S. WAWZONEK AND A. GUNDERSEN, *J. Electrochem. Soc.*, 111 (1964) 324.
13 I. A. KORSHUNOV AND JU. V. VODZINSKIJ, *Zh. Fiz. Khim.*, 27 (1953) 1152.
14 V. F. LAVRUSHIN, V. D. BEZUGLYJ AND G. G. BELOUS, *Zh. Obshch. Khim.*, 33 (1963) 1711.
15 S. G. MAJRANOVSKIJ, *Izv. Akad. Nauk SSSR, Ot. Khim. Nauk*, (1961) 2140.
16 A. RYVOLOVÁ, *Collection Czech. Chem. Commun.*, 22 (1957) 1114.
17 D. BARNES AND P. ZUMAN, *J. Electroanal. Chem.*, 16 (1968) 575.
18 D. BARNES AND P. ZUMAN, *Trans. Faraday Soc.*, in the press.
19 P. ZUMAN, D. BARNES AND A. RYVOLOVÁ-KEJHAROVÁ, *Discussions Faraday Soc.*, 45 (1968) 202.
20 P. ČÁRSKY, P. ZUMAN AND V. HORÁK, *Collection Czech. Chem. Commun.*, 30 (1965) 4316.
21 M. WAGNER, Thesis, ČSAV, Prague, 1968.
22 I. ŠESTÁKOVÁ, V. HORÁK AND P. ZUMAN, *Collection Czech. Chem. Commun*, 31 (1966) 3889.
23 P. ČÁRSKY, P. ZUMAN AND V. HORÁK, *Collection Czech. Chem. Commun.*, 29 (1964) 3044.
24 I. ŠESTÁKOVÁ, Thesis, ČSAV, Prague, 1967.
25 O. MANOUŠEK, personal communication.
26 P. ZUMAN AND J. KRUPIČKA, *Collection Czech. Chem. Commun.*, 23 (1958) 598.
27 P. ZUMAN, *Collection Czech. Chem. Commun.*, 33 (1968) 2548.
28 P. ZUMAN AND B. TURCSANYI, *Collection Czech. Chem. Commun.*, 33 (1968) 3090.
29 P. ZUMAN AND A. RYVOLOVÁ-KEJHAROVÁ, *Anal. Letters*, 1 (1968) 429.
30 S. G. MAJRANOVSKIJ AND L. I. LIŠČETA, *Collection Czech. Chem. Commun.*, 25 (1960) 3025.
31 L. HOLLECK AND D. MARQUARDING, *Naturwiss.*, 49 (1962) 468.
32 B. KASTENING AND L. HOLLECK, *Z. Elektrochem.*, 63 (1959) 166.
33 R. S. NICHOLSON, J. M. WILSON AND M. L. OLMSTEAD, *Anal. Chem.*, 38 (1966) 542.
34 P. ZUMAN AND D. BARNES, unpublished results.
35 P. ZUMAN AND E. LAVIRON, unpublished results.
36 A. RYVOLOVÁ-KEJHAROVÁ, unpublished results.

Vol. 21 No. 1 JOURNAL OF ELECTROANALYTICAL CHEMISTRY AND INTERFACIAL ELECTROCHEMISTRY APRIL 1969

CONTENTS

INORGANIC ELECTRONIC SPECTROSCOPY

by A. B. P. LEVER, Associate Professor of Chemistry,
York University, Toronto, Canada

The first monograph in the series PHYSICAL INORGANIC CHEMISTRY, edited by M. F. LAPPERT

Electronic spectroscopy has become, in recent years, a commonplace tool in inorganic research and development although few books dealing with the topic have appeared. Those books dealing with spectroscopy in general devote but a few pages to a discussion of the electronic spectra of inorganic compounds.

The aim of this book is (a) to provide the reader with a basic understanding of the methods and procedures involved in a study of the electronic spectra of inorganic compounds, (b) to discuss the information which may be derived from such study, with particular emphasis on stereochemistry and chemical bonding, and (c) to provide a reference text.

A beginning is made at a level which can be understood by an average student with a first degree, the first third of the book dealing with atomic theory, symmetry and group theory. In progressing further with the material presented, the reader can proceed from the construction of qualitative energy level diagrams and the assignment of transitions observed in the spectra of cubic molecules, to quantitative diagrams and the spectra of non-cubic molecules.

Having mastered this material the reader is shown how to derive useful information concerning stereochemistry and chemical bonding and even, qualitatively, such properties as effective nuclear charge and mean *d*-orbital radii. The spectra of the more common transition metal ions in their many oxidation states and stereochemistries are discussed in Chapter 9, which is a mine of information for the practising inorganic spectroscopist.

The book is unique in being the only reference work available which will bring the new graduate up to the level where he can read and usefully digest the original research papers in inorganic spectroscopy. Much of the material has not appeared in book form before and some of it has not appeared in print at all.

xii + 420 pages, 78 tables, 130 illus., 465 lit. refs., 1968, Dfl. 90.00, £11.10.0.

Elsevier
Publishing
Company

Amsterdam London New York

262 E